PhD-FSTM-2020-07
The Faculty of Sciences, Technology and Medicine

DISSERTATION

Defense held on 11/02/2020 in Luxembourg

to obtain the degree of

DOCTEUR DE L'UNIVERSITÉ DU LUXEMBOURG

EN INFORMATIQUE

by

Sumit GAUTAM
Born on 04 May 1990 in Jabalpur – Madhya Pradesh (INDIA)

DESIGN AND OPTIMIZATION OF SIMULTANEOUS WIRELESS INFORMATION AND POWER TRANSFER SYSTEMS

Dissertation defense committee

Dr Symeon CHATZINOTAS, dissertation supervisor
Professor, Université du Luxembourg

Dr Björn OTTERSTEN, Vice Chairman
Professor, Université du Luxembourg

Dr Miguel Angel MENDEZ OLIVARES, Chairman
Assistant Professor, Université du Luxembourg

Dr Luc VANDENDORPE
Professor, Université catholique de Louvain

Dr Bruno CLERCKX
Reader/Professor, Imperial College London

Let the future tell the truth, and evaluate each
one according to his work and accomplishments.
The present is theirs; the future, for which
I have really worked, is mine.

Nikola Tesla
Inventor

To
My Family and Friends

Abstract

The recent trends in the domain of wireless communications indicate severe upcoming challenges, both in terms of infrastructure as well as design of novel techniques. On the other hand, the world population keeps witnessing or hearing about new generations of mobile/ wireless technologies within every half to one decade. It is certain the wireless communication systems have enabled the exchange of information without any physical cable(s), however, the dependence of the mobile devices on the power cables still persist. Each passing year unveils several critical challenges related to the increasing capacity and performance needs, power optimization at complex hardware circuitries, mobility of the users, and demand for even better energy efficiency algorithms at the wireless devices. Moreover, an additional issue is raised in the form of continuous battery drainage at these limited-power devices for sufficing their assertive demands. In this regard, optimal performance at any device is heavily constrained by either wired, or an inductive based wireless recharging of the equipment on a continuous basis. This process is very inconvenient and such a problem is foreseen to persist in future, irrespective of the wireless communication method used. Recently, a promising idea for simultaneous wireless radio-frequency (RF) transmission of information and energy came into spotlight during the last decade. This technique does not only guarantee a more flexible recharging alternative, but also ensures its co-existence with any of the existing (RF-based) or alternatively proposed methods of wireless communications, such as visible light communications (VLC) (e.g., Light Fidelity (Li-Fi)), optical communications (e.g., LASER-equipped communication systems), and far-envisioned quantum-based communication systems. In addition, this scheme is expected to cater to the needs of many current and future technologies like wearable devices, sensors used in hazardous areas, 5G and beyond, etc. This Thesis presents a detailed investigation of several interesting scenarios in this direction, specifically concerning design and optimization of such RF-based power transfer systems.

The first chapter of this Thesis provides a detailed overview of the considered topic, which serves as the foundation step. The details include the highlights about its main contributions, discussion about the adopted mathematical (optimization) tools, and further refined minutiae about its organization. Following this, a detailed survey on the wireless power transmission (WPT) techniques is provided, which includes the discussion about historical developments of WPT comprising its present forms, consideration of WPT with wireless communications, and its compatibility with the existing techniques. Moreover, a review on various types of RF energy harvesting (EH) modules is incorporated, along with a brief and general overview on the system modeling, the modeling assumptions, and recent industrial considerations. Furthermore, this Thesis work has been divided into three main research topics, as follows. Firstly,

the notion of simultaneous wireless information and power transmission (SWIPT) is investigated in conjunction with the cooperative systems framework consisting of single source, multiple relays and multiple users. In this context, several interesting aspects like relay selection, multi-carrier, and resource allocation are considered, along with problem formulations dealing with either maximization of throughput, maximization of harvested energy, or both. Secondly, this Thesis builds up on the idea of transmit precoder design for wireless multigroup multicasting systems in conjunction with SWIPT. Herein, the advantages of adopting separate multicasting and energy precoder designs are illustrated, where we investigate the benefits of multiple antenna transmitters by exploiting the similarities between broadcasting information and wirelessly transferring power. The proposed design does not only facilitates the SWIPT mechanism, but may also serve as a potential candidate to complement the separate waveform designing mechanism with exclusive RF signals meant for information and power transmissions, respectively. Lastly, a novel mechanism is developed to establish a relationship between the SWIPT and cache-enabled cooperative systems. In this direction, benefits of adopting the SWIPT-caching framework are illustrated, with special emphasis on an enhanced rate-energy (R-E) trade-off in contrast to the traditional SWIPT systems. The common notion in the context of SWIPT revolves around the transmission of information, and storage of power. In this vein, the proposed work investigates the system wherein both information and power can be transmitted and stored. The Thesis finally concludes with insights on the future directions and open research challenges associated with the considered framework.

Acknowledgements

My journey in the Interdisciplinary Centre for Security, Reliability and Trust (SnT) at University of Luxembourg has been a wonderful experience. It could not have been so without the support of many people. As I submit my Ph.D. Thesis, I wish to extend my wholehearted gratitude to all those people who helped me in successfully completing this journey. First of all, I want to thank my advisors Prof. Symeon Chatzinotas and Prof. Björn Ottersten, for accepting me as a student and constantly guiding me. Their guidance has helped me improve not only as a researcher, but also as a person. Their help and support during difficult times strengthened and motivated me to move further. Additionally, I would specially like to extend my sincere gratitude to Dr. Eva Lagunas for being such an amazing mentor.

I would like to thank my collaborators: Dr. Eva Lagunas, Dr. Thang X. Vu, Dr. Satyanarayana Vuppala, Dr. Shree Krishna Sharma, Dr. Steven Kisseleff, Ashok Bandi, Prof. Symeon Chatzinotas and Prof. Björn Ottersten for helping me enhance my technical skills as well as the presentation qualities of the respective research articles. My swift research progress in Ph.D. requires a special dedication to my MS Thesis supervisor, Dr. P. Ubaidulla, who helped me back then in strengthening my research and technical skills. I would like to extend my special gratitude towards the teachers and lecturers who taught me several skill development courses at University of Luxembourg. I would also like to take this opportunity in thanking all my teachers (since my childhood) and all the people who came into my life, whose teachings and lessons have helped me in some way or the other on numerous instances. All these experiences have contributed towards the overall development of my persona.

I thank my colleagues and friends in SnT for providing a positive work environment. Many thanks to Renato, Jevgenij, Kostas, Anestis, Lei, Ashok, Hieu, Aakash, Satya and Sumit for extensive discussions and support. I would also like to thank Bhavani, Srikanth, Rig, Yogesh, Hossein, Saied, Ali, Lin, Yang, Alexander, Enjie, Liz, Tedros, and Anshuman for all the fun-filled moments in University of Luxembourg. Special thanks to Rucha, Maharshi, Neha, Soumi, Neera, Harika, Himadri, Luis, and Diana for being such amazing friends. Sincere gratitude to my good old friends and colleagues: Jitendra, Anudeep, Akshay, Sai Krishna, Kunal, Chandan, Nachiket, Prakash, Arpit, Sanchit, Arpita, Priyam, Rishabh, Roopal, Harsh, Farhan, and Ketan for being there with me in my good and bad times.

I could not have accomplished it without the support and understanding of my parents. I wish to thank my Grandparents and my sister Surbhi for being my constant support and motivation. Last, but not the least, thanks to the University of Luxembourg community for giving me an inspiring environment and lots of opportunities to grow.

The generous financial help from the Fonds National de la Recherche (FNR - Luxembourg National Research Fund) via University of Luxembourg is gratefully acknowledged.

List of Abbreviations

5G	Fifth Generation Mobile Technology.
AC	Alternating Current.
AF	Amplify-and-Forward.
AWGN	Additive White Gaussian Noise.
CDF	Cumulative Density Function.
CES	Consumer Electronics Show.
CL	Constant-Linear.
CLC	Constant-Linear-Constant.
CR	Cognitive Radio.
CRNs	Cognitive Radio Networks.
CSCG	Circularly Symmetric Complex Gaussian.
CSI	Channel State Information.
DC	Direct Current.
DF	Decode-and-Forward.
DPMA	Directional Power Maximization Algorithm.
EH	Energy Harvesting.
EM	Electromagnetic.
EYE	Energy Yield Escalation.
FCC	Federal Communications Commission.

FPP-SCA	Feasible Point Pursuit and Successive Convex Approximation.
FPP-SCA-e	Feasible Point Pursuit and Successive Convex Approximation for Energy Optimization.
Gu	Generating Unit.
IA	Integrated Architecture.
IC	Inductive Coupling.
ID	Information Decoding.
i.i.d.	independent and identically distributed.
IoT	Internet of Things.
IP	Intellectual Property.
IPT	Inductive Power Transfer.
IR	Infrared.
ITU-R	The ITU Radiocommunication Sector.
JMEP	Joint Multicast and Energy Precoding Design.
KKT	Karush-Kuhn-Tucker.
L	Linear.
LASER	Light Amplification by Stimulated Emission of Radiation.
Li-Fi	Light Fidelity.
LoS	Line-of-Sight.
LTE-A	Long Term Evolution - Advanced.
MC	Multicast.
MCM	Multi-Carrier Modulation.
MDP	Markov Decision Process.
MG	Multi-group.
MIT	Massachusetts Institute of Technology.
MIMO	Multiple-Input and Multiple-Output.
MISO	Multiple-Input and Single-Output.

ME	Maximum Permissible Exposure.
MPPT	Maximum Power Point Tracking.
MPT	Microwave Power Transfer.
NL	Non Linear.
NLoS	Non Line-of-Sight.
NOMA	Non-Orthogonal Multiple Access.
OFDM	Orthogonal Frequency Division Multiplexing.
OFDMA	Orthogonal Frequency Division Multiple Access.
PIEP	Per-User Information and/or Energy Precoding Design.
PS	Power Splitting.
PSD	Power Spectral Density.
QCQP	Quadratically Constrained Quadratic Problem.
QED	Quod Erat Demonstrandum.
QoS	Quality-of-Service.
R-E	Rate-Energy.
RF	Radio Frequency.
RFID	Radio Frequency Identification.
RIC	Resonant Inductive Coupling.
RPT	Resonant Power Transfer.
Ru	Recovery Unit.
RVs	Random Variables.
SA	Separated Architecture.
SBSP	Space-based Solar Power.
SDP	Semi-Definite Program.
SDR	Semi-Definite Relaxation.
SE	Storage Element.

SIMO	Single-Input and Multiple-Output.
SINR	Signal-to-Interference-and-Noise Ratio.
SMEP	Separate Multicast and Energy Precoding Design.
SNR	Signal-to-Noise Ratio.
SLP	Symbol Level Precoding.
SOCP	Second Order Conic Programming.
SPS	Solar-Power Satellite or Satellite Power System.
SRD	Sequential Resource Distribution.
SU	Secondary User.
SVR	Slack Variable Replacement.
SWIPT	Simultaneous Wireless Information and Power Transmission.
TS	Time Switching.
UL	Underwriters Laboratories.
ULAs	Uniform Linear Arrays.
VLC	Visible Light Communication.
WCP	Wireless Charging Pad.
WF	Water-Filing.
Wi-Fi	Wireless Fidelity.
WiMAX	Worldwide Interoperability for Microwave Access.
WIT	Wireless Information Transfer.
WPT	Wireless Power Transfer.
w.r.t.	with respect to.
WSNs	Wireless Sensor Network.
WSR	Weighted Sum Rate.
WWS	World Wireless System.
ZF	Zero-Forcing.

Notation

α, β	Constants related to the turn-on voltage of diode, capacitance and resistance.
δ_i	Caching gain coefficient at the i-th relay.
ϵ'	Threshold limit (breaking-point) for an iterative algorithm.
$\epsilon^{(t)}$	The step-size in an algorithm.
γ_i	SINR threshold/demand at the i-th user.
ι	Imaginary unit $\iota = \sqrt{-1}$.
$\hat{\lambda}$	Carrier wavelength.
π	Pi $\pi = 3.1416$.
$\mathbf{\Pi}_i$	The $M \times 1$ scalar vector indicating the path loss from M transmit (ULA) antennas to the i^{th} user.
Ψ	Variable to assist the precoder design metrics corresponding to three scenarios.
$\boldsymbol{\rho}$	Set of PS ratios at each user : $\{\rho_\ell\}$ where $\ell = 1, \ldots, L$.
σ_i^2	Antenna noise power at the i-th receiver node.
$\tau_i, \varpi_i, \hat{\tau}_i, \hat{\varpi}_i$	Time fractions between $[0, 1]$ corresponding to dynamic TS scheme.
θ_i	Direction of the i-th user from the transmitter (in radians).
Υ	The effective signal-to-noise ratio / signal-to-noise-and-interference ratio (SNR / SINR).
$\varkappa$	Constant to ensure zero-input/zero-output response for the sigmoidal function based non-linear (NL) energy harvesting model.
ϑ	The path loss exponent.
ξ	Demanded harvested energy at the user.
ζ	Energy conversion efficiency of the receiver.

$\mathbf{\Lambda}$	Denotes the vectors of the dual variables associated with the individual source and relays' power constraints : $(\lambda_S, \lambda_{R,1}, \ldots, \lambda_{R,K})$, during the power allocation step.
$\boldsymbol{\mu}$	Denotes the vectors of the dual variables associated with the individual source and relays' power constraints : $(\mu_S, \mu_{R,1}, \ldots, \mu_{R,K})$, during the power refinement step.
$\mathbf{\Phi}$	Binary matrix $(N \times N)$ for sub-carrier pairing.
$\log(x)$	Natural logarithm function of x.
e^x	Exponential function of x.
$\mathbb{E}\{\cdot\}$	Expected value.
$\mathbb{Re}\{\cdot\}$	Real part.
$\mathbb{Im}\{\cdot\}$	Imaginary part.
$\hat{a}$, $\hat{\mathbf{a}}$, $\hat{\mathbf{A}}$	A scalar, a column vector and a matrix.
$\lvert\hat{a}\rvert$	Modulus of scalar $\hat{a}$.
$\hat{\mathbf{A}}_{ij}$	The entry of the i-th row and j-th column of matrix $\hat{\mathbf{A}}$.
$\hat{\mathbf{a}}^T$, $\hat{\mathbf{A}}^T$	Transpose of vector $\hat{\mathbf{a}}$, transpose of matrix $\hat{\mathbf{A}}$.
$\hat{\mathbf{a}}^H$, $\hat{\mathbf{A}}^H$	Complex conjugate and transpose (hermitian) of vector $\hat{\mathbf{a}}$, complex conjugate and transpose (hermitian) of matrix $\hat{\mathbf{A}}$.
$\hat{\mathbf{A}} \succeq 0$	Matrix $\hat{\mathbf{A}}$ positive semidefinite.
$\hat{\mathbf{A}} \odot \hat{\mathbf{B}}$	Hadamard product between matrices $\hat{\mathbf{A}}$ and $\hat{\mathbf{B}}$, i.e., the element-wise multiplication of their elements.
$\hat{\mathbf{A}} \otimes \hat{\mathbf{B}}$	Kronecker product between matrices $\hat{\mathbf{A}}$ and $\hat{\mathbf{B}}$.
$\mathbf{Tr}(\hat{\mathbf{A}})$	Trace of matrix $\hat{\mathbf{A}}$.
$\mathbf{diag}(\hat{\mathbf{a}})$	Diagonal matrix whose entries are the elements of vector $\hat{\mathbf{a}}$.
$\mathbb{R}$	The set of real numbers.
$\mathbb{C}$	The set of complex numbers.
$\mathbb{R}^{n\times m}$	The set of $n \times m$ matrices with real-valued entries.
$\mathbb{C}^{n\times m}$	The set of $n \times m$ matrices with complex-valued entries.
$\mathbf{I}_Q$	Identity matrix of dimension Q.
arg	Argument.
max	Maximum.

min	Minimum.
argmax	Argument of Maximum.
$\mathcal{N}(\tilde{\mu}, \tilde{\sigma}^2)$	Gaussian or Normal distribution with mean $\tilde{\mu}$ and variance $\tilde{\sigma}^2$.
$d_{\mathcal{S},\mathcal{R}_i}$	The distance between the source and i-th relay.
$d_{\mathcal{R}_i,D}$	The distance between the i-th relay and destination node.
$\hat{d}$	Spacing between successive antenna elements in ULAs.
h	The channel gain coefficient metric.
$\mathbf{h}_i$	The $M \times 1$ conjugated channel vector for the corresponding receiver.
n	Sub-carrier index for the first hop where $n = 1, \ldots, N$.
n'	Sub-carrier index for the second hop where $n' = 1, \ldots, N$.
$\bar{\bar{n}}$	$\bar{\bar{n}}$-th iteration in an algorithm.
$\hat{n}$	Number of floors between the transmitter and the end-user(s).
$\tilde{n}$	Total number of iterations in an algorithm.
p	Transmitted power.
$\mathrm{p}(x)$	Harvested power as a function of input power x corresponding to the energy harvesting model.
r	Requested data rate at the destination node.
t_j	Slack variable corresponding to the j-th user's harvested energy.
$\mathbf{v}$	Slack penalties vector for QCQP reduction.
$\hat{w}_{(n,n'),k}$	Amplification coefficient of the k-th AF protocol-enabled relay.
$\widetilde{\mathbf{w}}_k$	The vector indicating the direction of k-th precoder.
$\mathbf{w}_k$	The $M \times 1$ complex precoding weight vector for the users in group $\mathcal{Z}_k$.
$\mathbf{A}$	Binary matrix ($N \times L$) for sub-carrier–user assignment.
B	Bandwidth.
$\mathcal{D}$	The destination node (end-user).
$\bar{\mathcal{D}}$	The set of all possible relay–user coupling $\mathbf{S} = \{s_{k,\ell}\}$, sub-carrier–user assignment $\mathbf{A} = \{a_{n,\ell}\}$, sub-carrier pairing $\mathbf{\Phi} = \{\phi_{(n,n')}\}$, and the PS ratio $\boldsymbol{\rho} = \{\rho_\ell\}$.
$\hat{D}$	Separation distance between the transmitter and end-user(s) (in meters).
E_{ext}	The external energy required at the relay for further transmission of the signal.
E_ℓ	Energy harvested at the ℓ-th user node (using a linear or a non-linear energy harvester).

$\mathcal{E}_\ell^{\mathcal{L}}$	Energy harvested using a linear energy harvester at the ℓ-th user node.
$\mathcal{E}_\ell^{\mathcal{N}}$	Energy harvested using a non-linear energy harvester at the ℓ-th user node.
$\mathcal{E}'$	Maximum harvested power in case of circuit saturation.
E_{R_i}	Energy demand at the i-th relay for harvesting.
$\hat{F}$	Operational Frequency.
K	Total number of available relays.
L	Total number of end-user nodes.
M	Number of Transmit antennas.
N	Total number of OFDMA sub-carriers in a hop.
$\hat{N}$	Distance power loss coefficient.
$\mathbf{P}_{\mathbf{in}}^{(\mathbf{Sat})}$	Saturation threshold of the RF-energy harvester.
$\mathbf{P}_{\mathbf{in}}^{(\mathbf{Sen})}$	Sensitivity threshold of the RF-energy harvester.
$\mathbf{P}_{\mathbf{Max}}$	Maximum power limitation at the transmit source.
$\mathbf{P}_{\mathbf{R}}^{(n)}$	Input power at the rectifier of the energy harvesting module.
R_i	Overall spectral efficiency at the i-th user.
$\mathcal{R}_k$	The k-th relay where $k = 1, \ldots, K$.
$\mathcal{S}$	The transmit source.
S_k	Set of active sub-carrier pairs $(n, \eta(n))$ assigned on relay k for user ℓ.
$\mathbf{S}$	Binary matrix $(K \times L)$ for relay–user coupling.
Z	Number of Multicasting groups.
$\mathcal{Z}_k$	The k-th Multicast group of users.

List of Tables

List of Figures

Contents

Preface

This Ph.D. Thesis has been carried out from May, 2017 to January, 2020 at the Interdisciplinary Centre for Security, Reliability and Trust (SnT), University of Luxembourg, Luxembourg, under the supervision of Prof. Symeon Chatzinotas and Prof. Björn Ottersten at SnT, University of Luxembourg, Luxembourg. Additionally, the Ph.D. Thesis was co-supervised by Dr. Eva Lagunas, firstly as a Research Associate and later as a Research Scientist (since 2018). The time-to-time evaluation of the Ph.D. Thesis was duly performed by the CET members constituting the supervisors at SnT, University of Luxembourg, Luxembourg and Prof. Luc Vandendorpe from Université catholique de Louvain, Belgium. The fruitful discussions during the INWIP-NET meetings and suggestions from the members of ICTEAM at UCLouvain, Belgium are also gratefully acknowledged.

Contents

This Ph.D. Thesis entitled *Design and Optimization of Simultaneous Wireless Information and Power Transfer Systems* is divided into six chapters. In Chapter 1, the objectives and contributions of this thesis are described. Chapter 2 provides a literature review on wireless power transfer and simultaneous wireless information and power transfer techniques. An investigation on simultaneous wireless information and power transmission (SWIPT) in cooperative systems is presented in Chapters 3. In order to take care of heterogeneous type of users, Precoding in Multi-group Multicasting for SWIPT systems is studied in Chapter 4. A novel SWIPT-Caching framework is analyzed in Chapter 5, where benefits of adding cache-based techniques to SWIPT systems are illustrated. Finally, Chapter 6 provides concluding remarks and future work.

Support of the Thesis

This Ph.D. Thesis has been fully supported by the Luxembourg National Research Fund under Project FNR-FNRS InWIP-NET (R-AGR-0700-10). The effort of collaborators and dissemination costs were supported by other projects, namely, FNR CORE ProCAST (R-AGR-3415-10), the European Research Council under Project AGNOSTIC (742648), and the European Cooperation in Science and Technology under project COST Action IC1301 - Wireless Power Transmission for Sustainable Electronics (WiPE). Additionally, the time-to-time support from SIGCOM is also gratefully acknowledged.

The major milestones of the Thesis are in-line with the timely deliverables of the FNR

- FNRS bilateral Project InWIP-NET (Integrated Wireless Information and Power Networks : R-AGR-0700-10) between the University of Luxembourg, Luxembourg and Université catholique de Louvain, Belgium. The main objective was to investigate InWIP-NET, where a wireless power transfer network composed of a variety of RF energy sources is incorporated into a heterogeneous wireless information network, in order to deliver on-demand information and power wirelessly in a cost-efficient manner.

Publications

Below is a list of original publications that have been produced during the period of Ph.D. candidacy, which are referred to in the text by **J** ≡ Journal, **B** ≡ Book Chapter, **C** ≡ Conference and **SP** ≡ Student Poster.

Journal Papers

[**J3**] S. Gautam, E. Lagunas, A. Bandi, S. Chatzinotas, S. K. Sharma, T. X. Vu, S. Kisseleff, B. Ottersten, **"Transmit Precoder Design for Energy Optimization in Wireless Multi-group Multicasting Systems"** in *IEEE Open Journal of the Communications Society (OJ-COMS)*, December, 2019.

[**J2**] S. Gautam, E. Lagunas, S. Chatzinotas and B. Ottersten, **"Relay Selection and Resource Allocation for SWIPT in Multi-User OFDMA Systems,"** in *IEEE Transactions on Wireless Communications*, vol. 18, no. 5, pp. 2493-2508, May 2019.

[**J1**] S. Gautam, T. X. Vu, S. Chatzinotas, B. Ottersten, **"Cache-aided Simultaneous Wireless Information and Power Transfer (SWIPT) with Relay Selection,"** in *IEEE Journal on Selected Areas In Communications*, vol. 37, no. 1, pp. 187-201, Jan. 2019.

Book Chapter

[**B1**] S. Gautam, T. X. Vu, S. Chatzinotas, B. Ottersten, **"Simultaneous Wireless Information and Power Transfer in UDNs with Caching Architecture,"** in *Wiley Book on Ultra-Dense Networks for 5G and Beyond: Modelling, Analysis, and Applications*, pp. 247-266, February 2019.

Conference Papers

[**C10**] S. Gautam, E. Lagunas, S. Kisseleff, S. Chatzinotas, B. Ottersten, **"Successive Convex Approximation for Transmit Power Minimization in SWIPT-Multicast Systems"** - accepted to *IEEE International Conference on Communications (IEEE ICC'20)*, June, 2020.

[**C9**] T. X. Vu, S. Chatzinotas, S. Gautam, E. Lagunas, B. Ottersten, **"Joint Optimization for PS-based SWIPT Multiuser Systems with Non-linear Energy Harvesting"** - accepted to *IEEE Wireless Communications and Networking Conference (IEEE WCNC'20)*, April, 2020.

[**C8**] S. Gautam, E. Lagunas, S. Chatzinotas, B. Ottersten, **"Wireless Multi-group Multicast Precoding with Selective RF Energy Harvesting,"** in *European Signal Processing Conference (IEEE EUSIPCO'19)*, A Coruña, SPAIN.

[**C7**] S. Gautam, E. Lagunas, S. Chatzinotas, B. Ottersten, **"Pricing Perspective for SWIPT in OFDM-based Multi-User Wireless Cooperative Systems,"** in *IEEE Wireless Communications and Networking Conference (IEEE WCNC'19)*, April, Marrakech, MOROCCO.

[**C6**] S. Gautam, E. Lagunas, S. Vuppala, S. Chatzinotas, B. Ottersten, **"QoS-Constrained Sum-Harvested Energy Maximization in OFDMA-based Wireless Cooperative Networks,"** in *IEEE International Conference on Advanced Networks and Telecommunications Systems 2018 (IEEE ANTS'18)*, December, Indore, INDIA.

[**C5**] S. Gautam, E. Lagunas, S. Chatzinotas, B. Ottersten, **"Sequential Resource Distribution Technique for Multi-User OFDM-SWIPT based Cooperative Networks,"** in *IEEE Global Communications Conference (IEEE GLOBECOM'18)*, December, Abu Dhabi, UAE.

[**C4**] S. Gautam, E. Lagunas, S. Chatzinotas, B. Ottersten, **"Resource Allocation and Relay Selection for Multi-User OFDM-Based Cooperative Networks with SWIPT,"** in *IEEE 15th International Symposium on Wireless Communication Systems 2018 (IEEE ISWCS'18)*, August, Lisbon, PORTUGAL.

[**C3**] S. Gautam, T. X. Vu, S. Chatzinotas, B. Ottersten, **"Joint Wireless Information and Energy Transfer in Cache-assisted Relaying Systems,"** in *IEEE Wireless Communications and Networking Conference (IEEE WCNC'18)*, 15-18 April 2018, Barcelona, SPAIN.

[**C2**] S. Gautam, E. Lagunas, S. K. Sharma, S. Chatzinotas, and B. Ottersten, **"Relay Selection Strategies for SWIPT-Enabled Cooperative Wireless Systems,"** in *28th Annual IEEE International Symposium on Personal, Indoor and Mobile Radio Communications (IEEE PIMRC'17)*, October 2017, Montreal, CANADA.

[**C1**] S. Gautam, and P. Ubaidulla, **"Joint Wireless Information and Energy Transfer in Cooperative Networks,"** in *IEEE 85th Vehicular Technology Conference (IEEE VTC-Spring'17)*, June 2017, Sydney, AUSTRALIA.

Student Poster Sessions

[**SP1**] S. Gautam, E. Lagunas, S. Chatzinotas, B. Ottersten, **"Optimal Relay Selection Strategy for Joint Data and Energy Transfer in Wireless Systems,"** in *IEEE Wireless Communications and Networking Conference (IEEE WCNC'18) - student poster session*, 15-18 April 2018, Barcelona, SPAIN.

Side Publications during PhD

[**J4**] S. Vuppala, T. X. Vu, S. Gautam, S. Chatzinotas, B. Ottersten, **"Cache-Aided Millimeter Wave Ad-Hoc Networks with Contention-Based Content Delivery,"** in *IEEE Transactions on Communications*, vol. 66, no. 8, pp. 3540-3554, Aug. 2018.

[**C11**] S. Vuppala, T. X. Vu, S. Gautam, S. Chatzinotas, B. Ottersten, **"Cache-Aided Millimeter Wave Ad-Hoc Networks,"** in *IEEE Wireless Communications and Networking Conference (IEEE WCNC'18)*, 15-18 April 2018, Barcelona, SPAIN.

Under Review

[**C12**] S. Gautam, E. Lagunas, S. Chatzinotas, S. K. Sharma, B. Ottersten, **"Max-Min Fairness Scheme for SWIPT-enabled Multicasting Systems with Heterogeneous Users"** - submitted to *International Conference on Signal Processing and Communications (SPCOM'20)*, 20-23 July 2020, Bangalore, INDIA.

Chapter 1

Introduction

Electricity has become one of the basic necessities for humans over the past several decades since its introduction. Transmission through wires is the most commonly adopted mechanism to transfer electricity from one place to another. The basic human curiosity to continuously explore has led the mankind to several groundbreaking innovations, whose benefits are reaped by the present generation of human kind. One such idea that has gathered an increasing public interest, is termed Wireless Power Transfer (WPT) or Wireless Energy Transfer (WET)[1] [1], which implies power transmission from an energy transmitter to an energy receiver without any wired connection. This notion introduced by Nikola Tesla inspired many researchers to explore novel possibilities of WPT techniques, which has led to several breakthrough innovations in the area of electromagnetic research during the past two centuries. It is needless to mention that the currently existing forms of WPT techniques are a result of contributions from various scientists and inventors over past many years. This has in-turn laid the foundation for modern electrical power transport systems [2]. At present, the researchers are inching closer to deliver even more superior forms of WPT methods with each passing day.

Based on the research developments in the field, it is found that power transmission may be realized via any of the three forms, viz., capacitive, inductive, or radiative. In the present day scenario, the most commonly associated terms in the context of WPT are inductive coupling, inductive power transfer (IPT) and resonant power transfer (RPT). As discussed above, the fundamental process of these methods include transmission of power from a source to an electrical load without any physical connectors (i.e., wires). Like the traditional wireless communication systems, a WPT system is also composed of a transmitter (also called as source) and a receiver (or a sink). In this context, an alternating current (AC) energizes the transmitter to produce a magnetic field which consequently induces a current in the receiver when brought within its vicinity. More details on the capabilities and limitations of WPT systems are broadly discussed in Chapter 2.

Technological advancements over the years, enabled the utilization of different kinds of Electromagnetic (EM) waves (such as infrared (IR), radio-frequency (RF), etc.) for general purpose applications in the domains of wireless communications and control systems [3]. In this regard, most of the present wireless communication technologies are designed to operate within the radio frequency (RF)/microwave range. This regime of frequencies is also suitable for radiative wireless power transmission, where the use of higher frequencies may provide a

[1]Note that the terms WPT and WET are used interchangeably in the literature.

more directive WPT. In this context, the extraction of energy from the received EM waves may be carried out with the help of a rectenna, which is a special type of antenna used to convert EM energy into direct current (DC) form of electricity [4]. An interesting concept called Space-based solar power (SBSP) aims at collection of solar power in space (via solar-power satellites (SPS) or satellite power systems) first, and then transmission of power to the earth's surface by using high intensity beams of microwaves [5]. In the similar direction, a mirrored concept is to wirelessly power spacecrafts leaving earth's orbit with the help of directed beamforming from the earth's surface [6]. Many research works with focus on WPT, have shown that microwaves are one of the prominent candidates to transfer large amounts of power wirelessly, however, under certain limitations. In 1975, experiments involving tens of kilowatts of WPT were performed at Goldstone in California [7, 8], and more recently (1997) at Grand Bassin on Reunion Island [9]. These methods achieved a successful WPT at distances in the order of a kilometer. In another experiment, Japanese scientists used microwaves to deliver 1.8 kilowatts of power (which is enough to run an electric kettle), through the air with pinpoint accuracy to a receiver kept 55 meters (170 feets) away from the transmit source [10]. Such breakthrough events motivate the humans towards the possibility of capturing a comprehensive power source in space one day. As a result, a sparking research interest is seen in the area of WPT and related fields. Due to the wide adoption of wireless communication methods, a natural alliance of WPT and wireless communication techniques is envisioned to address the increasing demands of power and data in the respective domains. In this vein, simultaneous wireless information and power transfer (SWIPT) systems are expected to gain more prominence after deployment of 5G (or even beyond).

Primal efforts in the development of WPT techniques focused on long-distance and high power applications. The further advancements in the domain revealed several concerns regarding limitations on the low efficiency of transmission process for such high-power applications, and adverse effect of radiation on human health. To combat such challenges, an alternative near-field power transmission technique called inductive coupling, has gathered tremendous attention from both academia and industry. This technique finds its utilization in several applications like e.g., for charging cell-phones, electrical vehicles, and medical implants [11, 12]. It is also noteworthy that the size of devices, such as sensors and wireless transceivers, has decreased many-fold. Additionally, drastic improvements in performance are seen in this context due to better energy optimization. However, the battery-limitations at the devices still remain a great cause of concern. As discussed previously, it cannot be denied that RF/microwaves will come in handy for unification of information and power transmission (simultaneously) to operate these devices. In this regard, SWIPT techniques may bring significant gains in terms of time delay, energy consumption, and interference management [13]. In the era of internet of things (IoT), SWIPT technologies may be relied upon by numerous ultra-low power sensors (which supports several heterogeneous sensing applications) in terms of information exchange and energy supply. In the case of future cellular systems with small cells, massive multiple-input multiple-output (MIMO), or millimeter-wave technique, SWIPT could potentially be integrated as an efficient way to jointly support high throughputs with energy sustainability.

In the following sections, we provide an overview of the problems in the field, the main motivation, and major contributions of this work. We further outline various forms of mathematical (optimization) problems, along with some optimization techniques involved for analyses in several stages of this Thesis. Finally, we provide details about the Thesis organization.

1.1 Problem Overview and Motivation

With the rapid development in the area of SWIPT, it is essential to investigate models that integrates the basic notion of SWIPT within several existing wireless communication systems. In this work, we consider different types of wireless communications based system models, where the concerned devices are capable of handling SWIPT mechanism. Due to the distance limitations of SWIPT systems, we first consider a cooperative network with multiple relays and multiple users to investigate the possibilities for extension of the information and energy delivery using a multi-carrier setting. We then study the precoder design for a multi-group multicasting system in order to tackle the assertive demands of the heterogeneous user types consisting the information users, and/or energy users, and/or both information and energy users, all served by single transmitter with multiple antennas. Finally, we introduce the notion of caching to the SWIPT systems, wherein both information and power could potentially be transmitted and stored unlike the traditional operations focusing on the transmission of information and storage of power. Herein, we assume perfectly known channel state information (CSI) in all cases. The system designing and definitions are succeeded by their analyses via corresponding mathematical (optimization problem) formulations. In this regard, several interesting problems to optimize wireless communications related metrics like information rate, harvested energy, transmit power, and multi-objective function with joint rate and harvested energy, are investigated under different sets of constraints. Based on different types of optimization problems in various scenarios, suitable optimization techniques are employed respectively. The corresponding solutions are validated using numerical results under various parameters and operating conditions. These investigations provide validation and adequate methodology for co-existence of SWIPT within existing wireless communications systems. In the following section, the main contribution of this Thesis are highlighted.

1.2 Main Contributions of this Thesis

In this Thesis, we investigate SWIPT in three different kinds of wireless communication systems. For all the case studies, we initially build up the respective system models that fuse existing wireless communication systems with SWIPT techniques. Since traditional information receivers are incapable of harvesting energy, therefore different forms of SWIPT receiver architectures are considered for analysis. Such kind of receivers are enhanced forms of information receivers along with an additional energy harvesting module. Based on either linear or non-linear behavior of EH operation, we formulate different optimization problems to investigate the considered system models. Further analysis and simplifications leads to suitable solutions. In this regard, a step-by-step discussion with highlights on main contributions of this work is provided below (A brief summary with key insights is also depicted in Fig. 1.1).

Considering the limitations of prior works related to relay selection in cooperative networks, orthogonal frequency division multiple access (OFDMA), and SWIPT, we present a framework in Chapter 3 to jointly optimize single relay selection from a pool of candidate relays, carrier assignment for the two-hop links, power allocation and power-splitting (PS) ratio optimization in a two-hop relay-assisted multiple user based OFDMA network with SWIPT. The relays employ the amplify-and-forward (AF) protocol which takes into account the channelization and sub-carrier switching to demultiplex, frequency convert and multiplex again, unlike its standard operation. We focus on the single relay selection over the multiple relay selection as the latter involves significant complexity in terms of control and synchronization among the relay nodes. We formulate the resource allocation and relay selection problem to

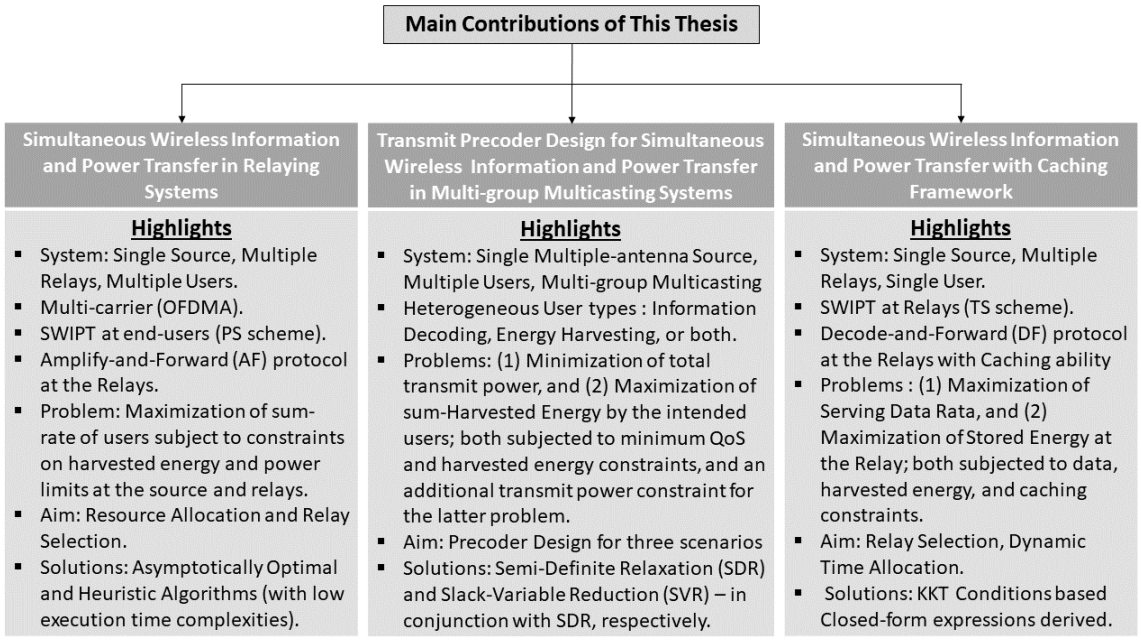

FIGURE 1.1: Brief overview on the main contributions of this Thesis.

maximize the total system throughput by satisfying the individual users' energy harvesting constraints while respecting the individual source and relays' transmit power limits. This is an extremely challenging problem due to the complexity caused by the joint optimization of several network resources, which requires an exhaustive analysis within the full search space. In order to circumvent this tedious and unaffordable optimization, we propose a) an extremely time-efficient and asymptotically optimal algorithm which yields nearly optimal results for high number of sub-carriers, and b) a heuristic method with good performance and even lesser computational complexity. Numerical results are presented, which show that the proposed low complexity schemes offer better performance than the one achieved with a semi-random resource assignment approach, where the relay and sub-carriers are randomly assigned followed by an optimal allocation of power and PS ratios.

Next, we study SWIPT in a Multi-group Multicasting system where precoder designing is desired for heterogeneous users in Chapter 4. Herein, we consider a MISO MG-MC precoding based-system wherein a transmit source equipped with multiple antennas provides coverage to multiple users with the help of beamforming through adequate precoder designs. We investigate the problems of minimization of total transmit power and maximization of sum-harvested energy (by the intended users), respectively, in three different scenarios incorporating the coexistence of heterogeneous users comprising three different types. Both problems are found to be non-convex in nature, such that in order to achieve a feasible (optimal or sub-optimal) solution, adequate relaxations and/or transformations are required. In this regard, we obtain reasonable solutions to the formulated problems with the help of semidefinite relaxation (SDR) and a slack variable replacement (SVR) technique. A comparative study between the three proposed scenarios is provided via numerical results based on the obtained solutions, where intensive investigation is carried out using parameter alterations under various practical conditions.

Finally, we investigate a SWIPT-Caching framework in Chapter 5, where we consider the aspect of relay selection in cache-equipped relays with SWIPT capabilities. Specifically, we

introduce a novel cache-assisted SWIPT architecture for decode-and-forward (DF)-enabled relaying systems under a dynamic TS-based scheme to study the interaction between caching capacity and SWIPT in the considered system. An optimization problem is formulated to maximize the throughput of the (serving) link between the relay and destination, taking into account the caching capacity, minimum harvested energy and quality-of-service (QoS) constraints. By using the KKT conditions with the aid of the Lambert function, a closed-form solution of the formulated problem is obtained for the dynamic TS factors and the transmit power at the relay. Based on this result, the best relay will be selected for cooperation. Thereafter, we formulate an optimization problem to maximize the energy stored at the relay subjected to the QoS constraint. Similar to the previous problem, a closed-form solution is obtained for optimization of the dynamic TS factors and the transmit power at the relay, by using the KKT conditions and the Lambert function. In this context, the effectiveness of the proposed schemes are demonstrated via intensive numerical results, through which the impacts of key system parameters are observed.

Thus, formulating novel optimization problems and providing respective solutions with optimal or sub-optimal results in the form of suitable closed-form or algorithms respectively, are the main areas of focus and contribution of this Thesis. In this direction, the different types of optimization problems encountered during the analyses of systems and some existing convex optimization tools are explained in the succeeding section.

1.3 Discussion on leveraged Mathematical (Optimization) Tools

It is well-known that decision making and analysis of physical systems involves *Optimization* as an important tool. From a mathematical view-point, an *optimization problem* is the problem of finding the *best* or a *suitable* solution from among the set of all *feasible* solutions. An appropriate model construction is the initial step of any optimization process. Herein, modeling is defined as a process to identify and express the *objective*, the *variable(s)*, and the *contraints* of the problem in mathematical terms. In this direction, the basic structure of an optimization problem may be described in sequence, as follows.

- *Objective*: This involves a quantitative measurement of the concerned system performance that we intend to either minimize or maximize. In wireless communications domain, we mostly intend to maximize metrics such as rate, signal-to-noise-ratio (SNR), sum-rate, profit function, etc., and minimize metrics like transmit power, power consumption at the devices, cost function, etc.

- *Optimization parameters (variables or unknowns)*: These refer to the system components whose optimal or sub-optimal values are intended after the optimization process. In wireless communications, these variables may be power allocation, index selection (usually for relays or sub-carriers), channel estimation, etc.

- *Constraints*: It can be one or several function(s) constituting the constraints which does not only describe the relationship among the variables, but also defines the allowable values of the optimization parameters. In wireless communications, certain limitations on the transmit power, rate or SNR demand, etc., constitutes as constraint(s) of the optimization problem(s).

The next step in the optimization process is to determine or observe the category in which the optimization problem belongs. Specifically, the optimization problem types may be broadly categorized into different forms, as shown in Fig. 1.2 [14].

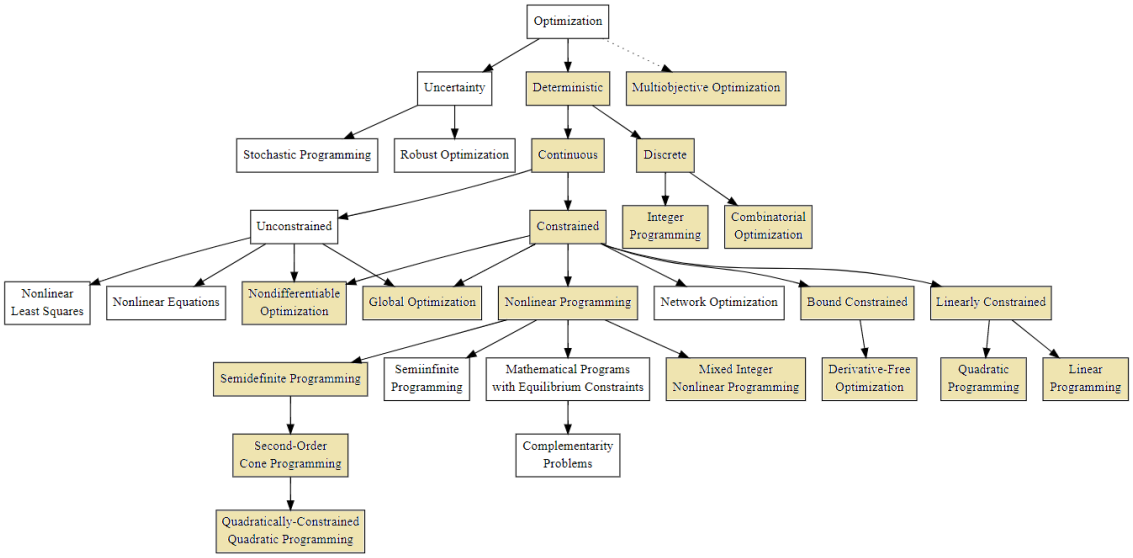

FIGURE 1.2: Different categories of Optimization Problems.

Herein, the optimization categories highlighted in light brown color indicates that these types of optimization problems were encountered while analysis of various system models, as presented in this work.

The final step in the optimization process is to employ suitable techniques to solve the problem, followed by validation via programming and selection of appropriate software. Some of the many possible optimization techniques (used to solve different categories of optimization problems) utilized in this Thesis are discussed in Appendix A. Detailed analysis with application of the aforementioned optimization problems and their solutions will be discussed in the forthcoming chapters. In the next section, we provide a brief schematic to understand the organization of this Thesis.

1.4 Organization of the Thesis

This Thesis is organized in six chapters as follows:

Chapter 1 : A general overview on the topic was provided, with motivation for the different problem settings. Detailed analyses on various optimization types and some convex optimization methods were presented. Additionally, a brief discussion on the major contributions of this work was provided.

Chapter 2 : As the basis for SWIPT in this chapter, we discuss the current state of the art methods in WPT. Herein, we present some details on various methods that facilitates WPT. In this direction, we present a chronology of major breakthroughs and events related to the development of WPT methodologies. As a foundation step for SWIPT, we confer upon the merger of WPT with traditional wireless communication systems. In order to estimate the energy harvesting operation at the corresponding energy harvester, we build-up a narrative on different types of available energy harvesting models. We then discuss about the various types of SWIPT receiver architectures, and compatibility of SWIPT with several existing

wireless communication systems. We cover another interesting aspect in the form of modeling SWIPT systems, and industrial consideration of the subject matter.

Chapter 3 : In this chapter, we propose a novel resource allocation and relay selection scheme for cooperative multi-user multi-relay OFDMA networks with SWIPT capabilities (assuming the non-linear energy harvesting modules) at the end-users. We find that the formulated problem corresponding to the sum-rate maximization of all the users is non-linear with mixed-integer programming. Therefore, it is difficult to obtain an explicit low-complexity solution. In this regard, we exploit the time-sharing criteria and choose sufficiently large number of sub-carriers to efficiently solve this combinatorial problem. We use the dual method with polynomial complexity in this case. Herein, we propose suitable methods which can noticeably improve the system performance and illustrate the effectiveness of the proposed algorithms via numerical results. Additionally, we show the asymptotic optimality of the solutions for sufficiently large parametric values of the number of OFDM sub-carriers, relays and users. Thereafter, we discuss several other interesting problems and their corresponding solutions considering the same systems set-up, however, with a linear EH module. We then provide a discussion on possible extensions of presented framework. The material presented in this chapter was partially published by the author in [15–21].

Chapter 4 : We consider precoding in multi-group multicast system(s) to guarantee the coexistence of three wireless user types, respectively capable of information decoding only, energy harvesting only, and information decoding and/or energy harvesting. In this context, we formulate two problems: (i) to minimize the total transmit power, and (ii) to maximize the overall harvested energy; both subjected to the constraints on minimum signal-to-intereference-and-noise ratio (SINR) and energy harvesting (EH) demands at the corresponding users. The aforementioned problems are transformed with the use of semidefinite relaxation (SDR) technique considering three scenarios, namely, Separate Multicast and Energy Precoding Design (SMEP), Joint Multicast and Energy Precoding Design (JMEP), and Per-User Information and/or Energy Precoding Design (PIEP), respectively. Moreover, an additional slack variable replacement (SVR) method is adopted to make the harvested energy maximization problem tractable. Suitable solutions are proposed to address the aforementioned problems, with considerably good efficiency. We show the performance benefits of SMEP over JMEP and PIEP, in terms of handling low-SINR user demands with no additional computational task for categorizing the EH users, unlike its sub-system counterpart, JMEP. This motivates the adoption of SMEP in practical scenarios. As a further step, we employ the feasible-point pursuit and successive convex approximation (FPP-SCA) to investigate the aforementioned problem of total transmit power minimization. The material presented in this chapter was partially published by the author in [22, 23], and submitted for review in [24, 25].

Chapter 5 : In this chapter, we propose and investigate relay selection strategy in a novel cache-assisted SWIPT architecture with dynamic time switching (TS) in dual-hop half duplex system, where the relays employ the DF protocol. We address the problem of relay selection for maximizing the data throughput between the relay and destination, under constraint on minimum energy stored at the relay; and relay selection for maximizing the energy stored at the relay under constraints on minimum rate and harvested energy, to guarantee a good performance in both the cases with regards to the QoS constraints. Besides, both the problems are formulated according to two separate yet distinct conventions over the time period. We present the closed-form solutions for the proposed relay system to enable SWIPT with caching. With the help of simulations, we illustrate the results corresponding to the solutions

obtained for the aforementioned problems with parameter variations. Consequently, we discuss several promising research directions and possible extensions of this work. The material presented in this chapter was partially published by the author in [26, 27].

Chapter 6 : Contains the conclusions of this Thesis and future work.

Chapter 2

Simultaneous Wireless Information and Power Transmission (SWIPT) - Survey

In modern day systems, the conventional transmission of power (mostly electricity) is carried out with the help of wires. As an outcome of technical advancements, there has been a tremendous progress in the field including the possibility of power transmission through a wireless medium. In this regard, the term wireless power transfer (WPT) is often used to describe the transmission of electrical energy to an electric load from a power source without interconnecting man-made conductors. In other words, WPT could be inferred as a novel paradigm developed to fulfill the electrical energy requirements without any use of wires. In WPT, a wireless transmitter is designated to design optimal (electromagnetic (EM)) signals that can propagate across an intervening space to one or more receivers, where the energy from the signal is extracted and utilized for various operations. In the scenarios where it is inconvenient to lay wires (as well as interconnect them), hazardous areas, costly operations, etc., WPT has emerged as a potential candidate to address such challenges.

Based on the research developments, WPT techniques may be categorized into two groups, viz., non-radiative and radiative. In non-radiative techniques, the power is typically transferred with the help of magnetic fields by using inductive coupling between the coils of wire. Several applications of non-radiative WPT include electric toothbrush chargers, RFID tags, smartcards, and chargers for implantable medical devices like artificial cardiac pacemakers, and inductive powering or charging of electric vehicles like cars, buses or trains. However, the primary focus in the domain lies in the development of wireless systems for charging mobiles and hand-held computing devices. Such equipment types include cellphones, digital music players and portable computers without being tethered to a wall plug. On the other hand, power may also be transferred by electric fields with the help of capacitive coupling between metal electrodes. In the case of radiative far-field WPT techniques (also called power beaming), power is transferred via beams formed by an electromagnetic radiation, like e.g., microwaves, infrared or LASER beams. These techniques are aimed at transporting power at longer distances, however, with a limitation of being pointed directly towards the receiver. In this context, high intensity non-directive beams may be harmful for users from a health perspective and hence, most radiative far-field WPT techniques are often regulated by the concerned authorities. When WPT is combined with wireless information transfer (WIT), the joint form is commonly termed as Simultaneous Wireless Information and Power Transfer (SWIPT).

Further sections of this chapter are organized as follows. We provide a brief discussion on the history related to developments of WPT techniques in Section 2.1. We discuss about various types of WPT methodologies in Section 2.2, and distinguish between the different types of WPT techniques in Section 2.3. Next, we motivate the merger of WPT techniques with existing wireless communication systems in Section 2.4. In this context, we present various forms of typical energy harvesting models in Section 2.5 and different types of receiver architectures supporting SWIPT in Section 2.6. We then discuss about the system modeling and industrial consideration of SWIPT in Section 2.7. Finally, we provide the summary of this chapter in in Section 2.8.

2.1 History of Wireless Power Transfer (WPT)

Over 5000 years ago, the discovery of electricity paved the way for several possibilities of its transmission. One of such possibilities was termed wireless power transfer (WPT), however, nobody fully understood its applications [28], [29], [30]. Many scientists performed several experiments in this domain, mostly after the Renaissance in the 15th century. This led to ground breaking research that characterized the natural phenomenon of WPT. Later in the 18th, 19th and 20th centuries, rapid experiments were carried out to explore further applications of electricity. During this period, it cannot be denied that some of these scientists were well ahead of their time whose contributions laid foundation to modern research. In this regard, several major events and breakthroughs are listed in Section 2.1.1, as follows.

2.1.1 Major events and breakthroughs

The current advancements in the field of WPT have been inspired by developments over past two to three centuries. Several scientists carried out important experiments in the field of WPT, which laid the foundation for modern systems aiming at joint information decoding and power harvesting. In this regard, a brief time-line with major events and breakthroughs in the field is provided below.

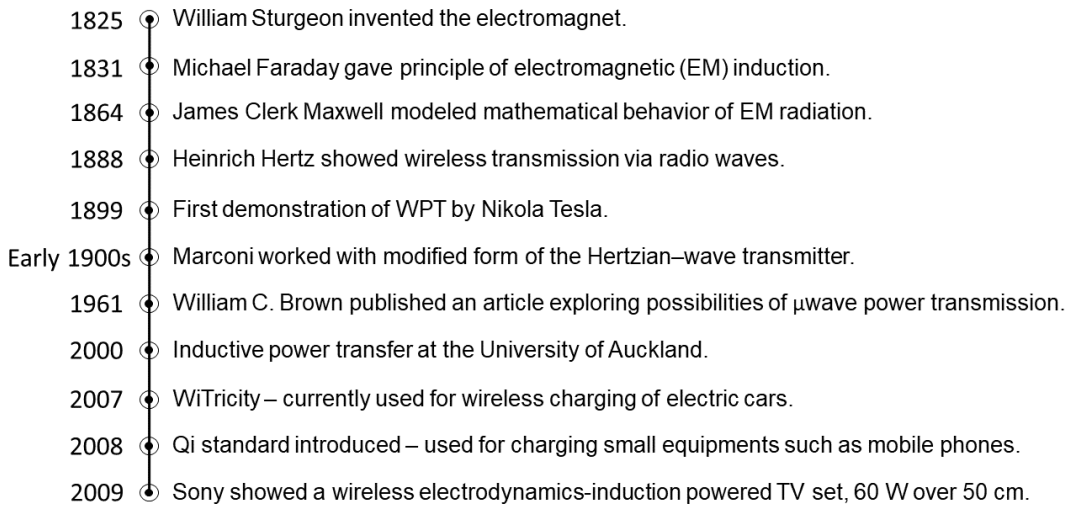

FIGURE 2.1: A brief time-line with major events and breakthroughs in the field of WPT.

Maxwell's theory of electromagnetism, published in 1864, mentions electromagnetic waves moving at the speed of light, and concluded that light itself was just such a wave. In 1888, Hertz performed a successful experiment with pulsed wireless power transfer. He produced an apparatus that produced and detected microwaves in the UHF region. However, these were the initial steps towards advancements in the WPT techniques. Further, we provide short discussions on Tesla's tower and Brown's rectenna, respectively, which happens to be the two most important developments that have paved the way for modern WPT systems.

2.1.2 Tesla's Tower

Nikola Tesla, a well renowned researcher and scientist in the field of electromagnetics, started working on WPT techniques in the late 1890s [31]. He was a pioneer of induction techniques for WPT. Tesla envisioned the possibility of a 'world wireless system (WWS)', where he intended to provide wireless electricity worldwide. In this vein, Tesla proposed to broadcast power with the help of a 187 feet tall tower which was later called the Tesla Tower (as depicted in Fig. 2.2). By realizing this model, Tesla had a vision that people can have access to free energy one day. However, the goals of this tower could not be completed due to shortage of funds and hence, this revolutionary idea eventually failed.

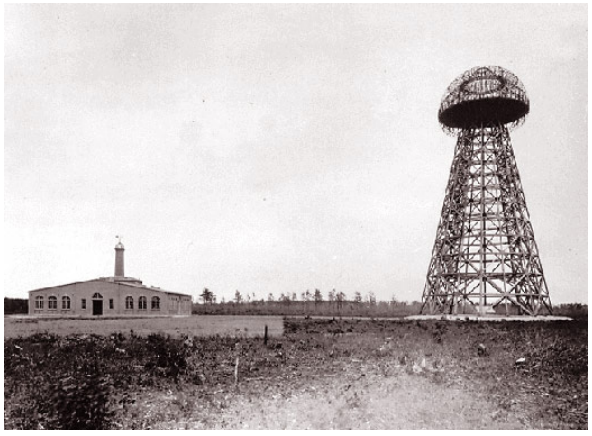

FIGURE 2.2: Tesla's tower [32].

It has been well documented that Tesla was able to transfer power (wirelessly) from one coil to another. Additionally, he designed a method to light 200 lamps from a distance of 40 km [33]. Inspired by this idea after nearly a decade, a team led by Marin Soljačić from MIT took this aspect into consideration in form of a project called 'WiTricity'. Several other existing methods of WPT have been brought to practice based on the same principle.

2.1.3 Brown's Rectenna

William C. Brown was another pioneer in the WPT technologies who designed and exhibited the possibilities of WPT via microwaves. In this context, the basic functionality of WPT could be understood in two parts, viz., transmit section and receive section. The transmit part is composed of microwave power source that generates microwave power which is controlled by the electronic control circuits. The microwave source is protected from the reflected power with the help of waveguide circulator, connected via co-axial waveguide adaptor. The impedance between the microwave source and transmit antenna is contested using the tuner.

Further, the directional coupler separates the attenuated signal based on the direction of signal propagation. The transmit antenna emits the power continuously through the free space to the receive antenna, which converts the received microwave power into DC power. In order to set the output impedance of a signal source equal to one in rectifying circuit, the filter and impedance matching circuit is provided.

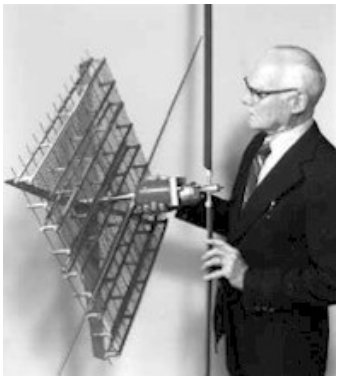

FIGURE 2.3: William C. Brown (1916 - 1999) [34].

As discussed above, the rectenna was a revolutionary device invented by William C. Brown in 1964 [35]. Brown later proposed the first wireless-powered aircraft in form of a helicopter model, which could be powered via microwaves beams from the ground. He also demonstrated a short range transmission of 475W of microwaves at 54% RF-DC efficiency. Robert Dickinson at NASA's jet propulsion laboratory, transmitted 30 kW DC output power across 1.5 km with 2.38 GHz microwaves from a 26 m dish to a 7.3 x 3.5 m rectenna array. Motivated by above-mentioned discussion, we provide a brief study on various types of WPT methods in the succeeding section.

2.2 Different Types of WPT Methods

The methods used to realize WPT may be broadly categorized in two ways, namely, near-field techniques (like inductive coupling, resonant inductive coupling, air ionization, etc.) and far-field techniques (like microwave power transmission, LASER power transmission, solar power satellites, etc.). In this regard, brief discussion on the two types of WPT techniques is provided below.

2.2.1 Near-Field Techniques

Concerning near-field WPT techniques, the three major possibilities include methods like inductive coupling, resonant inductive coupling, air ionization, which are discussed briefly in the following.

Inductive Coupling

The idea of inductive coupling dates back to 1800s, where transfer of power takes place between two coils. The coil which is used for transferring power is called a primary coil while the one receiving the power is called the secondary coil. In an inductive coupling, the primary and secondary coils are not connected via wires and the transfer of power is due to

mutual induction [36]. Generally, the devices used to transfer power in this case are usually air-cored. Some of the practical examples of inductive coupling are wireless charging pad (WCP), electric brushes, hair trimmers, etc. In order to carry out the WPT process, the charging pad (primary coil) and the device (secondary coil) have to be kept very near to each other. This technique is mostly preferred because it is very convenient to use. Additionally, inductive coupling is considered very reliable for general use since there is very limited use of wire and it is shock proof by nature.

(a) (b)

FIGURE 2.4: (a) Basic idea of Inductive Coupling [37], (b) Examples of Inductive Coupling [38].

Resonance Inductive Coupling (RIC)

In case of Resonant inductive coupling (RIC) or magnetic phase synchronous coupling, the "secondary" (load-bearing) side of the loosely coupled coil resonates to make the coupling stronger alongside the phenomenon with inductive coupling. This type of a resonant transformer is often used as a bandpass filter in analog circuitry. Concerning the WPT, some applications of RIC are found in computers, phones, and vehicles. Another type of RIC, termed as WiTricity, focuses on addition of another set of resonant coils on the "primary" (power source) side which pair with the coils on the secondary (load bearing) side. In simple terms, the combination of inductive coupling and resonance constitute towards the main working principle of RIC, i.e., resonance makes two objects interact very strongly and inductance induces current [39]. The basic working principle and the block diagram of RIC have been depicted in Figure 2.5, respectively.

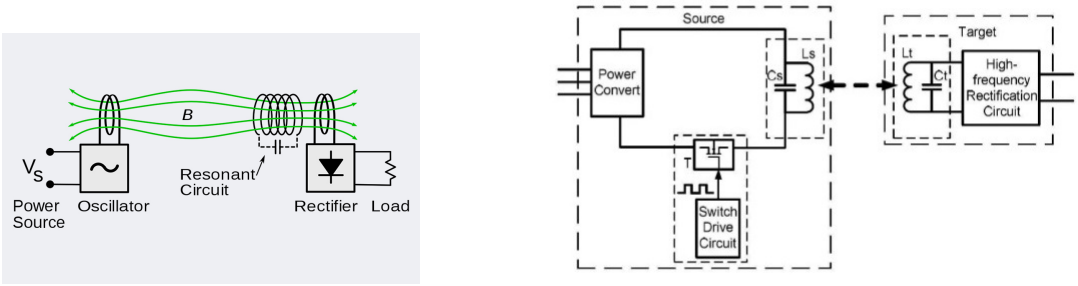

(a) (b)

FIGURE 2.5: (a) Resonance inductive coupling [40], (b) Block diagram of resonance inductive coupling (RIC) [41].

Air Ionization

Lying within several possibilities of near-field WPT techniques, air-ionization is considered to be one of the toughest methods [42]. The working principle of this techniques relies on the fact that air ionizes only when there is a high field. Specifically, a field as high as 2.11 MV/m is required to make this technique feasible. A practical example of air ionization method is natural lightening, as shown in Fig. 2.6. In general, this technique is not feasible for practical applications.

FIGURE 2.6: Air ionization [43].

2.2.2 Far-Field Techniques

As discussed previously, it is important to note that far-field techniques for WPT are usually radiative in nature. For such instances, the line-of-sight (LoS) may be considered a necessity for best performance while the cases with non-line-of-sight (NLoS) usually suffer from high losses. In this context, the LASER or microwave are mostly used as the means for realizing far-field WPT. The far-field techniques aims at achieving high power transfer, but they mostly encounter severe challenges due to power limitations at the transmit source and high power dissipation of the transmit signal with respect to distance. In order to demonstrate this technique, the construction of Tesla's tower may be considered as the best example. Some of the major proposed far-field techniques are discussed briefly in the following.

Microwave power transfer (MPT)

The microwave power transmission (MPT) is a form of WPT technique that utilizes the microwave regime of the electomagnetic spectrum to transfer high power from one place to another [30]. As mentioned above, the general requirement for ensuring the proper working of MPT is that the two concerned devices should usually be in the LoS for an optimal performance, as depicted in Fig. 2.7. In this context, the steps involved in MPT are (*i*) conversion of the electrical power to microwave power, (*ii*) trapping the microwave signal power with the help of a rectenna, and (*iii*) conversion of the microwave power into electrical power. Due to the limitations on alternating current (AC) of not being directly convertible to microwave power for transmission, it is firstly converted into a direct current (DC). In this regard, a magnetron is used to convert this DC equivalent to the desired microwave signal [44]. Upon the reception of the transmitted waves, the rectenna rectifies the received microwave signal in the process, and converts it back to the DC equivalent as its output. The final process involves conversion of DC back to AC which can be then used for different operations at the devices.

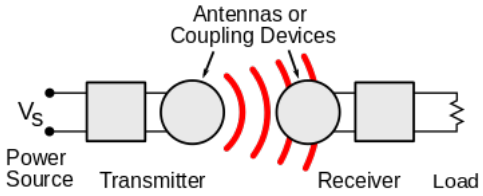

FIGURE 2.7: An example of MPT [45].

LASER transmission

LASER transmission is yet another form of far-field WPT technique, which is of importance due to its high directional nature and high coherence. LASER beams usually gets attenuated when they propagate through the atmosphere, however, most types of LASER specific beams do not disperse for very long distances. A photovoltaic cell is included in a simple receiver to extract power from the LASER beam, as shown in Fig. 2.8. In this vein, the process involved for realizing this technique is less complex and hence it is cost-efficient.

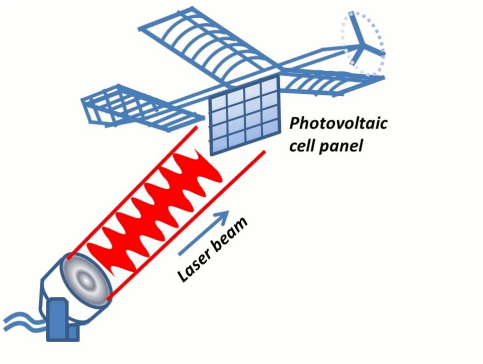

FIGURE 2.8: LASER transmission [46].

Solar power satellites (SPS)

In order to meet the earth's increasing power demands, solar power satellites (SPS) are presumably one of the potential candidates to meet the power requirements in future [47]. The solar power is more efficiently utilized by this technique. The SPS are placed in geostationary orbits, where the solar power are captured using photocells. Each SPS may involve nearly 400 million photocells on an average. The power absorbed via these photocells is then aggregated after conversion, and transmitted to the earth's surface in the form of microwaves/LASER. The received signal on the earth's surface is then converted to electrical power using the rectenna/photovoltaic cell. It is observed that the efficiency of this technique exceeds 85% if microwave is used [48].

Rectenna

As mentioned above, the term rectenna stands for rectifying antenna which is composed of an antenna and a rectifier circuit. The composition of rectenna includes dipole and a mesh of diodes, which is helpful in conversion of microwaves to DC. This arrangement helps in

conversion of microwaves into DC. The arrangements of diodes and dipoles are usually multi-element phased array. One practical application of rectenna is found in the US (of about one and a half mile long), which receives about 5000 MW of power from SPS [49]. A basic schematic of the overall operation is shown in Fig. 2.9.

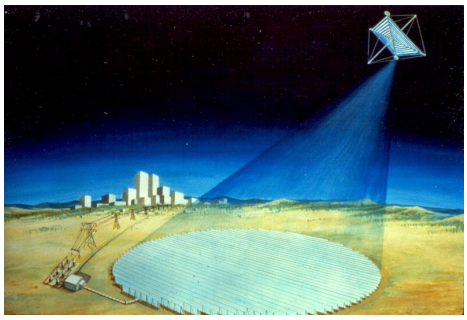

FIGURE 2.9: General working of a rectenna [50].

2.3 Comparison between various techniques of WPT and their Applications

Table 2.1 shows the comparison between the three major wireless energy transfer techniques. We observe that RF energy transfer technique has clear advantage in effective energy transfer distance. However, it has low RF-to-DC energy conversion efficiency especially when the harvested RF energy is small.

Wireless Energy Transfer Technique	**Field Region**	**Propagation**	**Effective Distance**	**Efficiency**
RF energy transfer	Far-field	Radiative	Depend on distance and frequency and the sensitivity of RF energy harvester (typically from several meters to several kilmeters)	0.4%, above 18.2%, and over 50% at -40 dBm, -20 dBm and -5 dBm input power, respectively [51].
Resonant inductive coupling	Near-field	Non-radiative	From a few millimeters to a few centimeters	From 5.81% to 57.2% when frequency varies from 16.2 kHz to 508 kHz [52].
Magnetic resonance coupling	Near-field	Non-radiative	From a few centimeters to a few meters	From above 90% to above 30 % when distance varies from 0.75m to 2.25m [53].

TABLE 2.1: Comparison of various wireless power transfer techniques.

The applications of near-field and far-field WPT techniques span over various areas of practical interest. In near field WPT, the distance is limited to centimeters (cms) or possibly few meters (m). Some potential applications of near field techniques are discussed below

Electric automobile charging: In case of electrical automobiles, WPT is made possible with the help of inductive methods where the vehicles may be static and moving. One practical example is the introduction of electric cars from Tesla motors.

Consumer electronics: Most of the presently available consumer electronics which supports WPT uses induction based coupling mechanism for transferring the power. Few practical examples include hair trimmers, electronic toothbrushes, Samsung Galaxy S-series (7 onwards) mobile phones, etc.

Industrial applications: The near field techniques can be used in industries where the environment is harsh and it is very difficult to set up wire lines to transfer power.

The far field WPT techniques aims at transferring high power in the range of kilometers. Potential applications of far field power transfer techniques include MPT, LASER transmission, SPS, rectenna, etc. These techniques are envisioned to be used for catering the increasing power demands in remote areas. In future, far-field power transfer techniques can also be used to broadcast power globally [54]. In the following section, we provide a discussion to motivate the merger of far-field WPT techniques with wireless communications.

2.4 Fusion of Wireless Communications with WPT

The emerging technologies in the broad area of communication systems continue to amaze the mankind in many ways. The wireless communication technologies introduce endless possibilities ranging from the transmission of information to near/far places without the help of wires, cables, or any other forms of electrical conductors, to transmission of wireless power. In this context, the distance between the source and destination can typically range from a few meters (e.g., remote control of a television) to thousands of kilometers (e.g., radio communication). With the advancement in the domain, several methods like: infrared (IR) based wireless communication, broadcast radio, microwave radio, and communication satellites came into existence. Television remote control, wireless fidelity (Wi-Fi), security systems, cellular telephone, computer interface devices (e.g., bluetooth) are some of the practical applications of wireless communications at present. Another potential application of wireless communication which has gathered considerable attention recently, is the WPT technique.

As discussed in the previous chapter, the WPT technology is in the forefront of electronic development. Since most of the WPT techniques used at present are based on inductive coupling, therefore they operate on the principle of two coil mechanism. Herein, the primary coil is the main source of power transfer while the secondary coil gains current due to induction. Generally, the primary coils are in the form of charging pads whereas the secondary coils are embedded within the device itself. This implies that such devices have to be kept very near to the charging pads for WPT operation to take place. Additionally, the energy conversion efficiency is very less due to the properties of inductance, which often leads to various losses. Moreover, induction based WPT technique fails to deliver on its promise when we consider direct supply of wireless power to wearable devices, sensors in hazardous areas, wireless sensor

network (WSN) nodes, etc, along with information transmission. In this context, it is interesting to exploit the possibility of incorporating data and energy transmission over a common electromagnetic (EM) wave. This type of technique which merges wireless communications or wireless information transfer (WIT) with WPT, is commonly termed as SWIPT.

SWIPT is a recent concept to not only enable devices charge wirelessly, but also allow free mobility with additional advantage of power harvesting. There are many potential applications of SWIPT like supplying wireless power to wearable devices, WSN nodes or sensors installed in hazardous areas, in the medical field (e.g., for powering the pacemaker), etc., along with the regular data services. It is evident that the present designs of transmitters and receivers (for information exchange) does not allow the possibility of supporting SWIPT. Therefore, this calls for a slight modification in the current transceiver design. Consequently, different designs of energy harvesters (EHs) have been proposed. Two common receiver architectures proposed in literature are: separated and integrated. In a separated receiver architecture, the energy harvester and information decoder operates as separate dedicated and individual units, which increases the complexity and cost of the circuit. On the other hand, in case of integrated receiver architecture joint processing of data and energy takes place over the transmission blocks, which is not only less complex but also cost efficient. The main focus of this thesis is on addressing the optimal and sub-optimal transceiver design algorithms for integrated type of architectures to support SWIPT.

In the following section, we discuss about typical RF energy receivers where we assume that the transmitter is capable of transmitting both information and energy simultaneously. This is followed by a general discussion about various types of receiver architectures which incorporates the SWIPT technique.

2.5 Various forms of a typical RF Energy Harvesting Receiver

After almost two decades of research in the field of wireless (RF) power transfer, it cannot be denied that the lifeline of all energy harvesting (EH) circuits lie in the rectenna, which is constituted of an antenna and a rectifier. The most common convention is to convert the input RF (AC) signal into a DC form via assistance from one or several diodes, which consequently introduces a non-linearity operation. The energy harvesting efficiency is found to improve with increasing number of diodes, however, at a cost of reduced receiver sensitivity [55]. In this regard, several models for rectifier circuits may be found in the literature, two of which are depicted in Fig. 2.10. The function of boost converter is amplification of the required voltage as well as the maximum power point tracking (MPPT), exactly due to the non-linear function of the rectifier output with respect to the input power, $\mathbf{P}_{\mathbf{R}}^{(n)}$ [56]. It is noteworthy that accurate or an approximate modeling of the non-linearity in the harvester is crucial from the view-point of SWIPT [57].

Several types of RF energy harvesting models are discussed below.

2.5.1 Linear (L) Energy Harvesting Model

The most primitive and widely adopted energy harvesting model by a large number of SWIPT related prior art is the linear (L) model. The harvested power (as a function of $\mathbf{P}_{\mathbf{R}}^{(n)}$) is expressed as follows

$$\mathrm{p}_{\mathrm{L}}(\mathbf{P}_{\mathbf{R}}^{(n)}) = \zeta_{\mathrm{L}}\mathbf{P}_{\mathbf{R}}^{(n)}; \qquad \mathbf{P}_{\mathbf{R}}^{(n)} \in \mathbb{R}_{+}, \tag{2.1}$$

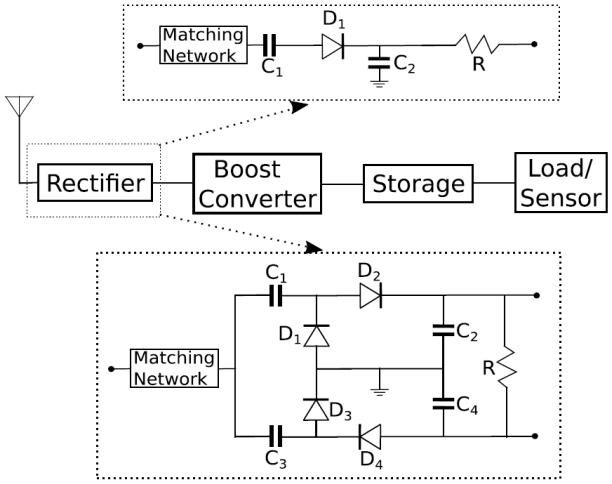

FIGURE 2.10: Basic schematic of RF energy harvester with single diode [57] (upwards) or multiple diodes [58] (downwards) within the rectifier circuit.

where $\zeta_{\mathrm{L}} \in [0, 1)$ is the constant corresponding to the energy conversion efficiency of the receivers. Typical behavior of a linearly harvested power is depicted in Fig. 2.11 with a solid curve. It is important to mention that this model does not take into consideration the following aspects

1. the dependence of RF energy harvesting efficiency on the input power,

2. the harvester is limited by the sensitivity threshold where it is unable to operate below a certain point, and

3. the saturation point of power when the input power level is above a power threshold.

2.5.2 Constant-Linear (CL) Energy Harvesting Model

For a constant-linear (CL) EH model, the harvested power is given by

$$\mathrm{p}_{\mathrm{CL}}(\mathbf{P}_{\mathbf{R}}^{(n)}) \triangleq \begin{cases} 0, & \mathbf{P}_{\mathbf{R}}^{(n)} \in [0, \mathbf{P}_{\mathbf{in}}^{(\mathrm{Sen})}], \\ \zeta_{\mathrm{CL}}(\mathbf{P}_{\mathbf{R}}^{(n)} - \mathbf{P}_{\mathbf{in}}^{(\mathrm{Sen})}; & \mathbf{P}_{\mathbf{R}}^{(n)} \in [\mathbf{P}_{\mathbf{in}}^{(\mathrm{Sen})}), \infty), \end{cases} \tag{2.2}$$

where $\zeta_{\mathrm{CL}} \in [0, 1)$ is the energy conversion efficiency of the receiver. In Fig. 2.11, the corresponding CL curve is depicted with dash-dotted line. The benefit of this model is that it takes the non-operability of the RF-harvester into account, below the sensitivity threshold of $\mathbf{P}_{\mathbf{in}}^{(\mathrm{Sen})}$). However, the CL model ignores the dependence of RF harvesting efficiency on the input power as it is a non-constant function, and the saturation of harvested power above a certain threshold $\mathbf{P}_{\mathbf{in}}^{(\mathrm{Sat})}$).

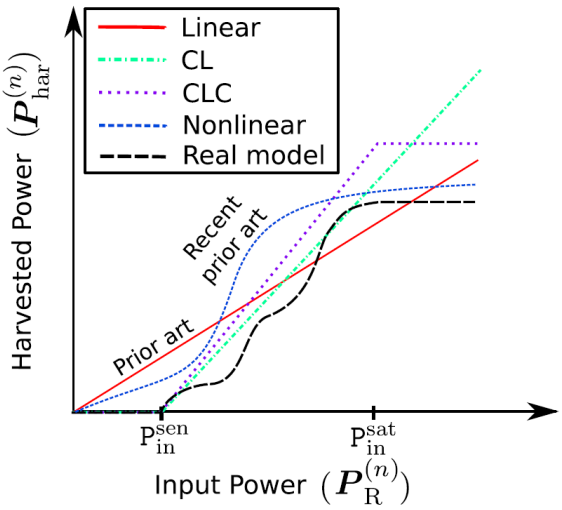

FIGURE 2.11: Plot of harvested power against the input power. In case of real rectenna model, the effect of harvester's sensitivity is taken into consideration where the harvested power is an increasing function of input power.

2.5.3 Constant-Linear-Constant (CLC) Energy Harvesting Model

In case of constant-linear-constant (CLC) EH model, the expression for harvested power is defined as

$$\mathrm{p}_{\mathrm{CLC}}(\mathbf{P}_{\mathbf{R}}^{(n)}) \triangleq \begin{cases} 0, & \mathbf{P}_{\mathbf{R}}^{(n)} \in [0, \mathbf{P}_{\mathbf{in}}^{(\mathrm{Sen})}], \\ \zeta_{\mathrm{CLC}}(\mathbf{P}_{\mathbf{R}}^{(n)} - \mathbf{P}_{\mathbf{in}}^{(\mathrm{Sen})}); & \mathbf{P}_{\mathbf{R}}^{(n)} \in [\mathbf{P}_{\mathbf{in}}^{(\mathrm{Sen})}, \mathbf{P}_{\mathbf{in}}^{(\mathrm{Sat})}], \\ \zeta_{\mathrm{CLC}}(\mathbf{P}_{\mathbf{in}}^{(\mathrm{Sat})} - \mathbf{P}_{\mathbf{in}}^{(\mathrm{Sen})}); & \mathbf{P}_{\mathbf{R}}^{(n)} \in [\mathbf{P}_{\mathbf{in}}^{(\mathrm{Sat})}, \infty), \end{cases} \tag{2.3}$$

where $\zeta_{\mathrm{CLC}} \in [0, 1)$. The performance of the CLC model is depicted as a dotted curve in Fig. 2.11. It is important to note that this model ignores the dependence of harvesting energy on input power.

2.5.4 Sigmoidal Function based Non-Linear (NL) Energy Harvesting Model

The harvested power via sigmoidal function based non-linear (NL) energy harvesting model is represented as

$$\mathrm{p}_{\mathrm{NL}}(\mathbf{P}_{\mathbf{R}}^{(n)}) \triangleq \frac{\mathcal{E}'}{1 - \varkappa} \cdot \left(\frac{1}{1 + \exp(-\alpha \mathbf{P}_{\mathbf{R}}^{(n)} + \alpha\beta)} - \varkappa \right), \tag{2.4}$$

where $\varkappa = \frac{1}{1+\exp(\alpha\beta)}$ is a constant to ensure zero-input/zero-output response for the model. The parameters α, β are related to the turn-on voltage of diode, capacitance and resistance, whereas $\mathcal{E}'$ denotes the maximum harvested power in case of circuit saturation. The corresponding values may be derived by using curve-fitting tool to the results reported in [59, 60].

2.5.5 Ground-Truth (Real) RF Energy Harvesting Model

Another form of non-linear EH model is presented in [55], which is motivated by a real implementation of the EH module as shown in Fig. 2.11. A step-by-step linear approximation

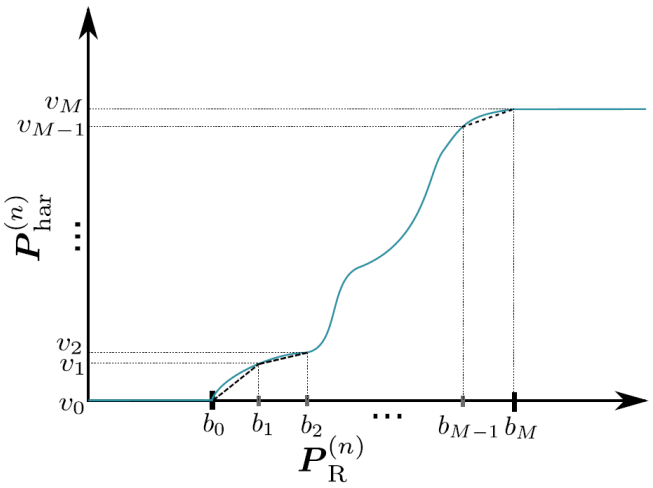

FIGURE 2.12: Graphical illustration of piece-wise linear approximation via ground-truth (real) RF EH model.

of the real model is intended. From the earlier discussions, the dependence of harvested power $\mathbf{P}_{\mathbf{har}}^{(n)}$ on the input power values $\mathbf{P}_{\mathbf{in}}$ is well established. In this regard, define $\{b_m\}_{m=0}^{M}$ as support points, with $b_0 = \mathbf{P}_{\mathbf{in}}^{(\text{Sen})}$, $b_{m-1} < b_m$, for $m \in [M]$, and $b_M = \mathbf{P}_{\mathbf{in}}^{(\text{Sat})}$. The corresponding set of image points $\{q_m\}_{m=0}^{M} \triangleq \{\text{p}(b_m)\}_{m=0}^{M}$ satisfying $q_{m-1} = \text{p}(b_{m-1}) \leq \text{p}(b_m) = q_m$, $m = 1, \ldots, M$, with $q_0 = 0$ and $q_m = \text{p}(\mathbf{P}_{\mathbf{in}}^{(\text{Sat})})$. We assume $0 = q_0 < q_1 < \ldots < q_{m-1} < q_m = \text{p}(\mathbf{P}_{\mathbf{in}}^{(\text{Sat})})$, without loss of generality.

Herein, the presented methodology approximates $\mathbf{P}_{\mathbf{har}}^{(n)}$ as a piece-wise linear function as follows

$$\text{p}_{\text{R}}(\mathbf{P}_{\mathbf{R}}^{(n)}) \triangleq \begin{cases} 0, & \mathbf{P}_{\mathbf{R}}^{(n)} \in [0, b_0], \\ \ell_m(\mathbf{P}_{\mathbf{R}}^{(n)} - b_{m-1}); & \mathbf{P}_{\mathbf{R}}^{(n)} \in (b_{m-1}, b_m], m \in [M] \\ q_m; & \mathbf{P}_{\mathbf{R}}^{(n)} \in [b_m, \infty), \end{cases} \tag{2.5}$$

where $\ell_m \triangleq \frac{q_m - q_{m-1}}{b_m - b_{m-1}}$, $m \in [M]$ are the slopes corresponding to $(M+1)$ points for $\{b_m\}_{m=0}^{M}$ and $\{q_m\}_{m=0}^{M}$. The corresponding depiction may be seen in Fig. 2.12.

2.5.6 Heuristic RF Energy Harvesting Model

The heuristic RF EH model proposes the energy conversion efficiency as a function of the input power [61] as follows

$$\zeta[\bar{x}] = \frac{\hat{a}_2\bar{x}^2 + \hat{a}_1\bar{x} + \hat{a}_0}{\hat{b}_3\bar{x}^3 + \hat{b}_2\bar{x}^2 + \hat{b}_1\bar{x} + \hat{b}_0}, \tag{2.6}$$

where $\bar{x}$ is the input power at the receiver and the parameters $\hat{a}_0, \hat{a}_1, \hat{a}_2, \hat{b}_0, \hat{b}_1, \hat{b}_2, \hat{b}_3$ are distinct for different types of RF-DC circuits [62]. Therefore, the output power can be obtained by

$$\text{p}_{\text{H}}(\mathbf{P}_{\mathbf{R}}^{(n)}) \triangleq \zeta[\mathbf{P}_{\mathbf{R}}^{(n)}]\mathbf{P}_{\mathbf{R}}^{(n)}. \tag{2.7}$$

2.5.7 General Discussion on above-mentioned EH models

From the analysis above, the main points to be taken into consideration are: (i) the nature of function depicting the EH model may either be linear or non-linear, (ii) the EH operation is a function of input power, and (iii) energy conversion efficiency of the receiver plays a vital role in the EH process. However, it is observed that various types of EH circuits may be designed and several non-linear forms of functions may be presented and analyzed accordingly. All the presented models may be considered tractable, however, the criteria of tractability lies in the type of scenario/method chosen. For example, Linear EH operation (along with CL, and CLC) may be considered intractable for general use at it (they) does not characterize the non-linear EH operation. In this context, several non-linear (Sigmoidal or Ground-Truth (reality based)) EH models may be put in parallel to yield a linearized (or CL or CLC) type of characteristic upon analysis [63, 64]. From the literature view-point, the two most widely adopted EH operation are linear (L) and the sigmoidal function based non-linear (NL) functions. Thus, we consider only these two models for our analysis, either together or distinctly.

It is well known that the sigmoidal model characterizes the saturation effect of the diode at high input power values at the EH receiver. Since SWIPT or EH only operation is limited by the distance and is feasible in an indoor scenario, two possibilities arise: (i) when receiver is very close to the transmitter – This case is similar to a coil-based near-field technique and there are no additional advantages, and (ii) when the receivers are placed at several meters of distance away from the transmitter – In this case, we expect to receive an input power in micro-Watts or even lower. This implies that the saturation effect at the EH module cannot be obtained in any case, except when the user(s) is/are very close to the transmitter. We use the sigmoidal model (the most widely adopted non-linear model in the literature) at low power of operation so that we may present system designs considering at-least a room sized space for analysis since the main target of SWIPT is to provide flexibility in terms of user mobility.

2.6 Different types of SWIPT Receivers and Techniques Compatible with SWIPT

Herein, we discuss various types of SWIPT receiver architectures available in the literature and briefly present some of the existing techniques compatible with SWIPT. In this context, the corresponding discussion is provided below.

2.6.1 Various Models of SWIPT Receivers

It is evident that the traditional information receiver architectures are designed to handle only the information reception, and they may not be considered optimal in the context of SWIPT. This is due to the reason that the information reception and RF power harvesting work at very different power sensitivity (e.g., -10 dBm for energy harvesters versus -60 dBm for information receivers) [65]. This inspires the research efforts toward the development of receivers capable of performing both information decoding as well as power harvesting together. In this regard, typically four types of receiver architectures which implements SWIPT are proposed in the literature. Brief description about these receivers are provided in the following subsections.

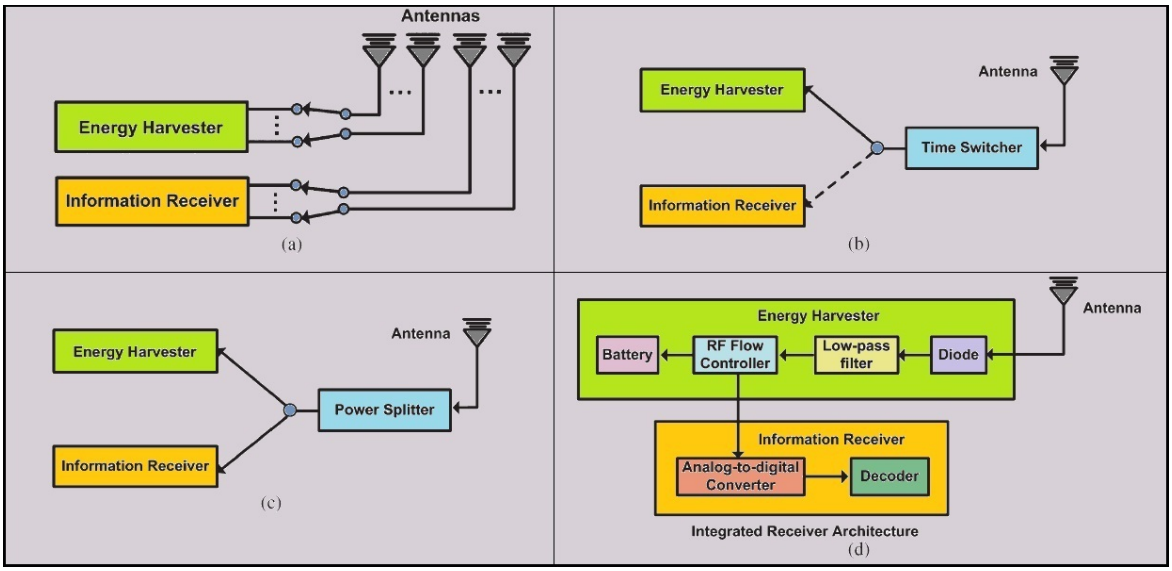

FIGURE 2.13: Different types of receiver architectures to support SWIPT.

Separated Receiver Architecture

In a separated receiver architecture, also known as antenna-switching [65], an energy harvester and information receiver are equipped with independent antenna(s) so that different channel coefficient(s) are observed by both. A generalized model for separated receiver architecture is shown in Fig. 2.13(a). Two sets of connections from antenna arrays virtually divides the system such that each set is connected to either energy harvester or information decoder. Consequently, independent and concurrent energy harvesting as well as information decoding can be performed with the help of this architecture. Apparently, the performance of the separated receiver architecture can be optimized by using the antenna-switching scheme [65].

Co-located Receiver Architecture

The co-located receiver architecture allows an energy harvester and an information receiver to share the same antenna(s) so that they observe the same channel(s). As a single antenna can be adopted, the co-located receiver architecture can be of a smaller size compared to the separated receiver architecture. This architecture can be categorized into two models, i.e., time-switching and power-splitting architectures. The time-switching architecture, as shown in Fig. 2.13(b), allows the network node to switch and use either the information receiver or the RF energy harvester for the received RF signals at a time. In the power-splitting architecture, as shown in Fig. 2.13(c), the received RF signals are split into two streams for the information receiver and RF energy harvester with different power levels. In practice, power splitting is based on a power splitter and time switching requires a simpler switcher. It has been recognized that theoretically power-splitting achieves better tradeoffs between information rate and the amount of RF energy transferred [65], [66]. However, it was shown in [67] that for high noise variance and under an assumption of non-linear EH module, TS was shown to perform better than PS. In the Thesis, we assumed noise variance of -90 dBm or lower wherein PS performs better than TS under the assumption of non-linear EH module.

Integrated Receiver Architecture

An integrated receiver architecture has been proposed in [66], where the energy harvester is integrated with the implementation of RF-to-base-band conversion for information decoding via rectifier. Hence, a small form factor is introduced as a consequence. The model for integrated receiver architecture has been depicted in Fig. 2.13(d). It should be noted that just like the co-located receiver architecture, the RF flow controller can also adopt a switcher or power splitter in a similar manner. However, the main difference is the adoption of switcher and power splitter in the integrated receiver architecture.

Ideal Receiver Architecture

In an ideal receiver architecture, it is assumed that the receiver is capable of extracting RF energy from the same signal used for decoding information. However, it has been pointed out in [66] that this assumption may not be guaranteed to work in practice. Present designs of receiver circuits does not allow extraction of RF energy and information decoding simultaneously from the recovered carrier. In other words, the process of information decoding incurs an energy loss that is carried by the received RF signals sent for an information receiver. Generalized analysis on the theoretical upper bound of the receiver performance are presented in the existing works, such as [68], [69], [70], [71], considering an ideal receiver architecture.

The work presented in [66] shows that the power consumed by receiver circuits are relatively small in comparison to the received signal. It is found that the integrated receiver architecture outperforms the co-located receiver architecture at high harvested energy region, whereas the co-located receiver architecture is superior at low harvested energy region. The integrated receiver architecture performs better in the case where circuit power consumption is high. When a system without minimum harvested energy requirement is considered, it is shown that the integrated receiver architecture performs better by providing high information rate in comparison to separated receiver for short transmission distances.

2.6.2 Techniques in WIT compatible with WPT to enable SWIPT

In this section, we provide a discussion on several existing (as well as emerging) wireless communication technologies wherein SWIPT could be integrated. Some SWIPT-enabled techniques are briefly discussed below.

Cooperative Relaying Systems

The most simple form of cooperative relaying system involves a transmitter, a relay node (which may employ an Amplify-and-Forward (AF) or Decode-and-Forward (DF) protocol), and a user. Further, the system may be expanded into a multi-relay and multi-user system, wherein optimal resource allocation may be desired. Considering the aspect of SWIPT mechanism, three possibilities arise

1. *Energy Harvesting at Relay only*: In such a system, the allocation of concerned resources takes place at the transmitter. The relay harvests energy as well as processes information using the transmit signal. The harvested energy may be used to amplify or re-transmit the desired signal to the end-user or may be stored for later use.

2. *Energy Harvesting at the end-User only*: Herein, the end-user is capable of simultaneous information decoding and energy harvesting. This mechanism is processed via received signal from the relay, which may further be enhanced via signal from the transmitter with the help of direct link, if it exists. The corresponding signal may be designed at the transmitter and/or relay and/or both.

3. *Energy Harvesting at both Relay and end-User*: In this case, the joint information decoding and energy harvesting operation takes place at both relay and end-user. The signal intended at the end-user may be designed at the transmit source or at the relay, whereas the signal intended at the relay is designed at the transmitter.

Related References: [72–81]

Full-Duplex Systems

A full duplex system involves simultaneous uplink and downlink between the concerned transceiver nodes, often referred to as bi-directional communication. In this regard, several existing works (in conjunction with SWIPT) provide analyses of full duplex systems via interesting problem formulations, such as weighted sum of transmit power minimization and weighted sum rate maximization. Additionally, other important aspects like resource allocation in full duplex SWIPT, multi-antenna relay systems and multiple-input multiple output (MIMO) have been investigated.

Related References: [82–95]

Cognitive Radio Networks (CRNs)

There are several works which provides the architectural design of (CRNs) and integration of RF-EH to CRNs. In this regard, the main focus lies in designing mechanism to support dynamic spectrum access with SWIPT.

Related References: [96–102]

Multi-Carrier Systems

A multi-carrier system involves multi-carrier modulation (MCM) wherein the transmit data is split into several components and each of these components are sent over separate carrier signals. The composite signal has a broad bandwidth, while individual carriers have narrow bandwidth. In case of SWIPT systems, two most widely adopted multi-carrier systems chosen for analysis are described below.

1. *Orthogonal Frequency Division Multiplexing (OFDM)/ Orthogonal Frequency Division Multiple Accesss (OFDMA):* With regard to SWIPT, several interesting problems includes resource allocation (e.g., carrier, power, etc.,) for single/multiple users and optimization of SWIPT parameters.

2. *Non-Orthogonal Multiple Access (NOMA):* This is another interesting form of multi-carrier setting. The use of power-domain and code-domain NOMA are of specific interest for SWIPT systems.

Related References: [103–110]

Precoding / Beamforming Systems

The precoding/beamforming frameworks are mostly based on multiple-input single-output (MISO) or multiple-input multiple-output (MIMO) systems. The main aim is to enhance the system performance with the help of focused or targeted beams at the end-user. Constructive interference among the concerned signals (often termed as Symbol Level Precoding (SLP)) constitutes as a source of energy for SWIPT systems.

Related References: [111–115]

Bistatic Scatter Radio

This kind of system involves a backscatter device, which reflects or sends a further modulated message to the intended user. Severe path-loss and limited communication range are the major drawbacks of these systems. However, such systems may facilitate SWIPT under several circumstances. A form of bistatic scatter radio is also used in the RFID systems.

Related References: [116–118]

Millimeter Wave Communication (mmWC) Systems for 5G

A millimeter wave communication system relies on the use of high frequencies for its operation. Even though SWIPT is limited by the usage of high frequencies, several interesting works have been carried out in this regard. Optimization of transmit power with distance limitations is one of the widely studied problem in this case.

Related References: [119–124]

Wireless Sensor Networks (WSNs)

The Internet-of-Things (IoTs) involves several small nodes (often termed as wireless sensor nodes (WSNs)), which usually suffers in terms of overall performance because of scarcity of energy due to limited battery sources. Moreover, such WSNs are difficult to reach in order to carry out continuous replacement of batteries. In this context, several interesting problems involve classification of nodes based on power usage and applying SWIPT to cooperative cluster of WSNs. Additionally, development of real time wireless recharging protocols still remain open challenges for WSNs with SWIPT capabilities.

Related References: [125–134]

Caching Systems

Several studies related to the cache-enabled systems have shown considerable performance improvements over traditional systems without caching. Further investigation of caching frameworks with SWIPT have shown tremendous improvements in system performance specifically in the context of rate-energy (R-E) trade-off. In this regard, time efficient systems with reduced delays may be modeled to exploit the benefits of caching with SWIPT.

Related References: [26, 27]

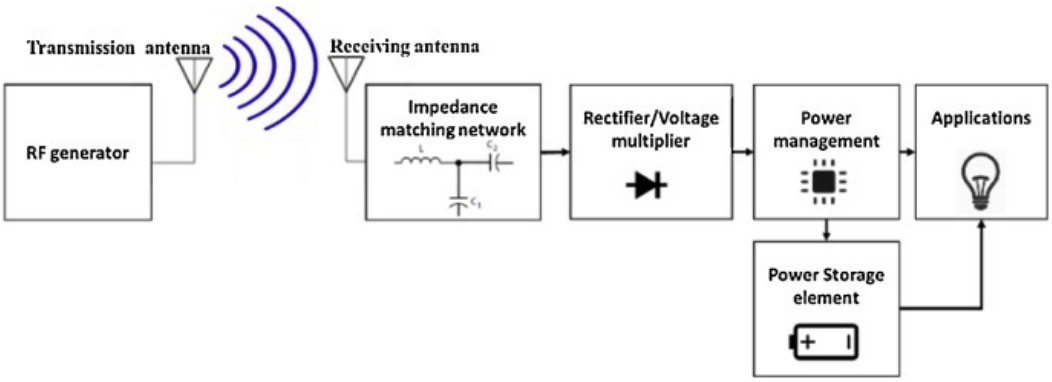

FIGURE 2.14: Basic schematic of RF-based WPT systems [145].

Security of the Systems

Most of the modern day systems rely on the quality-of-service (QoS) constraints, which does not take into consideration the security aspects of the system. In this context, physical layer security and secrecy performance analysis in SWIPT systems are taken up as potential research areas to address security related issues. Furthermore, several ways are proposed to study various receiver modes of SWIPT for increasing the system security via development of novel protocols.

Related References: [135–144]

2.7 System Modeling and Industrial Consideration of WPT/ SWIPT Techniques

In this section, we focus on describing the system modeling and assumptions for WPT and SWIPT systems, followed by a brief discussion on the industrial consideration of the concerned topic in the domain.

2.7.1 Modeling of WPT/SWIPT systems

Similar to the traditional wireless communication systems, the modeling components for WPT or SWIPT system includes a microwave source, a transmitting antenna, a receiving antenna and an energy harvesting module. Additionally, the power transmission process involves an assumption for the channel conditions used to facilitate WPT or SWIPT mechanism. In this regard, we discuss about the concerned components and assumptions below.

Microwave source and Transmit Antenna

A microwave source consisting of electron tubes or solid-state devices with electronics to control power output, is generally used for WPT mechanism. In this regard, the slotted

waveguide antenna, parabolic dish and microstrip patch are the most popular components. Since the slotted waveguide antenna provides high power handling capacity as well as high efficiency ($> 95\%$), they seems to be the most preferred option for WPT or SWIPT. In case of SWIPT, the existing WIT methods are used in conjunction with WPT techniques. Basic schematic of RF-based WPT systems is depicted in Fig. 2.14.

Assumptions on Channel Modeling for WPT/SWIPT

The most common channel modeling assumption while taking WPT or SWIPT systems into consideration, is their operation at microwave or RF bands ranging from 2.4 GHz to 5 GHz. Certain frequency bands find their utilization in a number of radio services according to the ITU-R radio regulations, including medical applications and industrial science. At present, the radio LANs and microwave ovens use the 2.4 GHz band while several applications like radio location service and dedicated short-range communications use the 5 GHz band heavily. This channel model assumption may provide accurate performance characteristics as for the real-life practical case. However, the conventional channel models used in WIT based on Rayleigh distribution with normalized channel conditions may also be used for theoretical validation of the concerned systems.

In this Thesis, we consider known channel state information (CSI). We assume that the optimization is carried out at a centralized controller, including all the implementations and computation via algorithms. The central controller is independent of the considered systems and it has its own power supply. Upon the successful optimization of the parameters, the central controller informs the concerned devices/nodes about the related/intended parameters. The signaling may be performed using orthogonal waveforms independently or using separate orthogonal multi-carrier framework. However, this would require more investigation and is currently out of the scope of this work. From the signaling overhead perspective, since the number of involved parameters is not too high, the signal overhead is not expected to cross its threshold until which it can facilitate the system with maximum benefits. Adequate feedback signaling may be accounted as the overhead in terms of collecting information from the limited power devices, which again should be acceptable provided the system efficiency is ensured.

In addition, it is noteworthy that the overall computation of involved parameters would be necessary at the first run. However, due to an indoor scenario, most of the conditions (CSI) may be fixed (or they will remain unaltered) unless in the case of signal blocking or signal jamming scenarios. In this case with known metrics, several parameters may be optimized and fixed accordingly while yielding a closed-form solution like scenario. In this regard, a time-to-time computation would be required depending on the system requirements e.g., the environmental effects on 5G signals is well known. In-line with this, computations (as well as CSI estimation) may be performed depending on the weather/temperature changes etc.

Receive Antenna and Energy Harvesting

At the receiver end, a rectenna is used to directly convert microwave energy into DC electricity at the energy harvesting module. Rectenna is composed of a receiving and converting unit at the WPT or SWIPT receiver. The basic components of this device (rectenna) includes diodes and mesh of dipoles which absorbs the microwave/RF energy from the received signal thereby converting it into electric power. The usual formation of these elements is in a multi-element phased array, with a mesh pattern reflector element for making it directional. In case

of SWIPT, the WIT and WPT mechanisms may be carried out distinctly or concurrently, depending on the capability of the receiver.

2.7.2 Industrial Consideration of WPT/SWIPT systems

With the tremendous growth and sparking research interest in the field over the last decade, several industrial organizations have shown enthusiasm in working towards making WPT a reality. However, it is worth mentioning that majority of such companies focus only on WPT techniques, which works independently with regard to WIT. The main aim of this Thesis is to bridge the gap between WIT and WPT, so as to motivate the consideration of SWIPT systems in future. Herein, we present a brief discussion on industrial consideration of the topic, where few major companies working in the domain are listed in Table 2.2.

Company	**Product**	**WPT Type**	**Operation Method**	**Reference**
Wi-Charge	Wi-Charge	Far-Field	Infrared (IR)	[146].
Energous Corporation	WattUp	Far-Field	Radio-Frequency (RF)	[147].
GuRu Wireless Inc. (formerly Auspion Inc.)	GuRu	Far-Field	Radio-Frequency (RF) - Millimeter Waves (mmWaves)	[148].
Ossia	Cota	Far-Field	Radio-Frequency (RF)	[149].
Powercast Corporation	Powercast	Far-Field	Radio-Frequency (RF)	[150].
WiTricity Corporation	WiTricity	Near-Field	Resonant Inductive Coupling (RIC)	[151].
Wireless Power Consortium (WPC)	Qi (Standard)	Near-Field	Inductive Coupling (IC)	[152].
Spansive (formerly Pi)	Spansive	Near-Field (mid-range)	Inductive Coupling (IC) - Loose	[153].
Freevolt	Freevolt	Near-Field	Inductive Coupling (IC)	[154].
Nowi	Nowi	Hybrid of Near- and Far-Field	Radio-Frequency (RF) + light movement + heat + other ambient energy sources	[155].

Table 2.2: Industrial consideration of WPT and SWIPT systems.

Detailed discussion about the companies and corresponding products as provided in Table 2.2 may be found in Appendix B.

2.8 Summary

In this chapter, we provided a discussion on history of WPT including major breakthroughs in the domain. We provided an insight to various types of WPT techniques, specifically the near-field and far-field methods. We provided a comparative study between the existing WPT

techniques and their applications. Further, we presented a discussion to motivate the merger of wireless communications with WPT. We then discussed about various type of energy harvesting models proposed in the literature. These models included linear (L), constant-linear (CL), constant-linear-constant (CLC), the sigmoidal function based non-linear (NL), ground-truth (real), and heuristic (H) based EH operations. We conferred upon different types of receiver architectures for SWIPT, followed by a brief discussion on techniques suitable for carrying out the SWIPT mechanism. Furthermore, we presented a discussion on system modeling and industrial consideration of WPT/SWIPT technologies. Based on some major insights from this chapter, we intend to develop the SWIPT framework in the succeeding parts of this Thesis.

Chapter 3

Simultaneous Wireless Information and Power Transfer in Relaying Systems

In this chapter, we investigate the resource allocation and relay selection in a two-hop relay-assisted multi-user Orthogonal Frequency Division Multiple Access (OFDMA) network, where the end-nodes support Simultaneous Wireless Information and Power Transfer (SWIPT) employing a Power Splitting (PS) technique. Our goal is to optimize the end-nodes' power splitting ratios as well as the relay, carrier and power assignment so that the sum-rate of the system is maximized subject to harvested energy and transmitted power constraints. Such joint optimization with mixed integer non-linear programming structure is combinatorial in nature. Due to the complexity of this problem, we propose to solve its dual problem which guarantees asymptotic optimality and less execution time compared to a highly-complex exhaustive search approach. Furthermore, we also present a heuristic method to solve this problem with lower computational complexity. Simulation results reveal that the proposed algorithms provide significant performance gains compared to a semi-random resource allocation and relay selection approach and close to the optimal solution when the number of OFDMA sub-carriers is sufficiently large.

The chapter is organized as follows. Introduction to the current state of the art is discussed in Section 3.1. Section 3.2 provides an overview of the system model. Section 3.3 describes the problem formulation for sum-rate maximization of all users. The proposed asymptotically optimal and heuristic solutions are illustrated in Sections 3.4 and 3.5, respectively. Numerical results are shown in Section 3.6. Further in Section 3.7, we provide brief summary of works related to the considered framework. Finally, Section 3.8 provides the summary of this chapter.

3.1 Introduction to SWIPT-based Cooperative Relaying Systems

Cooperative relaying is a promising technology where the information delivery from a source node to a user node is assisted via one or several intermediate nodes, referred to as relay nodes. In doing so, the network coverage is extended, fading effects are alleviated, and the whole network can be rolled out cost-effectively and rapidly [156, 157]. Besides, cooperative relaying has emerged as a promising alternative to alleviate the burden of installing multiple antennas on size-limited terminals [158].

Orthogonal Frequency Division Multiple Access (OFDMA) [159] is one of the most popular air interface for wireless access (e.g., LTE-A and WiMAX) given its spectral efficiency characteristics and its ability to handle frequency-selective fading. High data demands and energy requirements can be met by combining OFDMA and cooperative relaying [160]. However, optimal relay selection in relay-assisted OFDMA is not a straight forward problem since it depends highly on the OFDMA power and sub-carrier allocation across different hops. The selection of the most appropriate relay is one challenging problem by itself in general cooperative relaying scenarios. There are various protocols proposed in the literature to choose the best relay among a collection of available relays so that the performance of a single transmit-relay-receive link is optimized [161–163] where the respective strategies are to choose the best relay depending on its geographic position [161], maximization of end-to-end SNR [162], or based on the strongest bottleneck link (i.e., the weaker channel between the source-relay and relay-user channels) [163].

Recent studies have dealt with the joint optimization of relay selection and resource allocation in a single-user OFDMA relay network [164,165], while the multi-user extension of such a scenario was considered in [160] wherein the performance benefits of channel-dependent OFDMA sub-carrier pairing are illustrated for multi-hop systems. Considering a single source, multi-hop relaying and single user scenario, an OFDM-based selective relaying scheme was proposed in [166], where superior performance benefits of Selective OFDMA relaying with only symbol detection at each relay was shown over Selective OFDM relaying where decoding of whole OFDM block is required at each hop. However, all of these works does not take into account the energy efficiency aspects.

With the rapid development in wireless communication over recent years, the power demand to operate the wireless devices has increased manifold [167]. Simultaneous Wireless Information and Power Transmission (SWIPT) is an upcoming and promising technique to meet these requirements [168]. In this direction, several types of SWIPT receiver architectures were presented in [169], namely: separated, time-switching (TS), power-splitting (PS), and integrated architectures, where superior performance of PS-based SWIPT receiver is established. Implementation of SWIPT-OFDMA systems has attracted due attention recently [66, 170]. The incorporation of OFDMA with SWIPT does not only preserves its existing advantages, but simultaneous charging of multiple devices along with information exchange can be achieved. However, due to the rate-energy (R-E) trade-off [171], the information rate cannot be optimized without diminishing the harvested energy and vice-versa. In addition, the information and particularly the energy cannot be sent from one place to another over large distances. In this context, it has been proposed that the use of relays may come in handy for such cases [16, 17, 172–174].

There is limited work available in the literature addressing relay selection to enable SWIPT in multi-user OFDMA (MU-OFDMA) scenarios [175–178]. A simple relay selection algorithm in MU-OFDMA cooperative Cognitive Radio (CR) networks is analyzed in [175] to enhance the normalized sum-rate of secondary users (SUs) while a novel relay selection method for cooperative communication networks is proposed in [176] using fuzzy logic. Further, a relay selection problem based on co-channel interference is studied in [177], where the relays are assumed to employ the decode-and-forward (DF) protocol. It is noteworthy that [176] and [177] present a multi-user scenario but both the works neither consider OFDMA nor the energy harvesting aspects. On the other hand, performance benefits of relay selection

for SWIPT is shown in [178], where a trade-off between the information transfer to the target receiver and harvested energy at the remaining receivers is established. In [179], a relay selection method based on either maximum sum-throughput or minimum outage probability is proposed to facilitate the communication process between two transceivers in a full-duplex mode. However, the multi-user case is not investigated in [178,179]. In [180], Guo *et al.* consider energy constrained relay nodes within cooperative clustered WSNs and provide optimal strategies to prolong their lifetime using ambient RF signals which, however, do not incorporate the multicarrier setting. Similar to [180], the authors in [181] present a framework where two sources communicate with each other via two way DF and SWIPT-enabled relaying devices. Considering a SWIPT relay system, the authors in [182] proposed an optimal energy efficiency based joint resource allocation and relay selection scheme. Optimal transmission schemes (static and dynamic) for joint time allocation and power distribution are designed in [183], where single DF relay (with SWIPT capabilities) assists a source to transfer information to a destination. With a multiple-antenna source terminals and single-antenna energy harvesting (EH) relay, the performance analysis for an analog network coding based two-way relaying system is investigated in [184]. Noticeably, [180–184] considers energy harvesting at the relay nodes, and not at the end-users.

In contrast to the above studies, this chapter investigates the joint optimization of single relay selection from a pool of candidate relays, carrier assignment for the two-hop links, power allocation and power-splitting (PS) ratio optimization in a two-hop relay-assisted MU-OFDMA network with SWIPT. The relays employ the amplify-and-forward (AF) protocol which takes into account the channelization and sub-carrier switching to demultiplex, frequency convert and multiplex again, unlike its standard operation. We focus on the single relay selection over the multiple relay selection as the latter involves significant complexity in terms of control and synchronization among the relay nodes. We formulate the resource allocation and relay selection problem to maximize the total system throughput by satisfying the individual users' energy harvesting constraints while respecting the individual source and relays' transmit power limits. This is an extremely challenging problem due to the complexity caused by the joint optimization of several network resources, which requires an exhaustive analysis within the full search space. In order to circumvent this tedious and unaffordable optimization, we propose a) an extremely time-efficient and asymptotically optimal algorithm which yields nearly optimal results for high number of sub-carriers, and b) a heuristic method with good performance and even lesser computational complexity. Numerical results are presented, which show that the proposed low complexity schemes offer better performance than the one achieved with a semi-random resource assignment approach, where the relay and sub-carriers are randomly assigned followed by an optimal allocation of power and PS ratios.

This work builds on the authors' previous publications [16, 185]. In [16], the optimal transceiver design and relay selection for SWIPT in a single-transmitter single-receiver two-hop cooperative network is considered; while in [185] a single transmitter and multiple users scenario is considered with frequency-selective fading and multi-carrier transmission (without incorporation of cooperative systems). Moreover, a linear energy harvesting model was examined in [16,185] under a more generalized channel model while we do analysis by assuming a non-linear energy harvesting model in this work, under a more practically feasible scenario.

The main contributions of this chapter are four-fold, listed as follows

1. Firstly, we consider a dual-hop scenario where multiple AF-relays facilitate SWIPT from single source to multiple users with the help of OFDMA carriers in both the hops. Each end-user employs the PS-based SWIPT architecture[1] having a non-linear energy harvesting model. Our aim is to optimize and save network resources while easing the synchronization process amongst the relay nodes.

2. Secondly, we formulate an optimization problem for relay selection, carrier assignment in the two-hops for carrier pairing, power allocation, and the PS ratio for each user in order to maximize the overall sum-rate of the system subjected to transmit power and harvested energy constraints. One possible solution is proposed based on an exhaustive search mechanism within the full feasibility region, which imposes intractability at large dimensions due to extremely high (exponential) time-complexity.

3. Thirdly, we propose an asymptotically optimal solution by considering the dual of the aforementioned problem which reduces the computational complexity to polynomial time. Besides, we also present a heuristic solution with good performance and even lesser time-complexity. Additionally, we derive closed-form expressions for the power metrics by using the Karush-Kuhn-Tucker (KKT) conditions, and consequently determine respective PS ratios at the users.

4. Finally, we demonstrate the effectiveness of the proposed methods where significant gains are observed in comparison with a semi-random resource allocation and relay selection approach. In this vein, the impacts of varying the key system parameters is observed via numerical results. Additionally, the benefits of the proposed techniques are provided and some possible future directions of this work are discussed.

3.2 System Model

We consider a two-hop cooperative network of K fixed relays $(\mathcal{R}_1, \ldots, \mathcal{R}_k, \ldots, \mathcal{R}_K)$ assisting a source $\mathcal{S}$ that can transmit both information and energy to L users $(\mathcal{D}_1, \ldots, \mathcal{D}_\ell, \ldots, \mathcal{D}_L)$, where $L \leq K$ in general. The source, relays and end-user nodes are equipped with single antenna and each relay operates in a time-division half-duplex mode using the AF protocol. Each user is connected to the source via single relay, which is not shared with other users to avoid control channel and synchronization overhead. It is worth mentioning that the scenario considering only single relay with multiple antennas may be beneficial in some situations not only in terms of low synchronization overhead but also distance dependent effects for energy harvesting. This however limits the system performance and in this regard, multiple relays distributed within the network may help cater to the need of users with even lower synchronization overhead and higher efficiency. The transmission from the source to relays and from relays to users is based on OFDMA scheme. In particular, the available bandwidth on both the hops is divided into N sub-carriers ($1 \leq n \leq N$ for the first hop and $1 \leq n' \leq N$ for the second hop) in which the channel is assumed to be frequency-flat. The channel coefficient of the first hop between $\mathcal{S}$ and the $\mathcal{R}_k$ on the n-th sub-carrier is denoted as $h_{1,n,k}$,

[1]Please note that most of the aforementioned works consider EH at the relays. It is important to mention that for relays that are a part of the infrastructure with their own power supply (as in this chapter), EH at the end-users is crucial and this aspect has not been investigated widely. A practical example of the proposed framework can be its implementation in an indoor scenario (e.g., office workspace), where single source is located in the middle of a corridor and different AF relays are placed near the office doors so as to extend the SWIPT coverage inside the specific offices. In general, the role of the relays is of extreme importance in case of hindrance, which is highly experienced in indoor scenarios.

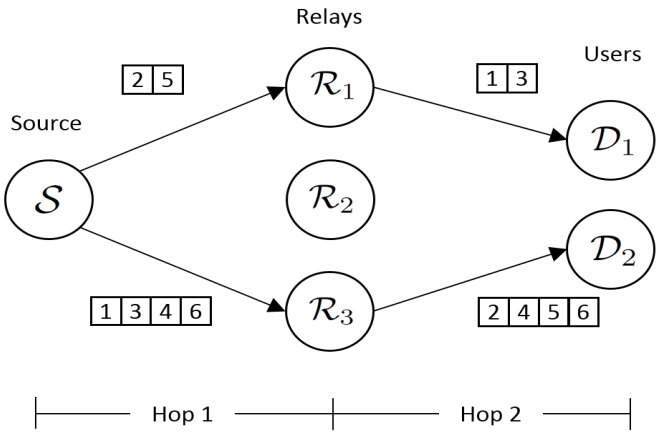

FIGURE 3.1: System model for multi-user relay-assisted OFDMA-based communications with SWIPT.

whereas the channel coefficient of the second hop between the $\mathcal{R}_k$ and the $\mathcal{D}_\ell$ on the n'-th sub-carrier is denoted as $h_{2,n',k,\ell}$. We assume that the users are out of reach of the source and therefore do not receive the direct signal during the first hop. We consider a sub-carrier pairing approach, where the sub-carriers of the first and second hops are paired such that each relay $\mathcal{R}_k$ employs a set of sub-carrier pairs. A sub-carrier pair is defined as the (n, n') sub-carriers such that the relay receives from sub-carrier n, amplifies it, and forwards it on the sub-carrier n'. Note that n and n' may be equal or not. We assume that each pair can only be assigned to one relay but one relay can employ multiple pairs. Fig. 3.1 illustrates the considered scenario and a particular sub-carrier pairing example for a network with $K = 3$ relays, $D = 2$ users and $N = 6$ sub-carriers.

The transmit power on the n-th sub-carrier at the source $\mathcal{S}$ in the first hop is denoted as $p_{1,n}$, while the relay $\mathcal{R}_k$ retransmits the received signal by applying the following amplification coefficient

$$\hat{w}_{(n,n'),k} = \sqrt{\frac{p_{2,n',k}}{p_{1,n}\left|h_{1,n,k}\right|^2 + \sigma_k^2}}, \tag{3.1}$$

which ensures that the relay transmit power on the n'-th sub-carrier is $p_{2,n',k}$. In (3.1), σ_k^2 denotes the noise power at the $\mathcal{R}_k$ relay. The total available power at the source $\mathcal{S}$ and at the relay $\mathcal{R}_k$ is fixed as P_S and $P_{\mathcal{R},k}$, respectively.

On the other hand, the receivers at the users are capable of decoding information as well as harvesting energy according to a PS SWIPT architecture. In particular, the received signal at the user $\mathcal{D}_\ell$ is split into two streams, with the power splitting ratio ρ_ℓ, as shown in Fig. 3.2. The fraction $\sqrt{\rho_\ell}$ of the received signal is used for energy harvesting, while the rest is sent to the information decoder. For simplicity, we assume a normalized transmission time for each hop so that the terms *energy* and *power* can be used interchangeably. In practice, the antenna noise $\tilde{d}_\ell \in \mathcal{CN}(0, \sigma^2_{\tilde{d}_\ell})$ has a negligible impact on both the information receiving and energy harvesting, since $\sigma^2_{\tilde{d}_\ell}$ is generally much smaller than the noise power introduced by the baseband processing circuit, and thus even lower than the average power of the received signal [186]. As a consequence, the antenna noise $\tilde{d}_\ell$ is neglected in this chapter. In addition, we assume that the relays are a part of the infrastructure having their own power supply and, therefore, they do not need to harvest energy from the received signals.

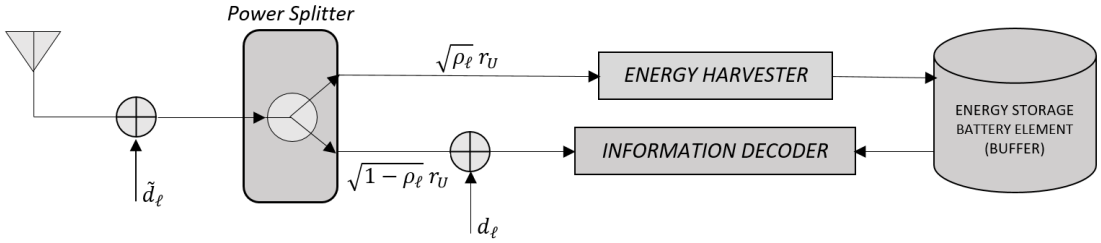

FIGURE 3.2: Receiver architecture based on PS scheme.

Let us denote $a_{n,\ell} \in \{0,\ 1\}$ as the binary variable for selection of $\mathcal{D}_\ell$ with $a_{n,\ell} = 1$ indicating $\mathcal{D}_\ell$ is assigned the sub-carrier n in the first hop and $a_{n,\ell} = 0$ otherwise. To comply with the fact that a sub-carrier can only be assigned to a unique user, we impose the following constraint,

$$\sum_{\ell=1}^{L} a_{n,\ell} = 1, \quad \forall n. \tag{3.2}$$

Assume $\phi_{(n,n')} \in \{0,\ 1\}$ denotes the indicator for sub-carrier pairing, where $\phi_{(n,n')} = 1$ means that sub-carrier n in the first hop is paired with sub-carrier n' in the second hop and $\phi_{(n,n')} = 0$ otherwise. Since each sub-carrier can be paired with one and only one sub-carrier, the binary variable $\phi_{(n,n')}$ must satisfy the following constraints

$$\sum_{n=1}^{N} \phi_{(n,n')} = 1, \ \sum_{n'=1}^{N} \phi_{(n,n')} = 1, \quad \forall (n, n'). \tag{3.3}$$

For the relay–user coupling, we define $s_{k,\ell} = \{0,\ 1\}$, where $s_{k,\ell} = 1$ means that $\mathcal{R}_k$ is selected for $\mathcal{D}_\ell$, $s_{k,\ell} = 0$ otherwise. One relay is assumed to assist single user. Therefore, the following relay–user constraints must be satisfied

$$\sum_{k=1}^{K} s_{k,\ell} = 1, \quad \forall \ell, \tag{3.4}$$

$$\sum_{\ell=1}^{L} s_{k,\ell} \leq 1, \quad \forall k. \tag{3.5}$$

The effective SNR seen at the decoding branch of the ℓ-th user for (n, n') sub-carrier pair over the $\mathcal{S} \to \mathcal{R}_k \to \mathcal{D}_\ell$ link is given by

$$\Upsilon_{(n,n'),k,\ell} = \frac{(1-\rho_\ell) p_{1,n} |h_{1,n,k} \hat{w}_{(n,n'),k} h_{2,n',k,\ell}|^2}{(1-\rho_\ell)\sigma_k^2 |h_{2,n',k,\ell} \hat{w}_{(n,n'),k}|^2 + \sigma_{d_\ell}^2}$$

$$= \frac{(1-\rho_\ell)\left(\frac{p_{1,n}|h_{1,n,k}|^2}{\sigma_k^2}\right)\left(\frac{p_{2,n',k}|h_{2,n',k,\ell}|^2}{\sigma_{d_\ell}^2}\right)}{1 + \left(\frac{p_{1,n}|h_{1,n,k}|^2}{\sigma_k^2}\right) + \left(\frac{p_{2,n',k}|h_{2,n',k,\ell}|^2}{\sigma_{d_\ell}^2}\right)}. \tag{3.6}$$

The above expression can be further simplified and re-written as follows

$$\Upsilon_{(n,n'),k,\ell} = \frac{(1-\rho_\ell)\Upsilon_{1,n,k}\Upsilon_{2,n',k,\ell}}{1+\Upsilon_{1,n,k}+(1-\rho_\ell)\Upsilon_{2,n',k,\ell}}, \tag{3.7}$$

where $\Upsilon_{1,n,k} = \frac{|h_{1,n,k}|^2 p_{1,n}}{\sigma_k^2}$, and $\Upsilon_{2,n',k,\ell} = \frac{|h_{2,n',k,\ell}|^2 p_{2,n',k}}{\sigma_{d_\ell}^2}$, with $\sigma_{d_\ell}^2$ being the baseband processing circuit noise power at $\mathcal{D}_\ell$. Further, we adopt the following approximation to make the analysis more tractable in the high SNR regime

$$\hat{\Upsilon}_{(n,n'),k,\ell} \approx \frac{(1-\rho_\ell)\Upsilon_{1,n,k}\Upsilon_{2,n',k,\ell}}{\Upsilon_{1,n,k}+(1-\rho_\ell)\Upsilon_{2,n',k,\ell}}, \tag{3.8}$$

since $\frac{|h_{1,n,k}|^2}{\sigma_k^2} >> 1$ and $\frac{|h_{2,n',k,\ell}|^2}{\sigma_{d_\ell}^2} >> 1$, therefore the unity term in the denominator of (3.7) may be ignored thereby causing a negligible impact on the system performance considering SWIPT.

The spectral efficiency achieved by the decoding branch of the (n, n') sub-carrier pair over the $\mathcal{S} \to \mathcal{R}_k \to \mathcal{D}_\ell$ link can thus be expressed as

$$R_{(n,n'),k,\ell} = \frac{1}{2}\ln\Big(1+\hat{\Upsilon}_{(n,n'),k,\ell}\Big), \tag{3.9}$$

where the factor $1/2$ is introduced to compensate for the two time slots of the considered relay assisted communication. The overall spectral efficiency at $\mathcal{D}_\ell$ is

$$R_\ell = \sum_{i=1}^{L}\sum_{k=1}^{K}\sum_{n=1}^{N}\sum_{n'=1}^{N} s_{k,\ell}a_{n,\ell}\phi_{(n,n')}R_{(n,n'),k,i}. \tag{3.10}$$

On the other hand, the energy harvested at the harvesting branch for the (n, n') sub-carrier pair over the $\mathcal{S} \to \mathcal{R}_k \to \mathcal{D}_\ell$ link is given by

$$E_{(n,n'),k,\ell} = \zeta\rho_\ell\Big[|\hat{w}_{(n,n'),k}h_{2,n',k,\ell}|^2(p_{1,n}|h_{1,n,k}|^2+\sigma_k^2)\Big], \tag{3.11}$$

where ζ is the energy conversion efficiency of the receiver. Furthermore, for a linear energy harvester, the overall harvested energy at $\mathcal{D}_\ell$ considering all intended sub-carriers is given by

$$\mathcal{E}_\ell^{\mathcal{L}} = \sum_{k=1}^{K}\sum_{n=1}^{N}\sum_{n'=1}^{N} E_{(n,n'),k,\ell}. \tag{3.12}$$

It is noteworthy that all the transmitted OFDM subcarriers are utilized for energy harvesting purpose. Using only the intended sub-carriers for energy harvesting purpose is an inefficient process as the energy available in sub-carriers allocated to other users may potentially be harvested [187].

From a practical viewpoint, it has been well established in the literature that the energy harvesting operation by the energy harvesters is non-linear in nature [59, 60, 188]. It is apparent from such studies that for small values of energy detection at the energy harvester, the gap between the performances of non-linear and linear energy harvesting models cannot be ignored. Besides, detection of high energy signals where the harvested energy is large or even larger than the demand, the linear energy harvesting model is incapable of capturing the characteristics of the energy harvesters. Thus, this calls for the adoption of a non-linear

EH model due to its practical feasibility. In this regard, we define the energy harvested at the receiver [59, 60] as follows

$$\mathcal{E}_{\ell}^{\mathcal{N}} = \rho_{\ell} \sum_{k=1}^{K} \sum_{n=1}^{N} \sum_{n'=1}^{N} \frac{\mathcal{E}'}{1-\varkappa} \cdot \left(\frac{1}{1+\exp(-\alpha p_{2,n',k} |h_{2,n',k,\ell}|^2 + \alpha\beta)} - \varkappa \right), \tag{3.13}$$

where $\varkappa \triangleq \frac{1}{1+\exp(\alpha\beta)}$, the constant $\mathcal{E}'$ is obtained by determining the maximum harvested energy on the saturation of the energy harvesting circuit, and α and β are specific for the capacitor and diode turn-on voltage metrics at the EH circuit. Practically, a standard curve-fitting tool based on analytical data may be used to decide the appropriate values of $\mathcal{E}'$, α, and β [59]. However, it should be noted that (3.13) is in its tractable form concerning the PS-type of scheme, which also simplifies the EH constraint. This is due to inconsistent values of correponding parameters as obtained from [59], and further feasibility concerns. The corresponding analysis is presented in Appendix C.1 of this Thesis.

Concerning the utilization of the harvested energy at each user, there are many interesting ways to do so. The harvested energy may be utilized by the user to recharge its battery or it may be stored for later use. Simultaneous powering to each information decoding sub-block is also a possibility. In order to convey its future energy harvesting demands to the central controller (which is responsible for performing all the computational and intimation task) using adequate signaling/feedback, the user may utilize the harvested energy for such purposes. This kind of mechanism may require a separate framework and analysis, as provided in [189]. However, any of the aforementioned methods may be adopted (as per the requirement) to utilize the harvested energy at the end-user.

Our goal is to optimize the network resources so as to maximize the total end-nodes' sum-rate under a set of harvested energy and transmitted power constraints. In the following section, we formulate the corresponding optimization problem and discuss about the possible solutions.

3.3 Problem Formulation

We consider the problem of relay selection, carrier assignment in the two-hops for carrier pairing, power allocation, and the computation of the optimal PS ratio at each user that maximizes the effective sum-rate of the end-user nodes, while ensuring that the harvested energy at each user is above a given threshold and that the total transmit power does not exceed a given limit. As such, the variables to be optimized are: relay–user coupling $\mathbf{S} = \{s_{k,l}\}$, sub-carrier–user assignment $\mathbf{A} = \{a_{n,\ell}\}$, sub-carrier pairing $\mathbf{\Phi} = \{\phi_{(n,n')}\}$, power allocation in the two-hops $\mathbf{P} = \{p_{1,n}, p_{2,n',k}\}$, and PS ratio at each user $\boldsymbol{\rho} = \{\rho_{\ell}\}$, where $n = 1, 2, \ldots, N$, $n' = 1, 2, \ldots, N$, $k = 1, 2, \ldots, K$, and $\ell = 1, 2, \ldots, L$. We assume that a central controller has access to channel state information (CSI) and rate/energy demands to solve such an optimization problem and informs the concerned nodes about the resulting allocation through a separate channel and appropriate signaling. Mathematically, the overall optimization problem can be represented as

$$(P1): \max_{\{\mathbf{P},\mathbf{A},\mathbf{\Phi},\mathbf{S},\boldsymbol{\rho}\}} \sum_{\ell=1}^{L} R_\ell \tag{3.14}$$

$$\text{subject to}: \quad (C1): E_\ell \geq \xi_\ell,\ \ell = 1,\ldots,L, \tag{3.15}$$

$$(C2): \sum_{\ell=1}^{L} a_{n,\ell} = 1,\ n = 1,\ldots,N, \tag{3.16}$$

$$(C3): \sum_{n=1}^{N} \phi_{(n,n')} = 1,\ n' = 1,\ldots,N, \tag{3.17}$$

$$(C4): \sum_{n'=1}^{N} \phi_{(n,n')} = 1,\ n = 1,\ldots,N, \tag{3.18}$$

$$(C5): \sum_{k=1}^{K} s_{k,\ell} = 1,\ \ell = 1,\ldots,L, \tag{3.19}$$

$$(C6): \sum_{\ell=1}^{L} s_{k,\ell} \leq 1,\ k = 1,\ldots,K, \tag{3.20}$$

$$(C7): \sum_{n=1}^{N} p_{1,n} \leq P_S, \tag{3.21}$$

$$(C8): \sum_{n'=1}^{N}\sum_{\ell=1}^{L}\sum_{n=1}^{N} s_{k,\ell} a_{n,\ell} \phi_{(n,n')} p_{2,n',k} \leq P_{\mathcal{R},k},\ k = 1,\ldots,K, \tag{3.22}$$

$$(C9): 0 \leq \rho_\ell \leq 1,\ \ell = 1,\ldots,L, \tag{3.23}$$

where E_ℓ is the harvested energy via linear or non-linear energy harvester (for further analysis, we assume $E_\ell = \mathcal{E}_\ell^{\mathcal{N}}$, unless specified otherwise), (3.21) and (3.22) represents the source power constraint and the relay power constraint, respectively. It is clear that $(P1)$ is a non-linear mixed integer programming problem involving computation of the optimal solutions $\{\mathbf{P}^*, \mathbf{A}^*, \mathbf{\Phi}^*, \mathbf{S}^*, \boldsymbol{\rho}^*\}$ with the total of $(K \cdot L)^{N!}$ possibilities of relay–user coupling, sub-carrier–user assignment, and sub-carrier pairing. These concurrent assignments become extremely complicated as the values of K, L, and N become large. In the following section, we present an asymptotic solution with appreciably lesser time complexity and good performance in comparison to the highly complex exhaustive search technique.

3.4 Proposed Asymptotically Optimal Solution

As mentioned previously, solving for $(K \cdot L)^{N!}$ possibilities of relay–user coupling, sub-carrier–user assignment, and sub-carrier pairing is a complicated process to obtain an optimal solution considering large values of K, L and N. In addition, discrete nature of the binary variables' assignment $(\mathbf{S}, \mathbf{A}, \mathbf{\Phi})$ when coupled with the power and harvested energy constraints, makes the problem very difficult to solve. In order to simplify this tedious computation task, we seek for other methods which does not only provide asymptotically optimal results, but also have far lesser time complexity in comparison to the aforementioned exhaustive search method. As shown in [190], under a certain aspect called the time-sharing condition, the duality gap of a non-convex resource allocation optimization problem is negligible. Furthermore, [190] proves

that the time-sharing condition is satisfied for practical multi-user spectrum optimization problems in multi-carrier systems for sufficiently large number of sub-carriers. From our optimization problem formulation, it is clear that the time-sharing condition is definitely satisfied (for sufficiently large N) and hence the dual method can be applied to obtain an asymptotically optimal solution in this regard. In the following sub-sections, we illustrate using the dual method that $(P1)$ can be solved in three stages with a polynomial time-complexity which is significantly less than its counterpart optimal exhaustive search method. In this vein, we provide an asymptotic technique based on the block-coordinate descent approach for joint optimization of intended variables.

3.4.1 Dual Problem Formulation

To proceed, we define $\bar{\mathcal{D}}$ as the set of all possible relay–user coupling $\mathbf{S} = \{s_{k,\ell}\}$, sub-carrier–user assignment $\mathbf{A} = \{a_{n,\ell}\}$, sub-carrier pairing $\mathbf{\Phi} = \{\phi_{(n,n')}\}$, the PS ratio $\boldsymbol{\rho} = \{\rho_\ell\}$, all satisfying (3.16), [(3.17), (3.18)], [(3.19), (3.20)], and [(3.15), (3.23)], respectively. We also define $\mathcal{P}(\mathbf{A}, \mathbf{\Phi}, \mathbf{S}, \boldsymbol{\rho})$ as the set of all power allocations $\mathbf{P} = \{p_{1,n}, p_{2,n',k}\}$ for given relay–user coupling, sub-carrier–user assignment, sub-carrier pairing, and PS ratio $(\mathbf{S}, \mathbf{A}, \mathbf{\Phi}, \boldsymbol{\rho})$ that satisfy $p_{1,n} \geq 0$, $p_{2,n',k} \geq 0$ for $s_{k,\ell}a_{n,\ell}\phi_{(n,n')} = 1$ and $\rho_\ell \in \bar{\mathcal{D}}$, and $p_{1,n} = p_{2,n',k} = 0$ for $s_{k,\ell}a_{n,\ell}\phi_{(n,n')} = 0$ and $\rho_\ell \in \bar{\mathcal{D}}$. Then, the Lagrange dual function of problem $(P1)$ can be written as

$$g(\mathbf{\Lambda}) \triangleq \max_{\substack{\mathbf{P}\in\mathcal{P}(\mathbf{A},\mathbf{\Phi},\mathbf{S},\boldsymbol{\rho}) \\ \{\mathbf{A},\mathbf{\Phi},\mathbf{S},\boldsymbol{\rho}\}\in\bar{\mathcal{D}}}} \mathcal{L}(\mathbf{P}, \mathbf{A}, \mathbf{\Phi}, \mathbf{S}, \boldsymbol{\rho}; \mathbf{\Lambda}) \tag{3.24}$$

where the Lagrangian is expressed as

$$\mathcal{L}(\mathbf{P}, \mathbf{A}, \mathbf{\Phi}, \mathbf{S}, \boldsymbol{\rho}; \mathbf{\Lambda}) = \sum_{\ell=1}^{L} R_\ell + \lambda_S\Big(P_S - \sum_{n=1}^{N} p_{1,n}\Big) + \sum_{k=1}^{K} \lambda_{R,k}\Big(P_{R,k} - \sum_{n'=1}^{N} p_{2,n',k}\Big), \tag{3.25}$$

with $\mathbf{\Lambda} = (\lambda_S, \lambda_{R,1}, \ldots, \lambda_{R,K}) \geq 0$ denoting the vectors of the dual variables associated with the individual power constraints. Hence, the dual optimization problem is

$$(P2): \min_{\mathbf{\Lambda}} \quad g(\mathbf{\Lambda}) \tag{3.26}$$

$$\text{subject to}: \quad \mathbf{\Lambda} \geq 0. \tag{3.27}$$

Since it is explicit that a dual function is always convex by definition [191], therefore the gradient or subgradient-based methods can be used to minimize $g(\mathbf{\Lambda})$ with guaranteed convergence. Let $\mathbf{P}^*(\mathbf{\Lambda})$ denote the optimal power allocation in (3.24) at dual point $\mathbf{\Lambda} = (\lambda_S, \lambda_{R,1}, \ldots, \lambda_{R,K})$, then the subgradient of $g(\mathbf{\Lambda})$ can be derived as follows

$$\Delta\lambda_S = P_S - \sum_{n=1}^{N} p^*_{1,n}(\mathbf{\Lambda}), \tag{3.28}$$

$$\Delta\lambda_{R,k} = P_{R,k} - \sum_{n'=1}^{N} p^*_{2,n',k}(\mathbf{\Lambda}), k = 1, \ldots, K. \tag{3.29}$$

Denoting $\Delta\mathbf{\Lambda} = (\Delta\lambda_S, \Delta\lambda_{R,1}, \ldots, \Delta\lambda_{R,K})$, the dual variables are updated as: $\mathbf{\Lambda}^{(t+1)} = \mathbf{\Lambda}^{(t)} + \epsilon^{(t)}\Delta\mathbf{\Lambda}$. Using the step size $\epsilon^{(t)}$ following the diminishing step size policy, the subgradient method above is guaranteed to converge to the optimal dual variables $\mathbf{\Lambda}^*$. Such an update method is of polynomial computational complexity in the number of dual variables $K + 1$.

$$p^*_{2,n',k} = \begin{cases} \left[\left(\frac{1}{c_{(n,n'),k,\ell}(1-\rho_\ell)x_1x_2}\right)\left(\frac{(1-\rho_\ell)^2x_1x_2^2-2\lambda_S(c_{(n,n'),k,\ell}x_1+(1-\rho_\ell)x_2)^2}{2\lambda_S(c_{(n,n'),k,\ell}x_1+(1-\rho_\ell)x_2)}\right)\right]^+, \\ \qquad \text{if } \ (1-\rho_\ell)^2x_1x_2^2 > 2\lambda_S(c_{(n,n'),k,\ell}x_1+(1-\rho_\ell)x_2)^2, \\ 0, \qquad \text{if } \ (1-\rho_\ell)^2x_1x_2^2 \le 2\lambda_S(c_{(n,n'),k,\ell}x_1+(1-\rho_\ell)x_2)^2. \end{cases} \tag{3.36}$$

$$c_{(n,n'),k,\ell} = \sqrt{\frac{\lambda_{R,k}(1-\rho_\ell)x_2}{\lambda_S x_1}}. \tag{3.37}$$

3.4.2 Optimizing Primal Variables at a Given Dual Point

Computation of the dual function $g(\mathbf{\Lambda})$ involves determining the optimal $\{\mathbf{P}^*, \mathbf{A}^*, \mathbf{\Phi}^*, \mathbf{S}^*, \boldsymbol{\rho}^*\}$ at the given dual point $\mathbf{\Lambda}$. In the following, we present the detailed derivation of the optimal primal variables in three phases. Before that, let us rewrite $g(\mathbf{\Lambda})$ in (3.24) as follows

$$g(\mathbf{\Lambda}) = \max_{\substack{\mathbf{P}\in\mathcal{P}(\mathbf{A},\mathbf{\Phi},\mathbf{S},\boldsymbol{\rho}) \\ \{\mathbf{A},\mathbf{\Phi},\mathbf{S},\boldsymbol{\rho}\}\in\mathcal{D}}} \sum_{\ell=1}^{L}\sum_{k=1}^{K}\sum_{n=1}^{N}\sum_{n'=1}^{N} \mathcal{L}_{(n,n'),k,\ell} + \lambda_S P_S + \sum_{k=1}^{K}\lambda_{R,k}P_{R,k}, \tag{3.30}$$

where

$$\mathcal{L}_{(n,n'),k,\ell} \triangleq R_\ell - \lambda_S p_{1,n} - \lambda_{R,k}p_{2,n',k}. \tag{3.31}$$

Optimal Power Allocation for Given Relay–User Coupling, Sub-carrier–User Assignment, Sub-carrier Pairing, and PS Ratio

Here we analyze the optimal power allocation $\mathbf{P}^*$ for given relay–user coupling ($\mathbf{S}$), sub-carrier–user assignment ($\mathbf{A}$), sub-carrier pairing ($\mathbf{\Phi}$), and the PS ratio ($\boldsymbol{\rho}$). Suppose that a sub-carrier pair (n, n') is valid and assigned to the user ℓ, k-th relay assigned to the user ℓ in a frame of transmission time, i.e., $s_{k,\ell}a_{n,\ell}\phi_{(n,n')} = 1$. The optimal power allocation over this sub-carrier pair – relay – user unit $\Big((n,n'),k,\ell\Big)$ can be determined by solving the following problem

$$(P3): \max_{\{p_{1,n},p_{2,n',k}\}} \quad \mathcal{L}_{(n,n'),k,\ell} \tag{3.32}$$

$$\text{subject to}: \quad p_{1,n} \ge 0, \tag{3.33}$$

$$p_{2,n',k} \ge 0. \tag{3.34}$$

It can be easily shown that $\mathcal{L}_{(n,n'),k,\ell}$ is a concave function of $(p_{1,n}, p_{2,n',k})$. Applying the KKT conditions [191], we obtain the optimal power allocation

$$p^*_{1,n} = \begin{cases} c_{(n,n'),k,\ell}p^*_{2,n',k}, & \text{if } \ p^*_{2,n',k} > 0, \\ \left(\frac{1}{\lambda_S} - \frac{1}{x_1}\right)^+, & \text{if } \ p^*_{2,n',k} = 0, \end{cases} \tag{3.35}$$

and $p_{2,n',k}$ is given in (3.36) at the top of this page, where $c_{(n,n'),k,\ell}$ is given in (3.37) with $x_1 = \frac{|h_{1,n,k}|^2}{\sigma_k^2}$, $x_2 = \frac{|h_{2,n',k,\ell}|^2}{\sigma_{d_\ell}^2}$ and $(\chi)^+ = \max(0, \chi)$.

It is indicated from (3.35) and (3.36) that for this particular path $\Big((n,n'),k,\ell\Big)$, if $(1-\rho_\ell)^2x_1x_2^2 \le 2\lambda_S(c_{(n,n'),k,\ell}x_1 + (1-\rho_\ell)x_2)^2$, no power is assigned in the second hop. The

$$g(\mathbf{\Lambda}) = \max_{\{\mathbf{A},\mathbf{\Phi},\mathbf{S},\boldsymbol{\rho}\}\in\bar{\mathcal{D}}} \sum_{i=1}^{L}\sum_{k=1}^{K}\sum_{n=1}^{N}\sum_{n'=1}^{N} a_{n,i}\phi_{(n,n')}s_{k,i}\mathcal{J}_{(n,n'),k,i}(\mathbf{\Lambda}) + \lambda_S P_S + \sum_{k=1}^{K}\lambda_{R,k}P_{R,k}. \quad (3.38)$$

$$\mathcal{J}_{(n,n'),k,i}(\mathbf{\Lambda}) \triangleq \frac{1}{2}\sum_{\ell=1}^{L}\ln\left(1+\frac{(1-\rho_\ell)^2x_1x_2^2 - 2\lambda_S(c_{(n,n'),k,\ell}x_1+(1-\rho_\ell)x_2)^2}{2\lambda_S\Big(c_{(n,n'),k,\ell}x_1+(1-\rho_\ell)x_2\Big)^2}\right) - \Big(c_{(n,n'),k,\ell}\lambda_S + \lambda_{R,k}\Big)\cdot\left(\frac{1}{c_{(n,n'),k,\ell}(1-\rho_\ell)x_1x_2}\right)\left(\frac{(1-\rho_\ell)^2x_1x_2^2 - 2\lambda_S(c_{(n,n'),k,\ell}x_1+(1-\rho_\ell)x_2)^2}{2\lambda_S\Big(c_{(n,n'),k,\ell}x_1+(1-\rho_\ell)x_2\Big)}\right). \quad (3.39)$$

inequality above can be further simplified and expressed as $f_1(\lambda_S) \leq f_2(\lambda_{R,k})$, where $f_1(\cdot)$ and $f_2(\cdot)$ are functions of λ_S and $\lambda_{R,k}$, respectively, with corresponding simplified expressions. From an economic outlook, the dual variables λ_S and $\lambda_{R,k}$ can be elucidated as the power prices at the source and k-th relay, respectively. After re-arranging the dual variables, the aforementioned inequality can be further re-written as $f_2^{-1}(\lambda_{R,k}) \leq f_1^{-1}(\lambda_S)$. Correspondingly, $f_1^{-1}(\lambda_S)$ can be viewed as the SNR gain at the user conceived by the source via the indirect link per cost metric, and $f_2^{-1}(\lambda_{R,k})$ the gain of SNR at the user created by the k-th relay per cost metric. In order to maximize the SNR gain at the user for a given tight comprehensive fee on the transmit power, it can be interpreted that all of the payment should be given to the source if $f_2^{-1}(\lambda_{R,k}) \leq f_1^{-1}(\lambda_S)$ or $f_1(\lambda_S) \leq f_2(\lambda_{R,k})$. Alternatively, if $f_1(\lambda_S) \geq f_2(\lambda_{R,k})$, then non-zero power allocation should be made at the source and k-th relay using the connecting parameter $c_{(n,n'),k,\ell}$ in (3.35).

Optimization of Relay–User Coupling, Sub-carrier–User Assignment, and Sub-carrier Pairing

Substituting the optimal power allocation expression (3.35) and (3.36) in (3.31) to eliminate the power variables and then into (3.30), we can obtain an alternative expression of the dual function as defined in (3.38) at the top of this page.

Here, the function $\mathcal{J}_{(n,n'),k,\ell}(\mathbf{\Lambda})$ is defined in (3.39) at the top of this page. Based on (3.38), we next determine the relay–user pairing $\mathbf{S}^*$, optimal sub-carrier–user assignment $\mathbf{A}^*$, and the sub-carrier pairing $\mathbf{\Phi}^*$. In this regard, we propose the following methods to obtain suitable solutions.

Suppose (n, n') is a valid sub-carrier pair in the given sub-carrier pairing scheme $\mathbf{\Phi}$, i.e., $\phi_{(n,n')} = 1$. Then, it is obvious that the optimal relay selected for the ℓ-th user corresponding to this sub-carrier pair should be the one having maximum value of $\mathcal{J}_{(n,n'),k,\ell}(\mathbf{\Lambda})$ in (3.39). That is

$$s_{k,\ell}^* = \begin{cases} 1, & k = k(n,n') = \arg\max\limits_{k} \mathcal{J}_{(n,n'),k,\ell}, \\ 0, & \text{otherwise.} \end{cases} \quad (3.40)$$

Similarly, it is obvious that the optimal sub-carrier allocated to the ℓ-th user corresponding to the $s_{k,\ell}^*$ obtained above, and for this sub-carrier pair, should be the one having maximum

value of $\mathcal{J}_{(n,n'),k,\ell}(\mathbf{\Lambda})$ in (3.39). That is

$$a^*_{n,\ell} = \begin{cases} 1, & \ell = \ell(n,n') = \arg\max\limits_{\ell} \mathcal{J}_{(n,n'),k,\ell}, \\ 0, & \text{otherwise.} \end{cases} \tag{3.41}$$

Therefore, the function $\mathcal{J}_{(n,n'),k,\ell}(\mathbf{\Lambda})$ defined in (3.39) serves as the optimal criterion for relay–user coupling as well as sub-carrier–user assignment.

Substituting $\mathbf{S}^*$ and $\mathbf{A}^*$ computed above, into (3.38), we obtain the corresponding dual function

$$g(\mathbf{\Lambda}) = \max_{\{\mathbf{\Phi},\boldsymbol{\rho}\}\in\bar{\mathcal{D}}} \sum_{\ell=1}^{L}\sum_{k=1}^{K}\sum_{n=1}^{N}\sum_{n'=1}^{N} \phi_{(n,n')}\mathcal{J}_{(n,n')} + \lambda_S P_S + \sum_{k=1}^{K}\lambda_{R,k}P_{R,k}, \tag{3.42}$$

where $\mathcal{J}_{(n,n')} \triangleq \mathcal{J}_{(n,n'),k(n,n'),\ell(n,n')}(\mathbf{\Lambda})$. Define $N \times N$ profit matrix $\mathbf{J} = [\mathcal{J}_{(n,n')}]$. In order to maximize the objective in (3.42), we should pick exactly one element in each row and each column of matrix $\mathbf{J}$ such that the sum of profits is as large as possible. Clearly, this is a standard linear assignment problem and can be efficiently solved by the Hungarian method [192], whose complexity is $\mathcal{O}(N^3)$.

Let $\eta(n)$ denote the sub-carrier index in the second hop optimally paired with the sub-carrier n in the first hop, for $n = 1, \ldots, N$. Then, the optimal sub-carrier pairing variables can be expressed as

$$\phi^*_{n,n'} = \begin{cases} 1, & n' = \eta(n), \\ 0, & \text{otherwise.} \end{cases} \tag{3.43}$$

Power Splitting Ratio

In order to optimize the values of $\boldsymbol{\rho}$, we substitute (3.43) in (3.42) and obtain the following dual function

$$g(\mathbf{\Lambda}) = \max_{\{\boldsymbol{\rho}\}\in\bar{\mathcal{D}}} \sum_{\ell=1}^{L}\sum_{k=1}^{K}\sum_{n=1}^{N}\sum_{n'=1}^{N} \mathcal{J}_{(n,n')} + \lambda_S P_S + \sum_{k=1}^{K}\lambda_{R,k}P_{R,k}. \tag{3.44}$$

It is clear that $\mathcal{J}_{(n,n')}$ is a decreasing function of $\boldsymbol{\rho}$. Therefore, the equality in (3.15) must hold. This yields the following solution

$$\rho^*_{\ell} = \frac{\xi_\ell}{\sum_{\forall k}\sum_{\forall n'}\sum_{\forall n}\frac{\mathcal{E}'}{1-\varkappa}\cdot\left(\frac{1}{1+\exp(-\alpha p^*_{2,n',k}|h_{2,n',k,\ell}|^2+\alpha\beta)} - \varkappa\right)}. \tag{3.45}$$

Combining the above three phases together, we have obtained the optimal primal variables $\{\mathbf{P}^*, \mathbf{A}^*, \mathbf{\Phi}^*, \mathbf{S}^*, \boldsymbol{\rho}^*\}$ for given dual variables $\mathbf{\Lambda}$. Suppose that the complexity of dual variable updates mentioned in Section IV-A and overall computation for such operation is in the order of $(K \cdot L \cdot N^5)^{\bar{\tau}}$. Then, the computational complexity of solving the dual problem (3.24) using the asymptotic approach is of $\mathcal{O}(N^3 \cdot (K \cdot L \cdot N^5)^{\bar{\tau}})$. This extremely reduced time-complexity implies a significant advantage over the exhaustive search method with immensely high computational complexity involving a span over the whole feasible regime with $(K \cdot L)^{N!}$ possibilities of relay–user coupling, sub-carrier–user assignment, and sub-carrier pairing.

3.4.3 Refinement of Power Allocation and PS Ratio

In this section, we now focus on obtaining the optimal solution for the corresponding primal problem in (3.14) after having acquired the optimal dual point $\mathbf{\Lambda}^*$ using the method as illustrated above. Because of a certain duality gap for fixed N, the optimal $\mathbf{P}^*(\mathbf{\Lambda}^*)$, $\mathbf{S}^*(\mathbf{\Lambda}^*)$, $\mathbf{A}^*(\mathbf{\Lambda}^*)$, $\mathbf{\Phi}^*(\mathbf{\Lambda}^*)$, and $\boldsymbol{\rho}^*(\mathbf{\Lambda}^*)$ may not completely lie within the feasibility set. Therefore to address this concern, we initially attain the solution for the relay–user coupling, sub-carrier-relay assignment, sub-carrier pairing and $\{\mathbf{S}^*(\mathbf{\Lambda}^*), \mathbf{A}^*(\mathbf{\Lambda}^*), \mathbf{\Phi}^*(\mathbf{\Lambda}^*)\}$, by applying the methods projected in the prior sub-sections. Next, we refine the power allocation $\mathbf{P}$ to meet the power constraints (3.21) and (3.22), and the PS ratio $\boldsymbol{\rho}$ to meet the PS ratio constraint (3.23) of the primal problem. It is also worth mentioning that this technique is asymptotically optimal due to the vanishing duality gap for adequately high values of N.

Let S_k denote the set of active sub-carrier pairs $(n, \eta(n))$ assigned on relay k for user ℓ. By substituting the value of $\{\mathbf{S}^*(\Lambda^*), \mathbf{A}^*(\Lambda^*), \mathbf{\Phi}^*(\Lambda^*)\}$ into (3.14), the power refinement problem can be equivalent to the following power allocation problem, which is convex

$$
\begin{aligned}
(P4): \max \ & \sum_{\ell=1}^{L} \hat{R}_\ell && (3.46)\\
\text{subject to}: \ & (C1): E_\ell \geq \xi_\ell, \ \ell = 1, \ldots, L, && (3.47)\\
& (C2): \sum_{(n,\eta(n))\in S_k} p_{1,n} \leq P_S, \ k = 1, \ldots, K, && (3.48)\\
& (C3): \sum_{(n,\eta(n))\in S_k} p_{2,n',k} \leq P_{\mathcal{R},k}, \ \forall k \text{ with } S_k \neq \emptyset, && (3.49)\\
& (C4): 0 \leq \rho_\ell \leq 1, \ \ell = 1, \ldots, L, && (3.50)
\end{aligned}
$$

where

$$
\hat{R}_\ell \triangleq \frac{1}{2} \sum_{i=1}^{L} \sum_{k=1}^{K} \sum_{(n,\eta(n))\in S_k} \ln\Big(1 + \tilde{\Upsilon}_{n,\eta(n),k,i}\Big), \tag{3.51}
$$

with $\tilde{\Upsilon}_{n,\eta(n),k,i} = \frac{(1-\rho_i)x_{1,n}p_{1,n}x_{2,\eta(n),k}p_{2,\eta(n),k}}{x_{1,n}p_{1,n}+(1-\rho_i)x_{2,\eta(n),k}p_{2,\eta(n),k}}$, $x_{1,n} = \frac{|h_{1,n,k}|^2}{\sigma_k^2}$ and $x_{2,\eta(n),k} = \frac{|h_{2,\eta(n),k,\ell}|^2}{\sigma_{d_\ell}^2}$.

Define $\bar{\mathcal{D}}$ as the set of all non-negative $\{p_{1,n}\}$, $\{p_{2,\eta(n),k}\}$ and ρ_ℓ. The Lagrangian of $(P4)$ over $\bar{\mathcal{D}}$ is

$$
\begin{aligned}
\mathcal{H}(\mathbf{P}, \boldsymbol{\rho}; \boldsymbol{\mu}) = \sum_{\ell=1}^{L} \hat{R}_\ell + \mu_S\Big(P_S - \sum_{(n,\eta(n))\in S_k} p_{1,n}\Big) \\
+ \sum_{k=1}^{K} \mu_{R,k}\Big(P_{R,k} - \sum_{(n,\eta(n))\in S_k} p_{2,\eta(n),k}\Big), \quad (3.52)
\end{aligned}
$$

with $\boldsymbol{\mu} = (\mu_S, \mu_{R,1}, \ldots, \mu_{R,K}) \geq 0$ being the vectors of the dual variables associated with the individual power constraints. Then, the dual function is

$$
g(\boldsymbol{\mu}) \triangleq \max_{\{\mathbf{P},\boldsymbol{\rho}\}\in\bar{\mathcal{D}}} \mathcal{H}(\mathbf{P}, \boldsymbol{\rho}; \boldsymbol{\mu}). \tag{3.53}
$$

Next, we intend to perform the power allocation and PS ratio refinements using the previously computed values of relay–user coupling, sub-carrier–user assignment, and optimal sub-carrier pairing. In the following sub-sections, we present the methods for the refinement of the power allocation and the corresponding PS ratio.

$$p^*_{2,\eta(n),k} = \begin{cases} \left[\left(\frac{1}{c_{(n,\eta(n)),k,\ell}(1-\rho_\ell)x_{1,n}x_{2,\eta(n),k}}\right)\right. \\ \left.\left(\frac{(1-\rho_\ell)^2x_{1,n}x^2_{2,\eta(n),k}-2\mu_S(c_{(n,\eta(n)),k,\ell}x_{1,n}+(1-\rho_\ell)x_{2,\eta(n),k})^2}{2\mu_S(c_{(n,\eta(n)),k,\ell}x_{1,n}+(1-\rho_\ell)x_{2,\eta(n),k})}\right)\right]^+, \\ \qquad \text{if } \ (1-\rho_\ell)^2x_{1,n}x^2_{2,\eta(n),k} > 2\mu_S(c_{(n,\eta(n)),k,\ell}x_{1,n}+(1-\rho_\ell)x_{2,\eta(n),k})^2, \\ 0, \qquad \text{if } \ (1-\rho_\ell)^2x_{1,n}x^2_{2,\eta(n),k} \leq 2\mu_S(c_{(n,\eta(n)),k,\ell}x_{1,n}+(1-\rho_\ell)x_{2,\eta(n),k})^2. \end{cases} \tag{3.55}$$

$$c_{(n,\eta(n)),k,\ell} = \sqrt{\frac{\mu_{R,k}(1-\rho_\ell)x_{2,\eta(n),k}}{\mu_S x_{1,n}}}. \tag{3.56}$$

Optimal Power Allocation for a given PS Ratio

Assuming a given PS ratio $\boldsymbol{\rho} \in \bar{\mathcal{D}}$ is valid. Then, employing the KKT conditions to compute the dual function at given dual point, it can be readily seen that the optimal power allocation follows the same expression as in (3.35) and (3.36). We rewrite them as follows for ease of presentation

$$p^*_{1,n} = \begin{cases} c_{(n,\eta(n)),k,\ell}p^*_{2,\eta(n),k}, & \text{if } \ p^*_{2,\eta(n),k} > 0, \\ \left(\frac{1}{\mu_S} - \frac{1}{x_{1,n}}\right)^+, & \text{if } \ p^*_{2,\eta(n),k} = 0, \end{cases} \tag{3.54}$$

where $p^*_{2,\eta(n),k}$ and $c_{(n,\eta(n)),k,\ell}$ are shown at the top of next page. The Lagrange multipliers μ_S and $\mu_{R,k}$ can be updated using the sub-gradient method and are chosen so as to satisfy the individual power constraints in (3.48) and (3.49) respectively.

Optimal PS Ratio

Substituting (3.55) in (3.47) and assuming that equality holds at the optimal point, we obtain the following

$$\rho^*_\ell = \frac{\xi_\ell}{\sum \frac{\mathcal{E}'}{1-\varkappa} \cdot \left(\frac{1}{1+\exp(-\alpha p^*_{2,\eta(n),k}|h_{2,\eta(n),k,\ell}|^2+\alpha\beta)} - \varkappa\right)}, \tag{3.57}$$

where $(n, \eta(n)) \in S_k$, $k = 1, 2, \ldots, K$, and $\ell = 1, 2, \ldots, L$.

The Lagrange multipliers in $\boldsymbol{\mu}$ are chosen to meet the power and PS ratio constraints in (3.47), (3.48), (3.49) and (3.50), and can be updated by the subgradient method. It can be easily observed that the computational complexity of the power refinement process is far more smaller than that of solving the dual problem. Thus, the overall complexity of our asymptotic solution is $\mathcal{O}(N^3(K \cdot L \cdot N^5)^{\bar{\tau}})$.

3.5 Proposed Heuristic Solution

In this section, we propose a sub-optimal low-complexity technique to solve the problem in $(P1)$. Intuitively, the major factor impacting the system performance is the decision on the appropriate selection of the intended variables $\mathbf{S}$, $\mathbf{A}$, and $\mathbf{\Phi}$. In the proposed asymptotic solution, computation of $\mathbf{S}$ and $\mathbf{A}$ follows a disjoint type of mechanism, which imposes some extra time-complexity. In this context, we provide a heuristic solution based on joint sequential assignment of the relay and sub-carrier pair that maximizes the equivalent $\mathcal{J}_{(n,n'),k,\ell}(\mathbf{\Lambda})$

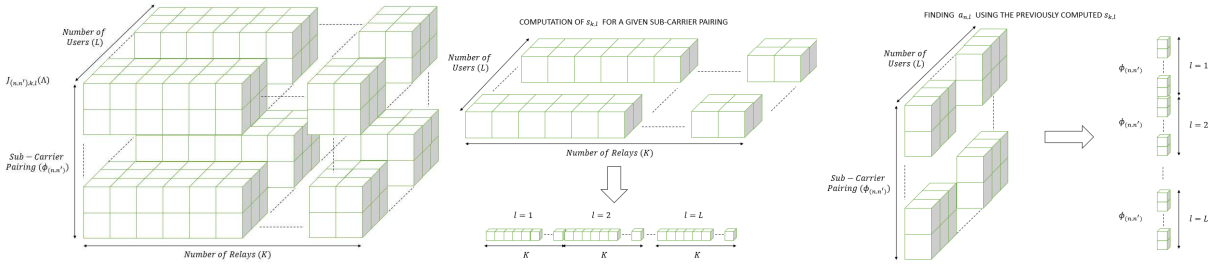

(a) (b) (c)

FIGURE 3.3: (a) 3-D visualization of the $\mathcal{J}_{(n,n'),k,\ell}(\mathbf{\Lambda})$ matrix, (b) Visualization of Algorithm 1 depicting the steps involved in computation of $s_{k,\ell}$ for a given $\phi_{(n,n')}$, and (c) Visualization of Algorithm 2 depicting the steps involved in computation of $a_{n,\ell}$ using the $s_{k,\ell}$ computed previously in (b).

metric in (3.39) to further reduce the time-complexity. The process for realizing this method is same as in the previous section, except for the step 3.4.2).

To perform this task, two dependent algorithms are designed, as depicted at the bottom of this page (Algorithm 1) and top of next page (Algorithm 2). Note that Algorithm 1 returns the relay assignment variable $\mathbf{S}$ but an incomplete version of the carrier related variables $\mathbf{\Phi}$ and $\mathbf{A}$, since only the sub-carrier pairs associated with the assigned relays have been determined. In order to fully determine the sub-carrier pairs and assign them to the corresponding user, we propose a similar approach where the remaining values of $\{\mathcal{J}_{(n,n'),k,\ell}\}$ are sequentially maximized, taking into account the previous relay selection. The carrier refinement algorithm is summarized in Algorithm 2. To facilitate better understanding, visualizations of $\mathcal{J}_{(n,n'),k,\ell}(\mathbf{\Lambda})$ metric, and the in-between procedures corresponding to both the algorithms is depicted in Fig. 3.3, placed at the top of this page. Finally, the power refinement and computation of optimal PS ratios are performed by using the method as in Section 3.4.3.

Algorithm 1 Relay and carrier assignment algorithm

1: **Require**:
- Number of users/destinations: L
- Number of relays: K
- Number of sub-carriers: N
- Function: $\mathcal{J}_{(n,n'),k,\ell}(\mathbf{\Lambda})$

2: **Initialize:** Iteration counter: $t = 1$
3: **while** t $\neq$ L **do**
4: Find the relay, user and sub-carrier pair that maximizes the equivalent $\mathcal{J}_{(n,n'),k,\ell}(\mathbf{\Lambda})$ metric of the remaining un-assign possibilities,

$$\{(n^*, n'^*), k^*, \ell^*\} = \max\{\mathcal{J}_{(n,n'),k,\ell}(\mathbf{\Lambda})\} \tag{3.58}$$

5: Assign $\phi_{(n^*,n'^*)} = 1$, $s_{k^*,\ell^*} = 1$ and $a_{n^*,\ell^*} = 1$.
6: $t = t + 1$.
7: **end while**
8: **Return:** Variables: $\mathbf{\Phi}, \mathbf{S}, \mathbf{A}$.

Algorithm 2 Carrier assignment refinement algorithm

1: **Require**:
- Number of users/destinations: L
- Number of relays: K
- Number of sub-carriers: N
- Function: $\mathcal{J}_{(n,n'),k,\ell}(\mathbf{\Lambda})$
- Relay selection: $\mathbf{S}$

2: **Initialize:** Iteration counter: $t = L + 1$
3: **while** t $\neq$ N **do**
4: Find the sub-carrier pair and user that maximizes the equivalent channel gain of the remaining un-assign possibilities,

$$\{(n^*, n'^*), \ell^*\} = \max\{\mathcal{J}_{(n,n'),k,\ell}(\mathbf{\Lambda})\} \tag{3.59}$$

5: Assign $\phi_{(n^*,n'^*)} = 1$ and $a_{n^*,\ell^*} = 1$.
6: $t = t + 1$.
7: **end while**
8: **Return:** Variables: $\mathbf{\Phi}, \mathbf{A}$.

Suppose that the complexity of dual variable updates required and overall computation for such operation to perform the above mentioned task is in the order of $(K \cdot L \cdot N^2)^{\bar{\tau}}$. Then, the proposed heuristic method provides a remarkable computational time-complexity advantage of $\mathcal{O}(N^3 \cdot (K \cdot L \cdot N^2)^{\bar{\tau}})$ over the BF approach with the order of $(K \cdot L)^{N!}$, significantly better than that of the proposed asymptotic approach with $\mathcal{O}(N^3 \cdot (K \cdot L \cdot N^5)^{\bar{\tau}})$.

3.6 Simulation Results

In this section, we present some simulation results to evaluate the performance of the proposed resource allocation and relay selection strategy. The simulations are performed for different parameter values to analyze the efficiency of proposed methods. For simplicity, we assume that the source and all the relays are subjected to the same power constraint i.e., $P_S = P_{R,1} = P_{R,2} = \ldots = P_{R,K}$, and the harvested energy demand at each user is assumed to be same i.e, $\xi_1 = \xi_2 = \ldots = \xi_\ell = \xi$ throughout this chapter.

We consider the node distribution as shown in Fig. 3.4, where a source is placed at a fixed point $(0, 5)$ m, the K relay nodes are placed randomly within a 4 m^2 region inside the coordinates (4,4) and (6,6) between the source and the users' area. The users are placed randomly as well within a 4×10 m^2 area between the coordinates (6,0) and (10,10). For our analysis, we generate several random combinations of relay and user placements from the source, within these specified room dimensions. The ITU Radiocommunication Sector (ITU-R) P.1238 [193] channel model is employed with the central frequency assumption at 1.9 GHz to emulate a wireless broadband network. We consider frequency-selective channel model, with 5-multipath arrivals averaged according to the Poisson process and the root mean square (rms) delay is set to 36.3078 ns as per the aforementioned room dimensions. During the first hop transmission from the source to relays, and the second hop transmission from the selected relays to the intended users, the path-loss model (with shadowing) is adopted for each multipath signal according to the corresponding parameters provided in [193]. The signal fading from the source to the relays and from relays to the users follow the Ricean

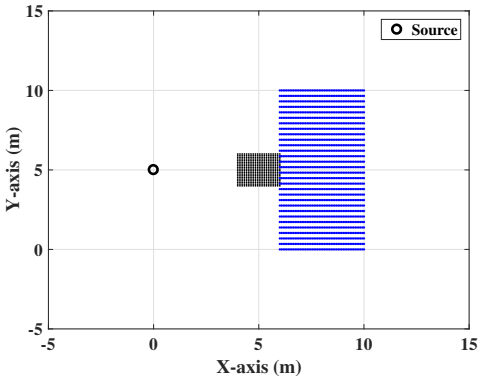

FIGURE 3.4: The simulation scenario comprises of room with dimension of 10×10 m^2 which includes a source placed at (0,5) m, pool of relays within the region (4,4) m and (6,6) m, and users placed inside (6,0) m and (10,10) m.

distribution with K-factor of 3.5. All the OFDM sub-carriers are assumed to experience a flat-fading and the total bandwidth is fixed to 20 MHz. The noise power at the relay and user nodes is assumed the same and equal to -110 dBW. Concerning the non-linear EH model, the constants $\mathcal{E}'$, α, and β are chosen to be $\mathcal{E}' = \mathrm{E_{Max}}$ where $\mathrm{E_{Max}}$ is the maximum harvested energy at which the EH circuit is saturated (calculated individually for each user), $\alpha = 1500$, and $\beta = 0.0022$, respectively [59, 60].

As a benchmark, the performance of a semi-random resource allocation and relay selection approach is also presented. This baseline approach operates as follows: (i) Choose any valid combination of $\mathbf{S}$, $\mathbf{A}$, and $\mathbf{\Phi}$ that satisfy (3.16), [(3.17), (3.18)], and [(3.19), (3.20)], respectively. (ii) Perform the OFDMA sub-carrier power allocation using the conventional WF approach [194]. (iii) Compute the PS ratios at all the user nodes and correspondingly the sum-rate of the system. However, the time-complexity of this method is very fast, but using this kind of hit-and-trial approach has the probability of getting the optimal choice as $1/(K \cdot L)^{N!}$. Therefore, this method is considered to provide a sub-optimal solution unless the hit-and-trial method coincides with optimal selection. To this end, it should be noted that due to unavailability of prior work in such a scenario, we use the semi-random scheme and the exhaustive search approach as the benchmarks to analyze the outcomes of the proposed algorithms.

Fig. 3.5 depicts the effect on sum-rate of all users with increasing harvested energy demands for the proposed solutions. We set $K = 3$, $L = 2$, $N = 6$ and $P_S = P_{R,1} = P_{R,2} = P_{R,3} = 0.1$ W. The results are evaluated and averaged over 100 Monte-Carlo random channel conditions for both the hops. A comparison of the proposed asymptotic and heuristic methods is depicted. For comparison purposes, we illustrate the exhaustive search solution as well. Due to computational limitations, the exhaustive search method is difficult to realize for higher values of N (specifically for $N \geq 6$). It is found that the proposed asymptotically optimal method performs better at lower harvested energy demands with narrower duality gap in comparison to the optimal exhaustive search method. However, this gap widens with growing demands of harvested energy because the proposed algorithm involves joint computations of $\mathbf{S}$, $\mathbf{A}$, and $\mathbf{\Phi}$ and due to the mixed-integer non-linear structure of this problem, the optimization task becomes cumbersome which reduces the optimality by some margin. Moreover, from the analysis presented in [190], it is clear that the time-sharing condition is not satisfied in case of Asymptotic method at lower N values. This leads to an increasing duality gap between the solutions of primal and dual problems. On the other

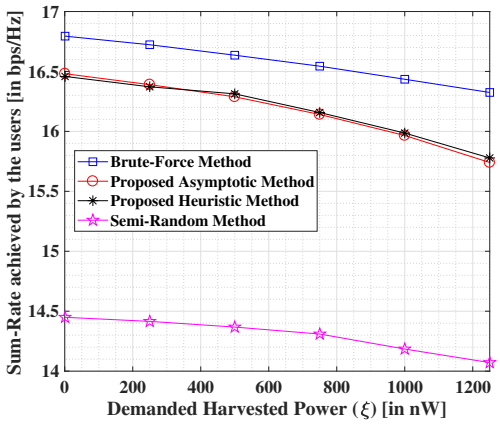

FIGURE 3.5: Sum-rate achieved by the system versus different harvested energy demands for comparison of the algorithms with $P_S = P_{R,1} = P_{R,2} = P_{R,3} = 0.1$ W, $K = 3$, $L = 2$, and $N = 6$ for 50 Monte-Carlo random channels.

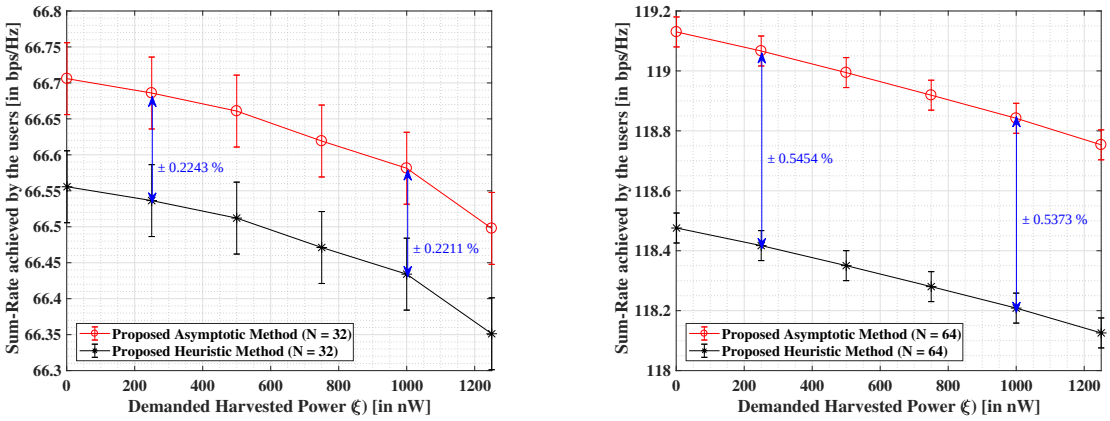

(a) (b)

FIGURE 3.6: Sum-rate achieved by the system versus different harvested energy demands for (a) $N = 32$ and (b) $N = 64$, for 50 Monte-Carlo random channel conditions for both the hops, respectively.

hand, it is found that the heuristic method performs better than the proposed asymptotic method for higher harvested energy demands at lower N values. However, we cannot claim its asymptotic optimality from the outcomes herein due to sub-optimal results. Higher N values are analyzed in subsequent figures, showing the asymptotic behavior of the proposed method.

We set $K = 10$, $L = 8$, and $P_S = P_{R,1} = \ldots = P_{R,10} = 0.5$ W in Fig. 3.6(a) with $N = 32$, and in Fig. 3.6(b) with $N = 64$. We observe that the proposed techniques improve the system performance with the increasing values of N. These results are evaluated and averaged over 50 Monte-Carlo random channel conditions for both the hops, respectively. Due to high time complexity of the exhaustive search case for higher parameter values, we have demonstrated the results using the proposed asymptotic, and heuristic methods only; to prove that the system performance improves considerably for higher values of N. Note that a ± 5 % tolerance limit is set for the error bars indicated in both 3.6(a) and 3.6(b). It is found that for $N = 32$, the asymptotic solution performs approximately 0.22% better than the

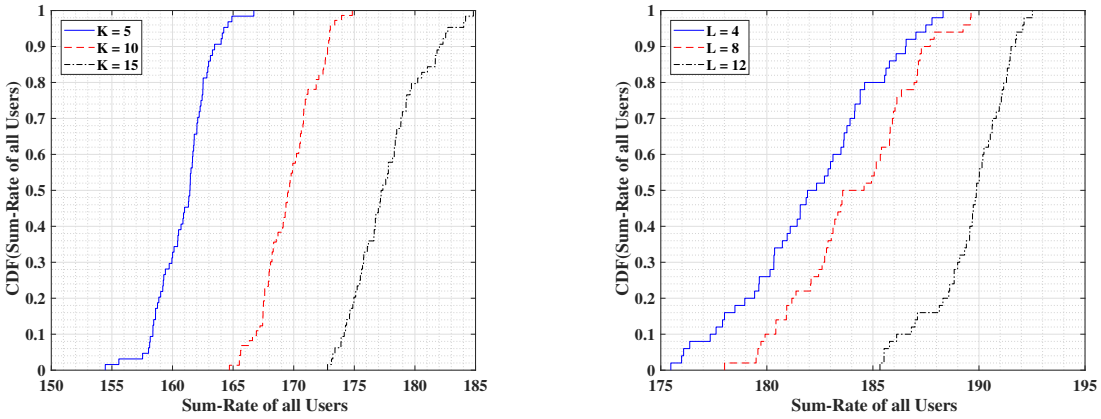

(a) (b)

FIGURE 3.7: (a) CDF plot of sum-rate of the system for different values of K with $L = 4$, $N = 64$ and (b) CDF plot of sum-rate of the system for different values of L with $K = 15$, $N = 64$.

EH Demand / Method	1 nW	50 nW	100 nW	150 nW	200 nW
Direct link only	49.1369	11.6324	2.8345	1.3219	0
Proposed (w/o direct link)	147.1453	147.1448	147.1443	147.1438	147.1433

TABLE 3.1: Sum-Rate (in bps/Hz) comparison of Direct Link only and Asymptotic Methods.

heuristic solution, while for $N = 64$, the asymptotic solution performs approximately 0.54% better than the heuristic solution. Additionally, the improvement in the system performances from $N = 32$ to $N = 64$ for the asymptotic method is of approximately 44% while for the heuristic method, the improvement is approximately 43.8%. From our observation, we find that there is a considerable improvement in the system performance for increasing values of N. Moreover, it is also noteworthy that the results from the proposed asymptotic algorithm are expected to asymptotically converge with the optimal solution, for sufficiently large value of N (ideally as $N \to \infty$) [190], as the time-sharing condition will be satisfied yielding an asymptotically zero duality gap between the corresponding Lagrange dual and primal problems.

Fig. 3.7(a) presents the performance of the proposed asymptotic algorithm in terms of the Cumulative Density Function (CDF) of users' sum-rate for different values of K with $L = 4$, $N = 64$ and $P_S = P_{R,1} = P_{R,2} = \ldots = P_{R,K} = 0.5$ W. The results are evaluated and averaged over 75 Monte-Carlo random channel conditions for both the hops. We set $\xi = 2.5$ μW. It is observed that there is a subtle increase in the sum-rate of the system by increasing the number of relays. Intuitively, more relay options provide an additional advantage due to better relay placements which may in-turn improve the system performance significantly.

Fig. 3.7(b) shows the CDF of the sum-rate of the system for different values of L with $K = 15$, $N = 64$ and $P_S = P_{R,1} = \ldots = P_{R,15} = 0.75$ W. The harvested energy demand is assumed to be $\xi = 5$ μW. The results are evaluated using the proposed asymptotic method and are averaged over 50 Monte-Carlo random channel conditions for both the hops. It is observed that the system performance improves by an appreciable margin when there is an increase in the number of users provided that the network resources are sufficient. However, this gap is expected to reduce as the number of relays approaches the number of users.

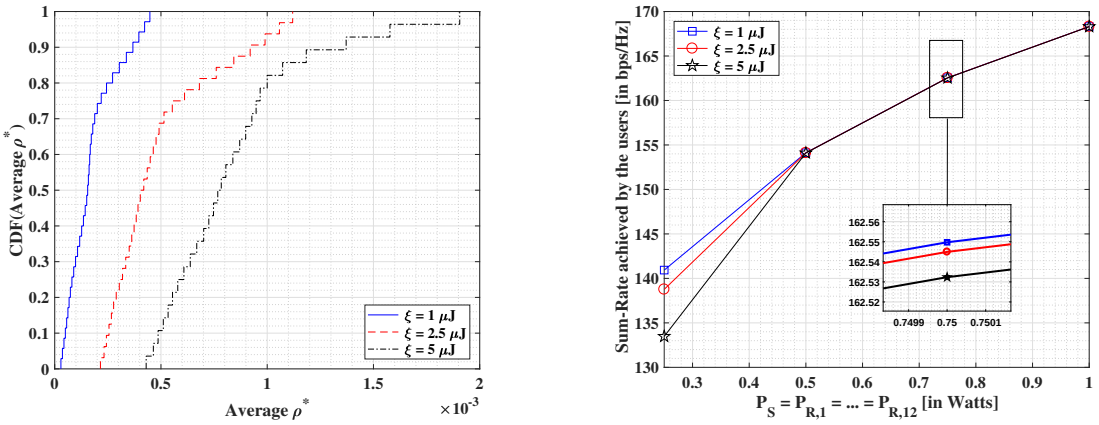

(a) (b)

FIGURE 3.8: (a) CDF plot of the average PS ratio (ρ^*) for different harvested energy demands with $K = 12$, $L = 8$, and $N = 64$ and (b) Sum-rate achieved by the system versus different harvested energy demands with $K = 12$, $L = 10$ and $N = 64$.

Fig. 3.8(a) illustrates the CDF plot of the average PS ratio (ρ^*) for different values of harvested energy demands using the proposed asymptotic algorithm. Here, we set $K = 12$, $L = 8$, $N = 64$ and $P_S = P_{R,1} = \ldots = P_{R,12} = 0.5$ W. The results are evaluated and averaged over 50 Monte-Carlo random channel conditions for both the hops. We observe that ρ^* increases significantly as the harvested energy demand keeps increasing. It is noteworthy that this depiction also accounts for the rate-energy (R-E) trade-off [171] which is well-known in the literature.

Fig. 3.8(b) depicts the plot of the sum-rate of the system against the different transmit power values at the source and relays. The simulations are performed using the proposed asymptotic method for various harvested energy demands. The results are evaluated and averaged over 20 Monte-Carlo random channel conditions for both the hops assuming $K = 12$, $L = 10$, and $N = 64$. It is noted that with increasing values of harvested energy, the sum-rate of the system decreases. However, with the increasing values of the source and relays' transmit powers, the sum-rate of the system increases considerably. This phenomenon is also an evidence of the R-E trade-off, as mentioned before. It is also noteworthy that once the harvested energy demand is fulfilled at the end-user, the sum-rate of the system nearly converge together when the individual transmit powers are sufficiently large.

In Fig. 3.9 we show that for $K = 10$, $L = 8$, $N = 128$, $\zeta = 0.8$ (for linear EH model), and $P_S = P_{R,1} = \ldots = P_{R,10} = 0.5$ W, the characteristic feature of a non-linear energy harvester in comparison to the linear one. It is seen that for increasing values of harvested energy demands, both the linear and non-linear energy harvesting models show a decreasing trend. From Fig. 3.9(a) and Fig. 3.9(b), it is clear that there is a significant impact of shadowing on energy harvesting. Specifically, we observe that there is 21.6% (approximately) difference between the results of the EH models for the cases with and without shadowing, when $\xi = 1$ nW.

Considering $K = 10$, $L = 6$, $N = 64$, and $P_S = P_{R,1} = \ldots = P_{R,10} = 0.5$ W, we show in Table 3.1 that the contribution from the direct link at the end-users is negligible in comparison to the proposed framework with cooperative relaying. For the case with direct link, separate CSIs are generated according to the ITU-R framework (as in the two

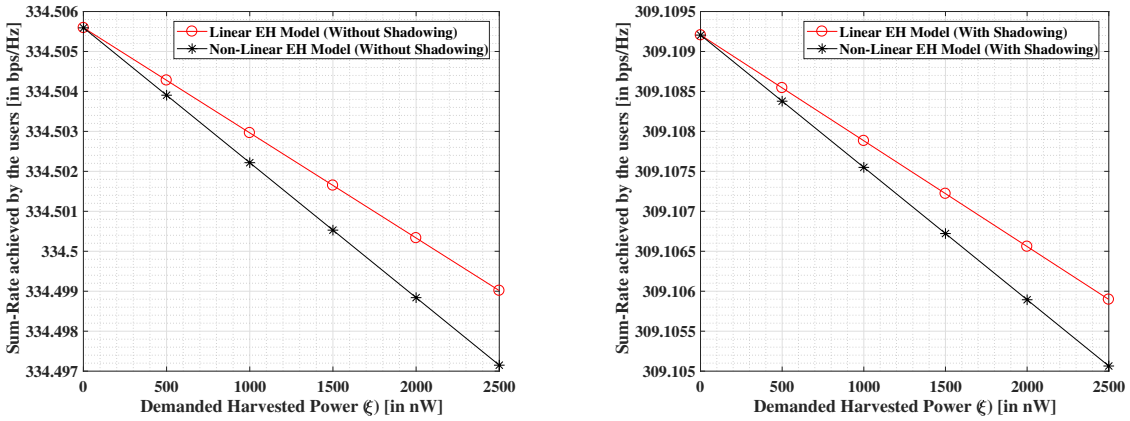

(a) (b)

FIGURE 3.9: Sum-rate achieved by the system versus different harvested energy demands to demonstrate the difference between the performances of Linear and Non-Linear EH models for : (a) Without Shadowing and (b) With Shadowing, with $K = 10$, $L = 8$ and $N = 128$ for 20 Monte-Carlo random channel conditions.

aforementioned hops). Then the sub-carriers are allocated based on maximum channel gain followed by WF technique. The PS ratio at each user is computed in a similar manner as for the proposed technique. Each value in Table 3.1 is computed after averaging over 20 Monte-Carlo experiments. The results prove that the system with only direct active link is incapable of providing sufficient sum-rate at end-users with increasing EH demands.

3.7 Other Contributions in-line with Considered Framework

Considering a similar system model as in this Chapter, several investigations via other interesting problem formulations such as maximization of sum-rate, maximization of sum-harvested energy, and maximization of joint sum-rate and sum-harvested energy (as a novel metric to introduce a pricing metric for SWIPT), were carried out. In this regard, various optimization techniques were used or developed to obtain a suitable (sub-optimal) solution with consideration of a linear EH module at the corresponding user(s). Brief summaries of the related works are provided below.

Relay Selection and Transceiver Design for Joint Wireless Information and Energy Transfer in Cooperative Networks [16]

In this work, we considered SWIPT in a cooperative network where half-duplex relays employing non-regenerative relay protocol assist a source node and a destination node to simultaneously transfer both data and energy to the destination node. It is assumed that the destination node is capable of harvesting energy and decoding information from the same received signal. Optimal selection of a relay as well as optimal allocation of resources is a challenging problem when additional requirement of energy harvesting is taken into account. We addressed the problem of optimal selection of relays and optimal receive processing to maximize the rate and total harvested energy. In this regard, we formulated problems for optimal relay selection and transceiver processing to maximize the rate under a constraint on

minimum harvested energy as well as to maximize the total harvested energy under constraint on minimum rate. Furthermore, this scenario was studied for both TS and PS schemes. We presented closed-form solutions for the proposed transceiver design problems by using the graphical analysis. With the help of simulations, we demonstrated a comparative study between TS and PS schemes for the aforementioned cases. The results show that PS scheme performs better in comparison to TS for same set of conditions.

Relay Selection Strategies for SWIPT-Enabled Cooperative Wireless Systems [17]

We studied a problem of relay selection in a two-hop relaying network where the destination was equipped with Simultaneous Wireless Information and Power Transmission (SWIPT) capabilities. In contrast to conventional cooperative networks, the destination node was considered to be capable of simultaneously decoding information and harvesting energy from both the source and the relay transmissions. In this context, we formulated two optimization problems for both time switching (TS) and power splitting (PS) based SWIPT schemes. The first problem was the maximization of the overall user data rate while ensuring a minimum harvested power. The second problem focused on the maximization of the overall harvested power at the user under the constraint on the minimum achievable rate. Assuming an amplify-and-forward (AF) relay protocol, closed-form solutions were obtained for the selection of an optimal relay, relay amplification coefficient and the optimal time or power splitting factor. The performance of the proposed relay selection strategies with the aforementioned objectives was evaluated and compared with the case of random relay selection. Furthermore, the Rate-Energy (R-E) trade-off performance of the scenario with both the direct and indirect relay-assisted links was compared to the case where only a relay-assisted link is available. Our simulation results demonstrated the significant benefits of combining direct and indirect links in SWIPT-enabled cooperative networks in terms of the R-E trade-off.

Resource Allocation and Relay Selection for Multi-User OFDM-Based Cooperative Networks with SWIPT [18]

This work investigated the single relay selection from a pool of candidate relays, subcarrier pairing, power allocation and PS ratio optimization in a two-hop relay-assisted multi-user network with SWIPT. Single relay is chosen over multiple relays to significantly reduce the control and synchronization process among the relay nodes. We formulated the resource allocation and relay selection problem as a maximization of the total system throughput by satisfying the individual users' energy harvesting constraints subjected to transmit power limits. The latter was found to be an extremely challenging problem due to the complexity caused by the joint optimization of several network resources, which required an analysis within the full search space. In order to circumvent this tedious and unaffordable optimization, we followed an heuristic approach based on the equivalent end-to-end channel gain computed with the harmonic mean. Numerical results were presented, which show that the proposed low complexity scheme was able to offer better performance than the one achieved with a semi-random resource assignment approach, where the relay and sub-carriers were randomly assigned, followed by an optimal power and PS ratios allocation according to the previous random decisions.

Sequential Resource Distribution Technique for Multi-User OFDM-SWIPT based Cooperative Networks [19]

Herein, we considered single source assisted by multiple half-duplex AF-enabled relays based on OFDM to forward both information and energy to multiple users. Considering this two-hop relay-assisted multi-user network with SWIPT, we investigated single relay selection from a pool of available relays and optimize the subcarrier pairing, power allocation, and SWIPT splitting factors. In order to significantly reduce the control and synchronization process among the relay nodes, single relay is chosen over multiple relays. We formulated a problem to optimize the relay selection and resource allocation based on maximization of the end-users' sum-rate constrained to minimum individual user's harvested energy and transmit power limits. Due to joint optimization of several resources, an analysis within the full search space imposed very high complexities thereby making the problem extremely challenging to solve. To circumvent this tedious and unaffordable optimization, we sought for a less complex heuristic solution. In this context, we proposed a novel sequential resource distribution (SRD) algorithm based on pairing the maximum channel gains of both the hops to maximize the end-users' sum-rate by jointly performing optimization of sub-carrier-destination assignment, sub-carrier pairing, and relay-destination coupling metrics, followed by power allocation to sub-carriers in each hop, and computation of SWIPT splitting factors at the destination.

QoS-Constrained Sum-Harvested Energy Maximization in OFDMA-based Wireless Cooperative Networks [20]

We investigated the performances of the time-switching (TS) and power-splitting (PS) based energy harvesting models in a two-hop relay assisted network where the end-users were capable of decoding information and harvesting energy concurrently. In particular, we considered joint resource allocation and relay selection to realize Simultaneous Wireless Information and Power Transfer (SWIPT) in a multi-carrier multi-user cooperative system where the relays employed the amplify-and-forward (AF) protocol. We formulated an optimization problem for relay selection, carrier assignment in the two hops, sub-carrier pairing, sub-carrier power allocation, and the SWIPT splitting factors for each user in order to maximize the sum of energy harvested at the users subjected to minimum QoS constraint at each user and power limitations at the transmitter and relays. In this context, we proposed an Energy Yield Escalation (EYE) algorithm with polynomial computation time-complexity and sub-optimal but good performance, to address the aforementioned problem. We illustrated the efficiency of the proposed technique via numerical results.

Pricing Perspective for SWIPT in OFDM-based Multi-User Wireless Cooperative Systems [21]

In this work, we proposed a novel formulation for joint maximization of total weighted sum-spectral efficiency and weighted sum-harvested energy to study Simultaneous Wireless Information and Power Transfer (SWIPT) from a pricing perspective. Specifically, we considered that a transmit source communicates with multiple destinations using Orthogonal Frequency Division Multiplexing (OFDM) system within a dual-hop relay-assisted network, where the destination nodes were capable of jointly decoding information and harvesting energy from the same radio-frequency (RF) signal using either the time-switching (TS) or power-splitting (PS) based SWIPT receiver architectures. Computation of the optimal solution for the aforementioned problem was found to be an extremely challenging task as joint optimization of

several network resources introduce intractability at high numeric values of relays, destination nodes and OFDM sub-carriers. Therefore, we presented a suitable algorithm with sub-optimal results and good performance to compute the performance of joint data processing and harvesting energy under fixed pricing methods by adjusting the respective weight factors, motivated by practical statistics. Furthermore, by exploiting the binary options of the weights, we showed that the proposed formulation could be regulated purely as a sum-spectral efficiency maximization or solely as a sum-harvested energy maximization problem. Numerical results illustrated the benefits of the proposed design under several operating conditions and parameter values.

3.8 Summary

In this chapter, we have proposed a novel resource allocation and relay selection scheme for cooperative multi-user multi-relay OFDMA networks with SWIPT capabilities at the end-users. The problem formulation for maximization of sum-rate of all the users was found to be non-linear with mixed-integer programming and hence an explicit low-complexity solution could not be obtained. By exploiting the availability of time-sharing criteria and choosing sufficiently large number of sub-carriers, we efficiently solved this combinatorial problem using the dual method with polynomial complexity. In this context, we proposed suitable methods which can noticeably improve the system performance and illustrated the effectiveness of the proposed algorithms via numerical results, where we showed the asymptotic optimality of the solutions for sufficiently large parametric values of the number of OFDM sub-carriers, relays and users. Additionally, brief descriptions on works with similar system set-ups were discussed. This work can be further extended to many promising directions including the study of current framework with non-orthogonal multiple access (NOMA) instead of OFDM, and incorporation of multi-antenna systems where each device in the system may be assumed to have multiple antennas. The latter case may offer several interesting problems like antenna-selection, and beamform designing for SWIPT in MIMO-OFDM/MIMO-NOMA systems. Additional benefits from contributions by the direct links (corresponding to signals in the first hop) at the end-users may also be leveraged.

Chapter 4

Transmit Precoder Design for Simultaneous Wireless Information and Power Transfer in Multi-group Multicasting Systems

The key to developing future generations of wireless communication systems lies in the expansion of extant methodologies, which ensures the coexistence of a variety of devices within a system. In this chapter, we assume several multicasting (MC) groups comprising three types of heterogeneous users including Information Decoding (ID), Energy Harvesting (EH) and both ID and EH. We present a novel framework to investigate the multi-group (MG) - MC precoder designs for three different scenarios, namely, Separate Multicast and Energy Precoding Design (SMEP), Joint Multicast and Energy Precoding Design (JMEP), and Per-User Information and/or Energy Precoding Design (PIEP). In the considered system, a multi-antenna source transmits the relevant information and/or energy to the groups of corresponding receivers using more than one MC streams. The data processing users employ the conventional ID receiver architectures, the EH users make use of a non-linear EH module for energy acquisition, while the users capable of performing both ID and EH utilize the separated architecture with disparate ID and non-linear EH units. Our contribution is threefold. Firstly, we propose an optimization framework to i) minimize the total transmit power and ii) to maximize the sum harvested energy, the two key performance metrics of MG-MC systems. The proposed framework allows the analysis of the system under arbitrary given quality of service and harvested energy requirements. Secondly, to deal with the non-convexity of the formulated problems, we transform the original problems respectively into equivalent forms, which can be effectively solved by semi-definite relaxation (SDR) and alternating optimization. The convergence of the proposed algorithms is analytically guaranteed. Thirdly, a comparative study between the proposed schemes is conducted via extensive numerical results, wherein the benefits of adopting SMEP over JMEP and PIEP models are discussed.

4.1 Introduction to Multi-group Multicasting Systems with SWIPT

Recent developments related to wireless communication systems of current and evolving generations have exposed several critical issues such as growing performance and capacity demands, complicated hardware designs, and need for energy-efficient architectures. Rapid battery drainage at power-limited wireless devices also raise concerns, while addressing the above-mentioned assertive demands. Consequently, two promising energy optimization techniques, namely, energy harvesting (as a recharging alternative) and minimization of power consumption (for enhancing the battery lifetime), respectively, may prove useful to address the aforementioned challenges [195,196]. Incorporation and implementation of such methods is likely to be considered essential from the Internet-of-Things (IoT) perspective [26,27,197]. The observed transitional trend of customers between any consequent generations of wireless mobile communications, i.e., NG to (N+1)G (where N = 1, ..., 4), reveals that it is almost impossible to switch directly into an advanced and superior technology altogether [198]. This implies that an intermediate time period is almost certain, until all the customer devices have been upgraded to the technology with the latest mobile generation. In the context of wireless energy harvesting (EH) devices based on radio-frequency (RF), e.g., sensors, smart devices and home gateways all under the same wireless network, we envision that a similar trend will be observed upon their launch. Therefore, it is necessary to make sure that different kinds of concerned devices such as information decoding (ID) specific, explicit to EH, and the ones performing ID and EH simultaneously, co-exist within the wireless networks and derive maximal gains, which is the main focus of this chapter.

Traditional information processing units have been shown to perform significantly better within a Multiple-Input Single-Output (MISO) set-up [199], in comparison to a one-to-one device communication scheme based on a single antenna. In [200], Varshney presented a framework to spark interest in the possibility of concurrent information and energy transmission using the RF signals. This work was later extended to multi-user MISO case in [195,201]. There has been a growing research interest in the field of simultaneous wireless information and power transmission (SWIPT) over the past decade [168]. A major outcome in this direction points towards the inability of the traditional ID receivers to harvest RF energy and thus, this calls for a change in the classical receiver architecture. In this context, researchers have proposed several interesting receiver designs for enabling SWIPT [202], with the four most viable designs being time-switching (TS), power-splitting (PS), separated architecture (SA) and integrated architecture (IA). The complex circuitries associated with TS, PS, and IA-based receivers for SWIPT includes one or more additional optimization parameter(s) in order to segregate the received signal for carrying out either distinct or simultaneous ID and EH operations. In this regard, the SA-based SWIPT receivers may come in handy to reduce the architectural demands within the transmit-receive systems.

In order to combat the aforementioned challenges, transmit precoding is a potential technique not only for enhancing the channel capacity and diversity, but also for mitigating interference in the context of multi-user MISO systems [203]. The authors in [195] presented a framework to jointly optimize the transmit beamforming and the receive power splitting (PS) ratio for SWIPT in MISO systems. Furthermore, energy efficiency optimization was considered in [204] with the same set-up targeting the Zero-Forcing (ZF) beamforming. In [205], Xu *et. al.*, studied the maximization of harvested energy for multi-user MISO SWIPT systems considering SA receiver architecture with a goal to optimize the ID and EH beamforming strategies. However, the above-mentioned works do not consider the non-linear EH model for

SWIPT, which is more realistic in comparison to its counterpart linear EH model. In [206], the advantages of employing precoding in MISO broadcast channels were presented for SWIPT systems, whereas joint multi-objective optimization for transmit precoding and receiver TS design was proposed in [207] considering a similar scenario with MISO and SWIPT systems.

Multi-group (MG) Multicasting (MC) is another promising technique to significantly improve the system performance. In [208], the authors proposed a framework for MG-MC beamformer design in the context of multiple-input single-output – orthogonal frequency division multiplexing (MISO-OFDM) with antenna selection. The benefits of precoding in a MG-MC scenario were demonstrated in [209–211]. The authors in [212] considered precoding for MG-MC with a common message to study the problem of maximization of weighted sum-rate (WSR) for two schemes where the transmitter superimposes common and multicast messages, and transmitter concatenates the multicast message vector with the common message, respectively. However, it was shown in [203] that an MC precoding problem is NP-hard by nature, even for a single group multicast. Several works have discussed joint information and energy transmission in the MG-MC scenario [213–215], however, with an assumption of a linear EH module. In [216], the authors studied SWIPT in MISO MG-MC system where each receiver employs the PS SWIPT receiver architecture for investigating the joint MC beamforming and receive power splitting problem to minimize the total transmit power under SINR and EH constraints. A framework to investigate PS-based SWIPT MC was presented in [217] with individual QoS constraints to meet the demands of energy sustainable IoT devices. It is noteworthy that these works do not consider the coexistence of different user types in the case of MG-MC within the MISO–SWIPT scenario.

In this chapter, we consider a MISO MG-MC precoding based-system wherein a transmit source equipped with multiple antennas provides coverage to multiple users with the help of beamforming through adequate precoder designs. We investigate the problems of minimization of total transmit power and maximization of sum-harvested energy (by the intended users), respectively, in three different scenarios incorporating the coexistence of heterogeneous users comprising three different types. Both problems are found to be non-convex in nature, such that in order to achieve a feasible (optimal or sub-optimal) solution, adequate relaxations and/or transformations are required. In this regard, we obtain reasonable solutions to the formulated problems with the help of semidefinite relaxation (SDR) and a slack variable replacement (SVR) technique. A comparative study between the three proposed scenarios is provided via numerical results based on the obtained solutions, where intensive investigation is carried out using parameter alterations under various practical conditions.

This work builds on the authors' previous publication [23], where the problem of transmit power minimization was addressed considering the three above-mentioned scenarios. As an extension, an alternate form of problem considering the maximization of sum-harvested energy is proposed here to address the concerns related to practical limitations of the prior problem (more details are provided in Section IV). Specifically, the main contributions and novelty of this work are listed below

1. We consider a novel MG-MC precoding framework which deals with the co-existence of three types of users capable of information decoding, energy harvesting, and joint information and energy extraction, respectively. In this context, it is important to mention that most of the existing works in the literature do not consider co-existence of multiple user types for analysis.

2. In order to introduce tractability in the minimization of the total transmit power, we provide adequate transformation to simplify the non-linear EH constraint to a linear

form. Without loss of generality, this transformation may come in handy to solve similar problems with non-linear EH constraints. With the help of SDR, the problem is further alleviated to an easily solvable convex-form. In comparison to other works, this chapter provides more practically oriented problem formulation for the minimization of total transmit power with the consideration of non-linear EH constraint.

3. Taking into consideration the practical implementation concerns of preceding problem, we formulate a sum-harvested energy maximization problem with a non-linear objective and transmit power limitation, in addition to other necessary constraints introduced earlier. In this context, we propose a slack variable replacement (SVR) technique (in conjunction with well-known SDR method) to make the problem tractable, which is then solved efficiently using an iterative algorithm. On the other hand, a simpler problem with linear EH objective and constraint is considered in most of the existing works that analyze the MG-MC framework.

4. Considering the existing works in the literature, it is noteworthy that an investigative comparison between the three proposed scenarios with heterogeneous users (including EH users with non-linear EH modules) has not been presented so far (to the best of authors' knowledge). Herein, we provide a comparative study among the three proposed schemes with separate information and/or energy precoder design, joint information and/or energy precoder design, and per-user information and/or energy precoder design. The latter scheme is considered as the benchmark for comparison purposes. We first draw the comparison between the systems based on a more generalized yet practically-inspired channel modeling scheme, in order to observe their corresponding behaviors under several test cases. Furthermore, we assume uniform linear arrays (ULAs) [218] at the transmitter to test the efficacy of the proposed algorithms over a channel that is simple and can be easily interpreted.

The rest of the chapter is organized as follows. Section 4.2 provides an insight into the system model. The total transmit power minimization problem and its corresponding solution are presented in Section 4.3, while the sum-harvested energy maximization problem and its (proposed) solution with an iterative algorithm are conferred in Section 4.4. Numerical results are shown in Section 4.5, followed by concluding remarks in Section 4.6.

4.2 System Model

We consider a multi-group multicasting (MG-MC) system where a transmit source equipped with M antennas serves L single-antenna users $(D_1, \ldots, D_L)$. Each user may be classified within one of the several possible groups, and is expected to perform either of the following operations, namely, information decoding (ID), energy harvesting (EH), or both ID and EH. In case a user performs both ID and EH, it is assumed to be equipped with disparate RF chains responsible for carrying out the desired operations. Such kind of receiver design is often referred to as the separated architecture (SA) in the literature for enabling joint information processing and energy harvesting [202]. In this work, we specifically categorize the ID users among Z multicasting (MC) groups while we assume that all the EH users are classified under the $(Z+1)^{\text{th}}$ group. Note that the users in $(Z+1)^{\text{th}}$ group may or may not be a part of any other pre-categorized Z MC groups of ID users. In the considered system, a user requesting joint ID and EH operations would participate in any one of the Z MC groups and also in $(Z+1)^{\text{th}}$ group. With regard to the categorization of users within the groups,

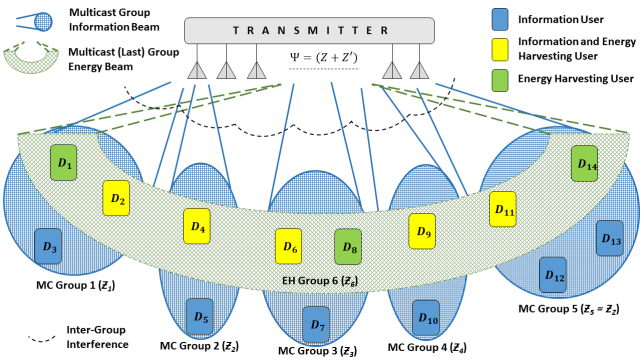

FIGURE 4.1: System model for Separate Multicast and Energy Precoding Design (SMEP). Herein, the intended EH users are served using the corresponding MC beam (blue) as well as a dedicated power beam (green).

several methods may be implemented. In this regard, channel co-linearity and orthogonality based user grouping is considered in [219] where initially $(Z+1)$ users (same as number of groups) with most orthogonal channels are considered as different groups. Further, the unallocated users are assigned to the groups based on co-linearity with the existing users in the groups. In [220], the authors consider message based user grouping where it is proved that ad-hoc user grouping is optimal for massive MIMO systems under max-min SINR design criterion. Regarding the categorization of users within specific groups in this work, naturally the users requesting the same (common) information will be a part of same group and thus, distinct groups may be formed and such groups may be assumed to be already known as considered herein. Therefore, for analytical convenience, we assume that all the users are already categorized among various groups and such arrangements are known [213, 214].

We propose and analyze three different precoding design methods for energy optimization, which are discussed below

1. *Separate Multicast and Energy Precoding Design (SMEP)*: In this case, we assume Z multicast information groups and an additional group devoted to EH specific users. Thus, we target design of at least $(Z+Z')$ precoders, where we intend to have $Z'=1$. However, the value of Z' may vary according to the technique used for designing criteria, which will be justified in the later sections.

2. *Joint Multicast and Energy Precoding Design (JMEP)*: Herein, no exclusive precoder is present for EH specific users. In particular, we target the design of Z multicast precoders taking into account the information and/or energy demands of the corresponding users[1].

3. *Per-User Information and/or Energy Precoding Design (PIEP)*: We assume in this case that each user is served by single dedicated precoder. Therefore, we target the design of L precoders (equal to the number of users). This case is very unlikely in practice but is considered as a baseline for comparison purposes.

[1]In JMEP, it is clear that for the EH users without ID request, classifications are performed within the Z MC groups. Regarding categorization of the EH users within the Z groups, certain methods e.g., distance from the nearest transmit antenna, distance from the nearest beam, etc., may be applied. This, however, involves rigorous analysis and is out of the scope of this work.

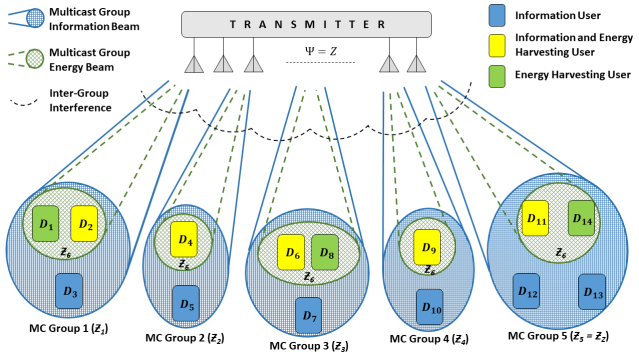

FIGURE 4.2: In Joint Multicast and Energy Precoding Design (JMEP), the EH users are categorized within the stipulated MC groups and all the users are served by their corresponding MC beam (blue). Note that there is/are no separate power beam(s) (green) as such, however, we have depicted the same for convenience to distinguish between the three types of wireless users.

For illustration purpose, we consider an example with $L = 14$ users, where 6 users are ID specific, 3 users only harvest energy, and 5 users have joint ID and EH capabilities, M transmit antennas (with $M \geq L$ for PIEP to be feasible), and $Z = 5$ MC groups. Correspondingly, the system set-up for the aforementioned three scenarios (SMEP, JMEP, and PIEP) are depicted in Fig. 4.1, Fig. 4.2, and Fig. 4.3, respectively. Let $\mathcal{Z}_k$ denote the k^{th} multicast users' group. Let us also define the following variable to assist the precoding design metrics (i.e., number of precoders) in three cases interchangeably

$$\Psi = \begin{cases} Z + Z' & : \quad \text{SMEP.} \\ Z & : \quad \text{JMEP.} \\ L & : \quad \text{PIEP.} \end{cases} \tag{4.1}$$

Each ID or joint ID and EH user belongs to only the MC group, i.e., $\mathcal{Z}_k \cap \mathcal{Z}_\ell = \varnothing$, $\forall k, \ell = \{1, \ldots, \Psi\}$ and $k \neq \ell$; whereas in case of EH, the user harvests energy using all the possible multicast signals[2].

The antenna array at the transmitter emits the signal $\mathbf{x}(t) = \sum_{k=1}^{\Psi} \mathbf{w}_k \bar{s}_k(t)$, where $\mathbf{w}_k$ is the related $M \times 1$ complex precoding weight vector for the users in group $\mathcal{Z}_k$, and $\bar{s}_k(t)$ is the corresponding information and/or energy signal. Additionally, we assume that the information and/or energy signals for each group $\{\bar{s}_k(t)\}_{k=1}^{\Psi}$ are mutually uncorrelated to each other with zero mean and unit variance, $\sigma^2_{\bar{s}_k} = 1$. The corresponding ID and/or EH signals may be separately designed according to the framework proposed in [221]. Distinct ID and EH signal forms motivate the use of SA-based devices. The total transmitted power can thus be given by $\sum_{k=1}^{\Psi} \mathbf{w}_k^H \mathbf{w}_k$.

The received signal at the i^{th} user is given by $y_i(t) = \mathbf{h}_i^H \mathbf{x}(t) + n_{R,i}(t)$, where $\mathbf{h}_i$ is the $M \times 1$ conjugated channel vector for the corresponding receiver and $n_{R,i}(t)$ is the additive white Gaussian noise at the corresponding i^{th} user's receiving antenna equipment with zero mean and variance $\sigma^2_{R,i}$. The source signals are assumed to be uncorrelated with $n_{R,i}(t)$. The signal received at the information decoding unit of the i^{th} receiver equipment is expressed as

[2]The other MCs are primarily taken into consideration due to interference causing side-lobes other than the desired MC, which is beneficial for EH.

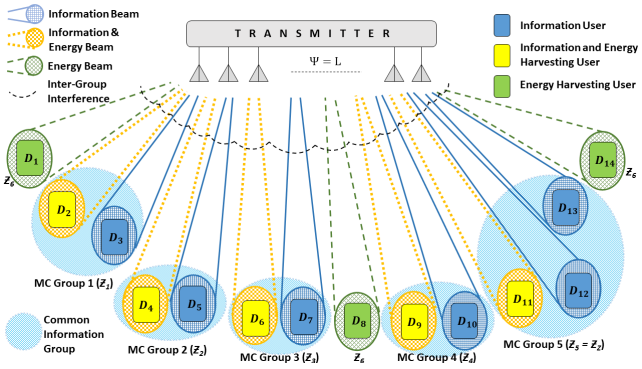

FIGURE 4.3: The system model for Per-User Information and/or Energy Precoding Design (PIEP) consists of dedicated precoders for each user. It is noteworthy that multiple transmissions of common message may occur while serving the set of users within the corresponding MC group.

$$y_{D,i}(t) = \Big(\mathbf{h}_i^H \mathbf{x}(t) + n_{R,i}(t)\Big) + n_{D,i}(t), \tag{4.2}$$

where $n_{D,i}(t)$ is the additional zero-mean Gaussian noise with a variance of $\sigma_{D,i}^2$ incurred due to the circuitry and other relevant operations at the ID block of the i^{th} receiver. For i^{th} receiver belonging to the k^{th} multicast group $\mathcal{Z}_k$, the signal-to-interference-and-noise ratio (SINR) is given by

$$\Upsilon_i = \frac{|\mathbf{w}_k^H \mathbf{h}_i|^2}{\sum\limits_{\substack{\ell=1 \\ \ell \neq k}}^{\Psi} |\mathbf{w}_\ell^H \mathbf{h}_i|^2 + \sigma_{R,i}^2 + \sigma_{D,i}^2}. \tag{4.3}$$

The signal dedicated for EH block of the i^{th} receiver is

$$y_{E,i}(t) = \mathbf{h}_i^H \mathbf{x}(t) + n_{R,i}(t). \tag{4.4}$$

Therefore, the energy extracted by the EH unit of i^{th} receiver is given as, $\mathcal{E}_i^{\mathcal{L}} = \zeta_i \Big(\sum_{k=1}^{\Psi} |\mathbf{w}_k^H \mathbf{h}_i|^2 + \sigma_{R,j}^2 \Big)$, where $0 < \zeta_i \leq 1$ is the energy conversion efficiency of the EH unit at the corresponding receiver [171]. Note that $\mathcal{E}_i^{\mathcal{L}}$ is theoretically valid in order to represent a linear EH operation, however its practical implementation is questionable. Thus, this calls for the adoption of a non-linear EH model. In this regard, we define the energy harvested at the receiver as follows [222]

$$\mathcal{E}_i^{\mathcal{N}} = \frac{\mathcal{E}'}{1 - \varkappa} \cdot \left(\frac{1}{1 + e^{(-\alpha(\sum_{k=1}^{\Psi} |\mathbf{w}_k^H \mathbf{h}_i|^2) + \alpha\beta)}} - \varkappa \right), \tag{4.5}$$

where $\varkappa \triangleq \frac{1}{1+\exp(\alpha\beta)}$, the constant $\mathcal{E}'$ is obtained by determining the maximum harvested energy on the saturation of the EH circuit, and α and β are specific for the capacitor and diode turn-on voltage metrics at the EH circuit. Practically, a standard curve-fitting tool based on analytical data may be used to decide the appropriate values of $\mathcal{E}'$, α, and β. A comparison between the linear and non-linear EH models is depicted in Fig. 4.4, where $\zeta_i = 0.75$ (for linear EH module), $\mathcal{E}' = 2.8\ mJ$, $\alpha = 1500$, and $\beta = 0.0022$ (for the non-linear EH module) [15, 222]. The non-linearity introduced due to the diode and capacitor elements is observed at lower input power at the EH module while a constant EH operation is seen for

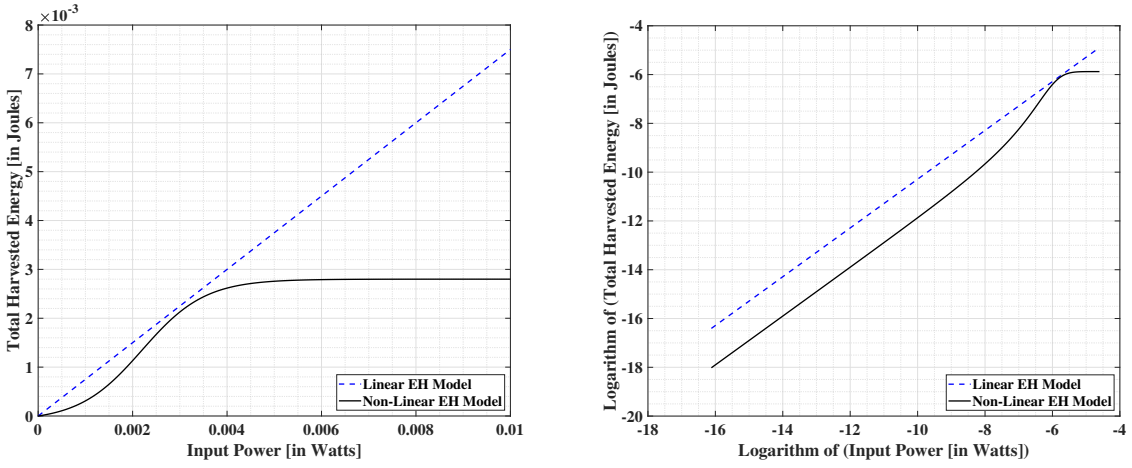

(a) (b)

FIGURE 4.4: Comparison between the energy extraction capabilities of linear and non-linear energy harvesting models (a) in general and (b) logarithmic scale.

higher values of input power which implies the saturation at diode element of the EH module. On the other hand, the linear EH model increases constantly based on the increasing input power at the EH module[3], without considering the saturation points of the circuit elements (such as diode) [222]. However, it is noted from Fig. 4.4(b) that the operation regime for the EH module in the proposed framework would range from milli-Joules to micro-Joules (or even lower), based on the separation distance between the transmitter and end-users. We assume normalized time slots to use the terms *power* and *energy* interchangeably.

In the following sections, we formulate the optimization problems corresponding to various precoder designs for minimization of the total transmit power and maximization of sum-harvested energy at the intended users, respectively, for the three scenarios, viz-a-viz., SMEP, JMEP and PIEP. Feasible solutions are obtained by employing suitable transformations and simplifications.

4.3 Transmit Power Minimization

In this section, we minimize the overall transmitted power subjected to minimum SINR and EH constraints at the corresponding users/groups.

4.3.1 Problem Formulation and Solution based on Semi-Definite Relaxation (SDR)

The overall optimization problem for precoder design (encapsulating three aforementioned scenarios) to minimize the total transmit power can be written in its analytical form as

[3]This is due to the assumption of a constant energy conversion efficiency at the EH module.

$$(P1): \min_{\{\mathbf{w}_k\}_{k=1}^{\Psi}} \sum_{k=1}^{\Psi} \mathbf{w}_k^H \mathbf{w}_k \tag{4.6}$$

$$\text{s.t. } (C1): \frac{\mathbf{w}_k^H \mathbf{H}_i \mathbf{w}_k}{\sum_{\ell \neq k} \mathbf{w}_\ell^H \mathbf{H}_i \mathbf{w}_\ell + \sigma_{R,i}^2 + \sigma_{D,i}^2} \geq \gamma_i,$$

$$\begin{cases} \text{SMEP}: \ \forall i \in \mathcal{Z}_k, \ \forall k \in \{1, \ldots, Z\}, \\ \qquad \forall \ell \in \{1, \ldots, Z+1\}, \\ \text{JMEP}: \ \forall i \in \mathcal{Z}_k, \ \forall k \in \{1, \ldots, Z\}, \\ \qquad \forall \ell \in \{1, \ldots, Z\}, \\ \text{PIEP}: \quad \forall i, \forall k, \forall \ell \in \{1, \ldots, L\}, i = k, \end{cases} \tag{4.7}$$

$$(C2): \mathcal{E}_j^{\mathcal{N}} \geq \xi_j, \forall j \in \mathcal{Z}_{Z+1}, \tag{4.8}$$

where γ_i is the SINR threshold at the i^{th} user, ξ_j is the harvested energy demand at j^{th} user (where i can be equal to j for some cases, in general), and $\mathbf{H}_i = \mathbf{h}_i \mathbf{h}_i^H$. It is clear that the formulated problem $(P1)$ is not convex due to constraints $(C1)$ and $(C2)$. Moreover, the feasibility of $(P1)$ is dependent on γ_i and ξ_i, corresponding to $(C1)$ and $(C2)$, respectively, which is additionally constrained by the rank of $\mathbf{H}_i$ [223]. On the other hand, it is interesting to note the hidden linearity aspect within the non-linear EH expression in (4.5), which can be useful in converting a non-linear EH constraint to a linear form, without loss of generality. The corresponding transformation is provided in (D.2) of Appendix D.1. To proceed, we define $\mathbf{w} = [\mathbf{w}_1^{\mathrm{T}} \ \mathbf{w}_2^{\mathrm{T}} \ \ldots \mathbf{w}_\Psi^{\mathrm{T}}]^{\mathrm{T}}$ and $\mathbf{W}_k = \mathbf{w}_k \mathbf{w}_k^H$. With the help of these notations, $(P1)$ can be reformulated into a semi-definite programming (SDP) problem as follows

$$(P2): \min_{\{\mathbf{W}_k\}_{k=1}^{\Psi}} \sum_{k=1}^{\Psi} \mathrm{Tr}\{\mathbf{W}_k\} \tag{4.9}$$

$$\text{s.t. } (C1): \mathrm{Tr}\{\mathbf{H}_i \mathbf{W}_k\} - \gamma_i \sum_{\ell \neq k} \mathrm{Tr}\{\mathbf{H}_i \mathbf{W}_\ell\} \geq \gamma_i (\sigma_{R,i}^2 + \sigma_{D,i}^2),$$

$$\begin{cases} \text{SMEP}: \ \forall i \in \mathcal{Z}_k, \ \forall k \in \{1, \ldots, Z\}, \\ \qquad \forall \ell \in \{1, \ldots, Z+1\}, \\ \text{JMEP}: \ \forall i \in \mathcal{Z}_k, \ \forall k \in \{1, \ldots, Z\}, \\ \qquad \forall \ell \in \{1, \ldots, Z\}, \\ \text{PIEP}: \quad \forall i, \forall k, \forall \ell \in \{1, \ldots, L\}, i = k, \end{cases} \tag{4.10}$$

$$(C2): \sum_{k=1}^{\Psi} \mathrm{Tr}\{\mathbf{H}_j \mathbf{W}_k\} \geq \frac{\xi_j'}{\zeta_j} - \sigma_{R,j}^2, \quad \forall j \in \mathcal{Z}_{Z+1}, \tag{4.11}$$

$$(C3): \mathbf{W}_k \succcurlyeq 0. \tag{4.12}$$

The SDP transforms the non-convex $(P1)$ into a convex problem as in $(P2)$, which can be solved using the well-known methods of convex optimization, cf. [224]. For our numerical evaluations, we employ the convex programming tool CVX, wherein we make use of the semi-definite relaxation (SDR) method to simplify $(P2)$ further [225, 226]. It is worth mentioning

that in the context of SDR, the well-known procedure is to drop the non-convex constraint of $\text{rank}(\mathbf{W}_k) = 1$. Let $\mathbf{W}^\star$ denote the solution of the relaxed problem in $(P2)$. Then, $\mathbf{W}^\star$ is considered the optimal solution iff $\text{rank}(\mathbf{W}_k^\star) = 1$ [227]. In this regard, technique like the eigen value decomposition (EVD) [228] or Gaussian randomization [203] may be employed to obtain a unit rank approximation of the precoder metrics.

4.3.2 Novel Feasible Point Pursuit Successive Convex Approximation Method for Energy Optimization (FPP-SCA-e)

In this section, we formulate an optimization problem to minimize the total transmit power with optimal precoder designs for the three aforementioned scenarios, under constraints on minimum signal-to-interference-and-noise ratio and harvested energy by the users with respective demands. The problem may be adapted to the well-known semi-definite program, which can be typically solved via relaxation of rank-1 constraint. However, the relaxation of this constraint may in some cases lead to performance degradation, which increases with the rank of the solution obtained from the relaxed problem. Hence, we develop a novel technique motivated by the feasible-point pursuit successive convex approximation method in order to address the rank-related issue. The benefits of the proposed method are illustrated under various operating conditions and parameter values, with comparison between the three above-mentioned scenarios.

Notation: In the remainder of this section, bold face lower case and upper case characters denote column vectors and matrices, respectively. The operators $(\cdot)^H$, $|\cdot|$ and $\otimes$ correspond to the conjugate transpose, the absolute value and the Kronecker product, respectively. An identity matrix of $Y \times Y$ dimensions is denoted as $\mathbf{I}_Y$, where its y^{th} column is represented as $\mathbf{e}_y$. Calligraphic indexed characters denote sets. $\mathbb{R}_\kappa^+$ denotes the set of real positive κ-dimensional vectors.

Herein, we present an enhanced technique motivated by a recently proposed alternative to SDR, namely, feasible-point pursuit successive convex approximation (FPP-SCA) [229, 230]. In contrast to the traditional FPP-SCA method applied to such frameworks [229], the technique proposed in this paper, FPP-SCA-e, takes care of an additional constraint of harvested energy demand at the intended users. It is clear that the problem $(P1)$ can be categorized within the general class of quadratically constrained quadratic problems (QCQPs), and thus a modified technique in-line with FPP-SCA can be developed which also takes into account an additional harvested energy constraint. To proceed, we define $\mathbf{w}_{\text{tot}} = [\mathbf{w}_1^H, \mathbf{w}_2^H, \ldots, \mathbf{w}_\Psi^H]^H$ such that the i^{th} SINR constraint reads as

$$\mathbf{w}_{\text{tot}}^H \mathbf{\Lambda}_i \mathbf{w}_{\text{tot}} \leq -\gamma_i(\sigma_{R,i}^2 + \sigma_{D,i}^2), \tag{4.13}$$

where $\mathbf{\Lambda}_i = \mathbf{\Lambda}_i^{(+)} + \mathbf{\Lambda}_i^{(-)}$ with $\mathbf{\Lambda}_i^{(+)} = \gamma_i(\mathrm{I}_\Psi - \text{diag}\{\mathbf{e}_k\}) \otimes \mathbf{h}_i\mathbf{h}_i^H$, $\mathbf{\Lambda}_i^{(-)} = -\text{diag}\{\mathbf{e}_k\} \otimes \mathbf{h}_i\mathbf{h}_i^H, \forall i \in \mathcal{Z}_k$, with $k \in \{1, \ldots, \Psi\}$. Let $\boldsymbol{\omega}$ denote any random point so that by the definition of a semi-definite matrix $\mathbf{\Lambda}_i^{(-)}$ we have $(\mathbf{w}_{\text{tot}} - \boldsymbol{\omega})^H \mathbf{\Lambda}_i^{(-)} (\mathbf{w}_{\text{tot}} - \boldsymbol{\omega}) \leq 0$. With further simplification, we express the linear constraint of $\mathbf{w}_{\text{tot}}$ around $\boldsymbol{\omega}$ as follows

$$\mathbf{w}_{\text{tot}}^H \mathbf{\Lambda}_i^{(-)} \mathbf{w}_{\text{tot}} \leq 2\text{Re}\{\boldsymbol{\omega}^H \mathbf{\Lambda}_i^{(-)} \mathbf{w}_{\text{tot}}\} - \boldsymbol{\omega}^H \mathbf{\Lambda}_i^{(-)} \boldsymbol{\omega}. \tag{4.14}$$

Subsequently, the SINR constaint in (4.14) is given by

$$\mathbf{w}_{\text{tot}}^H \mathbf{\Lambda}_i^{(+)} \mathbf{w}_{\text{tot}} + 2\text{Re}\{\boldsymbol{\omega}^H \mathbf{\Lambda}_i^{(-)} \mathbf{w}_{\text{tot}}\} - \boldsymbol{\omega}^H \mathbf{\Lambda}_i^{(-)} \boldsymbol{\omega} \leq -\gamma_i(\sigma_{R,i}^2 + \sigma_{D,i}^2), \tag{4.15}$$

wherein the unknown variables are quadratic over a semi-definite matrix. Following a similar trend, the harvested energy constraint at the $\tilde{\epsilon}^{\text{th}}$ user can thus be represented as

Technique →		JMEP			SMEP			PIEP		
Antennas ↓	(γ_i, ξ_i) ↓	SDP	FPP-SCA-e	FPP-SCA-e$^+$	SDP	FPP-SCA-e	FPP-SCA-e$^+$	SDP	FPP-SCA-e	FPP-SCA-e$^+$
$M = 20$	(0.1 dB, 1 μJ)	25.4	5.6	31.0	43.7	6.9	50.4	268.8	15.9	284.0
	(25 dB, 1 μJ)	31.5	6.0	37.0	55.5	6.9	62.4	354.0	17.0	366.5
	(0.1 dB, 5 μJ)	25.4	5.6	31.0	47.7	6.8	55.0	275.6	16.8	288.0
	(25 dB, 5 μJ)	29.8	6.1	35.3	55.4	6.9	62.1	373.7	16.3	389.0
	AVERAGE	**28.025**	**5.825**	**33.575**	**50.575**	**6.875**	**57.475**	**318.025**	**16.500**	**331.875**
$M = 10$	(0.1 dB, 1 μJ)	2.4	5.3	7.6	2.7	6.5	9.3	4.9	14.6	17.8
	(25 dB, 1 μJ)	2.6	5.4	7.8	3.6	6.6	10.2	6.6	14.8	18.4
	(0.1 dB, 5 μJ)	2.4	5.3	7.8	2.8	6.4	9.4	5.9	14.8	18.5
	(25 dB, 5 μJ)	2.9	5.7	8.2	3.5	6.5	10.0	7.6	14.9	20.4
	AVERAGE	**2.575**	**5.425**	**7.850**	**3.150**	**6.500**	**9.725**	**6.250**	**14.775**	**18.775**

TABLE 4.1: Computational complexity analysis (in seconds) of the proposed methods.

$$\zeta_{\tilde{\epsilon}}\Big[\boldsymbol{\omega}^{(j)H}\boldsymbol{\Lambda}_{\tilde{\epsilon}}^{(-)}\boldsymbol{\omega}^{(j)} - 2\mathrm{Re}\{\boldsymbol{\omega}^{(j)H}\boldsymbol{\Lambda}_{\tilde{\epsilon}}^{(-)}\mathbf{w}_{\mathrm{tot}}\} - \mathbf{w}_{\mathrm{tot}}^{H}\hat{\boldsymbol{\Lambda}}_{\tilde{\epsilon}}^{(+)}\mathbf{w}_{\mathrm{tot}} + \sigma_{R,\tilde{\epsilon}}^{2}\Big] \geq \xi'_{\tilde{\epsilon}}, \tag{4.16}$$

where $\hat{\boldsymbol{\Lambda}}_{\tilde{\epsilon}}^{(+)} = (\mathrm{I}_{\Psi} - \mathrm{diag}\{\mathbf{e}_k\}) \otimes \mathbf{h}_{\tilde{\epsilon}}\mathbf{h}_{\tilde{\epsilon}}^{H}$, $\forall \tilde{\epsilon} \in \mathcal{Z}_{Z+1}$, with $k \in \{1, \ldots, \Psi\}$. By adding the slack penalties $\mathbf{v} \in \mathbb{R}_{(Z+2)}^{+}$, the QCQP problem in $(P1)$ can be approximated as follows

$$(P3): \min_{r, \mathbf{w}_{\mathrm{tot}}, \mathbf{v}} \; r + \lambda||\mathbf{v}|| \tag{4.17}$$

$$\text{s.t. } (C1): \mathbf{w}_{\mathrm{tot}}^{H}\boldsymbol{\Lambda}_{i}^{(+)}\mathbf{w}_{\mathrm{tot}} + 2\mathrm{Re}\{\boldsymbol{\omega}^{(j)H}\boldsymbol{\Lambda}_{i}^{(-)}\mathbf{w}_{\mathrm{tot}}\}$$
$$-\boldsymbol{\omega}^{(j)H}\boldsymbol{\Lambda}_{i}^{(-)}\boldsymbol{\omega}^{(j)} \leq -\gamma_i(\sigma_{R,i}^{2} + \sigma_{D,i}^{2}) + \mathrm{v}_{\mathcal{I}},$$
$$\begin{cases} \text{SMEP}: \; \forall i \in \mathcal{Z}_k, \; \forall k \in \{1, \ldots, Z\}, \\ \qquad\qquad \forall \ell \in \{1, \ldots, Z+1\}, \\ \text{JMEP}: \; \forall i \in \mathcal{Z}_k, \; \forall k \in \{1, \ldots, Z\}, \\ \qquad\qquad \forall \ell \in \{1, \ldots, Z\}, \\ \text{PIEP}: \quad \forall i, \forall k, \forall \ell \in \{1, \ldots, L\}, i = k, \end{cases}$$
$$\mathcal{I} \in \{1, \ldots, Z\}, \tag{4.18}$$

$$(C2): \zeta_{\tilde{\epsilon}}\Big[\boldsymbol{\omega}^{(j)H}\boldsymbol{\Lambda}_{\tilde{\epsilon}}^{(-)}\boldsymbol{\omega}^{(j)} - 2\mathrm{Re}\{\boldsymbol{\omega}^{(j)H}\boldsymbol{\Lambda}_{\tilde{\epsilon}}^{(-)}\mathbf{w}_{\mathrm{tot}}\}$$
$$-\mathbf{w}_{\mathrm{tot}}^{H}\hat{\boldsymbol{\Lambda}}_{\tilde{\epsilon}}^{(+)}\mathbf{w}_{\mathrm{tot}} + \sigma_{R,\tilde{\epsilon}}^{2}\Big] \geq \xi'_{\tilde{\epsilon}} - \mathrm{v}_{Z+1},$$
$$\forall \tilde{\epsilon} \in \mathcal{Z}_{Z+1}, \tag{4.19}$$

$$(C3): \mathbf{w}_{\mathrm{tot}}^{H}\mathbf{w}_{\mathrm{tot}} \leq r + \mathrm{v}_{Z+2}, \tag{4.20}$$

where $r \in \mathbb{R}^{+}$, $\lambda \in \mathbb{R}$ is a fixed input parameter and $\boldsymbol{\omega}^{(j)}$ is the j^{th} instance of the introduced auxiliary variable. Herein, $(P3)$ is a convex QCQP and can be solved via well-known convex optimization techniques [224]. Similar to FPP-SCA as in [230], $(P3)$ is solved with starting point selection as $\boldsymbol{\omega}^{(j+1)} = \mathbf{w}_{\mathrm{tot}}^{(j)}$ in each instance of the FPP-SCA-e algorithm. This iterative process is repeated until guaranteed convergence [229,230]. The convergence proof is straightforward. Since the modification to the problem is treated in the same way, i.e., eigenvalue separation; there is no change in the behavior of FPP-SCA-e technique with respect to the original FPP-SCA.

Technique / ξ_i	SDP	FPP-SCA-e	FPP-SCA-e$^+$
1 μJ	10.6347 dBW	10.1224 dBW	9.4784 dBW
2 μJ	13.6151 dBW	12.8914 dBW	12.4496 dBW
3 μJ	15.3523 dBW	14.7874 dBW	14.0671 dBW
4 μJ	16.5805 dBW	15.7903 dBW	15.5425 dBW
5 μJ	17.5288 dBW	16.8827 dBW	16.4088 dBW

TABLE 4.2: Total Transmit Power for SMEP, optimized using SDP, SCA, and FPP-SCA-e$^+$ schemes, with $\gamma_i = 5$ dB and $M = 16$.

Technique / ξ_i	SDP	FPP-SCA-e	FPP-SCA-e$^+$
1 μJ	10.6347 dBW	9.8102 dBW	9.2665 dBW
2 μJ	13.6152 dBW	12.6895 dBW	12.3341 dBW
3 μJ	15.3527 dBW	14.8355 dBW	14.0506 dBW
4 μJ	16.5805 dBW	15.7481 dBW	15.4584 dBW
5 μJ	17.5288 dBW	16.7515 dBW	16.3696 dBW

TABLE 4.3: Total Transmit Power for JMEP, optimized using SDP, SCA, and FPP-SCA-e$^+$ schemes, with $\gamma_i = 5$ dB and $M = 16$.

4.3.3 Analysis of Computation Complexity

Assume that the CVX solver encounters the computation complexities of $\nu(\Psi, M, \gamma_i, \xi_i)$ orders for yielding a solution corresponding to $(P2)$. Therefore, the computational complexities for SMEP, JMEP, and PIEP are respectively given by $\mathcal{O}\Big(((Z+1)^3 \cdot Z^2 \cdot L^4)^{\nu(Z+1,M,\gamma_i,\xi_i)}\Big)$, $\mathcal{O}\Big((Z^5 \cdot L^4)^{\nu(Z,M,\gamma_i,\xi_i)}\Big)$, and $\mathcal{O}\Big((L^6 \cdot Z^3)^{\nu(L,M,\gamma_i,\xi_i)}\Big)$. More discussion is provided in the numerical results section.

To proceed, we consider the evaluation of the optimization problem with FPP-SCA-e method. Firstly, we focus on two different possibilities related to the initial point selection for $\boldsymbol{\omega}$ in the proposed method corresponding to $(P3)$. Let the starting point of $\boldsymbol{\omega}$ be denoted by $\widehat{\mathbf{w}}_{\text{tot}}$. The first possibility considers any random selection of $\widehat{\mathbf{w}}_{\text{tot}}$, which we term as FPP-SCA-e. Whereas for the second possibility, we provide the solution obtained via SDR as the input to $\widehat{\mathbf{w}}_{\text{tot}}$, which we refer to as FPP-SCA-e$^+$.

Next, we consider the computational complexities of the proposed techniques, wherein we present their run-time analysis in Table 4.1 using the tic-toc function in MATLAB R2017a, with all the reported values in seconds. On one hand, we observe that the execution time of SDP is faster than FPP-SCA-e for lower number of transmit antennas, in all the three scenarios. While on the other hand, significant run-time increment is seen in the case of SDP over FPP-SCA-e, for high number of transmit antennas. The FPP-SCA-e$^+$ technique relies on the starting point of SDP and thus behaves according to the execution times of both SDP and FPP-SCA-e. Specifically, the increased run-time for SDP ranges approximately between 150% and 200% (depending on the type of scheme chosen), whereas the increment in case of FPP-SCA-e is around 5% to 15% (for the three scenarios).

Finally, we compare the three methods, namely, SDP, FPP-SCA-e, and FPP-SCA-e$^+$ in Tables 4.2 and 4.3, respectively for the SMEP and JMEP scenarios. We find that the solution

via SDR is considered the best starting point for FPP-SCA-e, as also illustrated for similar method in [229]. Hence, we consider only SDP and FPP-SCA-e^{+} methods for further analysis in the numerical results section.

4.3.4 Motivation for an Alternative Problem Formulation

The results propound a strong motivation for the practical implementation of proposed framework. However, the possibility of a real-life application (from an indoor-environment perspective) is still doubtful. This is due to the presence of a very hard constraint on harvested energy, i.e., (4.11) and no limitation on the transmit power. Intuitively, the transmit power has to increase for higher demands of harvested energies. As a result, the total transmit power may not always be guaranteed to respect the Federal Communications Commission (FCC) regulations [231] in general. Therefore, this calls for an alternative formulation focusing on the maximization of the harvested energies of the intended users with a limitation on maximum transmit power, in addition to other necessary constraints. Such kind of problem is more suitable from application view-point as it is both safe and efficient for the users. In this vein, the relevant developments are outlined in the subsequent section.

4.4 Harvested Energy Maximization

We maximize the sum harvested energy by the intended users subjected to predefined SINR and EH constraints at the corresponding users/groups, and an upper limit on the total transmit power.

4.4.1 Problem Formulation and Solution

The overall optimization problem (encapsulating the three considered scenarios) to ensure the co-existence of the three user types in MG-MC precoding scheme can subsequently be written in its analytical form as follows

$$(P4): \max_{\{\mathbf{w}_k\}_{k=1}^{\Psi}} \sum_{\forall j \in \mathcal{Z}_{Z+1}} \mathcal{E}_j^{\mathcal{N}} \tag{4.21}$$

$$\text{s.t. } (C1): \frac{|\mathbf{w}_k^H \mathbf{h}_i|^2}{\sum_{\ell \neq k} |\mathbf{w}_\ell^H \mathbf{h}_i|^2 + \sigma_{R,i}^2 + \sigma_{D,i}^2} \geq \gamma_i,$$

$$\begin{cases} \text{SMEP}: \ \forall i \in \mathcal{Z}_k, \ \forall k \in \{1, \ldots, Z\}, \\ \qquad \forall \ell \in \{1, \ldots, Z+1\}, \\ \text{JMEP}: \ \forall i \in \mathcal{Z}_k, \ \forall k \in \{1, \ldots, Z\}, \\ \qquad \forall \ell \in \{1, \ldots, Z\}, \\ \text{PIEP}: \quad \forall i, \forall k, \forall \ell \in \{1, \ldots, L\}, i = k, \end{cases} \tag{4.22}$$

$$(C2): \mathcal{E}_j^{\mathcal{N}} \geq \xi_j, \ \ \forall j \in \mathcal{Z}_{Z+1}, \tag{4.23}$$

$$(C3): \sum_{k=1}^{\Psi} \mathbf{w}_k^H \mathbf{w}_k \leq \mathrm{P}_{\mathrm{Max}}, \tag{4.24}$$

where γ_i is the SINR threshold at the i^{th} user, ξ_j is the harvested energy demand at j^{th} user (where i can be equal to j for some cases[4], in general), $\mathrm{P}_{\mathrm{Max}}$ is the overall available transmit power. Since the problem in $(P4)$ involves a non-linear fractional program, it is non-convex and difficult to solve directly using conventional solvers. In addition, the feasibility of $(P4)$ is dependent on γ_i and ξ_i, which is constrained by the rank of $\mathbf{H}_i$ as well [223]. Moreover, unlike the previous problem in $(P2)$, it is difficult to transform the objective directly into a simpler form, even with the help of SDR. Herein, we intend to find a possibility for an equivalent CVX-solvable problem. In this regard, we propose to transform the fractional form objective function into a slack-variable replacement (SVR) form using the following proposition.

Proposition 1: The maximum achievable sum-harvested energy, $\sum_{\forall j\in\mathcal{Z}_{Z+1}} t_j^{\star}$, by the intended users can be obtained provided that

$$\begin{aligned}\max_{\widehat{\mathbf{w}}} \; & \sum_{\forall j\in\mathcal{Z}_{Z+1}} t_j \\ & = \sum_{\forall j\in\mathcal{Z}_{Z+1}} t_j^{\star} = \sum_{\forall j\in\mathcal{Z}_{Z+1}} \mathcal{E}_j^{\mathcal{N}}(\widehat{\mathbf{w}}^{\star}) \end{aligned} \tag{4.25}$$

for $t_j \geq \xi_j$ and $\mathcal{E}_j^{\mathcal{N}}(\widehat{\mathbf{w}}) \geq \xi_j$, where

$$\mathcal{E}_j^{\mathcal{N}}(\widehat{\mathbf{w}}) = \frac{\mathcal{E}'}{1-\varkappa} \cdot \left(\frac{1}{1+e^{(-\alpha(\sum_{k=1}^{\Psi} |\mathbf{w}_k^H \mathbf{h}_j|^2)+\alpha\beta)}} - \varkappa \right), \tag{4.26}$$

with $t_j^{\star}$, $\forall j \in \mathcal{Z}_{Z+1}$, denoting the optimal SVR-parameters, and $\widehat{\mathbf{w}}^{\star} = \{\mathbf{w}_k^{\star}\}_{k=1}^{\Psi}$ representing the set of precoders for the respective scenarios, obtained upon the convergence i.e., when the objective function achieves its maximum.

Proof: We first analyze the nature of the objective in $(P4)$, where we observe that the function is concave within the feasible regime. The corresponding proof is provided in Appendix D.2. Next, we assume that $(P4)$, i.e., [(4.21)-(4.24)], is a feasible problem and based on the prior findings, it is obvious that $(P4)$ involves maximization of a concave function subjected to non-linear constraints in (4.23) and (4.24). However, the corresponding constraint may be reduced to a simplified (convex) form with the use of adequate transformation or reduction, e.g., SDR. Thus $(P4)$ can subsequently be pared down into a standard convex form (after plausible transformations). Since the objective is a monotonically increasing function of the optimization variables, an optimal (local or global) solution is guaranteed within the feasible set of constraints. Therefore, assuming $\widehat{\mathbf{w}}^{\star}$ as the optimal set of precoders satisfying the requirements in $(P4)$, the maximum achievable (optimal) objective is given by $\sum_{\forall j\in\mathcal{Z}_{Z+1}} \mathcal{E}_j^{\mathcal{N}}(\widehat{\mathbf{w}}^{\star})$. ■

Proposition 1 provides an adequate and compulsory condition for developing the optimal resource allocation scheme. In particular, based on the original optimization problem with a fractional form-objective function, an equivalent optimization problem with an objective function based on SVR (e.g., $\sum_{\forall j\in\mathcal{Z}_{Z+1}} t_j$, s.t. $\mathcal{E}_j^{\mathcal{N}} \geq t_j$) can be found such that the same solution is achieved for both optimization problems. Moreover, it is explicit that the optimal solution is achieved with equality in (4.25), and thus we could use this equality condition to validate the optimality of the solution. Hence, rather than tackling the original fractional form-objective function, we develop an alternating algorithm for the equivalent SVR - objective function whilst meeting the conditions in *Proposition 1*. In this regard, we reformulate $(P4)$ with the help of SDR and *Proposition 1*, represented in its mathematical form as

[4]For users within an MC as well as the last group, i can be equal to j.

$$(P5): \max_{\substack{\{\mathbf{W}_k\}_{k=1}^{\Psi} \\ \{t_j\}_{\forall j \in \mathcal{Z}_{Z+1}}}} \sum_{\forall j \in \mathcal{Z}_{Z+1}} t_j \tag{4.27}$$

$$\text{s.t. } (C1): \mathrm{Tr}\{\mathbf{H}_i \mathbf{W}_k\} - \gamma_i \sum_{\ell \neq k} \mathrm{Tr}\{\mathbf{H}_i \mathbf{W}_\ell\} \geq \gamma_i (\sigma_{R,i}^2 + \sigma_{D,i}^2),$$

$$\begin{cases} \text{SMEP}: \ \forall i \in \mathcal{Z}_k, \ \forall k \in \{1, \ldots, Z\}, \forall \ell \in \{1, \ldots, Z+1\}, \\ \text{JMEP}: \ \forall i \in \mathcal{Z}_k, \ \forall k \in \{1, \ldots, Z\}, \forall \ell \in \{1, \ldots, Z\}, \\ \text{PIEP}: \quad \forall i, \forall k, \forall \ell \in \{1, \ldots, L\}, i = k, \end{cases} \tag{4.28}$$

$$(C2): \frac{1}{1 + e^{(-\alpha(\sum_{k=1}^{\Psi} \mathrm{Tr}\{\mathbf{H}_j \mathbf{W}_k\}) + \alpha\beta)}} \geq t_j \left(\frac{1 - \varkappa}{\mathcal{E}'} \right) + \varkappa, \ \ \forall j \in \mathcal{Z}_{Z+1}, \tag{4.29}$$

$$(C3): t_j \geq \xi_j, \ \ \forall j \in \mathcal{Z}_{Z+1}, \tag{4.30}$$

$$(C4): \sum_{k=1}^{\Psi} \mathrm{Tr}\{\mathbf{W}_k\} \leq \mathrm{P}_{\mathrm{Max}}, \tag{4.31}$$

$$(C5): \mathbf{W}_k \succcurlyeq 0, \tag{4.32}$$

where t_j denotes the introduced intermediary slack-variable corresponding to the j^{th} user, $\forall j \in \mathcal{Z}_{Z+1}$, with other parameters having same definitions as described previously. Note that the non-convex constraint of $\mathrm{rank}(\mathbf{W}_k) = 1$ is dropped as a part of standard SDR procedure. Since the objective function in $(P5)$ is an affine[5] (or concave) function and the constraint set is also convex, the modified optimization problem in $(P5)$ is in the standard form of a convex programming problem that can be solved by standard numerical methods such as the interior-point method [232]. It is obvious that joint optimization of the involved parameters $\left(\{\mathbf{W}_k\}_{k=1}^{\Psi} \text{ and } \{t_j\}_{\forall j \in \mathcal{Z}_{Z+1}}\right)$ corresponding to $(C2) \cdots (C4)$ is difficult to realize using the CVX solver, in general. However, an iterative-based computation of parameters is possible to seek a suitable solution. Therefore, $(P5)$ can be successfully solved by the proposed convex programming based on an iterative method for maximization of harvested energy, as summarized in Algorithm 1. The pivotal stage for the proposed iterative method based solution is to develop an intermediate SVR-parameter update policy for solving the formulated problem. In order to understand the method behind the proposed alternating algorithm for harvested energy maximization, we subdivide it into two steps. In the first step (lines 3-9), we compute the precoder metrics $\{\mathbf{W}_k\}_{k=1}^{\Psi}$ for fixed values of $\{t_j\}_{\forall j \in \mathcal{Z}_{Z+1}}$, where any values are permissible, respectively, provided that $(P5)$ remains tractable. The corresponding optimized values of $\{\mathbf{W}_k\}_{k=1}^{\Psi}$ are then used in the second step of the algorithm (lines 10-17), where joint optimization of $\{t_j\}_{\forall j \in \mathcal{Z}_{Z+1}}$ is carried out. Upon the completion of the second step, the optimized values of $\{t_j\}_{\forall j \in \mathcal{Z}_{Z+1}}$ are fed again to the first step and this iterative process is repeated until the convergence of objective in $(P5)$. To proceed further, we propose the following proposition.

Proposition 2: For a given $\{t_j\}_{\forall j \in \mathcal{Z}_{Z+1}}$, the objective function (4.27) is affine in $\{\mathbf{W}_k\}_{k=1}^{\Psi}$.

Proof: From $(C2)$, and $(C3)$ of $(P5)$, it is clear that the objective is directly related to $\{\mathbf{W}_k\}_{k=1}^{\Psi}$. Therefore, each iterative computation of $\{\mathbf{W}_k\}_{k=1}^{\Psi}$ corresponding to $(C4)$ would affect $\{t_j\}_{\forall j \in \mathcal{Z}_{Z+1}}$. Based on the nature of $(P5)$, it is obvious that the objective is an increasing affine function which attains the maximum when equality in $(C4)$ is reached. The proof is straightforward from this analytical reasoning. ■

[5]Note that the sum of affine functions is an affine function. Additionally, an affine function is both convex as well as concave in nature [224]. Herein, it may be claimed that we tackle maximization of a concave function.

Algorithm 3 Iterative Algorithm for Harvested Energy Maximization

Initialize: $\{t_j\}_{\forall j \in \mathcal{Z}_{Z+1}}$, and ϵ' as the threshold limit;
REPEAT
  Given $\{t_j\}$, $\forall j$, solve (4.27)-(4.32) to obtain $\{\mathbf{W}_k(\bar{\bar{n}})\}_{k=1}^{\Psi}$;
  IF $(t_j(\bar{\bar{n}}) - t_j(\bar{\bar{n}}-1) \leq \epsilon')$ & $(\bar{\bar{n}} > 2)$
    Convergence_1 = **TRUE**;
    RETURN $\{\mathbf{W}_k^{\star}\}_{k=1}^{\Psi} = \{\mathbf{W}_k(\bar{\bar{n}}-1)\}_{k=1}^{\Psi}$, $t_j^{\star} = t_j(\bar{\bar{n}}-1)$;
  ELSE
    Convergence_1 = **FALSE**;
  END IF
  Given $\{\mathbf{W}_k(\bar{\bar{n}})\}_{k=1}^{\Psi}$, solve (4.27)-(4.32) to get $\{t_j(\bar{\bar{n}})\}_{\forall j \in \mathcal{Z}_{Z+1}}$;
  IF $(t_j(\bar{\bar{n}}) - t_j(\bar{\bar{n}}-1) \leq \epsilon')$ & $(\bar{\bar{n}} > 2)$
    Convergence_2 = **TRUE**;
    RETURN $t_j^{\star} = t_j(\bar{\bar{n}}-1)$, $\{\mathbf{W}_k^{\star}\}_{k=1}^{\Psi} = \{\mathbf{W}_k(\bar{\bar{n}}-1)\}_{k=1}^{\Psi}$;
  ELSE
    $t_j(\bar{\bar{n}}+1) = t_j(\bar{\bar{n}})$, $\forall j$, and $\bar{\bar{n}} = \bar{\bar{n}} + 1$;
    Convergence_2 = **FALSE**;
  END IF
UNTIL Convergence_1 = **TRUE** & Convergence_2 = **TRUE**.

To prove the convergence of the proposed SVR-based solution, we first prove that the corresponding slack-variable metric, $\{t_j\}_{\forall j \in \mathcal{Z}_{Z+1}}$, increases in each iteration. Then, we prove that if the number of iterations is large enough, then the SVR-parameters $\{t_j\}_{\forall j \in \mathcal{Z}_{Z+1}}$ converge to the optimal $\{t_j^{\star}\}_{\forall j \in \mathcal{Z}_{Z+1}}$ such that the optimality condition in *Proposition 2* is satisfied, i.e., $\sum_{\forall j \in \mathcal{Z}_{Z+1}} t_j^{\star} = \sum_{\forall j \in \mathcal{Z}_{Z+1}} \mathcal{E}_j^{\mathcal{N}}(\mathbf{W}^{\star})$. Let $\{\mathbf{W}_k(\bar{\bar{n}})\}_{k=1}^{\Psi}$ denote the precoder metrics in the $\bar{\bar{n}}$-th iteration. Suppose $t_j(\bar{\bar{n}}) \neq t_j^{\star}$ and $t_j(\bar{\bar{n}}+1) \neq t_j^{\star}$, $\forall j \in \mathcal{Z}_{Z+1}$, represent the SVR-values in the iterations $\bar{\bar{n}}$ and $\bar{\bar{n}}+1$, respectively. It is obvious from *Proposition 2* that $t_j(\bar{\bar{n}}) > 0$ and $t_j(\bar{\bar{n}}+1) > 0$ will hold and that $\sum_{\forall j \in \mathcal{Z}_{Z+1}} t_j(\bar{\bar{n}}+1) > \sum_{\forall j \in \mathcal{Z}_{Z+1}} t_j(\bar{\bar{n}})$. Therefore, we can show that as long as the number of iterations is large enough, $\sum_{\forall j \in \mathcal{Z}_{Z+1}} t_j(\bar{\bar{n}})$ will eventually approach the maximum and satisfy the optimality condition as stated in *Proposition 1*. However, the global optimality of the solution may not be guaranteed due to prior constraint relaxation according to SDR.

4.4.2 Power-Refinement Process

We observe that the solution obtained for $(P5)$ via CVX yields similar outcomes like the ones attained in the previous section. The JMEP and PIEP achieve rank-1 solutions for most of the experiments, however this outcome is not certain in general. The solutions corresponding to SMEP are indeed rank-1 for the MC group precoders, while multi-rank solutions are achieved for last group (with EH users). Again, this implicates that Z MC precoders would easily serve the ID users and the EH users will be aided with the help of rank($\mathbf{W}_{Z+1}$) precoders. From a hardware implementation perspective, such sub-optimal solution makes it difficult to ensure the practical tractability of SMEP system. Therefore, the Gaussian randomization technique [203] is employed to curtail the multi-ranked $\{\mathbf{W}_{Z+1}\}$ into a unit rank, which in-turn induces additional computational complexities. In order to ensure the optimality condition in *Proposition 2*, we first compute the individual directions using the eigen value decomposition (EVD) [228] or randomization technique (as above) [203] for Z MC precoders and use the randomization method for the precoder corresponding to

$\{\mathbf{W}_{Z+1}\}$. Then, the vector indicating the direction of k^{th} precoder is given by $\widetilde{\mathbf{w}}_k = \frac{\mathbf{w}_k}{||\mathbf{w}_k||_2}$. We reformulate $(P5)$ and obtain the problem $(P6)$, as follows

$$(P6): \max_{\substack{\{\mathrm{p}_k\}_{k=1}^{\Psi} \\ \{t_j\}_{\forall j \in \mathcal{Z}_{Z+1}}}} \sum_{\forall j \in \mathcal{Z}_{Z+1}} t_j \tag{4.33}$$

$$\text{s.t. } (C1): |\widetilde{\mathbf{w}}_k^H \mathbf{h}_i|^2 \mathrm{p}_k - \gamma_i \sum_{\ell \neq k} |\widetilde{\mathbf{w}}_\ell^H \mathbf{h}_i|^2 \mathrm{p}_\ell \geq \gamma_i(\sigma_{R,i}^2 + \sigma_{D,i}^2),$$

$$\begin{cases} \text{SMEP}: \ \forall i \in \mathcal{Z}_k, \ \forall k \in \{1,\ldots,Z\}, \\ \qquad\qquad \forall \ell \in \{1,\ldots,Z+1\}, \\ \text{JMEP}: \ \forall i \in \mathcal{Z}_k, \ \forall k \in \{1,\ldots,Z\}, \\ \qquad\qquad \forall \ell \in \{1,\ldots,Z\}, \\ \text{PIEP}: \quad \forall i, \forall k, \forall \ell \in \{1,\ldots,L\}, i = k, \end{cases} \tag{4.34}$$

$$(C2): \frac{1}{1 + e^{(-\alpha(\sum_{k=1}^{\Psi} |\widetilde{\mathbf{w}}_k^H \mathbf{h}_j|^2 \mathrm{p}_k) + \alpha\beta)}} \geq t_j\left(\frac{1-\varkappa}{\mathcal{E}'}\right) + \varkappa, \ \forall j \in \mathcal{Z}_{Z+1}, \tag{4.35}$$

$$(C3): t_j \geq \xi_j, \ \forall j \in \mathcal{Z}_{Z+1}, \tag{4.36}$$

$$(C4): \sum_{k=1}^{\Psi} \mathrm{p}_k \leq \mathrm{P}_{\text{Max}}, \tag{4.37}$$

$$(C5): \mathrm{p}_k \geq 0, \tag{4.38}$$

where p_k is the power term associated to the k^{th} precoder with $\widetilde{\mathbf{w}}_k$ as its direction, and other terms have the same meaning as defined previously. In other words, the scalar p_k is optimized in the direction of $\widetilde{\mathbf{w}}_k$. Thereafter, the solution to $(P5)$ can be obtained directly using the CVX solver, which is summarized in Algorithm 2. Consequently, Directional Power Maximization Algorithm (DPMA) ensures that the optimality condition in *Proposition 2* is always satisfied with rank-1 solutions for all precoders. Consequently, the proof of convergence of Algorithm 2 would follow the same process as presented in the previous section. From the programming viewpoint, the convergence of Algorithm 1 and Algorithm 2 could be determined by setting an extremely low threshold value (say ϵ'), such that the stopping criteria is defined by $\sum_{\forall j \in \mathcal{Z}_{Z+1}} t_j(\bar{\bar{n}}+1) - \sum_{\forall j \in \mathcal{Z}_{Z+1}} t_j(\bar{\bar{n}}) \leq \epsilon'$.

4.4.3 Computational Complexity Analysis

Suppose that the CVX solver incurs the computational complexities of $\kappa_1(\Psi, M)$ orders for carrying out the operations 4: to 9:, and $\kappa_2(M)$ orders to process 11: to 17:, respectively, corresponding to Algorithm 1, and linear orders for Algorithm 2. Consequently, the overall computation complexities for SMEP, JMEP, and PIEP are respectively

$\mathcal{O}\left(\left(\left(L^5 \cdot (Z+1)^3 \cdot Z^2\right)^{\left(\kappa_1(Z+1,M)+\kappa_2(M)\right)}\right)^{\chi(\tilde{n},\gamma_i,\xi_i)}\right)$, $\mathcal{O}\left(\left(\left(L^5 \cdot Z^6\right)^{\left(\kappa_1(Z,M)+\kappa_2(M)\right)}\right)^{\chi(\tilde{n},\gamma_i,\xi_i)}\right)$, and

$\mathcal{O}\left(\left(\left(L^7 \cdot Z^2\right)^{\left(\kappa_1(L,M)+\kappa_2(M)\right)}\right)^{\chi(\tilde{n},\gamma_i,\xi_i)}\right)$, where $\chi(\tilde{n},\gamma_i,\xi_i)$ denotes the factor dependent on

Algorithm 4 Directional Power Maximization Algorithm (DPMA)

Initialize: $\{t_j\}_{\forall j \in \mathcal{Z}_{Z+1}}$, $\{\widetilde{\mathbf{w}}_k\}_{k=1}^{\Psi}$, and ϵ';
REPEAT
  Given $\{t_j\}$, $\forall j$, solve (4.33)-(4.38) to obtain $\{\mathrm{p}_k(\bar{\bar{n}})\}_{k=1}^{\Psi}$;
  IF $(t_j(\bar{\bar{n}}) - t_j(\bar{\bar{n}}-1) \leq \epsilon')$ & $(\bar{\bar{n}} > 2)$
    Convergence_1 = **TRUE**;
    RETURN $\{\mathrm{p}_k^{\star}\}_{k=1}^{\Psi} = \{\mathrm{p}_k(\bar{\bar{n}}-1)\}_{k=1}^{\Psi}$, $t_j^{\star} = t_j(\bar{\bar{n}}-1)$;
  ELSE
    Convergence_1 = **FALSE**;
  END IF
  Given $\{\mathrm{p}_k(\bar{\bar{n}})\}_{k=1}^{\Psi}$, solve (4.33)-(4.38) to get $\{t_j(\bar{\bar{n}})\}_{\forall j \in \mathcal{Z}_{Z+1}}$;
  IF $(t_j(\bar{\bar{n}}) - t_j(\bar{\bar{n}}-1) \leq \epsilon')$ & $(\bar{\bar{n}} > 2)$
    Convergence_2 = **TRUE**;
    RETURN $t_j^{\star} = t_j(\bar{\bar{n}}-1)$, $\{\mathrm{p}_k^{\star}\}_{k=1}^{\Psi} = \{\mathrm{p}_k(\bar{\bar{n}}-1)\}_{k=1}^{\Psi}$;
  ELSE
    $t_j(\bar{\bar{n}}+1) = t_j(\bar{\bar{n}})$, $\forall j$, and $\bar{\bar{n}} = \bar{\bar{n}} + 1$;
    Convergence_2 = **FALSE**;
  END IF
UNTIL Convergence_1 = **TRUE** & Convergence_2 = **TRUE**.

$\tilde{n}$ iterations of algorithm(s), γ_i and ξ_i, corresponding to each of the respective scenarios. We demonstrate the effectiveness of proposed methods in the following section.

4.5 Simulation Results

In this section, we present a comparative study between SMEP, JMEP and PIEP. The three cases viz-a-viz., SMEP, JMEP, and PIEP are implemented using MATLAB R2017a, with optimization performed via convex programming tool CVX [225, 226], and the solutions obtained with the help of SEDUMI solver.

4.5.1 Simulation Environment

We assume an ITU-R indoor model (2-floor office scenario) [193] to generate channel realizations with the path-loss exponent given by

$$\mathrm{PL\ (in\ dB)} = 20\log_{10}(\hat{F}) + \hat{N}\log_{10}(\hat{D}) + P_f(\hat{n}) - 28, \tag{4.39}$$

where $\hat{F}$ is the operational frequency (in MHz), $\hat{N}$ is the distance power loss coefficient, $\hat{D}$ is the separation distance (in metres) between the transmitter and end-user(s) (with $\hat{D} >$ 1m), $P_f(\hat{n}) = 15 + 4(\hat{n}-1)$ is the floor penetration loss factor (in dB), and $\hat{n}$ is the number of floors between the transmitter and the end-user(s) (with $\hat{n} \geq 0$). Specifically, the chosen parametric values are $\hat{F} = 2.4$ GHz, $\hat{D}$ is randomly chosen between 4m and 5m (unless specified otherwise), $\hat{N} = 30$, and $P_f(2) = 19$ dB. It is noteworthy that the channel state information (CSI) will not be affected largely, due to the assumption of an indoor scenario . Moreover, the CSI loops within the coherence time of the channel where the dynamic nature in CSI may be assumed to be introduced from the environment as well as user mobility in some way [193]. In this context, wider beam widths could be desirable from a signal reception point of view (due to mobility), while narrow beams might be better to control the interference.

The transmitter is assumed to be equipped with $M = 20$ antennas (unless specified otherwise), while $L = 10$ users are distributed within $(Z + 1) = 5$ groups as follows: $\mathcal{Z}_1 = \{D_1, D_3, D_4\}$, $\mathcal{Z}_2 = \{D_2, D_5\}$, $\mathcal{Z}_3 = \{D_6, D_8\}$, $\mathcal{Z}_4 = \{D_7, D_9, D_{10}\}$, and $\mathcal{Z}_5 = \{D_1, D_5, D_8, D_{10}\}$, where $\mathcal{Z}_5$ is the EH group of users while the remaining ($\mathcal{Z}_1$,..., $\mathcal{Z}_4$) MC groups are comprised of ID users. We set $\sigma^2_{R,i}$ = -110 dBW, $\sigma^2_{D,i}$ = -80 dBW and $\zeta_i = 0.6$. Furthermore, an average of 500 random channel realizations (with random placement of end-users in every realization) is presented for each experiment corresponding to the transmit power minimization problem, while an average of 100 experiments is performed to analyze the harvested energy maximization problem. The constants corresponding to the non-linear EH circuit are chosen as $\mathcal{E}' = 2.8$ mJ, $\alpha = 1500$, and $\beta = 0.0022$ [15, 222].

4.5.2 Discussion on Optimization Solutions

Before we provide detailed discussion on the optimization solutions, it is important to highlight the challenges related to the adoption of considered non-linear EH model in comparison to a linear EH scheme. Due to the introduction of a non-linear (exponential) function to characterize the EH operation, the traditional equations and definitions with linear form require alteration accordingly. With regard to the optimization problems, incorporation of the non-linear EH model leads to intractability which requires rigorous transformations and relaxations in comparison to the case with the linear EH model. Moreover, several challenges are encountered while seeking suitable solution(s) in this context. Specifically, the problems require adequate transformations to be solved by the convex optimization solvers (e.g., we use the CVX in this work, which requires a particular form of input problem formulation).

It has been shown in [233] that a solution pertaining to $\text{rank}(\mathbf{W}_k^\star) = 2$ can still be viewed as optimal. Furthermore, it can be reduced to $\text{rank}(\mathbf{W}_k^\star) = 1$ at an additional computation cost thereby penalizing the system performance and increasing the chance that not all constraints will be satisfied. Therefore, we consider the $\text{rank}(\mathbf{W}_k^\star) \leq 2$ solution as optimal. In other cases, i.e., for $\text{rank}(\mathbf{W}_k^\star) > 2$, the solution is considered sub-optimal with further scope of improvement.

In the context of both the energy optimization problems, i.e., total transmit power minimization (in $(P1)$) and sum-harvested energy maximization (in $(P4)$), it is found that the solutions of both JMEP and PIEP are indeed rank-1 for most of the experiments whereas such an outcome cannot be assured to be always true, in general. The solution corresponding to SMEP is found to be unit rank for lower values of SINR and harvested energy demands. Further, this effect seems to vanish with higher demands of SINR and harvested energy where multi-rank solutions are obtained for the last group (harvested energy serving precoders). One interpretation of multi-rank solution obtained for $\{\mathbf{W}_{Z+1}\}$ corresponding to the EH group implies that in order to serve EH specific users, more precoders $\Big(Z'$ in number(s), with $Z' = \text{rank}(\mathbf{W}_{Z+1})\Big)$ would be required. The ID users are served using the beams of corresponding Z MC precoders while the EH users utilize $\text{rank}(\mathbf{W}_{Z+1})$ precoders for collecting energy, which is sub-optimal and difficult to implement from a hardware perspective. Therefore, the randomization technique [203] is implemented to reduce the multi-rank solution for $\{\mathbf{W}_{Z+1}\}$ to a unit rank thereby introducing additional computational penalties while ensuring tractability in terms of hardware implementation. Another interpretation that the multi-rank solution suggests is to split the EH group into multiple groups, so that the energy can be better focused across the respective group channel vectors. However, it is noteworthy that the presence of energy-specific precoder for last group becomes redundant for very high demands of SINR,

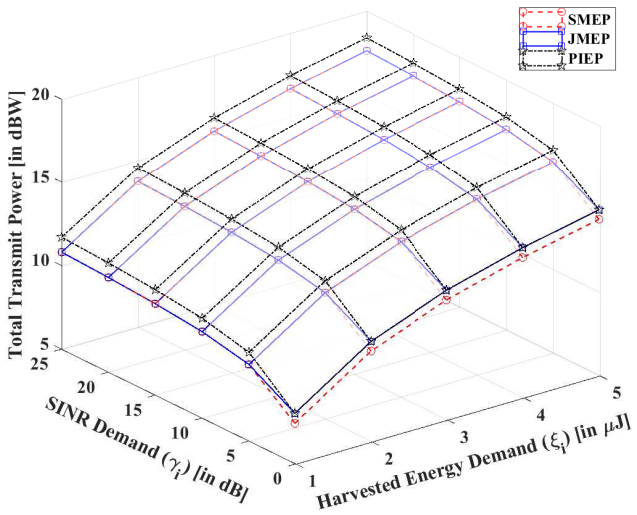

FIGURE 4.5: Performance analysis of SMEP, JMEP and PIEP via SDR, in terms of total transmit power versus the harvested energy demands and the SINR demands of users where $\hat{D}$ = 5m and M = 20.

where SMEP is found to yield similar performance as JMEP. Regarding the realization of algorithms in practical systems, offloading may be performed where the computation task is carried out by a centralized node [234, 235]. In this context, adequate signaling or feedback mechanism may be utilized by the central controller to inform the concerned nodes.

4.5.3 Numerical Analysis

In Fig. 4.5, we illustrate the effect on the total transmit power (in dBW) with increasing demand of the harvested energy and the SINR threshold with results obtained via SDR. Performance benefits of the proposed SMEP are seen over JMEP and PIEP, where SMEP is observed to perform best at low SINR and/or EH demands. Apparently, JMEP encounters a contradictory SINR-EH demand constraint at lower values of SINR demand which makes it difficult to attain optimal precoder designs. However, it is clear that the performance of SMEP and JMEP would converge together at higher SINR demand, where the contribution from energy-dedicated precoder in SMEP can be considered negligible. It is needless to mention that SMEP can successfully take care of distinct user types without any complications, while JMEP would require additional computation to categorize the EH users within the intended Z groups to ensure its efficient performance. In general, the total transmit power increases with higher demands of SINR and/or EH thresholds for all the three cases viz-a-viz., SMEP, JMEP, and PIEP.

Fig. 4.6 shows the variation in total transmit power (in dBW) with increasing number of array antennas at the transmitter for $\gamma_i = 5$ dB and $\xi_i = 1$ μJ, where the results are obtained via SDR. Herein, we compare the proposed SMEP with the two benchmarks JMEP and PIEP, respectively. It is observed that the system performance for all the scenarios improves considerably in terms of the total transmit power with increasing number of transmit array antennas, where SMEP is seen to perform the same as JMEP, while both SMEP and JMEP outperforms PIEP. Furthermore, a similar trend is observed when the distance between the transmitter and end-users is increased with the placement in between $\hat{D}$ = 6.5m and $\hat{D}$ =

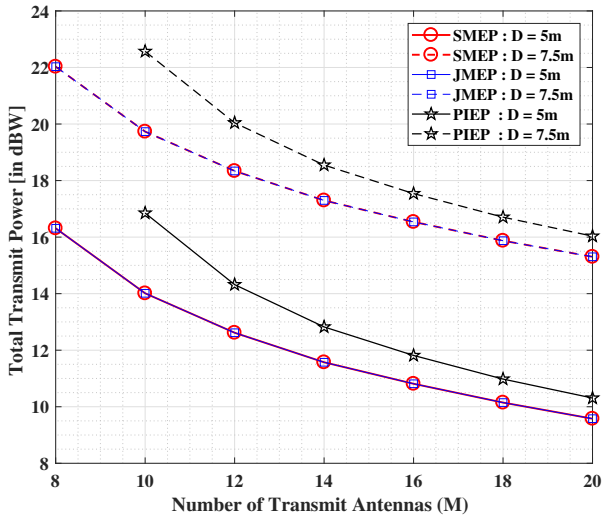

FIGURE 4.6: Performance analysis of SMEP, JMEP and PIEP in terms of total transmit power versus the number of transmit antennas via SDR, with variation in distance where $\gamma_i = 5$ dB and $\xi_i = 1$ μJ.

7.5m. However, an expected increase in the total transmit power is also observed in this case. It is also noteworthy that JMEP and SMEP are operational even with lower number of transmit array antennas in comparison to the number of end-users while the former (number of transmit array antennas) should be equal or greater than the latter (number of end-users) to ensure operability of PIEP.

Considering the case where the impact on the scenarios with respect to the number of users, it is noteworthy that the SINR and EH demands in Fig. 4.5 may be synonymously translated into the number of users. In simple terms, this duality with more number of users would correspond to high SINR and EH demands and vice-versa. It is observed that the total transmit power increases or decreases with the increase or decrease in number of users, respectively. Regarding the number of antennas, it is observed from Fig. 4.6 that increasing number of antennas would facilitate the users with optimized transmit power at the the precoders. Therefore, similar trend should be observed as above, where more number of antennas would be beneficial in terms of improving the system performance(s).

Herein, we present the results obtained via numerical experiments for the proposed FPP-SCA-e$^+$. In comparison with [230] and [229], we consider a more practical channel model whereas the problem formulated in this work involves an additional EH constraint. Based on the experimental findings, we set $\lambda = 10^{12}$ for FPP-SCA-e$^+$, and $\lambda = 10^{15}$ for FPP-SCA-e. These values are chosen to ensure the feasibility of considered problem in $(P3)$, and to force the slack variables in $\mathbf{v}$ towards zero. Specifically, with the considered channel model, and given that γ_i and ξ_i are both non-zeros, we propose to choose $\lambda \geq 1/\Big(\min(\gamma_i/1\text{dB}, \xi_i/1\text{J})\Big)^2$.

In Fig. 4.7, we investigate the performances of the three scenarios, namely, SMEP, JMEP, and PIEP, wherein the effect of increasing SINR demands on the total transmit power is examined for fixed $\xi_i = 2.5$ μJ. We observe that the total transmit power increases with growing SINR demands, for all the three above-mentioned secenarios. In addition, the proposed FPP-SCA-e$^+$ method provides a better estimate to the total transmit power in comparison to SDP.

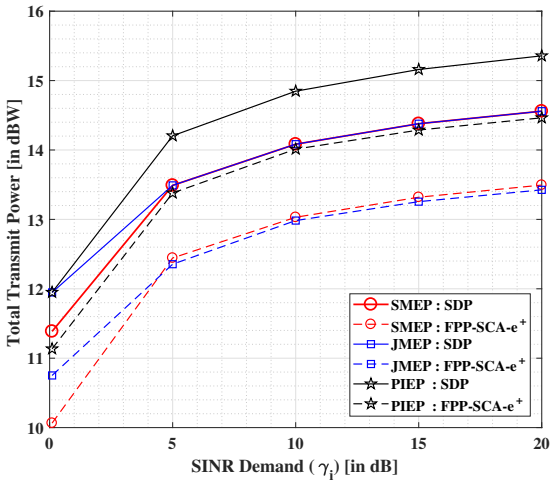

FIGURE 4.7: Total transmit power versus the SINR demands at the users with SDP and FPP-SCA-e$^+$ techniques, where $\xi_i = 2.5\mu$J.

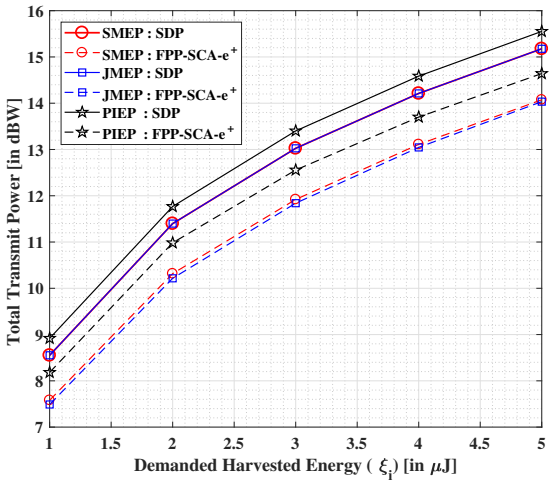

FIGURE 4.8: Total transmit power versus the harvested energy demands at the users with SDP and FPP-SCA-e$^+$, where $\gamma_i = 1$ dB.

As noticed via both SDP and FPP-SCA-e$^+$ techniques, SMEP is found to perform better than JMEP in the low-SINR regimes while JMEP shows marginal advantages over SMEP in higher SINR regions. However, both JMEP and SMEP are seen to outperform PIEP in terms of total transmit power optimization for increasing SINR demands.

In Fig. 4.8, we present the impact on the total transmit power with increasing values of EH demands, where $\gamma_i = 1$ dB. The objective is seen to increase with growing EH demands for all the three considered scenarios, viz., SMEP, JMEP, and PIEP. The performances of SMEP and JMEP are found to be considerably better in comparison to PIEP, for both SDP and FPP-SCA-e$^+$ techniques. The optimized values of total transmit powers are nearly same

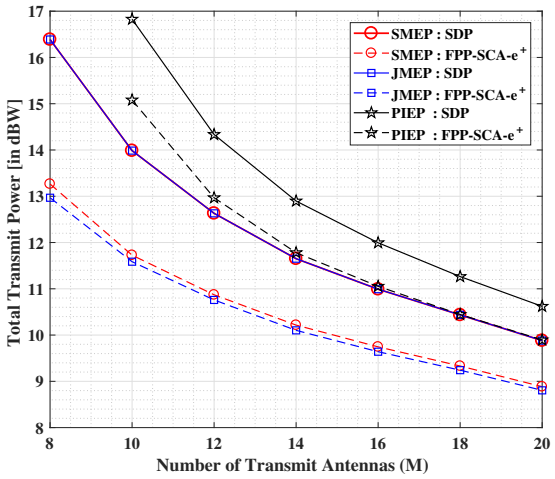

FIGURE 4.9: Total transmit power versus number of antennas, using SDP and FPP-SCA-e$^+$ techniques, with $\gamma_i = 5$ dB and $\xi_i = 1\mu$J.

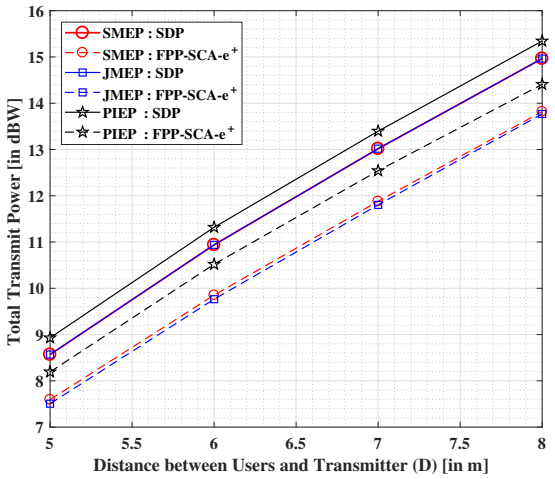

FIGURE 4.10: Total transmit power versus the distance between the users and transmitter, with $\gamma_i = 1$ dB and $\xi_i = 1\mu$J.

for SMEP and JMEP in case of SDP. However, JMEP is observed to perform slightly better than SMEP in terms of transmit power optimization via FPP-SCA-e$^+$ method, for increasing EH demands.

Fig. 4.9, shows the result of increasing the number of transmit antennas on the total optimized transmit power for $\gamma_i = 5$ dB and $\xi_i = 1$ μJ. A general decreasing trend of total transmit power is observed from both SDP and FPP-SCA-e$^+$ techniques for growing number of antennas, with latter (FPP-SCA-e$^+$) providing better solutions in comparison to the former (SDP). From an overall performance perspective, both JMEP and SMEP outperforms PIEP. However, similar outcomes are obtained for JMEP and SMEP through SDP, while JMEP is

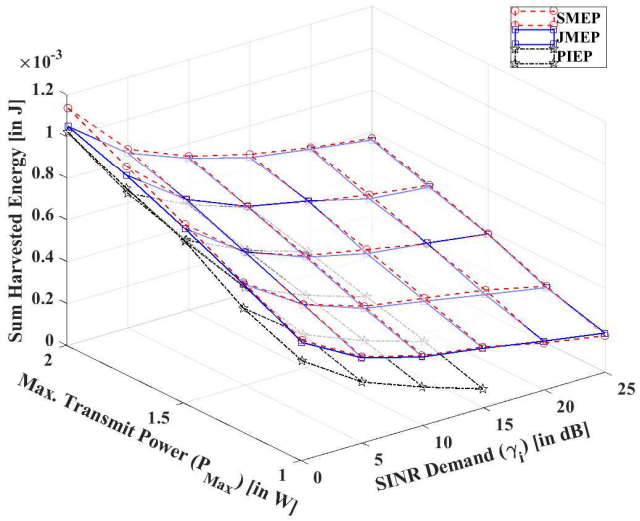

FIGURE 4.11: Performance analysis of SMEP, JMEP and PIEP in terms of sum-harvested energy versus the maximum transmit power limits and variation in the SINR of users with $\xi_i = 10$ nJ.

found to perform marginally better than SMEP. This marginal effect is due to the presence of an extra precoder in SMEP over JMEP.

We depict in Fig. 4.10 the performance analysis of the three scenarios (SMEP, JMEP and PIEP) in terms of total transmit power against increasing distance between the transmitter and users, with $\gamma_i = 1$ dB and $\xi_i = 1$ μJ. Please note that any point corresponding to $(\hat{D})$ on the x-axis portrays the result for random arrangements of each user between $(\hat{D})$ and $(\hat{D}-1)$ for each instance of the experimental realizations. The total transmit power escalates significantly with increasing values of distances between the transmitter and users. Similar as above, we find that the SMEP and JMEP systems exceed over PIEP for both SDP and FPP-SCA-e$^+$ techniques. A slender gap is observed between the performances of SMEP and JMEP in case of FPP-SCA-e$^+$ technique while both shows identical performances with SDP.

In Fig. 4.11, we present the impact on the sum-harvested energy (in Joules) with increasing SINR threshold and maximum power limitations with $\xi_i = 10$ nJ. The objective increases with rising values of maximum transmit power limitations while it is seen to decrease with growing SINR demands for all the three scenarios namely SMEP, JMEP and PIEP. Both SMEP and JMEP are found to provide superior performances over PIEP, with SMEP operating nearly same as JMEP at lower $\mathrm{P_{Max}}$ values and higher SINR demands. However, the efficiency of SMEP is significantly higher than JMEP at higher values of $\mathrm{P_{Max}}$ and SINR demands. In addition, PIEP is found to approach an infeasible regime at higher values of SINR demands (for most of the experiments) and thus the results appear to terminate at $\gamma_i = 15$ dB. Moreover, it is noteworthy that the working characteristic of SMEP is naturally viable to take care of separate information and/or energy users more competently in comparison to JMEP and PIEP, with a remarkable performance.

Fig. 4.12 depicts the variation in sum-harvested energy (in Joules) with increasing number of transmit antenna arrays with $\gamma_i = 1$ dB, $\xi_i = 1$ nJ and $\mathrm{P_{Max}} = 1.5$ W. It is seen that SMEP provides better performance in comparison to JMEP and PIEP, where the objective

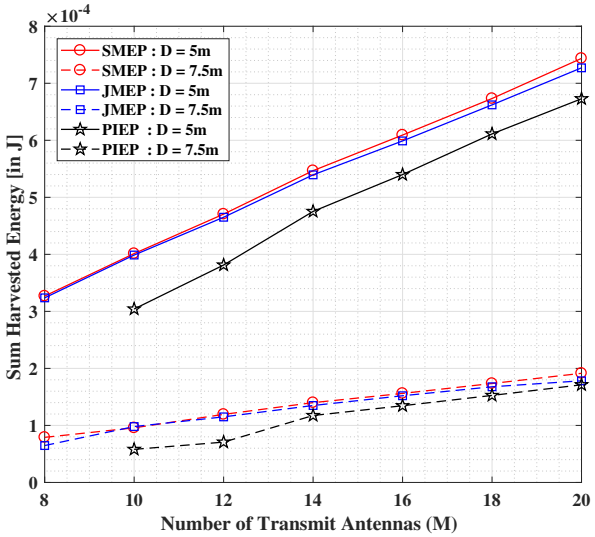

FIGURE 4.12: Performance analysis of SMEP, JMEP and PIEP in terms of sum harvested energy versus the number of transmit antennas with variation in distance where $\gamma_i = 1$ dB, $\xi_i = 1$ nJ and $\mathrm{P_{Max}} = 1.5$ W.

increases appreciably with growing number of antennas. Similar trend is observed when the designated users are placed randomly between $\hat{D} = 6.5$m and $\hat{D} = 7.5$m, from the ULA-equipped transmitter. As noticed previously, SMEP and JMEP are functional even at lower number of antennas in comparison to the number of users, while the minimum number of antennas should atleast be same as the number of users for PIEP to be operational.

In this direction, it is important to discuss about the system performance with varying number of users. As mentioned previously, the duality between the user demands and the number of users may be assumed. In this regard, the results from Fig. 4.11 indicate that for a fixed number of transmit antennas, the sum-harvested energy would decrease or increase with growing or depreciating number of users (synonymous with SINR and EH demands). Whereas, the results in Fig. 4.12 shows the benefits of increasing the number of antennas on system performance under a specific transmit power limitation. Moreover, the number of heterogeneous user types and their placement would also affect the overall performance corresponding to the maximization of sum-harvested energy by the intended users.

Next, we set $\gamma_i = 0.1$ dB, $\xi_i = 1$ μJ in Fig. 4.13 and $\gamma_i = 0.1$ dB, $\xi_i = 1$ nJ and $\mathrm{P_{Max}} = 1.5$ W in Fig. 4.14, and consider any random realization of $\mathbf{h}_i$, to investigate the effectiveness of the exclusive precoder in SMEP designated to serve the group of EH users in comparison to the JMEP and PIEP scenarios, corresponding to the two energy optimization problems in (4.6) and (4.21), respectively. Herein, we consider two experiments to study the problems on energy optimization more keenly. In the first test, we assume that the inequality in the SINR constraint i.e., $(C1)$ of all the formulated problems $(P1)$, $(P2)$, $(P4)$, $(P5)$, $(P6)$ holds; which we refer to as the flexible (Flexi) form of the problem since there is no hard boundation on the computed SINR and each user may obtain equal to or more than the demanded SINR threshold. Whereas in the other (second) test, we consider that a strict equality (Str-Eq) holds in $(C1)$ of $(P1)$, $(P2)$, $(P4)$, $(P5)$, $(P6)$, meaning that each user will be provided neither more nor less, but equal to the exact SINR demand. Before we

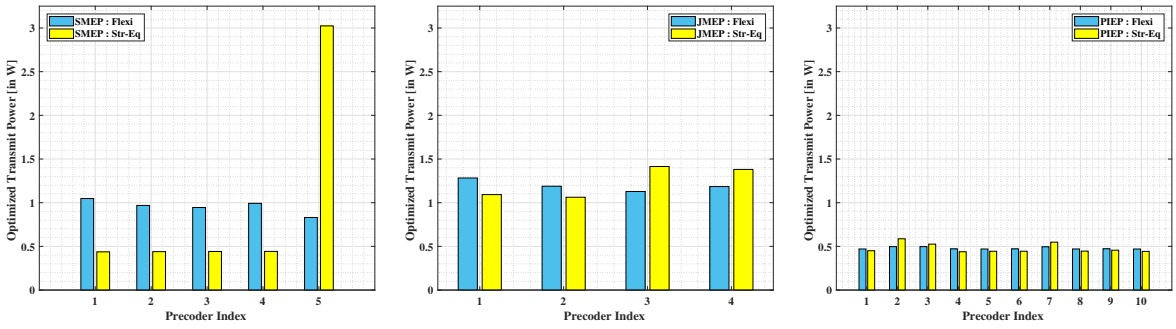

(a) (b) (c)

FIGURE 4.13: Optimized transmit power of the precoders via SDR, following the total transmit power minimization problem for (a) SMEP, (b) JMEP and (c) PIEP.

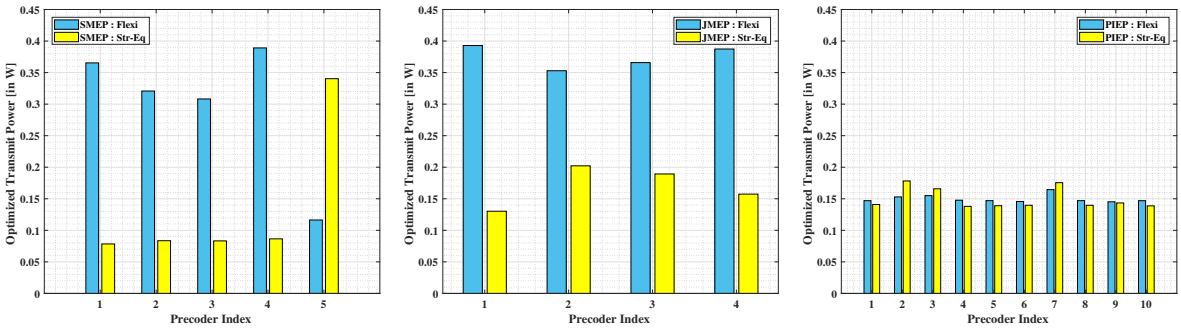

(a) (b) (c)

FIGURE 4.14: Optimized transmit power of the precoders via SDR, following the sum-harvested energy maximization problem for (a) SMEP, (b) JMEP and (c) PIEP.

proceed, it is important to mention that all the prior simulation results were obtained via first experiment trial (which is more general from practical perspective). From our previous observations in the performance analysis of SMEP, JMEP and PIEP, we find that the main investigation lies in the low SINR demand regime, where the impact of the precoder for energy group in SMEP is maximum.

Considering the total transmit power minimization problem, we show in Fig. 4.13 the comparison between the three considered schemes namely, SMEP, JMEP and PIEP. As discussed above, we perform the evaluation over the two experiments viz., Flexi and Str-Eq. The significance of the exclusive precoder in SMEP corresponding to the group of EH users is explicitly visible (with reference to Precoder Index = 5) in Fig. 4.13(a), when compared with JMEP in Fig. 4.13(b) and PIEP in Fig. 4.13(c). From the outcomes of the two experiments in all cases, we find that the exclusive precoder in SMEP corresponding to the group of EH users becomes more significant in terms of reducing the complexity in power allocations at the stipulated precoders. Whereas the other systems (JMEP and PIEP) require more transmit power to take care of the contradictory constraints of low SINR and high EH demands at the corresponding users.

In Fig. 4.14, we consider the problem of sum-harvested energy to illustrate the comparison between SMEP (in Fig. 4.14(a)), JMEP (in Fig. 4.14(b)) and PIEP (in Fig. 4.14(c)) for a

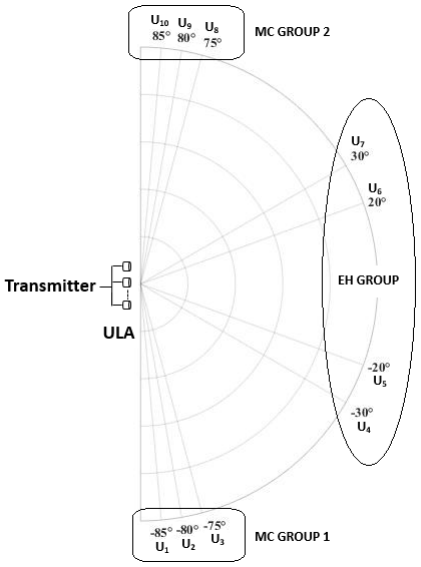

FIGURE 4.15: User placing within groups, served via ULA-equipped transmitter.

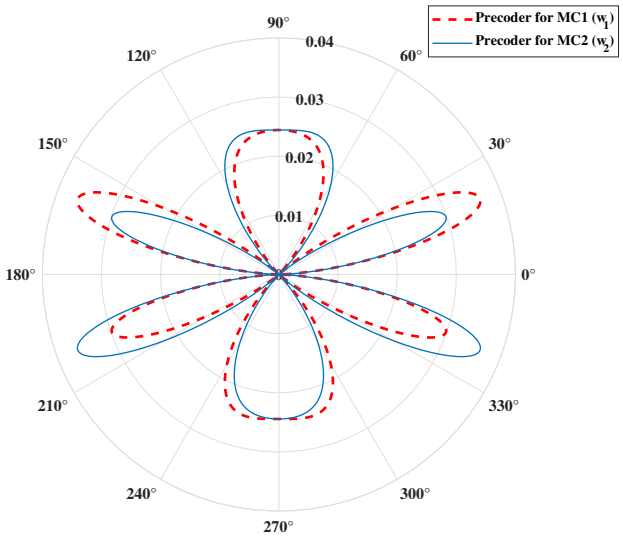

FIGURE 4.16: Antenna radiation beam pattern for JMEP.

fixed maximum transmit power limitation of $P_{Max} = 1.5$ W. The results are obtained after the two experiments (Flexi and Str-Eq., respectively), are performed for the aforementioned three schemes. Herein, we observe similar outcomes like in the above-mentioned analysis, indicating the benefits of adopting an exclusive precoder in SMEP for the group of EH users, over JMEP and PIEP schemes in the low SINR and high EH demand regimes.

4.5.4 Further Investigation via Uniform Linear Arrays

In this section, we consider a more generalized line-of-sight (LoS)-based channel model in comparison to the previous cases, for investigating the performances of SMEP and JMEP

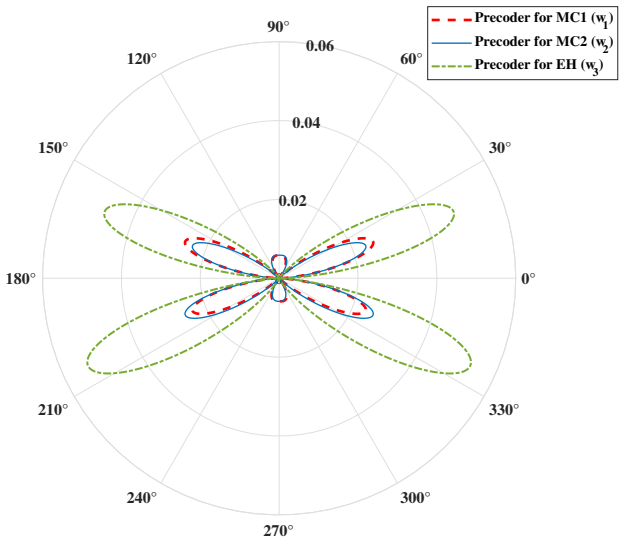

FIGURE 4.17: Antenna radiation beam pattern for SMEP.

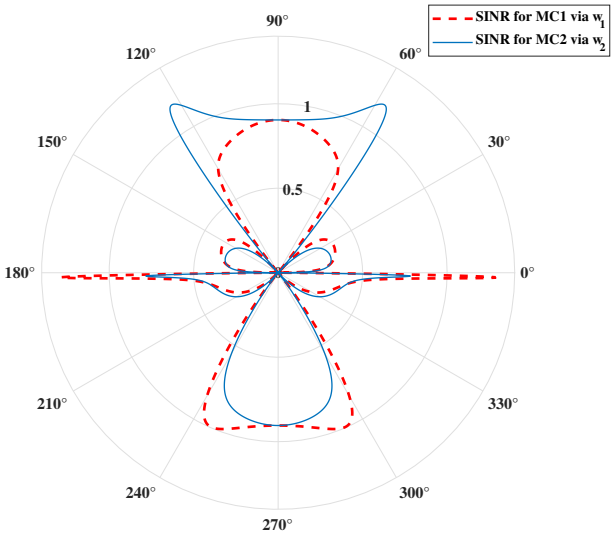

FIGURE 4.18: SINR pattern of MC precoders in SMEP.

further. Herein, we assume a scenario similar to 802.11 frameworks [236] (e.g., 802.11b), where the bandwidth is considered to be 20 MHz with an operational frequency of 2.4 GHz. A uniform linear arrays (ULAs)-based transmitter is presumed for investigating the proposed methods in a practically motivated environment. Please note that in this case, an antenna gain of 10 dB is also taken into consideration, along with (4.39). The corresponding $M \times 1$ complex vectors indicating the phase shift from each element of transmit antenna array to the receive antenna of i^{th} user, where $i \in \{1, \ldots, L\}$, are Vandermonde

$$\mathbf{v}(\varphi_i) = [1 \quad e^{\iota\varphi_i} \quad e^{\iota 2\varphi_i} \quad \ldots \quad e^{\iota(M-1)\varphi_i}]^T, \tag{4.40}$$

where $\varphi_i = -2\pi\hat{d}\sin(\theta_i)/\hat{\lambda}$, and $\iota = \sqrt{-1}$. Herein, $\hat{d}$ denotes the spacing between successive antenna elements, $\hat{\lambda}$ is the carrier wavelength, and the angles θ_i (in radians) define the direction of the i^{th} user from the transmitter. Assume $\mathbf{\Pi}_i$ as the $M \times 1$ scalar vector indicating the path loss from M transmit (ULA) antennas to the i^{th} user modeled according to (4.39). Then, the equivalent channel vector for the i^{th} user is given by $\mathbf{h}_i = \mathbf{v}(\varphi_i) \odot \mathbf{\Pi}_i$, where $\odot$ denotes the Hadamard product. Note that the phase orientation of ULA set-up must be unaffected due to this operation.

The transmitter is assumed to be equipped with $M = 4$ antennas (unless specified otherwise) spaced $\hat{d} = \hat{\lambda}/2$ apart, while $L = 10$ users are distributed within $(Z+1) = 3$ groups as follows: $\mathcal{Z}_1 = \{D_1(-85^\circ), D_2(-80^\circ), D_3(-75^\circ)\}$, $\mathcal{Z}_2 = \{D_8(75^\circ), D_9(80^\circ), D_{10}(85^\circ)\}$, $\mathcal{Z}_3 = \{D_4(-30^\circ), D_5(-20^\circ), D_6(20^\circ), D_7(30^\circ)\}$, where $\mathcal{Z}_3$ is the EH group of users while the remaining ($\mathcal{Z}_1$, $\mathcal{Z}_2$) MC groups are comprised of ID users. Note that $D_i(\theta_i)$ denotes the angular placement of i^{th} user at an angle θ_i from the ULA. This arrangement is depicted in Fig. 4.15 for better visual understanding. Further, we perform the numerical evaluation corresponding to the sum-harvested maximization problem in $(P4)$ for SMEP and JMEP, wherein we assume $\mathrm{P}_{\text{Max}} = 0.1$ W, $\gamma_i = 0.2$ dB[6], and $\xi_i = 1$ nJ.

For further analysis, the ULA radiation beam-pattern for each precoder is obtained by using the sum of transmit power via corresponding precoder in all the directions between $[-\pi, \pi]$ radians. Specifically, the radiation beam-pattern for k^{th} precoder is defined as $\sum_{\forall\varphi_i} \mathbf{w}_k^H \mathbf{v}(\varphi_i)$, where $\varphi_i = -2\pi\hat{d}\sin(\theta_i)/\hat{\lambda}$, with $\theta_i \in [-\pi, \pi]$. Similarly, the SINR pattern for k^{th} MC precoder is expressed by $\sum_{\forall\varphi_i} \mathbf{w}_k^H \mathbf{v}(\varphi_i) / \sum_{\substack{\ell=1 \\ \ell\neq k}}^{\Psi} \sum_{\forall\varphi_i} \mathbf{w}_\ell^H \mathbf{v}(\varphi_i)$, where $\varphi_i = -2\pi\hat{d}\sin(\theta_i)/\hat{\lambda}$, with $\theta_i \in [-\pi, \pi]$.

In Fig. 4.16, the ULA radiation beam-pattern is depicted using the SDR-based precoder solutions of the considered sum-harvested maximization in JMEP. It is observed that the two designated precoders fulfill the information and energy demands of the users in distinct groups. Similarly, we depict in Fig. 4.17 the ULA radiation beam-pattern for the above-mentioned problem considering the case of SMEP. It is seen that the precoder corresponding to the EH group of users meets their demands via exclusively designed beams, with slight assistance from the other two MC-specific precoders, as expected. Such a case emphasizes on the need of separate waveform designs for ID and EH operations for further improvement in system efficiency [221]. Next, we show the SINR-based beam patterns in Fig. 4.18, for the same case of SMEP. The operations of the two dedicated precoders for MC groups are presented, wherein they provide the requested SINR demands at the MC groups. As anticipated (with the help of observations in prior section), SMEP is found to perform better than JMEP, specifically with $\left(\sum_{\forall j\in\mathcal{Z}_{Z+1}} \mathcal{E}_j^{\mathcal{N}}\right)_{\text{SMEP}} = 5.4403$ μJ and $\left(\sum_{\forall j\in\mathcal{Z}_{Z+1}} \mathcal{E}_j^{\mathcal{N}}\right)_{\text{JMEP}} = 4.3615$ μJ, respectively, for the presented ULA-based results.

4.5.5 Remarks

The overall outcomes imply that the solutions for JMEP and PIEP are (locally) optimal while (local) sub-optimal results are obtained for SMEP, which are rectified with the help of Gaussian randomization approach. From the hardware implementation perspective, this means that even with additional precoder(s) in comparison to JMEP, SMEP is seen to provide relatively better performance. However, both SMEP and JMEP provide comparably similar

[6]This demand enables the provision of data speeds same or higher than 5 Mbps at each user, which is sufficient for HD quality video streaming [237].

performance at higher demands of SINR implying that enough power could be harvested from the corresponding SINR beams and that the last group's energy precoder becomes redundant in case of SMEP[7]. *It is important to highlight that the adoption of separate precoder designs for ID and EH operations does not only reduce the complexity at the transmit source, but also improves the overall system performance both in terms of transmit power minimization as well as maximization of sum-harvested energy. Besides, the proposed JMEP method may be considered a special case or a sub-system of SMEP. Moreover, SMEP has another advantage where its flexibility may facilitate the adoption of different waveform designs, for the ID and EH operations, respectively. In this regard, recent studies, e.g., [221], have shown that the structure of the two waveforms can be rather different.* The operation of PIEP involves same number of precoders as the users, which is good for individual users but it naturally imposes an overall high power consumption, thereby imposing large computational complexities. Moreover, PIEP may even fail to provide the minimum (high) demands of SINR and EH demands at relevant users due to insufficient transmit power in case of sum-harvested energy maximization of the corresponding users.

4.6 Summary

We considered precoding in multi-group multicast system(s) to guarantee the coexistence of three wireless user types, respectively capable of information decoding only, energy harvesting only, and information decoding and/or energy harvesting. In this context, two problems were formulated to minimize the total transmit power, and to maximize the overall harvested energy, respectively; both subjected to the constraints on minimum SINR and EH demands at the corresponding users. The aforementioned problems were transformed with the use of semidefinite relaxation technique considering three scenarios, namely, Separate Multicast and Energy Precoding Design (SMEP), Joint Multicast and Energy Precoding Design (JMEP), and Per-User Information and/or Energy Precoding Design (PIEP), respectively. In addition, we proposed a novel technique named FPP-SCA-e, to address the problem of total transmit power minimization in three considered scenarios, namely, SMEP, JMEP, and PIEP. The developed technique was found to be suitable for solving a QCQP problem that consisted of both ID and EH users. Moreover, co-existence of heterogeneous user types was established under a practically motivated system model. Performance benefits of the FPP-SCA-e technique were shown over SDP via numerical results. Moreover, an additional slack variable reduction method was adopted to make the harvested energy maximization problem tractable. Suitable solutions with considerably good performance were proposed to address the aforementioned problems. Performance benefits of SMEP were shown over JMEP and PIEP, in terms of handling low-SINR user demands with no additional computational task for categorizing the EH users, unlike its sub-system counterpart, JMEP. This motivates the adoption of SMEP in practical cases. Further, we investigated the problem for minimization of total transmit power minimization with the feasible point pursuit and successive convex approximation, wherein much improved outcomes were obtained for the three scenarios in comparison the results via to SDP. This work can be extended to several interesting directions, such as the analysis of the proposed framework with alternative low-complexity based techniques, investigation of the optimization problems with optimized grouping techniques, consideration of MIMO systems, and further analysis with massive MIMO.

[7]It is worth mentioning that the case with contradictory constraints of low SINR and high EH demands is also difficult to realize in the JMEP scenario.

Chapter 5

Simultaneous Wireless Information and Power Transfer with Caching Framework

In this chapter, we investigate the performance of cache-assisted simultaneous wireless information and power transfer (SWIPT) cooperative systems, in which one source communicates with one destination via the aid of multiple relays. In order to prolong the relays' serving time, the relays are assumed to be equipped with a cache memory and energy harvesting (EH) capability. Based on the time-splitting mechanism, we analyze the effect of caching on the system performance in terms of the serving throughput and the stored energy at the relay. In particular, two optimization problems are formulated to maximize the relay-destination throughput and the energy stored at the relay subject to some quality-of-service (QoS) constraints, respectively. By using the KKT conditions and with the help of the Lambert function, closed-form solutions are obtained for the two formulated problems. In order to further improve the performance, a relay selection policy is introduced to select the best relay based on either the maximum throughput between the relays' and destination link or maximum stored energy at the relay, for conveying information to the destination. Numerical results reveal significant benefits of incorporating caching capabilities to SWIPT systems, in terms of improved serving time, throughput and energy harvesting performance at the relays.

This chapter is organized as follows. The next Section introduces the current state of the art in SWIPT with Caching. Section 5.2 provides an insight to the system model. Section 5.3 presents the problem for maximization of link throughput between the relay and destination. Section 5.4 addresses the problem of maximization of the stored energy at the relay. Section 5.5 comprises of simulation results for the proposed algorithms. Finally, Section 5.6 provides the summary of this chapter.

5.1 Introduction to the SWIPT-Caching Framework

The exponential increase in the usage of wireless devices like smart-phones, wearable gadgets, or connected vehicles, has not only posed substantial challenges to meet the performance and capacity demands [17, 238], but also revealed some serious environmental concerns with alarming energy consumption and CO_2 emissions [239]. These concerns become more significant as the forecast number of devices will exceed 50 billions by the end of 2020 [240]. Recent developments in the upcoming paradigm of Internet-of-Things (IoT) emphasize the interconnection between equipments, commodities, functionalities, and customers, with or without

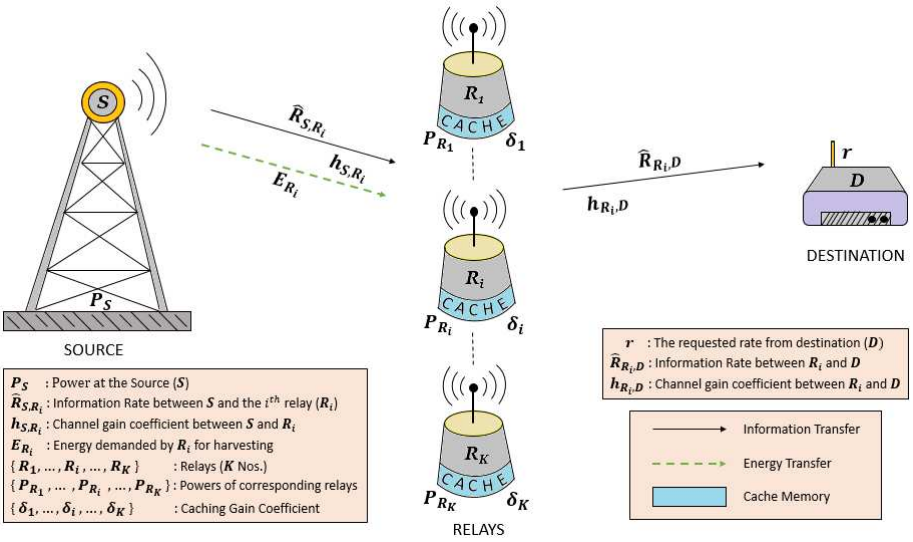

FIGURE 5.1: System model for simultaneous wireless information and power transfer (SWIPT) with caching.

human mediation. Since most of these connecting operations involve wireless sensor nodes or equivalent battery-limited devices that may not be continuously powered, energy becomes a sparse and pivotal resource. These challenges require the future communication networks to have not only efficient energy management but also capability of being self-powered from redundant energy sources, which is known as energy harvesting (EH).

Among potential EH techniques, simultaneous wireless information and power transfer (SWIPT) has received much attention as the key enabling technique for future IoT networks [168]. The basic premise behind SWIPT is to allow concurrent data reception and EH from the same radio frequency (RF) input signal. Considering rapid drainage of battery sources in wireless devices, it has almost become essential to take up such techniques in order to compensate for this issue. Since the conventional receiver architectures are capable of performing information decoding with focus on increasing the data rate only and are unable to harvest energy, this calls for alternative receiver architectures to support SWIPT [167]. Two notable architectures have been proposed based on time switching (TS) and power splitting (PS) schemes [66,171]. In the former, the received signal is switched between the information decoder and energy harvester. It is noted in the TS scheme that full received power is used for either information decoding or energy harvesting. In the latter, both the information decoder and energy harvester are active simultaneously, each of them receive parts of the signal power. The research on SWIPT has received much attention recently [16,168,185]. The Rate-Energy (R-E) trade-off is analyzed in [241] under both TS and PS based SWIPT. The authors in [242] investigate the performance of SWIPT ad-hoc networks in terms of transmission capacity and the harvested energy per unit area. The harvested energy density can be maximized by optimizing the density of the deployed information decoding nodes in TS architecture, and the power splitting ratio in PS architecture. In [243], a tractable model of the rectifier non-linearity is developed to support general multi-carrier modulated input waveforms, which is then used to model a wireless information and power transfer architecture based on the superposition of multi-carrier modulated and unmodulated waveforms. The authors in [244] propose an adaptive scheduling scheme for EH based multiuser systems to jointly maximize achievable rate and harvested energy. In [245], the performance of cooperative networks with battery-powered EH relays is analyzed considering direct source-relay link. The authors

in [246] have investigated various relaying protocols to realize SWIPT in a dual-hop system under static (equal) time distribution. A comprehensive review on SWIPT is presented in [247].

Another major problem the future networks have to face is network congestion, which usually occurs during peak hours when the network resource is scarce. The cause of this congestion is mainly due to the fact that replicas of a common content may be demanded by various mobile users. A promising solution to overcome network congestion is to shift the network traffic from peak hours to off-peak times via content placement or caching [248]. In (off-line) caching, there is usually a placement phase and a delivery phase. In the placement phase, which usually occurs during off-peak times when the network resources are abundant, popular content is prefetched in distributed caches close to the end users. The latter usually occurs during peak hours when the actual users' requests are revealed. If the requested content is available in the user's local storage, it can be served without being requested from the core network. Various advantages brought by caching have been observed in terms of backhaul's load reduction [248–250] and system energy efficiency improvement [27, 251, 252].

A generic concept outlining joint EH and caching has recently been proposed for 5G networks to exploit the benefits of both techniques. A so-called framework GreenDelivery is proposed in [239], which enables efficient content delivery in small cells based on energy harvesting small base stations. In [253], an online energy-efficient power control scheme for EH with caching capability is developed. In particular, by adopting the Poisson distribution for the energy sources, a dynamic programming problem is formulated and solved iteratively by using numerical methods. The authors in [254] propose a caching mechanism at the gateway for the energy harvesting based IoT sensing service to maximize the hit rate. In [255], the authors investigate the performance of heterogeneous vehicular networks with renewable energy source. A network planning problem is formulated to optimize cache size and energy harvesting rate subject to backhaul capacity limits. We note that these works either address an abstract EH with general external energy sources or consider EH separated from caching.

On one hand, the SWIPT-based systems are inevitably impacted by the phenomenon of R-E trade-off [256]. On the other hand, cooperative systems with incorporated caches are proven to perform far better in terms of information exchange compared to traditional communication systems without caching [257]. In this chapter, we intend to develop a joint relationship between caching and SWIPT to study the corresponding performance benefits. Besides, significant benefits are anticipated from cache-assisted SWIPT systems, in terms of: (i) prolonged serving time of the relays, (ii) reduced content delivery time, (iii) increased transmission throughput, and (iv) improved energy storage at the relay (including energy harvesting capabilities). In this regard, we investigate the performance of EH based cooperative networks, in which the relay node is equipped with both SWIPT and caching capabilities. In particular, we aim at developing a framework to realize the integration of SWIPT with caching architectures. The considered system is assumed to operate in the TS based mode, since the PS counterpart imposes complex hardware design challenges of the power splitter [171]. The main contributions of this chapter are four-fold, listed as follows.

1. Firstly, we introduce a novel cache-assisted SWIPT architecture for decode-and-forward (DF)-enabled relaying systems under a dynamic TS-based scheme to study the interaction between caching capacity and SWIPT in the considered system.

2. Secondly, an optimization problem is formulated to maximize the throughput of the (serving) link between the relay and destination, taking into account the caching capacity, minimum harvested energy and quality-of-service (QoS) constraints. By using

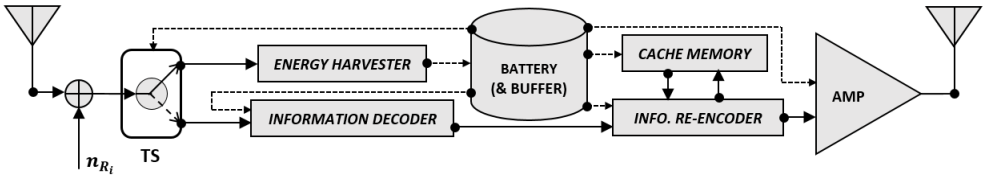

FIGURE 5.2: Proposed DF relay transceiver design for hybrid SWIPT and caching with time switching (TS) architecture.

the KKT conditions with the aid of the Lambert function, a closed-form solution of the formulated problem is obtained for the dynamic TS factors and the transmit power at the relay. Based on this result, the best relay will be selected for cooperation.

3. Thirdly, we formulate an optimization problem to maximize the energy stored at the relay subjected to the QoS constraint. Similar to the previous problem, a closed-form solution is obtained for optimization of the dynamic TS factors and the transmit power at the relay, by using the KKT conditions and the Lambert function.

4. Finally, the effectiveness of the proposed schemes are demonstrated via intensive numerical results, through which the impacts of key system parameters are observed. Furthermore, a discussion on practical implementation and future directions is provided.

5.2 System Model

We consider a generic TS based SWIPT system, which consists of one source, K relays, and one destination, as depicted in Fig. 5.1. Each device within the network is equipped with single antenna. Due to limited coverage, e.g., transmit power limit or blockage, there is no direct connection between the source and the destination. The considered model can find application on the downlink where the base station plays the source's role and sends information to a far user via a small- or femto- cell base station. The relays operate in DF mode and are equipped with single antenna. We consider a general cache-aided SWIPT model, in which each relay contains an information decoder, an energy harvester, and a cache in order to store or exchange information. The block diagram of a typical relay architecture is shown in Fig. 5.2.

We consider block Rayleigh fading channels, in which the channel coefficients remain constant within a block (or coherence time), and independently change block to block. One communication session (broadcasting and relaying) takes place in T seconds (T does not exceed the coherence time). In the broadcasting phase, the source-relay links are active for information decoding (at the relay) and energy harvesting. The relays employ the TS scheme so that the received signal is first provided to the the energy harvester for some fraction of the time allocated for transmitter-relay communication link, and then to information decoder for the remaining fraction. In case of equal time slots in both the hops, this mechanism is also known as harvest-then-forward protocol [258]. Correspondingly, due to the changing nature of the TS factors', we refer to this analogous operation as "dynamic harvest-then-forward" protocol. In the relaying phase, the selected relay forwards the information to the destination. Full channel state information (CSI) is assumed to be available at a centralized base station which performs all the computations and inform the relevant devices via adequate signaling.

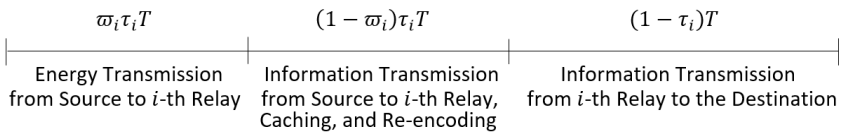

FIGURE 5.3: Convention assumed for distribution of time to investigate the throughput maximization problem.

The relay with the best reward will be selected for sending information to the destination. Details on relay selection will be presented later.

Fig. 5.3 presents a convention for allocation of time fractions in the TS scheme: *i)* energy transmission from the source to i-th relay, *ii)* information processing at the relay, and *iii)* information forwarding to the destination. The link between the transmitter and i-th relay with cache is active for a fraction of $\tau_i T$ seconds, while the link between the i-th relay and destination is active for the remaining $(1-\tau_i)T$, where $0 \leq \tau_i \leq 1$. Furthermore, we assume that the energy harvesting at the relays takes place for a fraction of $\varpi_i\tau_i T$ seconds and the information decoding at the relay takes place for a fraction of $(1-\varpi_i)\tau_i T$ seconds, where $0 \leq \varpi_i \leq 1$. For ease of representation, we assume normalized time to use energy and power interchangeably without loss in generality.

5.2.1 Signal model

We define the information transfer rates from the source to the i-th relay as $\hat{R}_{\mathcal{S},\mathcal{R}_i}$, and from the i-th relay to the destination as $\hat{R}_{\mathcal{R}_i,\mathcal{D}}$, with $1 \leq i \leq K$, where $i \in \mathbb{Z}$.

Let $h_{\mathcal{S},\mathcal{R}_i}$ and $h_{\mathcal{R}_i,\mathcal{D}}$ denote the channel coefficients between the source and the i-th relay and between the i-th relay and the destination, respectively, and $d_{\mathcal{S},\mathcal{R}_i}$ and $d_{\mathcal{R}_i,\mathcal{D}}$ denote the distance between the source and i-th relay, and the distance between the i-th relay and destination, respectively. Furthermore, $P_{\mathcal{S}}$ and $P_{\mathcal{R}_i}$ denote the transmit power at the source and the i-th relay, respectively.

Let $x \in \mathbb{C}$ be the transmitted symbol by the source satisfying $E\{|x|^2\} = 1$. The signal received at the i-th relay is given by

$$y_{\mathcal{R}_i} = \sqrt{P_{\mathcal{S}}}\; d_{\mathcal{S},\mathcal{R}_i}^{-\vartheta/2}\; h_{\mathcal{S},\mathcal{R}_i}\; x \;+\; n_{\mathcal{R}_i}, \tag{5.1}$$

where ϑ is the path loss exponent, $n_{\mathcal{R}_i}$ is the additive white Gaussian noise (AWGN) at the relay, which is an independent and identically distributed (i.i.d.) complex Gaussian random variable with zero mean and variance $\sigma^2_{n_{\mathcal{R}_i}}$.

Upon receiving the desired signal from the source, the relay decodes to obtain the estimate of the original signal. Then the (selected) relay re-encodes and forwards it to the destination. The signal received at the destination as transmitted by the i-th relay is given by

$$y_D = \sqrt{P_{\mathcal{R}_i}}\; d_{\mathcal{R}_i,\mathcal{D}}^{-\vartheta/2}\; h_{\mathcal{R}_i,\mathcal{D}}\; \tilde{x} \;+\; n_{\mathcal{D}}, \tag{5.2}$$

where $\tilde{x}$ is the transmit symbol from the relay, and $n_{\mathcal{D}}$ is the AWGN at the destination node which is an i.i.d. complex Gaussian random variable with zero mean and variance $\sigma^2_{n_{\mathcal{D}}}$. We note that in the proposed cached-aid architecture, the relayed symbol can be either decoded source symbol or from the relay's cache.

The effective signal-to-noise ratio (SNR) of the source-relay and relay-destination links are given as

$$\Upsilon_{\mathcal{S},\mathcal{R}_i} = \frac{P_{\mathcal{S}}\ d_{\mathcal{S},\mathcal{R}_i}^{-\vartheta}\ |h_{\mathcal{S},\mathcal{R}_i}|^2}{\sigma_{n_{\mathcal{R}_i}}^2};\ \Upsilon_{\mathcal{R}_i,\mathcal{D}} = \frac{P_{\mathcal{R}_i}\ d_{\mathcal{R}_i,\mathcal{D}}^{-\vartheta}\ |h_{\mathcal{R}_i,\mathcal{D}}|^2}{\sigma_{n_{\mathcal{D}}}^2}. \tag{5.3}$$

By assuming a Gaussian codebook, the achievable information rate on the source-relays' link is

$$\hat{R}_{\mathcal{S},\mathcal{R}_i} = B\ \log_2(1+\Upsilon_{\mathcal{S},\mathcal{R}_i}), \quad \forall i, \tag{5.4}$$

and the achievable information rate at the destination is

$$\hat{R}_{\mathcal{R}_i,\mathcal{D}} = B\ \log_2(1+\Upsilon_{\mathcal{R}_i,\mathcal{D}}), \forall i, \tag{5.5}$$

where B is the channel bandwidth.

5.2.2 Caching model

A general caching model is considered at the relays. In particular, in addition to the information sent from the source, the relays have access to the information stored in their individual caches to serve the destination. For robustness, we assume that for $i = 1, \ldots, K$, the i-th relay does not have information about the content popularity. Therefore, it will store $0 \leq \delta_i \leq 1$ parts of every file in its cache [248, 251] [1]. For convenience, we call δ_i as the caching coefficient throughout the chapter. This caching scheme will serve as the lower bound benchmark compared to the case where priori information of content popularity is available. When the destination requests a file from the library, δ_i parts of that file are already available at the i-th relay's cache. Therefore, the source need to send only the remaining portions of that file to the relay.

5.2.3 Power assumption at the relay

For robustness, we assume that the relays are powered by an external source, E_{ext}, on top of the harvested energy. This general model allows to analyze the impact of various practical scenarios. As an usecase, the purely SWIPT relay is obtained by setting E_{ext} to zero. The harvested energy at the i-th relay is given by

$$E_{\mathcal{R}_i} = \zeta \varpi_i \tau_i (P_{\mathcal{S}} d_{\mathcal{S},\mathcal{R}_i}^{-\vartheta} |h_{\mathcal{S},\mathcal{R}_i}|^2 + \sigma_{n_{\mathcal{R}_i}}^2), \tag{5.6}$$

where ζ is the energy conversion efficiency of the receiver.

5.3 Maximization of the serving information rate

In this section, we aim at maximizing the serving information data between the selected relay and the destination, by taking into consideration the caching capacity at the relay, while assuring the predefined QoS constraint and that the total transmit power at the source does not exceed the limit. The corresponding optimization problem (P1) is stated as follows

$$(P1): \max_{i\in\mathcal{K},\varpi_i,\tau_i,P_{\mathcal{R}_i}} \quad (1-\tau_i)\hat{R}_{\mathcal{R}_i,\mathcal{D}} \tag{5.7}$$

$$\text{subject to}: \quad (C1): (1-\varpi_i)\tau_i(\hat{R}_{\mathcal{S},\mathcal{R}_i} + (\delta_i \cdot r)) \geq (1-\tau_i)\hat{R}_{\mathcal{R}_i,\mathcal{D}}, \tag{5.7a}$$

$$(C2): (1-\tau_i)P_{\mathcal{R}_i} \leq E_{\mathcal{R}_i} + E_{ext}, \tag{5.7b}$$

$$(C3): 0 < P_{\mathcal{S}} \leq \mathrm{P}_{\mathrm{Max}}, \tag{5.7c}$$

$$(C4): 0 \leq \varpi_i \leq 1, \tag{5.7d}$$

$$(C5): 0 \leq \tau_i \leq 1, \tag{5.7e}$$

[1] This caching method is also known as probabilistic caching.

where $\mathcal{K} = \{1, \ldots, K\}$, $E_{\mathcal{R}_i}$ is given in (5.6), E_{ext} is the external energy required at the relay for further transmission of the signal, $\mathrm{P}_{\mathrm{Max}}$ is the maximum power limit at the transmitter, and r is the QoS constraint. The objective in (5.7) is to maximize the transfered data to the destination, since the relay-destination link is active only in $1 - \tau_i$ (active times normalized by T). Constraint (5.7a) is to assure non-empty buffer at the relay. Constraint (5.7b) is to assure that the used energy at the relay cannot exceed the input. It is noteworthy that E_{ext} is stipulated in each time slot which thereby translates into stored energy for the successive time slot, provided the relays are battery driven. In other case, E_{ext} can be assumed to be constant in each time slot if the relays are part of the infrastructure with sufficient power supply, as in [259].

This is a mixed-integer programming problem implying that relay selection along with joint computations of ϖ_i, τ_i, and $P_{\mathcal{R}_i}$ is a difficult task. Therefore, we recast $(P1)$ into a pair of coupled optimization problems namely, outer optimization for choosing the best relay, and inner optimization for joint computations of ϖ_i, τ_i, and $P_{\mathcal{R}_i}$. In the following sections, we address the optimal solutions to the inner and outer optimizations, respectively.

5.3.1 Optimization of TS Factors and the Relay Transmit Power

In this subsection, we address the inner optimization problem of $(P1)$ involving joint computations of ϖ_i, τ_i, and $P_{\mathcal{R}_i}$, assuming that the i-th relay is active. The consequent sub-problem is formulated as follows

$$\begin{aligned} (P2): \max_{\varpi_i, \tau_i, P_{\mathcal{R}_i}} \quad & (1-\tau_i)\hat{R}_{\mathcal{R}_i,\mathcal{D}} \\ \text{subject to}: \quad & (5.7\text{a}) - (5.7\text{e}). \end{aligned} \tag{5.8}$$

This is a non-linear programming problem involving joint computations of ϖ_i, τ_i, and $P_{\mathcal{R}_i}$, which is challenging to find the exact solution. Since the constraints are partially convex on each variable while fixing the others, we propose to solve this problem using the Karush-Kuhn-Tucker (KKT) conditions.

The Lagrangian corresponding to $(P2)$ can be denoted as follows

$$\begin{aligned} \mathcal{L}(\varpi_i, \tau_i, P_{\mathcal{R}_i}; \lambda_1, \lambda_2, \lambda_3, \lambda_4) = F(\varpi_i, \tau_i, P_{\mathcal{R}_i}) - \lambda_1\, G(\varpi_i, \tau_i, P_{\mathcal{R}_i}) - \lambda_2\, H(\varpi_i, \tau_i, P_{\mathcal{R}_i}) \\ -\lambda_3\, I(\varpi_i, \tau_i, P_{\mathcal{R}_i}) - \lambda_4\, J(\varpi_i, \tau_i, P_{\mathcal{R}_i}), \end{aligned} \tag{5.9}$$

where

$$F(\varpi_i, \tau_i, P_{\mathcal{R}_i}) = (1-\tau_i) B \log_2(1 + \Upsilon_{\mathcal{R}_i,\mathcal{D}}), \tag{5.10}$$

$$G(\varpi_i, \tau_i, P_{\mathcal{R}_i}) = (1-\tau_i) B \log_2(1 + \Upsilon_{\mathcal{R}_i,\mathcal{D}}) - (1-\varpi_i)\tau_i [B \log_2(1 + \Upsilon_{\mathcal{S},\mathcal{R}_i}) + (\delta_i \cdot r)] \leq 0, \tag{5.11}$$

$$H(\varpi_i, \tau_i, P_{\mathcal{R}_i}) = (1-\tau_i) P_{\mathcal{R}_i} - \zeta \varpi_i \tau_i (P_{\mathcal{S}} d_{\mathcal{S},\mathcal{R}_i}^{-\vartheta} |h_{\mathcal{S},\mathcal{R}_i}|^2 + \sigma_{n_{\mathcal{R}_i}}^2) - E_{ext} \leq 0, \tag{5.12}$$

$$I(\varpi_i, \tau_i, P_{\mathcal{R}_i}) = \varpi_i - 1 \leq 0, \tag{5.13}$$

$$J(\varpi_i, \tau_i, P_{\mathcal{R}_i}) = \tau_i - 1 \leq 0. \tag{5.14}$$

For (local) optimality[2], it must hold $\nabla \mathcal{L}(\varpi_i, \tau_i, P_{\mathcal{R}_i}; \lambda_1, \lambda_2, \lambda_3, \lambda_4) = 0$. Thus, we can represent the equations for satisfying the optimality conditions as

[2]Note that a KKT point is not necessarily a local optimum, but can also be saddle point and even maximum points [224].

$$\frac{\partial \mathcal{L}(\varpi_i, \tau_i, P_{\mathcal{R}_i}; \lambda_1, \lambda_2, \lambda_3, \lambda_4)}{\partial \varpi_i} \implies -\lambda_1\Big(\tau_i\Big(B\log_2(1+\Upsilon_{\mathcal{S},\mathcal{R}_i}) + (\delta_i \cdot r)\Big)\Big) - \lambda_2\Big(-\zeta\tau_i(P_{\mathcal{S}} d_{\mathcal{S},\mathcal{R}_i}^{-\vartheta}|h_{\mathcal{S},\mathcal{R}_i}|^2 + \sigma^2_{n_{\mathcal{R}_i}})\Big) - \lambda_3 = 0, \quad (5.15)$$

$$\frac{\partial \mathcal{L}(\varpi_i, \tau_i, P_{\mathcal{R}_i}; \lambda_1, \lambda_2, \lambda_3, \lambda_4)}{\partial \tau_i} \implies -B\log_2(1+\Upsilon_{\mathcal{R}_i,\mathcal{D}}) - \lambda_1\Big(-B\log_2(1+\Upsilon_{\mathcal{R}_i,\mathcal{D}}) - (1-\varpi_i)\Big(B\log_2(1+\Upsilon_{\mathcal{S},\mathcal{R}_i}) + (\delta_i \cdot r)\Big)\Big) - \lambda_2\Big(-P_{\mathcal{R}_i} - \zeta\varpi_i(P_{\mathcal{S}} d_{\mathcal{S},\mathcal{R}_i}^{-\vartheta}|h_{\mathcal{S},\mathcal{R}_i}|^2 + \sigma^2_{n_{\mathcal{R}_i}})\Big) - \lambda_4 = 0, \quad (5.16)$$

$$\frac{\partial \mathcal{L}(\varpi_i, \tau_i, P_{\mathcal{R}_i}; \lambda_1, \lambda_2, \lambda_3, \lambda_4)}{\partial P_{\mathcal{R}_i}} \implies \frac{\ln(2) d_{\mathcal{R}_i,\mathcal{D}}^{-\vartheta}|h_{\mathcal{R}_i,\mathcal{D}}|^2}{\sigma^2_{n_{\mathcal{D}}} + P_{\mathcal{R}_i} d_{\mathcal{R}_i,\mathcal{D}}^{-\vartheta}|h_{\mathcal{R}_i,\mathcal{D}}|^2} - \lambda_1\left(\frac{\ln(2) d_{\mathcal{R}_i,\mathcal{D}}^{-\vartheta}|h_{\mathcal{R}_i,\mathcal{D}}|^2}{\sigma^2_{n_{\mathcal{D}}} + P_{\mathcal{R}_i} d_{\mathcal{R}_i,\mathcal{D}}^{-\vartheta}|h_{\mathcal{R}_i,\mathcal{D}}|^2}\right) - \lambda_2 = 0. \quad (5.17)$$

The conditions for feasibility are as expressed in (5.11), (5.12), (5.13), and (5.14). Complementary slackness expressions can be represented as follows

$$\lambda_1 \cdot G(\varpi_i, \tau_i, P_{\mathcal{R}_i}) = 0, \quad (5.18)$$
$$\lambda_2 \cdot H(\varpi_i, \tau_i, P_{\mathcal{R}_i}) = 0, \quad (5.19)$$
$$\lambda_3 \cdot I(\varpi_i, \tau_i, P_{\mathcal{R}_i}) = 0, \quad (5.20)$$
$$\lambda_4 \cdot J(\varpi_i, \tau_i, P_{\mathcal{R}_i}) = 0. \quad (5.21)$$

The conditions for non-negativity read $\varpi_i, \tau_i, P_{\mathcal{R}_i}, \lambda_1, \lambda_2, \lambda_3, \lambda_4 \geq 0$. It is straightforward to verify that if $\lambda_3 \neq 0$, then $I(\varpi_i, \tau_i, P_{\mathcal{R}_i}) = 0$ implying that $\varpi_i = 1$. Since this is not a feasible solution, therefore $\lambda_3 = 0$. Similarly, it can be shown that $\lambda_4 = 0$.

The final solution can be postulated in the following theorem.

Theorem 1. *If $\lambda_1 \neq 0 \implies G(x, P_{\mathcal{R}_i}) = 0$; $\lambda_2 \neq 0 \implies H(x, P_{\mathcal{R}_i}) = 0$, then we obtain the following optimal values*

$$P_{\mathcal{R}_i} = \left(\exp\left(\mathcal{W}\Big(\frac{\mathcal{A}}{B}\exp\Big(-\frac{1}{B}\log^2(2)\Big) * \log(2)\Big) + \frac{\log^2(2)}{B}\right) - 1\right)\left(\frac{\sigma^2_{n_{\mathcal{D}}}}{d_{\mathcal{R}_i,\mathcal{D}}^{-\vartheta}\ |h_{\mathcal{R}_i,\mathcal{D}}|^2}\right), \quad (5.22)$$

where $\mathcal{A} = \frac{(\ln(2) d_{\mathcal{R}_i,\mathcal{D}}^{-\vartheta}|h_{\mathcal{R}_i,\mathcal{D}}|^2)(\zeta(P_{\mathcal{S}} d_{\mathcal{S},\mathcal{R}_i}^{-\vartheta}|h_{\mathcal{S},\mathcal{R}_i}|^2 + \sigma^2_{n_{\mathcal{R}_i}}))}{\sigma^2_{n_{\mathcal{D}}}}$ and $\mathcal{W}(\cdot)$ is the Lambert W function [260].

$$\tau_i = \frac{\varphi_1 \cdot \varphi_2 + P_{\mathcal{R}_i} - E_{ext} \cdot \varphi_3}{\varphi_1 \cdot \varphi_2 + \varphi_2 \cdot \varphi_3 + P_{\mathcal{R}_i} \cdot \varphi_3}, \quad (5.23)$$

where $\varphi_1 = B\log_2(1+\Upsilon_{\mathcal{R}_i,\mathcal{D}})$, $\varphi_2 = \zeta(P_{\mathcal{S}} d_{\mathcal{S},\mathcal{R}_i}^{-\vartheta}|h_{\mathcal{S},\mathcal{R}_i}|^2 + \sigma^2_{n_{\mathcal{R}_i}})$, and $\varphi_3 = B\log_2(1+\Upsilon_{\mathcal{S},\mathcal{R}_i}) + (\delta_i \cdot r)$.

$$\varpi_i = \frac{(1-\tau_i)P_{\mathcal{R}_i} - E_{ext}}{\zeta\tau_i(P_{\mathcal{S}} d_{\mathcal{S},\mathcal{R}_i}^{-\vartheta}|h_{\mathcal{S},\mathcal{R}_i}|^2 + \sigma^2_{n_{\mathcal{R}_i}})}. \quad (5.24)$$

Proof. See Appendix E.1.

Remark: Since there is one and only one feasible solution (as derived using the KKT conditions), therefore, the obtained solution must be in-line with respective conditions in

Theorem 1. Alternatively if the conditions in Theorem 1 are not satisfied, then it is reasonable to discard the solution as the problem becomes infeasible.

It is proved in our analysis above $\Big((5.9)$ - $(5.21)\Big)$ that the necessary conditions for KKT are satisfied. Assume that KKT yields the following solutions: (i) Primal variables: $\varpi_i^\star$, $\tau_i^\star$, $P_{\mathcal{R}_i}^\star$, (ii) Dual Variables: $\lambda_1^\star$, $\lambda_2^\star$. The second order derivatives can therefore be represented using these solutions as: $\nabla^2_{\varpi_i\varpi_i}\mathcal{L}(\varpi_i^\star, \tau_i^\star, P_{\mathcal{R}_i}^\star; \lambda_1^\star, \lambda_2^\star) = 0$, $\nabla^2_{\tau_i\tau_i}\mathcal{L}(\varpi_i^\star, \tau_i^\star, P_{\mathcal{R}_i}^\star; \lambda_1^\star, \lambda_2^\star) = 0$, and $\nabla^2_{P_{\mathcal{R}_i}P_{\mathcal{R}_i}}\mathcal{L}(\varpi_i^\star, \tau_i^\star, P_{\mathcal{R}_i}^\star; \lambda_1^\star, \lambda_2^\star) \geq 0$. It is found that the sufficiency criteria are not strictly met and hence the function is not strictly constrained local minimum. However, the sufficiency conditions are satisfied, the solutions obtained above does not guarantee global optimality.

From an economic view-point, the Lagrange Multipliers λ_1 and λ_2 can be expounded as the prices for data and energy in cost/bit and cost/Joule, respectively. Leveraging the results from our analysis in Appendix E.1, we find that $\lambda_1 = \frac{f_1(P_\mathcal{S})}{f_2(P_\mathcal{S},\delta_i,r)} \cdot \lambda_2$, where $f_1(P_\mathcal{S}) = \zeta(P_\mathcal{S} d_{\mathcal{S},\mathcal{R}_i}^{-\vartheta}|h_{\mathcal{S},\mathcal{R}_i}|^2 + \sigma^2_{n_{\mathcal{R}_i}})$, and $f_2(P_\mathcal{S}, \delta_i, r) = B\log_2(1 + \Upsilon_{\mathcal{S},\mathcal{R}_i}) + (\delta_i \cdot r)$. Correspondingly, it is clear that if more data rate is demanded by the user provided the caching capacity is fixed, then we are enforced to compensate for the request by using the energy metric per cost unit in order to satisfy the respective data and energy constraints in $(P2)$. This action would however add more to the energy price. Similarly, it is apparent that increasing the transmit power will readily add to the cost of data transfer in addition to an increased energy price. In the context of caching, it would be needless to mention that *the higher the cache capacity is, the lower will be the prices for data and energy transmissions.*

5.3.2 Relay Selection

In this subsection, we consider optimal selection of a relay to address the solution of outer optimization of $(P1)$. Based on the above developments, we find the best relay which provides maximum throughput corresponding to (5.7). The best relay index is selected as $j^\star = \arg\max_{j\in\{1,\ldots,K\}}(1-\tau_j^\star)\hat{R}^\star_{R_j,D}$, where $\tau_j^\star$ and $\hat{R}^\star_{R_j,D}$ are the solutions of problem (5.8). It is worth to mention that this relay selection is based on exhausted search and provides the best performance with high cost of complexity. Finding a compromise relay selection is of interest in the future research.

5.4 Maximization of the Energy Stored at the Relay

In this section, we aim at maximizing the energy stored at the relay. The stored energy is calculated by subtracting the input energy, e.g., E_{ext} plus the harvested energy, by the output energy, e.g., used for forwarding information to the destination. Our motivation behind this section is that the stored energy at the relay can be used to perform extra processing task, e.g., sensing, or to recharge a battery for future use. In particular, an optimization problem is formulated to jointly select the best relay and maximize the stored energy, while satisfying a given QoS.

For convenience, we introduce a new convention for fractions of time in the TS scheme, as shown in Fig. 5.4. However, the corresponding inter-relationships between the two conventions in Fig. 5.3 and Fig. 5.4 are established in Appendix E.3. For the newly adopted convention, the link between the transmitter and relay with cache is considered to be active for a fraction of $(\hat{\varpi}_i + \hat{\tau}_i)T$ seconds, while the link between the relay and destination is active for the remaining $(1-(\hat{\varpi}_i + \hat{\tau}_i))T$, where $0 \leq \hat{\varpi}_i + \hat{\tau}_i \leq 1$. As mentioned earlier, since the relay adopts a TS type of scheme for SWIPT, we assume that the energy harvesting at the

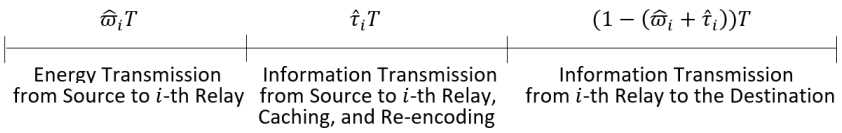

FIGURE 5.4: Convention assumed for distribution of time to investigate the stored energy maximization problem.

relay takes place for a fraction of $\hat{\varpi}_i T$ seconds and the information decoding at the relay takes place for a fraction of $\hat{\tau}_i T$ seconds. Similarly, we assume normalized time to use energy and power interchangeably without loss in generality. We remind that the harvested energy at the relay i is given as

$$E_{\mathcal{R}_i} = \zeta \hat{\varpi}_i (P_{\mathcal{S}} d_{\mathcal{S},\mathcal{R}_i}^{-\vartheta} |h_{\mathcal{S},\mathcal{R}_i}|^2 + \sigma_{n_{\mathcal{R}_i}}^2), \tag{5.25}$$

where ζ is the energy conversion efficiency of the receiver.

We now consider the problem of relay selection for maximization of the energy stored at the relay, while ensuring that the requested rate between relay-destination is above a given threshold and that the total transmit powers at the transmitter and relay does not exceed a given limit. The corresponding optimization problem (P3) can be expressed as

$$(P3): \max_{i\in\mathcal{K},\hat{\varpi}_i,\hat{\tau}_i,P_{\mathcal{R}_i}} \; [\zeta \hat{\varpi}_i (P_{\mathcal{S}} d_{\mathcal{S},\mathcal{R}_i}^{-\vartheta} |h_{\mathcal{S},\mathcal{R}_i}|^2 + \sigma_{n_{\mathcal{R}_i}}^2) + E_{ext} - (1-(\hat{\varpi}_i+\hat{\tau}_i))P_{\mathcal{R}_i}]^+ \tag{5.26}$$

$$\text{subject to}: \; (C1): \hat{\tau}_i(\hat{R}_{\mathcal{S},\mathcal{R}_i} + (\delta_i \cdot r)) \geq (1-(\hat{\varpi}_i+\hat{\tau}_i))\hat{R}_{\mathcal{R}_i,\mathcal{D}}, \tag{5.26a}$$

$$(C2): (1-(\hat{\varpi}_i+\hat{\tau}_i))P_{\mathcal{R}_i} \leq E_{\mathcal{R}_i} + E_{ext}, \tag{5.26b}$$

$$(C3): (1-(\hat{\varpi}_i+\hat{\tau}_i))\hat{R}_{\mathcal{R}_i,\mathcal{D}} \geq r, \tag{5.26c}$$

$$(C4): 0 < P_{\mathcal{S}} \leq \mathrm{P}_{\mathrm{Max}}, \tag{5.26d}$$

$$(C5): 0 \leq \hat{\varpi}_i + \hat{\tau}_i \leq 1, \tag{5.26e}$$

where the objective in (5.26) is non-zero and the constraint (5.26c) is to satisfy the QoS requirement.

The problem $(P3)$ is difficult to solve, since it is a mixed-integer programming problem involving relay selection along with joint computations of $\hat{\varpi}_i$, $\hat{\tau}_i$, and $P_{\mathcal{R}_i}$. So, we recast $(P3)$ into pair of coupled optimization problems for performing the outer optimization to choose the best relay, and inner optimization for joint computations of $\hat{\varpi}_i$, $\hat{\tau}_i$, and $P_{\mathcal{R}_i}$. In the following subsections, we address the optimal solutions to the inner and outer optimizations, respectively.

5.4.1 Optimization of TS Factors and the Relay Transmit Power

In this subsection, we consider the inner optimization problem of (P3). We determine the technique for joint computations of $\hat{\varpi}_i$, $\hat{\tau}_i$, and $P_{\mathcal{R}_i}$, for maximizing the energy stored at the relay while ensuring that the requested rate between relay-destination is above a given threshold and that the total transmit powers at the transmitter and relay does not exceed a

given limit. Correspondingly, the sub-problem $(P4)$ can be formulated as

$$(P4): \max_{\hat{\varpi}_i,\hat{\tau}_i,P_{\mathcal{R}_i}} \; [\zeta\hat{\varpi}_i(P_{\mathcal{S}}d_{\mathcal{S},\mathcal{R}_i}^{-\vartheta}|h_{\mathcal{S},\mathcal{R}_i}|^2+\sigma_{n_{\mathcal{R}_i}}^2)+E_{ext}-(1-(\hat{\varpi}_i+\hat{\tau}_i))P_{\mathcal{R}_i}]^+ \tag{5.27}$$

$$\text{subject to}: \; (C1): \hat{\tau}_i(\hat{R}_{\mathcal{S},\mathcal{R}_i}+(\delta_i\cdot r))\geq(1-(\hat{\varpi}_i+\hat{\tau}_i))\hat{R}_{\mathcal{R}_i,\mathcal{D}}, \tag{5.27a}$$

$$(C2): (1-(\hat{\varpi}_i+\hat{\tau}_i))P_{\mathcal{R}_i}\leq E_{\mathcal{R}_i}+E_{ext}, \tag{5.27b}$$

$$(C3): (1-(\hat{\varpi}_i+\hat{\tau}_i))\hat{R}_{\mathcal{R}_i,\mathcal{D}}\geq r, \tag{5.27c}$$

$$(C4): 0<P_{\mathcal{S}}\leq \mathrm{P}_{\mathrm{Max}}, \tag{5.27d}$$

$$(C5): 0\leq\hat{\varpi}_i+\hat{\tau}_i\leq 1. \tag{5.27e}$$

This is a non-linear programming problem involving joint computations of $\hat{\varpi}_i$, $\hat{\tau}_i$, and $P_{\mathcal{R}_i}$, which introduces intractability. Therefore, we propose to solve this problem using the Karush-Kuhn-Tucker (KKT) conditions.

The Lagrangian for $(P4)$ can be expressed as follows

$$\mathcal{L}(\hat{\varpi}_i,\hat{\tau}_i,P_{\mathcal{R}_i};\mu_1,\mu_2,\mu_3,\mu_4)=F(\hat{\varpi}_i,\hat{\tau}_i,P_{\mathcal{R}_i})-\mu_1\,G(\hat{\varpi}_i,\hat{\tau}_i,P_{\mathcal{R}_i})-\mu_2\,H(\hat{\varpi}_i,\hat{\tau}_i,P_{\mathcal{R}_i})$$
$$-\mu_3\,I(\hat{\varpi}_i,\hat{\tau}_i,P_{\mathcal{R}_i})-\mu_4\,J(\hat{\varpi}_i,\hat{\tau}_i,P_{\mathcal{R}_i}), \tag{5.28}$$

where

$$F(\hat{\varpi}_i,\hat{\tau}_i,P_{\mathcal{R}_i})=\zeta\hat{\varpi}_i(P_{\mathcal{S}}d_{\mathcal{S},\mathcal{R}_i}^{-\vartheta}|h_{\mathcal{S},\mathcal{R}_i}|^2+\sigma_{n_{\mathcal{R}_i}}^2)+E_{ext}-(1-(\hat{\varpi}_i+\hat{\tau}_i))P_{\mathcal{R}_i}, \tag{5.29}$$

$$G(\hat{\varpi}_i,\hat{\tau}_i,P_{\mathcal{R}_i})=(1-(\hat{\varpi}_i+\hat{\tau}_i))B\log_2(1+\Upsilon_{\mathcal{R}_i,\mathcal{D}})-\hat{\tau}_i[B\log_2(1+\Upsilon_{\mathcal{S},\mathcal{R}_i})+(\delta_i\cdot r)]\leq 0, \tag{5.30}$$

$$H(\hat{\varpi}_i,\hat{\tau}_i,P_{\mathcal{R}_i})=(1-(\hat{\varpi}_i+\hat{\tau}_i))P_{\mathcal{R}_i}-E_{ext}-\zeta\hat{\varpi}_i(P_{\mathcal{S}}d_{\mathcal{S},\mathcal{R}_i}^{-\vartheta}|h_{\mathcal{S},\mathcal{R}_i}|^2+\sigma_{n_{\mathcal{R}_i}}^2)\leq 0, \tag{5.31}$$

$$I(\hat{\varpi}_i,\hat{\tau}_i,P_{\mathcal{R}_i})=r-(1-(\hat{\varpi}_i+\hat{\tau}_i))B\log_2(1+\Upsilon_{\mathcal{R}_i,\mathcal{D}})\leq 0, \tag{5.32}$$

$$J(\hat{\varpi}_i,\hat{\tau}_i,P_{\mathcal{R}_i})=(\hat{\varpi}_i+\hat{\tau}_i)-1\leq 0. \tag{5.33}$$

with μ_1,μ_2,μ_3,μ_4 being the Lagrange Multipliers for the corresponding constraints (C1), (C2), (C3), and (C5). Note that the objective function in (5.27) is non-differentiable, and hence we relax the $(x)^+=\max(0,x)$ constraint as represented in (5.29). However, only positive values should be the acceptable solutions as the problem becomes infeasible with negative values.

For optimality, $\nabla\mathcal{L}(\hat{\varpi}_i,\hat{\tau}_i,P_{\mathcal{R}_i};\mu_1,\mu_2,\mu_3,\mu_4)=0$. Thus, we can represent the equations for satisfying the optimality conditions as

$$\frac{\partial\mathcal{L}(\hat{\varpi}_i,\hat{\tau}_i,P_{\mathcal{R}_i};\mu_1,\mu_2,\mu_3,\mu_4)}{\partial\hat{\varpi}_i}\implies[\zeta(P_{\mathcal{S}}d_{\mathcal{S},\mathcal{R}_i}^{-\vartheta}|h_{\mathcal{S},\mathcal{R}_i}|^2+\sigma_{n_{\mathcal{R}_i}}^2)+P_{\mathcal{R}_i}]-\mu_1[-B\log_2(1+\Upsilon_{\mathcal{R}_i,\mathcal{D}})]$$
$$-\mu_2[-P_{\mathcal{R}_i}-\zeta(P_{\mathcal{S}}d_{\mathcal{S},\mathcal{R}_i}^{-\vartheta}|h_{\mathcal{S},\mathcal{R}_i}|^2+\sigma_{n_{\mathcal{R}_i}}^2)]-\mu_3[B\log_2(1+\Upsilon_{\mathcal{R}_i,\mathcal{D}})]-\mu_4=0, \tag{5.34}$$

$$\frac{\partial\mathcal{L}(\hat{\varpi}_i,\hat{\tau}_i,P_{\mathcal{R}_i};\mu_1,\mu_2,\mu_3,\mu_4)}{\partial\hat{\tau}_i}\implies P_{\mathcal{R}_i}-\mu_1[-B\log_2(1+\Upsilon_{\mathcal{R}_i,\mathcal{D}})-(B\log_2(1+\Upsilon_{\mathcal{S},\mathcal{R}_i})+(\delta_i\cdot r))]$$
$$-\mu_2[-P_{\mathcal{R}_i}]-\mu_3[B\log_2(1+\Upsilon_{\mathcal{R}_i,\mathcal{D}})]-\mu_4=0, \tag{5.35}$$

$$\frac{\partial\mathcal{L}(\hat{\varpi}_i,\hat{\tau}_i,P_{\mathcal{R}_i};\mu_1,\mu_2,\mu_3,\mu_4)}{\partial P_{\mathcal{R}_i}}\implies -(1-(\hat{\varpi}_i+\hat{\tau}_i))-\mu_1\left[(1-(\hat{\varpi}_i+\hat{\tau}_i))\left(\frac{\ln(2)d_{\mathcal{R}_i,\mathcal{D}}^{-\vartheta}|h_{\mathcal{R}_i,\mathcal{D}}|^2}{\sigma_{n_{\mathcal{D}}}^2+P_{\mathcal{R}_i}d_{\mathcal{R}_i,\mathcal{D}}^{-\vartheta}|h_{\mathcal{R}_i,\mathcal{D}}|^2}\right)\right]$$
$$-\mu_2(1-(\hat{\varpi}_i+\hat{\tau}_i))-\mu_3\left[-(1-(\hat{\varpi}_i+\hat{\tau}_i))\left(\frac{\ln(2)d_{\mathcal{R}_i,\mathcal{D}}^{-\vartheta}|h_{\mathcal{R}_i,\mathcal{D}}|^2}{\sigma_{n_{\mathcal{D}}}^2+P_{\mathcal{R}_i}d_{\mathcal{R}_i,\mathcal{D}}^{-\vartheta}|h_{\mathcal{R}_i,\mathcal{D}}|^2}\right)\right]=0. \tag{5.36}$$

The conditions for feasibility are as expressed in (5.30), (5.31), (5.32), and (5.33). Complementary slackness expressions can be represented as follows

$$\mu_1 \cdot G(\hat{\varpi}_i, \hat{\tau}_i, P_{\mathcal{R}_i}) = 0, \tag{5.37}$$
$$\mu_2 \cdot H(\hat{\varpi}_i, \hat{\tau}_i, P_{\mathcal{R}_i}) = 0, \tag{5.38}$$
$$\mu_3 \cdot I(\hat{\varpi}_i, \hat{\tau}_i, P_{\mathcal{R}_i}) = 0, \tag{5.39}$$
$$\mu_4 \cdot J(\hat{\varpi}_i, \hat{\tau}_i, P_{\mathcal{R}_i}) = 0. \tag{5.40}$$

The conditions for non-negativity are: $\hat{\varpi}_i, \hat{\tau}_i, P_{\mathcal{R}_i}, \mu_1, \mu_2, \mu_3, \mu_4 \geq 0$. It is clear that if $\mu_4 \neq 0$, then $J(\hat{\varpi}_i, \hat{\tau}_i, P_{\mathcal{R}_i}) = 0$ implying that $\hat{\varpi}_i + \hat{\tau}_i = 1$. Since this is not a feasible solution, therefore $\mu_4 = 0$. The two possible solution are as mentioned in the following theorems, respectively.

Theorem 2. *If* $\mu_1 \neq 0 \implies G(\hat{\varpi}_i, \hat{\tau}_i, P_{\mathcal{R}_i}) = 0$; $\mu_2 = 0 \implies H(\hat{\varpi}_i, \hat{\tau}_i, P_{\mathcal{R}_i}) \neq 0$; $\mu_3 \neq 0 \implies I(\hat{\varpi}_i, \hat{\tau}_i, P_{\mathcal{R}_i}) = 0$, *then we obtain the following optimal values*

$$P^{\dagger}_{\mathcal{R}_i} = (\nu - 1)\left(\frac{\sigma^2_{n_{\mathcal{D}}}}{d^{-\vartheta}_{\mathcal{R}_i,\mathcal{D}}|h_{\mathcal{R}_i,\mathcal{D}}|^2}\right), \tag{5.41}$$

$$\hat{\tau}^{\dagger}_i = \frac{r}{B\log_2(1 + \Upsilon_{\mathcal{S},\mathcal{R}_i}) + (\delta_i \cdot r)}, \tag{5.42}$$

$$\hat{\varpi}^{\dagger}_i = 1 - r\left(\frac{1}{B\log_2(1 + \Upsilon_{\mathcal{S},\mathcal{R}_i}) + (\delta_i \cdot r)} + \frac{1}{B\log_2\left(1 + \frac{P^{\dagger}_{\mathcal{R}_i} d^{-\vartheta}_{\mathcal{R}_i,\mathcal{D}}|h_{\mathcal{R}_i,\mathcal{D}}|^2}{\sigma^2_{n_{\mathcal{D}}}}\right)}\right), \tag{5.43}$$

where

$$\nu = \exp\left(\mathcal{W}\left(-\frac{\mathcal{A}}{B}\exp\left(-\frac{1}{B}\log^2(2)\right) * \log(2)\right) + \frac{\log^2(2)}{B}\right), \tag{5.44}$$

with $\mathcal{A} = \ln(2) - \left(\frac{\zeta}{\sigma^2_{n_{\mathcal{D}}}}\right)(\ln(2) d^{-\vartheta}_{\mathcal{R}_i,\mathcal{D}}|h_{\mathcal{R}_i,\mathcal{D}}|^2)(P_{\mathcal{S}} d^{-\vartheta}_{\mathcal{S},\mathcal{R}_i}\ |h_{\mathcal{S},\mathcal{R}_i}|^2 + \sigma^2_{n_{\mathcal{R}_i}})$.

Theorem 3. *If* $\mu_1 \neq 0 \implies G(\hat{\varpi}_i, \hat{\tau}_i, P_{\mathcal{R}_i}) = 0$; $\mu_2 \neq 0 \implies H(\hat{\varpi}_i, \hat{\tau}_i, P_{\mathcal{R}_i}) = 0$; $\mu_3 \neq 0 \implies I(\hat{\varpi}_i, \hat{\tau}_i, P_{\mathcal{R}_i}) = 0$, *then the following values are optimal*

$$P^{*}_{\mathcal{R}_i} = (\tilde{\eta}_{_L} - 1)\left(\frac{\sigma^2_{n_{\mathcal{D}}}}{d^{-\vartheta}_{\mathcal{R}_i,\mathcal{D}}|h_{\mathcal{R}_i,\mathcal{D}}|^2}\right), \tag{5.45}$$

$$\hat{\tau}^{*}_i = \frac{r}{B\log_2(1 + \Upsilon_{\mathcal{S},\mathcal{R}_i}) + (\delta_i \cdot r)}, \tag{5.46}$$

$$\hat{\varpi}^{*}_i = \frac{rP^{*}_{\mathcal{R}_i} - E_{ext} B\log_2\left(1 + \frac{P^{*}_{\mathcal{R}_i} d^{-\vartheta}_{\mathcal{R}_i,\mathcal{D}}|h_{\mathcal{R}_i,\mathcal{D}}|^2}{\sigma^2_{n_{\mathcal{D}}}}\right)}{\zeta(P_{\mathcal{S}} d^{-\vartheta}_{\mathcal{S},\mathcal{R}_i}|h_{\mathcal{S},\mathcal{R}_i}|^2 + \sigma^2_{n_{\mathcal{R}_i}})}, \tag{5.47}$$

where $\tilde{\eta}_{_L}$ = *Largest Root of* $[\mathcal{A} - B\log_2(\tilde{\eta})\Big(\mathcal{B} + \mathcal{C}\tilde{\eta} + \mathcal{D}B\log_2(\tilde{\eta})\Big) = 0]$, *with* $\mathcal{A} = a \cdot b \cdot r$, $\mathcal{B} = a \cdot b + a \cdot r \cdot \left(\frac{\sigma^2_{n_{\mathcal{D}}}}{d^{-\vartheta}_{\mathcal{R}_i,\mathcal{D}}|h_{\mathcal{R}_i,\mathcal{D}}|^2}\right) - b \cdot r$, $\mathcal{C} = -a \cdot r \cdot \left(\frac{\sigma^2_{n_{\mathcal{D}}}}{d^{-\vartheta}_{\mathcal{R}_i,\mathcal{D}}|h_{\mathcal{R}_i,\mathcal{D}}|^2}\right)$, *and* $\mathcal{D} = a \cdot E_{ext}$, *where* $a = B\log_2(1 + \Upsilon_{\mathcal{S},\mathcal{R}_i}) + (\delta_i \cdot r)$, *and* $b = \zeta(P_{\mathcal{S}} d^{-\vartheta}_{\mathcal{S},\mathcal{R}_i}|h_{\mathcal{S},\mathcal{R}_i}|^2 + \sigma^2_{n_{\mathcal{R}_i}})$.

Proof. See Appendix E.2.

To summarize the solutions obtained above, we propose the following algorithm to maximize the stored energy in the relay supporting SWIPT - Caching system (MSE-WC Algorithm)

Algorithm. *MSE-WC Algorithm*

Input: The parameters $h_{\mathcal{S},\mathcal{R}_i}$, $h_{\mathcal{R}_i,\mathcal{D}}$, δ_i, r, and E_{ext}.
Output: The maximized value of energy stored at the relay: $\{E_S\}$.

1. : Initialize: $\zeta \in (0,1]$, $P_T \in (0, \varepsilon P_{Max}]$, $0.5 < \varepsilon < 1$, $\sigma^2_{n_{\mathcal{R}_i}} = 1$, and $\sigma^2_{n_{\mathcal{D}}} = 1$.
2. : Compute $P^{\dagger}_{\mathcal{R}_i}$, $\hat{\tau}^{\dagger}_i$, and $\hat{\varpi}^{\dagger}_i$ using (5.41), (5.42), and (5.43) respectively.
3. : Define: $E^{\dagger}_S = \zeta \hat{\varpi}^{\dagger}_i (P_{\mathcal{S}} d^{-\vartheta}_{\mathcal{S},\mathcal{R}_i} |h_{\mathcal{S},\mathcal{R}_i}|^2 + \sigma^2_{n_{\mathcal{R}_i}}) + E_{ext} - (1 - (\hat{\varpi}^{\dagger}_i + \hat{\tau}^{\dagger}_i)) P^{\dagger}_{\mathcal{R}_i}$.
4. : Compute $P^{*}_{\mathcal{R}_i}$, $\hat{\tau}^{*}_i$, and $\hat{\varpi}^{*}_i$ using (5.45), (5.46), and (5.47) respectively.
5. : Define: $E^{*}_S = \zeta \hat{\varpi}^{*}_i (P_{\mathcal{S}} d^{-\vartheta}_{\mathcal{S},\mathcal{R}_i} |h_{\mathcal{S},\mathcal{R}_i}|^2 + \sigma^2_{n_{\mathcal{R}_i}}) + E_{ext} - (1 - (\hat{\varpi}^{*}_i + \hat{\tau}^{*}_i)) P^{*}_{\mathcal{R}_i}$.
6. : $E_S = \max(E^{\dagger}_S, E^{*}_S)$.
7. : **return** E_S.

The algorithm proposed above returns the maximized value of the objective function as its output. First, we initialize all the necessary values as indicated in 1). Then, we compute the optimal values of $P^{\dagger}_{\mathcal{R}_i}$, $\hat{\tau}^{\dagger}_i$, and $\hat{\varpi}^{\dagger}_i$ in 2), and define the energy stored at the relay in 3). 2) and 3) corresponds to the solutions obtained for Case VI during the analysis. Similarly, we find the optimal values of $P^{*}_{\mathcal{R}_i}$, $\hat{\tau}^{*}_i$, and $\hat{\varpi}^{*}_i$ in 4), and define the energy stored at the relay in 5) accordingly. 4) and 5) corresponds to the solutions obtained for Case VIII during the analysis. Next, we find the maximum of the two computed local optimal solutions for the energy stored at the relay, which in turn maximizes the objective function. It should also be noted that the solutions proposed in (P2) for maximizing the energy stored at the relay are not necessarily global optimum, as the problem is non-linear in nature. However, the KKT conditions guarantees the local optimal solutions.

From our analysis above $\Big((5.28)\text{-}(5.40)\Big)$, it is clear that the necessary conditions for KKT are satisfied. Let us assume that the optimal solutions obtained via KKT are (i) Primal variables: $\hat{\varpi}^{\star}_i$, $\hat{\tau}^{\star}_i$, $P^{\star}_{\mathcal{R}_i}$, (ii) Dual Variables: $\mu^{\star}_1$, $\mu^{\star}_2$, $\mu^{\star}_3$. With the help of these solutions, we find that the second order derivatives : $\nabla^2_{\hat{\varpi}_i \hat{\varpi}_i} \mathcal{L}(\hat{\varpi}^{\star}_i, \hat{\tau}^{\star}_i, P^{\star}_{\mathcal{R}_i}; \mu^{\star}_1, \mu^{\star}_2, \mu^{\star}_3) = 0$, $\nabla^2_{\hat{\tau}_i \hat{\tau}_i} \mathcal{L}(\hat{\varpi}^{\star}_i, \hat{\tau}^{\star}_i, P^{\star}_{\mathcal{R}_i}; \mu^{\star}_1, \mu^{\star}_2, \mu^{\star}_3) = 0$, and $\nabla^2_{P_{\mathcal{R}_i} P_{\mathcal{R}_i}} \mathcal{L}(\hat{\varpi}^{\star}_i, \hat{\tau}^{\star}_i, P^{\star}_{\mathcal{R}_i}; \mu^{\star}_1, \mu^{\star}_2, \mu^{\star}_3) \geq 0$; are sufficient conditions for KKT, but does not meet the sufficiency criteria strictly. Hence, the function is not strictly constrained local minimum. Therefore, the presented solutions are not necessarily global optimal.

In order to analyze the proposed approach from an economic perspective, we denote the equivalent relationship between the Lagrange Multipliers μ_1 and μ_3 as μ_R and rename μ_2 as μ_E which corresponds to the the prices for data and energy, respectively, in cost units. Using the results from our analysis in Appendix E.2, we find that $\mu_E = \frac{f_1(P_{\mathcal{S}}, \delta_i, r)}{f_2(P_{\mathcal{S}})} \cdot \mu_R$, where $f_1(P_{\mathcal{S}}, \delta_i, r)$, and $f_2(P_{\mathcal{S}})$ are functions computed as per the illustrated technique. Correspondingly, if more energy is required by the relay with fixed caching capacity, then we are forced to compensate for the request by using the energy metric per cost unit at the source in order to satisfy the respective data and energy constraints in $(P2)$. This action

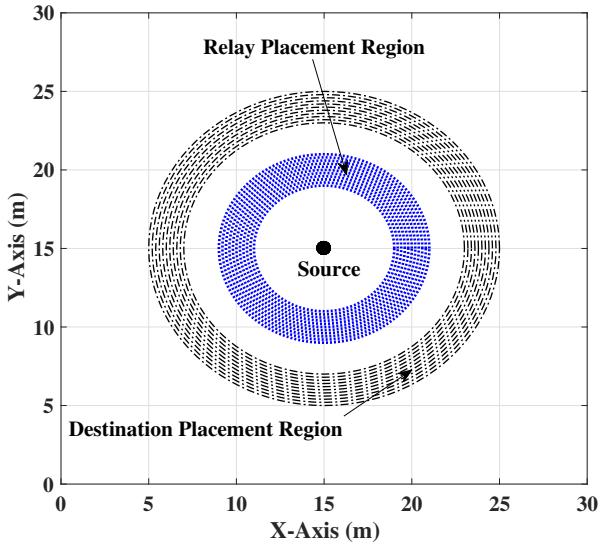

FIGURE 5.5: Simulated Scenario: An ITU-R P.1238 framework implemented with the relays spatially distributed within the blue region (4m to 6m from the source) and the destination placed randomly within the black region (8m to 10m from the source).

would however add more to the data price as well. Similarly, it is apparent that increasing the transmit power will readily add to the cost of energy transfer in addition to an increased data price. Furthermore in the context of caching, it is worth mentioning that *extra cache capacity implies subordinate prices for data and energy transmissions per cost unit.*

5.4.2 Relay Selection

From the methods proposed above, optimal TS ratios and the relay transmit power can be computed easily. Herein, we propose to find the best relay which provides maximized harvested power corresponding to (5.26). In this context, the index of the optimally selected relay can be expressed as $j^{\star} = \arg\max_{j\in\{1,\ldots,K\}} E^{\star}_{S_j}$, where $E^{\star}_{S_j}$ is the optimal energy stored at the j-th relay as the solution of problem (5.27).

5.5 Numerical Results

In this section, we evaluate the performance of the proposed system for the solutions presented in this chapter. We employ the ITU Radiocommunication Sector (ITU-R) P.1238 channel model [193] with central frequency assumption at 450 MHz. The signal fading in both the hops follow Ricean distribution with K-factor of 3.5. The overall emulation setup is depicted in Fig. 5.5. Additionally, we consider a total bandwidth of $B = 1$ MHz, $\zeta = 0.50$ [261], $\sigma^2_{n_{\mathcal{R}_i}} = -100$ dBW, and $\sigma^2_{n_{\mathcal{D}}} = -100$ dBW. All the relays are assumed to have the same caching coefficient, i.e., $\delta_i = \delta, \forall i$. All the results are evaluated over 500 Monte-Carlo random channel realizations. The proposed architecture is compared with a reference scheme using a fix time-splitting. The reference scheme spends the first half period for information broadcasting and energy harvesting, and uses the second half period for relaying [246, 258].

Fig. 5.6 plots the performance of the cache-aided SWIPT as a function of the total number of relays. The result is calculated based on the best relay selected as in Section 5.3 and Section 5.4. In both cases, $\delta = 0.5$, and $E_{ext} = 1\mu$J. It is observed from Fig. 5.6(a) that

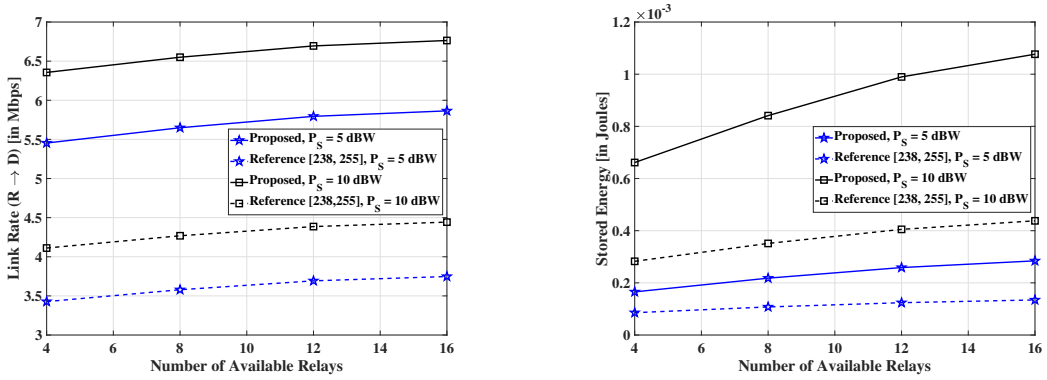

(a) (b)

FIGURE 5.6: Performance comparison between the proposed cache-aided SWIPT and the reference scheme for different number of available relays with $\delta = 0.5$, $r = 3$ Mbps, and $E_{ext} = 1\mu$J. (a) Link rate performance. (b) Stored energy performance.

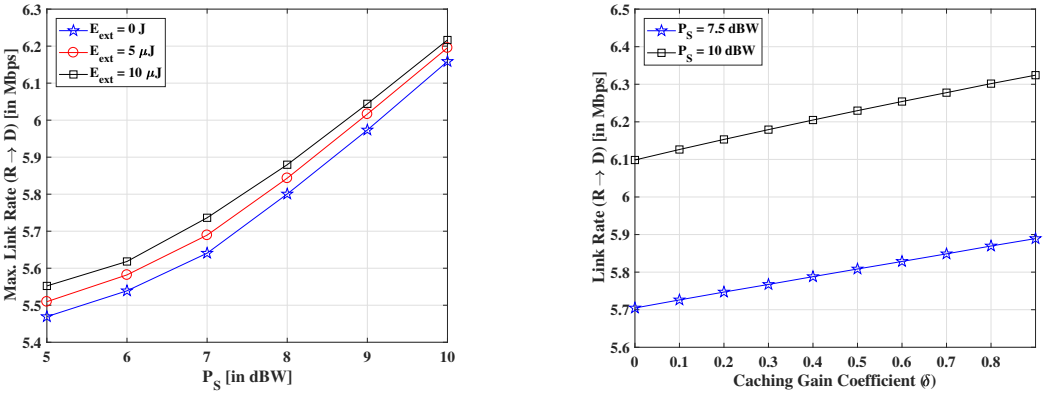

(a) (b)

FIGURE 5.7: Link-rate maximization: (a) Maximum link rate versus increasing values of $P_{\mathcal{S}}$ for various values of E_{ext} with total number of available relays $K = 8$, caching coefficient $\delta = 0.5$, and $r = 5$ Mbps. (b) Maximized link rate versus the caching coefficient for various $P_{\mathcal{S}}$ with total number of available relays $K = 8$, $E_{ext} = 10$ μJ, and $r = 5$ Mbps.

the proposed architecture significantly outperforms the reference and the gain is larger as the number of available relays increases. In particular, the proposed architecture achieves a performance gain of 15% for $P_{\mathcal{S}} = 5$ dBW and 20% for $P_{\mathcal{S}} = 10$ dBW over the reference scheme. This result confirms the effectiveness of the proposed optimization framework. It is also shown that having more relays results in a better serving rate thanks to inherent diversity gain brought by the relays. The harvested energy comparison between the proposed and the reference is plotted in Fig. 5.6(b). A similar conclusion is observed that the proposed architecture surpasses the reference in all cases. In addition, having more available relays improves the harvested energy.

Fig. 5.7(a) illustrates the results corresponding to the solutions proposed for the rate maximization problem, assuming that an optimal relay is chosen as per the solutions corresponding to the outer optimization of (5.7). It is observed from the figure that the source transmit power has a significant influence on the achievable rate. In particular, by increasing the source transmit power by 5 dBW, the serving rate is increased by 30%. This result can be explained from the fact that for a given caching coefficient, the source does not have to send the whole requested content to the relay. In this case, having a larger source power results

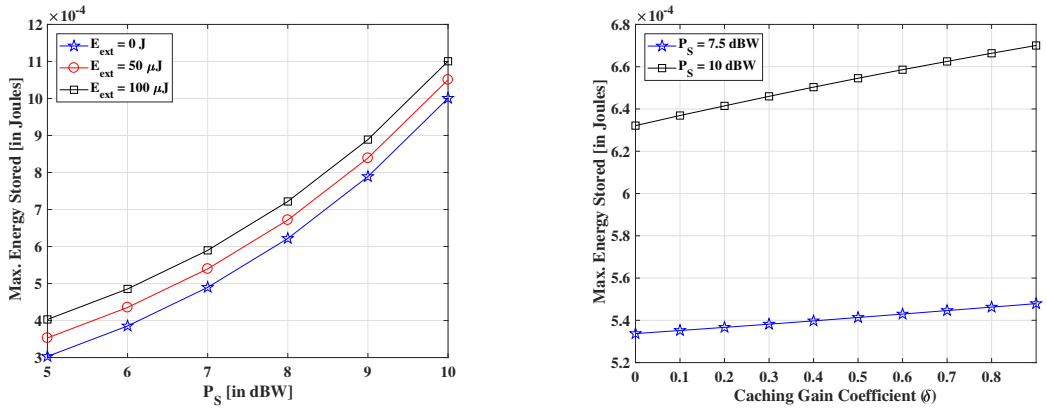

FIGURE 5.8: Stored Energy maximization: (a) Stored energy performance as a function of the source transmit power for various values of E_{ext}. $K = 8$ relays, $\delta = 0.5$ and $r = 1$ Mbps. (b) Stored energy performance as a function of the caching coefficient for various values of $P_{\mathcal{S}}$. $K = 8$ relays, $E_{ext} = 0.5$ mJ, and $r = 5$ Mbps.

in more harvested energy, which in turn increase the relay's transmit power. Especially, this observation is also obtained when there is not external energy source, e.g., $E_{ext} = 0$, which shows the effectiveness of the proposed cache-aided SWIPT architecture.

Fig. 5.7(b) plots the maximum throughput as a function of the caching gain coefficient with $E_{ext} = 10$ μJ and $r = 5$ Mbps. It is observed that the caching gain has similar impact on the achievable throughput for different values of $P_{\mathcal{S}}$. In general, a larger cache size (or equivalent larger caching coefficient) results in a higher serving rate. This result together with result in Fig. 5.7(a) suggest an interactive role of the caching capacity and the transmit power. In particular, a smaller source power system can still achieve the same throughput by increasing the cache size.

Fig. 5.8(a) presents the stored energy at the chosen relay, according to the solution of outer optimization of (5.26), as a function of the source's transmit power and different external energy values. It is shown from the results that the source transmit power has large impacts on the stored energy at the relay. In particular, increasing the source's transmit power by 2 dBW will double the stored energy at the relay. It is also observed that increasing the external energy can significantly improve the stored energy at high $P_{\mathcal{S}}$ values. However, when $P_{\mathcal{S}}$ is small, increasing E_{ext} does not bring considerable improvement. This is because at low $P_{\mathcal{S}}$ values, most of the time is used for information transfer from the source to the relay.

Fig. 5.8(b) depicts the plot of the energy stored at the selected relay as a function of the cache capacity δ, with $E_{ext} = 0.5$ mJ and $r = 5$ Mbps. The case with $\delta = 0$ implies that there is no caching at the relay. It is shown that caching helps to increase the saved energy at the relay for all $P_{\mathcal{S}}$ values. And the increased stored energy are almost similar for different $P_{\mathcal{S}}$. This is because of the linear model of the caching system.

Fig. 5.9(a) presents an evaluation of the energy stored at the chosen relay against the increasing values of r. It is seen that the energy stored at the relay decreases with increasing values of requested rate (r), for $\delta = 0.5$ and $E_{ext} = 0.1$ mJ. On the other hand, it is clear that with increasing values of $P_{\mathcal{S}}$, the energy stored at the relay increases non-linearly. The former variation is due to the fact that in order to meet the demand of requested rate at the destination, more energy would be required for resource allocation at the relay which utilizes

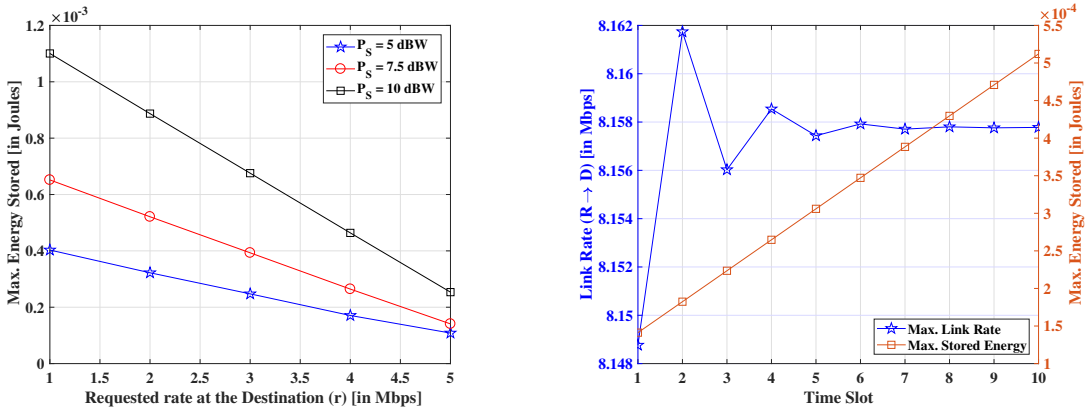

FIGURE 5.9: Rate-Energy trade-off and comparison of the two proposed relay selection schemes. (a) Stored energy performance as a function of QoS requirements with different source transmit power. $K = 8$ relays, $\delta = 0.5$ and $E_{ext} = 0.1$ mJ. (b) Performance of the two proposed relay selection schemes for ten time slots. $K = 8$ relays, $P_{\mathcal{S}} = 7.5$ dBW, $E_{ext} = 1\mu$J, $r = 3$ Mbps.

the harvested energy.

Fig. 5.9(b) illustrates the comparison between the two proposed relay selection schemes for various time slots with $K = 8$ relays, $P_{\mathcal{S}} = 7.5$ dBW, $E_{ext} = 1$ μJ, $r = 3$ Mbps. Herein, we assumed $E_{ext} = 1$ μJ as the initial external energy in the first slot, while in the subsequent slots, the value for E_{ext} was assumed as the stored energy value in the previous slot. The results helps in simultaneously studying impact of the relay selection using the two problems, where it is seen that the throughput saturates after some time-slots implying that $E_{ext} \to 0$ while the stored energy increases linearly. These respective cases for throughput and stored energy maximization provides useful insight on the benefits of relay selection on the system performance.

5.6 Summary

In this chapter, we proposed and investigated relay selection strategy in a novel cache-assisted SWIPT architecture with dynamic time switching (TS) in dual-hop half duplex system, where the relays employ the DF protocol. We addressed the problem of relay selection to maximize the data throughput between the relay and destination under constraint on minimum energy stored at the relay; and relay selection for maximizing the energy stored at the relay under constraints on minimum rate and harvested energy, guaranteeing a good performance in both the cases with regards to the QoS constraints. Besides, both the problems were formulated according to two separate yet distinct conventions over the time period. We presented the closed-form solutions for the proposed relay system to enable SWIPT with caching. With the help of simulations, we illustrated the results corresponding to the solutions obtained for the aforementioned problems with parameter variations. This work can be further extended to many fascinating directions like multiuser and multicarrier scenario, and relaying with full duplexing mode. Another promising research topic is to consider multiple antennas systems where an additional dimension is how to optimally select antennas or design beamforming vectors for information transmission or energy transfer. In addition, the energy queuing model and adoption of Markov Decision Process (MDP) to model the aforementioned problems can be another interesting direction to this work, wherein the same problems can be studied using

stochastic methods with uncertain CSI. Therefore, by leveraging from the benefits of caching, we intend to improve system efficiency to enhance SWIPT performance. This can be realized by dynamic adjustment of the TS factors, which can significantly improve the throughput and energy storage capabilities at the relay.

Chapter 6

Conclusions and Future Works

A summary and the main conclusions of the work performed in this Thesis are provided in Section 6.1. Finally, Section 6.2 provides an outlook for possible future works.

6.1 Main Conclusion

With each passing year, the advancements in the field of wireless power transfer (WPT) continue to motivate the researchers in proposing some interesting ideas. Based on the recent developments in the domain, one of the promising approaches is to incorporate the information or data transfer (i.e., wireless communication techniques) with WPT, which is termed as simultaneous wireless information and power transfer (SWIPT). In this Thesis, we focused on the design and optimization of SWIPT systems. We provided an overview of the topic in this regard, followed by an thorough survey on the existing (and proposed) SWIPT systems. In order to address the distance limitations, co-existence of heterogeneous user types (ID, and/or EH and/or both) within a single system, and transmission and storage of both information and energy; we investigated the possibilities of SWIPT in three categories of frameworks including cooperative relaying, precoder designing for multi-group multicasting, and caching, respectively, as discussed below.

Firstly, we proposed a novel resource allocation and relay selection scheme for cooperative multi-user multi-relay OFDMA networks with SWIPT capabilities at the end-users. Our aim was to optimize the end-nodes' power splitting (PS) ratios as well as the relay, carrier and power assignment so that the sum-rate of the system could be maximized, subjected to harvested energy and transmitted power constraints. In this regard, we provided a solution with the help of dual problem formulation, which guaranteed an asymptotic optimality and less execution time in comparison to a highly-complex exhaustive search approach. Furthermore, we also presented a heuristic method to solve this problem with lower computational complexity.

Secondly, we assumed several multicasting (MC) groups comprising three types of heterogeneous users including information decoding (ID), EH and both ID and EH. We presented a novel framework to investigate the multi-group (MG) - MC precoder designs for three different scenarios, namely, Separate Multicast and Energy Precoding Design (SMEP), Joint Multicast and Energy Precoding Design (JMEP), and Per-User Information and/or Energy Precoding Design (PIEP). In the considered system, a multi-antenna source was assumed to transmit the relevant information and/or energy to the groups of corresponding receivers

using more than one MC streams. In this context, two problems were formulated to minimize the total transmit power, and to maximize the overall harvested energy, respectively; both subjected to the constraints on minimum SINR and EH demands at the corresponding users. The aforementioned problems were transformed with the use of semidefinite relaxation technique considering three scenarios, viz., SMEP, JMEP and PIEP, respectively. Moreover, an additional slack variable reduction method was adopted to make the harvested energy maximization problem tractable. Suitable solutions with considerably good performance were proposed to address the aforementioned problems.

Lastly, we investigated the performance of cache-assisted SWIPT cooperative systems, in which one source was assumed to communicate with one destination via the aid of multiple relays. In order to prolong the relays' serving time, the relays were assumed to be equipped with a cache memory and EH capability. Based on the time-splitting mechanism, we analyzed the effect of caching on the system performance in terms of the serving throughput and the stored energy at the relay. Particularly, two optimization problems were formulated for (i) maximizing the relay-destination throughput and (ii) the energy stored at the relay, both subjected to some quality-of-service (QoS) constraints, respectively. By using the KKT conditions and with the help of the Lambert function, we obtained closed-form solutions for the two formulated problems. In order to further improve the performance, a relay selection policy was introduced to select the best relay based on either the maximum throughput between the relays' and destination link or maximum stored energy at the relay, for conveying information to the destination.

Towards this end, the main contributions of this Thesis are summarized below.

1. Different from several existing works in the literature, this Thesis considered three distinctly novel system designs for investigation of SWIPT mechanism.

2. The assumed frameworks were individually scrutinized with the help of rigorous mathematical (optimization) analysis.

3. For the above-mentioned problems, we presented suitable closed-form solutions, algorithms, or solutions via different types of convex-optimization methods.

4. The algorithms proposed in this Thesis were designed for an optimal (as well as suboptimal) performance for the respective scenarios, however, ensuring extremely less execution time complexities.

5. Supporting results based on MATLAB simulations were provided, which included practically motivated designing and optimization methods for the SWIPT systems.

6.2 Future Works

Although the results presented in this Thesis have demonstrated the effectiveness of the proposed designs and optimization methods for different types of SWIPT systems, many opportunities for extending the scope of this Thesis still remain open. This section discusses some of the topics that we consider particularly interesting for extension and new problems.

6.2.1 Possible Extensions

- **Further analysis of the SWIPT-Caching Framework**: The SWIPT-Caching framework investigated in Chapter 5 could be further extended into many fascinating directions. Some of these possibilities include extension of the current work to multiple-users and/or multi-carrier scenario. Moreover, the non-linear EH model may be used for investigation. From the machine learning view-point, several appealing directions open up based on the optimization of caching coefficient with regard to the proposed SWIPT-caching framework. The main outcome of this investigation points towards a unified framework which combines information/energy transmission and storage, which was missing from the literature. In this direction, information processing could also be considered in ultra-low power fog computing SWIPT-based networks. Further discussion on other (in-line) possibilities is provided in the next section.

- **More Insights on the Multi-group Multicasting with SWIPT framework**: In Chapter 4 of this Thesis, a comparative study between three different scenarios for Multi-group Multicasting in SWIPT systems with heterogeneous users was provided. In the process, the most simple form of optimization problem (i.e., semidefinite programming (SDP)) and a simple relaxation technique (i.e., semidefinite relaxation) were used for analysis. However, several other possibilities still remain open, specifically concerning the technical analysis for better optimization of the system parameters. In this regard, certain methods like feasible-point pursuit and successive convex approximation, second-order conic programming (SOCP), etc., may be explored. Furthermore, alternate optimization problems may also be formulated and analyzed for the proposed systems, e.g., combined objective with rate and harvested energy, fractional optimization including rate, harvested energy and transmit power, etc. Several other extension possibilities includes: (i) consideration of TS and/or PS schemes at the end-users for theoretical analysis, (ii) adaptive beamforming, (iii) antenna splitting and per-antenna power constraints, (iv) incorporation of practically-motivated power consumption models, and (v) behavior of system with consideration of minimum input power at the EH models. From a practical (lab) implementation view-point, the proposed framework could be tested by using the USRPs and energy harvesting test-beds. As an initial step, the work proposed in Chapter 4 of this Thesis could be taken up and implemented for practical experiments. Based on further theoretical developments, the system performance could be made more efficient.

- **Consideration of Interference aspect in the OFDMA scenario**: The framework provided in Chapter 3 considers an investigation assuming the orthogonal frequency division multiple access (OFDMA) type of multi-carrier setting, however, without consideration of the interference aspect. As an extension, a more practical scenario may be considered for investigation which also takes interference into account. The same framework could be further extended by using the non-orthogonal multiple access (NOMA), with possible considerations of the power-domain and/or code-domain based NOMA schemes.

- **Imperfect channel state information (CSI)**: Although more practical centric computer simulations were provided in the Thesis, the channel conditions were assumed to be known throughout. As a possible extension, all the proposed scenarios and results could be investigated again with an assumption of an imperfect CSI, to drive the systems more closer to the practical systems, e.g., unknown channel for EH devices only

since there might not necessarily be a return link like actuators.

6.2.2 New Problems

- **Waveform Designing for SWIPT**: Based on the research developments in the domain, there are primarily two options to tackle SWIPT systems: (i) optimization of the system (or network) and relevant parameters and (ii) focus on waveform optimization for enhancement in the system performance. In this Thesis, we have mostly focused on system designing and optimization problems with an assumption of Gaussian signaling for simplicity. In case of non-linearities, the proposed methods in this Thesis may be considered as benchmark performances in contrast to the systems with enhanced performances with different waveform designing. It is also noteworthy that most of the works in the literature considers Gaussian signaling which may be used to describe a generalized framework with regard to the several types of EH models. There may be possibilities where specific EH waveforms may be designed to serve a certain type of EH module while the performance may not be guaranteed to enhance the EH characteristic at another EH receiver. In simple terms, we present generalized solutions in this Thesis (similar to traditional methods in wireless communications), which would provide suitable solutions under any circumstance.

  Waveform designing for SWIPT systems is an emerging and promising topic in the domain [221, 243, 262–266]. With an intention of designing separate waveforms for both information and energy transmissions, SWIPT waveform designing would be an interesting choice for investigation with the Separate Multicast and Energy Precoding Design (SMEP) model presented in the Chapter 4 of this Thesis. The benefits provided by this flexible form of system (SMEP) seems to be an ideal candidate for investigation with SWIPT waveform designing.

- **Backscattering-SWIPT system design**: There are several existing works in the literature considering the Backscatter communications [267–271]. In terms of SWIPT, it is noteworthy that most of the existing works assume a linear EH model at the SWIPT receiver. An investigation with similar system model as presented in Chapter 3 may be carried out, with the replacement of relays by Backscatter devices.

- **IoT systems with ultra-low power fog computing SWIPT-based networks**: The IoT systems are new paradigm which assist the development future generations of wireless communications. Most of the IoT networks are composed of ultra-low power wireless sensor nodes, which have limited batteries and frequent recharging is difficult process. In this regard, there has been some recent progress in the domain of IoT systems with ultra-low power fog computing SWIPT-based networks [207,238,272–274]. In conjunction with the framework proposed in Chapter 5, interesting possibilities may be realized both from systems and mathematical analysis view-point. Some possible extensions include consideration of (i) Caching in IoT systems with ultra-low power fog computing SWIPT-based networks, (ii) non-linear energy harvesting model at the receivers, and (iii) different types of SWIPT receiver architectures such as TS and PS.

- **Rate-Splitting for SWIPT**: Rate-splitting is emerging as another interesting scheme to enhance rate, robustness and Quality-of-Service (QoS) for future generations of wireless communication systems. In the context of SWIPT, there are limited works available

in the literature [275]. The availability of different types of EH models and consideration of variable scenarios (such as multi-user MIMOs, SWIPT TS/PS schemes at the receivers, etc.), several interesting optimization problems including maximization of harvested energy, maximization of SINR/Rate, etc., under certain QoS and EH constraints, may be formulated and analyzed in the domain.

Appendix A

Relevant Optimization Techniques

A.1 Graphical Analysis of Optimization Problem

The most trivial method to understand the behavior of the objective function and constraints (or the optimization problem as a whole) and seek an optimal solution, is to perform analysis via graphical method. In this context, let us consider an example aiming at minimization of two (optimization) variable based function with relevant constraints [276] as follows

$$(P1): \min_{x,y} \quad F(x,y) \tag{A.1}$$

$$\text{s.t.} \quad (C1): G(x,y) \leq 5, \tag{A.2}$$

$$(C2): H(x,y) \geq -1, \tag{A.3}$$

where $F(x,y) = -x + 2y$, $G(x,y) = x^2 + y^2$, and $H(x,y) = x + y$, with $x, y \in \mathbb{Z}$.

To proceed, we consider plotting the constraint $(C1)$ on the x-y cartesian coordinate system as follows

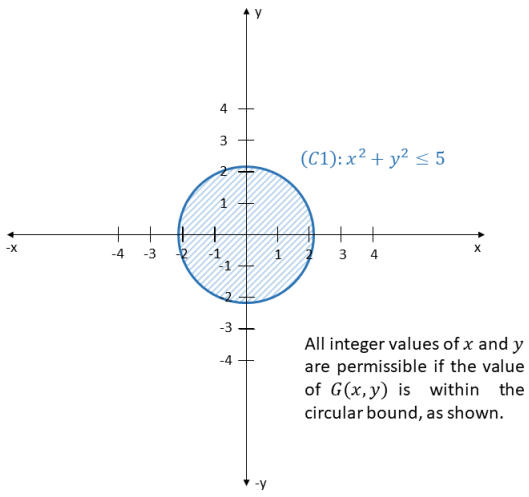

In a similar manner(as above), we plot the function in constraint $(C2)$ as provided below

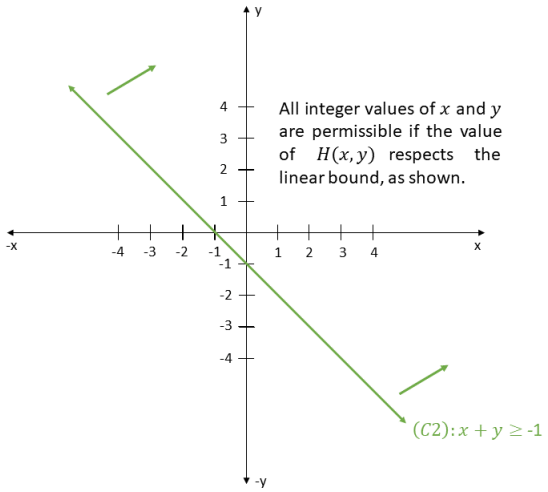

For the other cases or types of optimization problems (with several constraints), all the constraints of that problem may be plotted in a similar fashion.

Next, it is necessary to combine all the plots of constraints in order to find a feasibility set for the corresponding optimization problem in the considered example. Therefore, we have the following feasibility space.

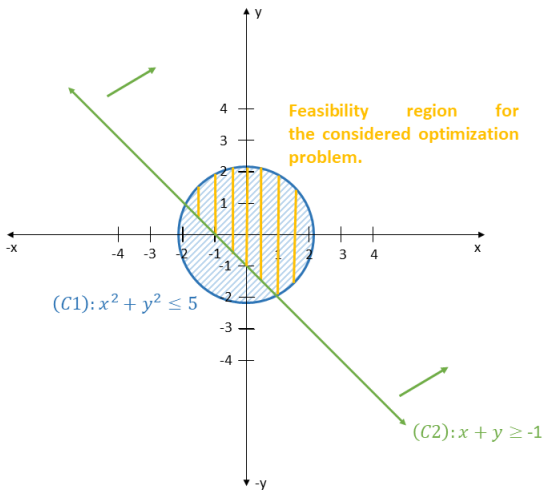

Finally, we observe the nature of the objective function in the optimization problem. To begin with, we set $F(x, y) = 0$ whose plot is indicated in the following figure. Then we assume any value less than zero (say -2) for minimizing the objective, and plot $F(x, y) = -2$. This process is repeated until the minimum value within the feasibility set of the optimization problem is reached, as shown in the figure below.

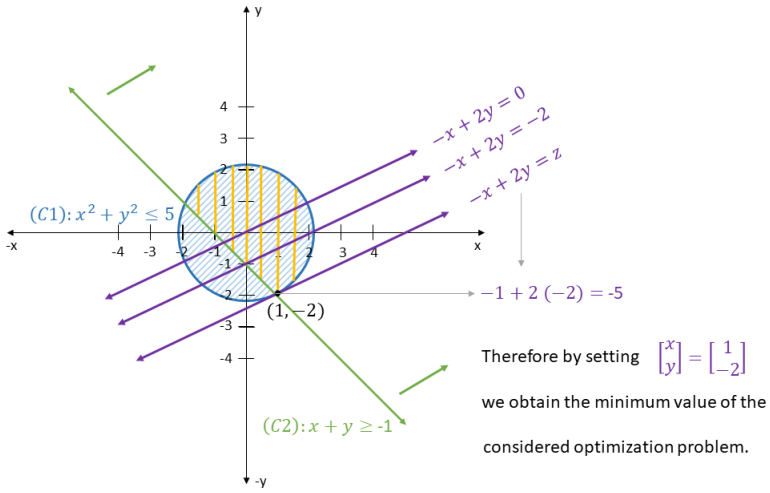

This method is often used to solve convex form of optimization problems, where an optimal solution could be obtained. This method was used for analysis in [**C1**] and partially in [**C2**].

A.2 Lagrangian and Dual Problem

Let us consider a generic optimization problem [277] where we intend to minimize an objective function $\mathbf{F}(\mathbf{x})$, which has n variables. The optimization problem has m equality constraints and p inequality constraints. Then, the (primal) optimization problem is mathematically represented as

$$(P1): \min_{\mathbf{x}} \quad \mathbf{F}(\mathbf{x}) \qquad [\mathbf{F}(\mathbf{x}) : \mathbb{R}^n \rightarrow \mathbb{R}] \tag{A.4}$$

$$\text{s.t.} \quad (C1): \mathbf{H}(\mathbf{x}) \leq 0, \qquad [\mathbf{H}(\mathbf{x}) : \mathbb{R}^n \rightarrow \mathbb{R}^m] \tag{A.5}$$

$$(C2): \mathbf{G}(\mathbf{x}) = 0. \qquad [\mathbf{G}(\mathbf{x}) : \mathbb{R}^n \rightarrow \mathbb{R}^p] \tag{A.6}$$

Here, we aim to relax the constraints by associating a penalty parameter with each of them. Thus, we associate with each of the m equality constraints a penalty parameter $\boldsymbol{\lambda}$, such that $\boldsymbol{\lambda} \in \mathbb{R}^m$. In other words, $\boldsymbol{\lambda}$ will be a vector of $\mathbb{R}^m$ because we have m equality constraints. In a similar manner, we associate the penalties for the inequality constraints using $\boldsymbol{\mu}$, where $\boldsymbol{\mu} \in \mathbb{R}^p$. Therefore, the relaxation of these constraints by moving them into the objective function will generate a function called the Lagrangian, which is denoted as

$$\mathcal{L}(\mathbf{x}; \boldsymbol{\lambda}, \boldsymbol{\mu}) = \mathbf{F}(\mathbf{x}) + \boldsymbol{\lambda}^T \mathbf{H}(\mathbf{x}) + \boldsymbol{\mu}^T \mathbf{G}(\mathbf{x}). \tag{A.7}$$

Next, we define the dual function, $\mathbf{Q} : \mathbb{R}^{m+p} \rightarrow \mathbb{R} : \mathbf{Q}(\boldsymbol{\lambda}, \boldsymbol{\mu})$, where

$$(P2): \mathbf{Q}(\boldsymbol{\lambda}, \boldsymbol{\mu}) = \min_{\mathbf{x} \in \mathbb{R}^n} \quad \mathcal{L}(\mathbf{x}; \boldsymbol{\lambda}, \boldsymbol{\mu}). \tag{A.8}$$

Note that $(P2)$ is unconstrained problem as all the constraints are moved to the objective.

Now, we need to treat the equality and inequality constraints differently i.e., $\mathbf{G}(\mathbf{x}) \leq 0$. This implies that we are required to pay a penalty only when the constraint is "violated" when $\mathbf{G}(\mathbf{x}) > 0$. Correspondingly, we have $\mu^T \mathbf{G}(\mathbf{x}) \geq 0$, which implies that $\mu \geq 0$.

We now explore more on the notion of Dual bounds. In this regard, we have the following Theorem.

Theorem 4. *Consider $\boldsymbol{x}^\star$ is an optimal solution of the primal. If $\boldsymbol{\lambda} \in \mathbb{R}^m$ and $\mu \in \mathbb{R}^p$, $\boldsymbol{\mu} \geq 0$, then $\boldsymbol{Q}(\boldsymbol{\lambda}, \boldsymbol{\mu}) \leq \boldsymbol{F}(\boldsymbol{x}^\star)$.*

Proof. Based on the considered optimal value of the primal, we have

$$\mathbf{Q}(\boldsymbol{\lambda}, \boldsymbol{\mu}) = \min_{\mathbf{x} \in \mathbb{R}^n} \quad \mathcal{L}(\mathbf{x}; \boldsymbol{\lambda}, \boldsymbol{\mu}) \leq \mathcal{L}(\mathbf{x}^\star; \boldsymbol{\lambda}, \boldsymbol{\mu}) = \mathbf{F}(\mathbf{x}^\star) + \boldsymbol{\lambda}^T \mathbf{H}(\mathbf{x}^\star) + \boldsymbol{\mu}^T \mathbf{G}(\mathbf{x}^\star). \quad \text{(A.9)}$$

Since $\mathbf{x}^\star$ is a verified optimal solution, thus $\boldsymbol{\lambda}^T \mathbf{H}(\mathbf{x}^\star) = 0$. Also, from the above discussion, we have $\boldsymbol{\mu}^T \mathbf{G}(\mathbf{x}^\star) \leq 0$ as $\boldsymbol{\mu} \geq 0$ and $\mathbf{G}(\mathbf{x}^\star) \leq 0$. Therefore, we have

$$\mathbf{Q}(\boldsymbol{\lambda}, \boldsymbol{\mu}) = \mathbf{F}(\mathbf{x}^\star) + \boldsymbol{\lambda}^T \mathbf{H}(\mathbf{x}^\star) + \boldsymbol{\mu}^T \mathbf{G}(\mathbf{x}^\star) \leq \mathbf{F}(\mathbf{x}^\star). \quad \text{(A.10)}$$

□

Based on the Theorem above, we have the following Corollary.

Corollary 1. *Given $\boldsymbol{x}^\star$ is an optimal solution of the primal and $\boldsymbol{x}$ is a feasible solution of the primal. If $\boldsymbol{\lambda} \in \mathbb{R}^m$ and $\mu \in \mathbb{R}^p$, $\boldsymbol{\mu} \geq 0$, then $\boldsymbol{Q}(\boldsymbol{\lambda}, \boldsymbol{\mu}) \leq \boldsymbol{F}(\boldsymbol{x}^\star) \leq \boldsymbol{F}(\boldsymbol{x})$.*

This leads us to an in-line "Weak Duality Theorem", as defined below.

Theorem 5. ***[Weak Duality Theorem]:*** *If $\boldsymbol{x}^\star$ is an optimal solution of the primal and $(\lambda^\star, \mu^\star)$ is the optimal solution of the dual, then $\boldsymbol{Q}(\boldsymbol{\lambda}, \boldsymbol{\mu}) \leq \boldsymbol{F}(\boldsymbol{x}^\star)$.*

Towards this end, we can summarize the duality and feasibility of primal and dual problems in the table below.

Problem Type → ↓	**Dual Problem**			
Primal Problem	*Feasibility* → ↓	Optimal	Unbounded	Infeasible
	Optimal	YES	NO	NO
	Unbounded	NO	NO	YES
	Infeasible	NO	YES	(??) – YES (but cannot be derived from Duality Theorem)

From the discussion above, we can infer that the primal and dual problems are strongly related. The value of the dual is a lower bound on the value of the primal. Moreover, solving the dual problem means fining the best lower bound on the primal problem. This method was adopted for analysis of the optimization problem in [**J2**].

A.3 Karush-Kuhn-Tucker (KKT) Conditions

As discussed in the previous section, an optimization problem constrained to one or more equalities may be solved via method of Lagrange Multipliers. However, this method may be extended via Karush-Kuhn-Tucker (KKT) conditions when inequalities are included in the constraints [278]. In this vein, we consider the following problem

$$(P1) : \mathbf{x}^\star = \underset{\mathbf{x}}{\operatorname{argmin}} \quad F(\mathbf{x}) \tag{A.11}$$

$$\text{s.t.} \quad (C1) : H_i(\mathbf{x}) = 0, \forall i = 1, \ldots, m \tag{A.12}$$

$$(C2) : G_i(\mathbf{x}) \leq 0, \forall i = 1, \ldots, n. \tag{A.13}$$

In order to fond a solution that minimizes $F(\mathbf{x})$, we need to ensure that all equalities in $H_i(\mathbf{x}) = 0$ and the inequalities in $G_i(\mathbf{x}) \leq 0$ hold. Following the discussion in previous section, we define the Lagrangian with λ_i and μ_i as the KKT multipliers corresponding to the m-equalities and n-inequalities, as follows

$$\mathcal{L}(\mathbf{x}; \lambda, \mu) = F(\mathbf{x}) + \sum_{i=1}^{m} \lambda_i H_i(\mathbf{x}) + \sum_{i=1}^{n} \mu_i G_i(\mathbf{x}). \tag{A.14}$$

Thus, the optimization problem becomes

$$\mathbf{x}^\star = \underset{\mathbf{x}}{\operatorname{argmin}}\, \mathcal{L}(\mathbf{x}; \lambda, \mu). \tag{A.15}$$

We find the extremum of the function by determining the roots of the gradient of the loss function with respect to $\mathbf{x}$. In this context, it is important to note the dependence of $\mathbf{x}$ on λ and μ. Moreover, there are only k equations (where k is the number of parameters as elements in $\mathbf{x}$), yielded from gradient with respect to $\mathbf{x}$. Whereas, the total number of optimization parameters are k plus the number of multipliers $(m+n)$. However, it is still possible to obtain m-more equations by differentiating the function with respect to each Lagrange multiplier λ_i corresponding to the equality constraints. We intend to find n-more equations, which may possibly be derived from inequality constraints. To proceed, we note that if the extremum of the original function is in $G_i(\mathbf{x}^\star) \leq 0$, then this constraint will not affect the extremum in comparison to the problem without constraint. Therefore, μ_i can be set to zero in this case. On the other hand, if the new solution is at the border of the constraint, the $G_i(\mathbf{x}^\star) = 0$ and μ_i may be zero or non-zero. This concept may be visualized with the help of following graphical representation

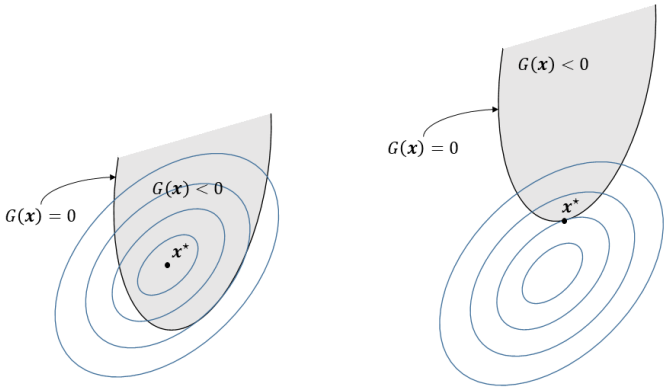

We find that in both the cases, the equation $\mu_i G_i(\mathbf{x}) = 0$ is *necessary* for the solution to our considered problem. Thus, we obtain n equations from the inequality constraints. In the set of possible solutions, the constraint terms are always zero, which does not affect the result of the loss function. It is clear the λ_i can have any value (due to equality constraint(s)), while μ_i are limited to non-negative values. We show in the figure below, a case when $\mathbf{x}^\star$ is in the region $G_i(\mathbf{x}) = 0$ so that μ_i can be different from zero.

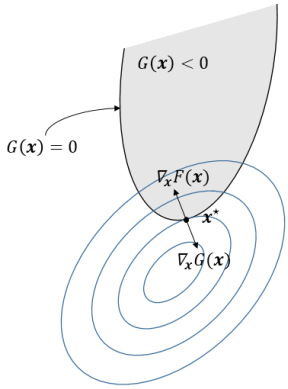

$$\begin{aligned} \mathbf{x}^\star &= \underset{\mathbf{x}}{\operatorname{argmin}}\, F(\mathbf{x}) + \mu_i G_i(\mathbf{x}) \\ 0 &= \nabla_x F(\mathbf{x}) + \mu_i \nabla_x G_i(\mathbf{x}) \\ \text{or } \mu_i &= -\frac{\nabla_x F(\mathbf{x})}{\nabla_x G_i(\mathbf{x})}. \end{aligned} \tag{A.16}$$

In such a case, the gradients of $F(\mathbf{x})$ and $G_i(\mathbf{x})$ with respect to $\mathbf{x}$ have opposite directions. Therefore, μ_i must be positive from equation (A.16).

Following this discussion, we may enumerate the KKT conditions as follows

1. *Stationarity*

$$\nabla_x F(\mathbf{x}) + \sum_{i=1}^{m} \nabla_{\mathbf{x}} \lambda_i H_i(\mathbf{x}) + \sum_{i=1}^{n} \nabla_{\mathbf{x}} \mu_i G_i(\mathbf{x}) = 0, \quad \text{(Minimization)} \tag{A.17}$$

$$\nabla_x F(\mathbf{x}) + \sum_{i=1}^{m} \nabla_{\mathbf{x}} \lambda_i H_i(\mathbf{x}) - \sum_{i=1}^{n} \nabla_{\mathbf{x}} \mu_i G_i(\mathbf{x}) = 0. \quad \text{(Maximization)} \tag{A.18}$$

2. *Equality Constraints*

$$\nabla_\lambda F(\mathbf{x}) + \sum_{i=1}^{m} \nabla_\lambda \lambda_i H_i(\mathbf{x}) - \sum_{i=1}^{n} \nabla_\lambda \mu_i G_i(\mathbf{x}) = 0. \tag{A.19}$$

3. *Inequality Constraints or Complementary Slackness Condition*

$$\mu_i G_i(\mathbf{x}) = 0, \forall i = 1, \ldots, n. \tag{A.20}$$

4. *Non-Negativity*

$$\mu_i \geq 0, \forall i = 1, \ldots, n. \tag{A.21}$$

Moreover, the operations may further be classified into binding and non-binding KKT conditions, based on the inequality constraints as summarized below

- $G_i(\mathbf{x}) < 0$ (Inactive) $\implies \mu_i = 0$ (Just Binding case).
- $\mu_i = 0$ does not imply $G_i(\mathbf{x})$ is inactive in general. In such cases KKT condition may be non-binding.

The KKT conditions were used in [**J1**], as well as partially in [**J2**].

A.4 Semi-Definite Programming (SDP)

Semidefinite programming (SDP) is a subfield of convex optimization concerned with the optimization of a linear objective function (an objective function is a user-specified function that the user wants to minimize or maximize) over the intersection of the cone of positive semidefinite matrices with an affine space, i.e., a spectrahedron. Semidefinite programming is a relatively new field of optimization which is of growing interest for several reasons [279]. SDP has several applications in many fields such as traditional convex constrained optimization, control theory, and combinatorial optimization. Efficient ways for solving SDP includes interior point methods, which are very reliable both in theory as well as practice [280].

Let $\mathbf{X}$ be a matrix or equivalently an array of n^2 components with form $(\mathrm{x}_{11}, \ldots, \mathrm{x}_{nn})$, such that $\mathbf{X} \in S^n$. Whereas $\mathbf{X}$ could also be an object (a vector) in the space S^n. Any of the three forms may be encountered while dealing with different types of scenarios/problems.

It is now interesting to explore how a linear function of $\mathbf{X}$ would look like. In case $\mathbf{C}(\mathbf{X})$ is a linear function of $\mathbf{X}$, then $\mathbf{C}(\mathbf{X})$ may be simply written as $\mathbf{C} \cdot \mathbf{X}$, where $\mathbf{C} \cdot \mathbf{X} = \sum_{i=1}^{n} \sum_{j=1}^{n} C_{ij} X_{ij}$. It is clear that if $\mathbf{X}$ is a symmetric matrix, the $\mathbf{C}$ will also be a symmetric matrix without any loss of generality. Keeping this notion into consideration, a generalized form of SDP may be represented as an optimization problem as below

$$(P1): \min \quad \mathbf{C} \cdot \mathbf{X} \tag{A.22}$$

$$\text{s.t.} \quad (C1): \mathbf{A}_i \cdot \mathbf{X} = b_i, \;\; i = 1, \ldots, m, \tag{A.23}$$

$$(C2): \mathbf{X} \succeq 0. \tag{A.24}$$

It is noteworthy that the variable in the SDP above is matrix $\mathbf{X}$. In this regard, $\mathbf{X}$ could be assumed as an array of n^2 numbers or a vector in S^n (for simplicity). Therefore, a linear objective function $\mathbf{C} \cdot \mathbf{X}$ and m-linear $\mathbf{X}$-dependent equations, namely, $\mathbf{A}_i \cdot \mathbf{X} = b_i$, $i = 1, \ldots, m$, constitutes the minimization problem, as above. It is important to note that X must also lie in the (closed convex) cone of the positive semi-definite symmetric matrices S_+^n. Another point to be highlighted is that the data for SDP consists of the symmetric matrix $\mathbf{C}$ (which corresponds to objective function) and the m-symmetric matrices $\mathbf{A}_1, \ldots, \mathbf{A}_m$, and the m-vector $\mathbf{b}$, which forms the m-linear equations.

In the wireless communications domain, problem transformations via SDP are mostly encountered in precoding and beamforming systems. Herein, the well-known method of semi-definite relaxation (SDR) is to drop the rank constraint on precoder or beamforming vectors and solving the relaxed convex problem via traditional convex optimization methods, such as interior point method. Correspondingly, this technique was used for analysis in [**J3**], [**C8**] and partially in [**C10**].

A.5 Slack Variable Reduction (SVR) Technique

Slack variable reduction (SVR) technique is an interesting way to solve complicated set of optimization problems, especially in case of non-convex program [281]. Specifically, consider

the following forms of optimization problems with optimization parameter $x \in \mathbb{R}$.

$$(P1): \max_{x} \quad F(x) \tag{A.25}$$
$$\text{s.t.} \quad (C1): G(x) \geq 0, \tag{A.26}$$
$$(C2): H(x) \leq 0. \tag{A.27}$$

and

$$(P2): \min_{x} \quad F(x) \tag{A.28}$$
$$\text{s.t.} \quad (C1): G(x) \leq 0, \tag{A.29}$$
$$(C2): H(x) \geq 0. \tag{A.30}$$

Let us assume the case where both $(P1)$ and $(P2)$ are distinct, feasible and non-convex. Additionally, the difficulty in finding a suitable solution lies with the objective $F(x)$. Consider that $(C1)$ and $(C2)$ are both convex (In other case, certain methods like approximation or suitable transformations may be used to reduce the constraints into equivalent or approximate convex form). In this regard, we make use of a slack variable to reduce the problems into following forms

$$(P3): \max_{x,v} \quad v \tag{A.31}$$
$$\text{s.t.} \quad (C1): G(x) \geq 0, \tag{A.32}$$
$$(C2): H(x) \leq 0, \tag{A.33}$$
$$(C3): F(x) \geq v. \tag{A.34}$$

and

$$(P4): \min_{x,v} \quad v \tag{A.35}$$
$$\text{s.t.} \quad (C1): G(x) \leq 0, \tag{A.36}$$
$$(C2): H(x) \geq 0, \tag{A.37}$$
$$(C3): F(x) \leq v. \tag{A.38}$$

Based on this reduction, the constraints $(C3)$ in both the problems may further be approximated (e.g., using Taylor series), reduced or transformed into a convex form. Once $(C3)$ is convex, the problem becomes a convex program and may easily be solved via well-known convex optimization techniques (like e.g., interior point method), or directly via convex optimization solvers (e.g., CVX). An application of SVR method is provided in [**J3**].

A.6 Feasible Point Pursuit and Successive Convex Approximation (FPP-SCA)

Considering several wide range of applications like e.g., transmit precoding for beamforming in wireless networks, portfolio risk management in financial engineering, etc., quadratically constrained quadratic programs (QCQPs) have emerged as another important class of optimization problems [230]. In this regard, a simple form (example) of QCQP problem may be represented as

$$(P1): \min_{\mathbf{x} \in \mathbb{C}^n} \quad \mathbf{x}^H \mathbf{A}_0 \mathbf{x} \tag{A.39}$$
$$\text{s.t.} \quad \mathbf{x}^H \mathbf{A}_m \mathbf{x} \leq b_m, \;\; m = 1, \ldots, M. \tag{A.40}$$

Based on the limits of the constraint(s), $(P1)$ may be feasible or not whereas establishing (in)feasibility is usually NP-hard. In case of infeasibility,a compromise may be explored to minimize constraint violations in some sense. Herein, we take potential infeasibility into account and introduce slack variables $\mathbf{v} \in \mathbb{R}^M$ and a slack penalty to $(P1)$, as defined below

$$(P2): \min_{\mathbf{x}\in\mathbb{C}^n, \mathbf{v}\in\mathbb{R}^M} \quad \mathbf{x}^H\mathbf{A}_0\mathbf{x} + \lambda||\mathbf{v}|| \tag{A.41}$$

$$\text{s.t.} \quad (C1): \mathbf{x}^H\mathbf{A}_m\mathbf{x} \leq \hat{b}_m + v_m, \;\; m = 1, \ldots, M. \tag{A.42}$$

$$(C2): u_m \geq 0. \;\; m = 1, \ldots, M. \tag{A.43}$$

where λ is a trade-off term between the original objective function and the slack penalty term, and $||\cdot||$ is usually the norm.

Assuming $(\mathbf{x}_0, \mathbf{v}_0)$ as the optimal solution of $(P2)$ and iff $\mathbf{u}_0 = 0$, the $\mathbf{x}_0$ is the optimal solution of $(P1)$, since $(P2)$ is always feasible. In case when ℓ_1 norm of $(P2)$, the sum of slack variables is reduced due to the non-negativity constraints. Additionally, this promotes a sparsity in terms of constraint violations. However, the difficulty in solving $(P2)$ remains due to its non-convex and NP-hard nature, in general. In this regard, *Successive Convex Approximation (SCA)* comes in handy. We use the eigen-value decomposition of $\mathbf{A}_m$, which is expressed as: $\mathbf{A}_m = \mathbf{A}_m^{(+)} + \mathbf{A}_m^{(-)}$, where $\mathbf{A}_m^{(+)} \succeq 0$ and $\mathbf{A}_m^{(-)} \preceq 0$ (negative semi-definite).

Let $\mathbf{z}, \mathbf{x} \in \mathbb{C}^{n\times 1}$, $(\mathbf{x}-\mathbf{z})^H\mathbf{A}_m^{(-)}(\mathbf{x}-\mathbf{z}) \leq 0$. The left-hand side of the inequality may be expanded as

$$\mathbf{x}^H\mathbf{A}_m^{(+)}\mathbf{x} \leq 2Re\{\mathbf{z}^H\mathbf{A}_m^{(-)}\mathbf{x}\} - \mathbf{z}^H\mathbf{A}_m^{(-)}\mathbf{z}. \tag{A.44}$$

Therefore, by using the linear restriction (A.45) around the point $\mathbf{z}$, we replace the m^{th} (non-convex) constraint of $(P2)$ with the convex constraint

$$\mathbf{x}^H\mathbf{A}_m^{(+)}\mathbf{x} \leq 2Re\{\mathbf{z}^H\mathbf{A}_m^{(-)}\mathbf{x}\} \leq \hat{b}_m + \mathbf{z}^H\mathbf{A}_m^{(-)}\mathbf{z} + v_m. \tag{A.45}$$

Consequently, we have the following convex-optimization problem

$$(P3): \min_{\mathbf{x}\in\mathbb{C}^n, \mathbf{v}\in\mathbb{R}^M} \quad \mathbf{x}^H\mathbf{A}_0\mathbf{x} + \lambda\sum_{m=1}^{M} v_m \tag{A.46}$$

$$\text{s.t.} \quad (C1): \mathbf{x}^H\mathbf{A}_m^{(+)}\mathbf{x} \leq 2Re\{\mathbf{z}^H\mathbf{A}_m^{(-)}\mathbf{x}\} \leq \hat{b}_m + \mathbf{z}^H\mathbf{A}_m^{(-)}\mathbf{z} + v_m, \tag{A.47}$$

$$(C2): v_m \geq 0. \;\; m = 1, \ldots, M. \tag{A.48}$$

In this regard, an iterative solution may be used to find a suitable solution as provided in [230]. With regard to this work, the FPP-SCA technique is employed and the corresponding results are demonstrated in [**C8**].

A.7 Alternating Optimization and Other Heuristic Methods

In case of multi-variable problem formulations, an alternating optimization approach may be employed when the problem is convex with respect to each of the concerned parameters individually. In this method, we primarily initiate by selecting one parameter (as the optimization variable) while fixing the values of other variables. These (fixed) values may be randomly chosen, however, the problem feasibility must always be ensured. Then, any of the convex optimization methods (including the ones described above) may be employed to find a suitable solution. Next, we fix this value of the optimized parameter and choose another parameter for optimization, while keeping remaining parameters fixed with random values,

as above. This process is repeated sequentially until all the parameters have been optimized. This approach is termed as an alternative optimization. It should be noted that the complete process must be repeated iteratively until the convergence of objective function is reached. This convergence could be derived or proved mathematically as well. In this regard, [**J1**], [**J2**], and [**J3**] employ such form of alternating optimization method.

Similar to above, some optimization problems (either convex or non-convex) may be solved by employing several heuristic ways. These methods may not necessary lie in the category of any optimization methods (in contrast to above-mentioned techniques). The target of heuristic methods is to provide a suitable solution (mostly sub-optimal) with good performance. We propose some heuristic methods in [**J1**], [**C4**], [**C5**], [**C6**] and [**C7**].

Based on the discussion above, it is essential to understand the nature and type of optimization problem in hand. After the corresponding analysis, the problem may be transformed, relaxed, or reduced into a convex optimization problem. Certain methods (as described above) may be used to find the suitable solution(s). The optimality or sub-optimality may be determined by the type of method used.

Appendix B

Industrial Consideration of WPT and SWIPT

B.1 WiCharge [146]

In 2012, Victor Vaisleib, Ori Mor and Ortal Alpert founded a company named *Wi-Charge*, with an aim to develop technology and products for far-field wireless power transfer using focused infrared beams. The first prototype of Wi-Charge was demonstrated in 2015, which facilitated charging of small electronic devices. In 2018, Wi-Charge demonstrated simultaneous charging of multiple devices from a single transmitter. Wi-Charge uses the invisible infrared (IR) light of the electromagnetic spectrum to deliver power using focused beams. The company claims to deliver several watts of power to a device at certain distance (in meters) away from the IR-based transmitter. The core technology of Wi-Charge is based on a distributed LASER resonator, which is formed by the retro-reflectors within the transmit and receive units. Multiple devices without any moving components can be charged with this unique concept whereas in case where an opaque object enters one of the beams, the corresponding power transfer is automatically turned off. The company announced in April 2019 that it has earned Underwriters Laboratories (UL) safety approval. Due to the straight and narrow transmit beaming, the received beam is contained within a small spot and all the energy falls inside the receiver. Hence, the human exposure to the radiated power is minimal as long as the path between the transmitter and the receiver is not crossed. In other case when the path between transmitter and receiver is blocked, the transmission is terminated immediately which is later resumed after the line-of-sight is restored. Wi-Charge claims that this mechanism ensures that power exposure to people, animals or unrelated objects is always below the maximum permissible exposure (MPE).

B.2 WattUp by Energous [147]

Energous Corporation developed the WattUp technology, which can support fast and efficient contact-based charging, as well as charging over-the-air. WattUp is an RF-based WPT technology, scalable to offer substantial improvements in contact-based charging efficiency, foreign object detection, orientation freedom and thermal performance in comparison to older (existing), coil-based charging technologies. The technology finds its applications into many different sized electronic devices for the home and office, as well as the medical, industrial,

retail and automotive industries, while ensuring an interoperability across all its products. Energous develops silicon-based WPT technologies and customizable reference designs including innovative silicon chips, antennas and software, for a large variety of applications, such as smartphones, fitness trackers, hearables, medical sensors and more. The company has received the world's first FCC Part 18 certification for at-a-distance wireless charging. Additionally, the company has more than 215 awarded patents/allowed applications for its WattUp wireless charging technology to-date.

B.3 GuRu Wireless Inc. (formerly Auspion Inc.) [148]

GuRu Wireless Inc. (formerly known as Auspion Inc.) was founded in 2017 by a team of Caltech electrical engineers, applied physicists, and integrated circuit and phased array experts. The goal of this company is to enable a zero contact energy system by powering the devices in homes and workspaces. In this regard, the radio waves from the generator carries power through the air to the receive device, where the beams intelligently find the devices and power them. The overall system is composed of a Generating Unit (GU) where the wireless power originates, and a Recovery Unit (Ru) which is composed of small, thin array of circuits. The RU announces its presence to GU and the GU then uses concentrated beams of radio wave power to serve the RU. Then the RU determines the power requirement of the device and converts the incoming radio wave beams into electric power. Herein, Radio Frequency Lensing (RF Lensing) enables concentrated beaming of radio frequency waves through the air, and to the concerned devices. Moreover, GuRu's design was created with such an extraordinary and deliberate attention that the power beams have shallow penetration depth and cannot reach internal organs of humans (unlike cell phone and WiFi signals). Additionally, GuRu's sensing technology and safety interlocks pause power beams within milliseconds, if a person or pet approaches a beam's path.

B.4 Cota by Ossia [149]

Hatem Zeine, a physicist and a technologist, founded Ossia in 2008 to challenge people's core assumptions about what is possible with wireless power. He later made the core discovery of *Cota*, which was publicly revealed at the Techcrunch Disrupt in 2013. The development of the Cota wireless power receiver, transmitter, and cloud software are based on company's extensive technological research. The Cota technology does not involve wireless charging pads or other induction or contact-based charging methods. Ossia is a privately held technology development company that licenses Cota Real Wireless Power, which is headquartered in Bellevue, Washington.

B.5 Powercast [150]

In 2003, a small team of enthusiasts focusing on development of real-life wireless power solutions discussed about the possibilities in a coffee shop meeting near downtown Pittsburgh, that led to the foundation of Powercast Corporation. After spending several years of refining its wireless charging technology, the team entered the market at the 2007 Consumer Electronics Show (CES). The demonstration of this technology with transmission of radio-frequency (RF) where its energy could potentially be harvested for powering small-receiver equipped embedded devices, bagged them several awards including CNET's Best of CES for Emerging

Technology. The company has been actively working in the areas like wireless charging challenges, powering of wireless sensor networks, waterproof designs, reusable smart bands, RFID tags and many other commercial and industrial applications. Powercast launched solutions designed to power consumer electronic devices in 2017. In addition to several accumulated awards, the company has created significant intellectual property (IP) surrounding RF-based wireless power, including 42 patents worldwide (21 in the U.S.) and 29 pending patents.

B.6 WiTricity [151]

Under the leadership of Professor Marin Soljačić, a team of physicists from the Massachusetts Institute of Technology (MIT) founded the WiTricity Corporation in 2007. The aim of the company was to commercialize a novel technology for wireless electricity, invented and patented by the founders two years prior its foundation. Professor Soljačić and team proved the magnetic fields of two properly designed devices with closely matched resonant frequencies can couple into a single continuous magnetic field. This enabled the transfer of power from one device to the other at high efficiency and over a distance range that is useful for real-world applications. Considering a power source placed 2 meters away from a 60-watt light bulb, the team demonstrated the technology successfully by illuminating it, thereby dubbed as "highly resonant wireless power transfer". Based on this experiment, their theoretical models were validated where relationship between the geometry, distance and electrical properties of the devices and WPT mechanism was established. At present, WiTricity is actively developing the core technology and additional intellectual property that will take this spectacular invention and apply it to electric vehicle wireless charging.

B.7 Qi Standard for Wireless Charging [152]

The Wireless Power Consortium (WPC) developed Qi (pronounced as CHEE) as an open interface standard that realized WPT via inductive charging over distances of up to 4 cm (1.6 inches). In this context, the concept of wireless charging was employed using the resonant inductive coupling (RIC), which involved a charging pad and a compatible device. Mobile device manufacturers that are working with the standard include Apple, Asus, Google, HTC, Huawei, LG Electronics, Motorola Mobility, Nokia, Samsung, BlackBerry, Xiaomi, and Sony. Since its first release in 2008, the Qi standard finds its application in more than 160 smartphones, tablets and other devices till date.

B.8 Pi Standard for Wireless Charging - Spansive [153]

Spansive (previously known as Pi standard for wireless charging) was founded in 2014 by John MacDonald and Lixin Shi, while they met working at MIT. Spansive is based on software-defined inductive technology, which primarily facilitates the concerned devices through loose-coupling. As Pi, the company had been working on a cone-shaped wireless charger that would sit on a desk and allow the user to charge devices placed within about 12 inches in any direction. It would require a case to work with existing devices, with the trade-off of not requiring the user to place their device directly on top of a charging pad. They showed this device at TechCrunch Disrupt SF in 2017, where the company won the Startup Battlefield competition. The company has launched and shipped over fifteen products at companies like Apple, Intel, and Texas Instruments.

B.9 Freevolt [154]

Freevolt is a London, UK based company that focuses on RF energy harvesting and associated power and control technologies. The company holds several proprietary, patents and patent pending technologies that recycle and harvest RF energy from radio transmission networks such as NFC, cellular, Wi-Fi, etc. The harvested energy is then used to power electrical devices such as smart cards, sensors, and wearables. As an initial commercial application, the company used smart cards with a mission to enable fraud protection and improved security without any impact on existing infrastructure or user experience.

B.10 Nowi [155]

Founded in 2015, Nowi is a company that focuses on the Internet of Things (IoT) devices. In order to address the power constraints, Nowi is actively working towards its Wi-Fi powered sensors. Precisely, Nowi powers small internet of things devices with wireless power by using RF signals like Wi-Fi not only for communication, but also as a power source. Besides RF signals, the company also takes into consideration several ambient energy sources such as energy via light movement, heat, etc., which could be used to power the devices. The company has a vision to completely eradicate the battery sources from low power devices, such as smart wearables or sensors. Nowi claims that their devices can gain continuous power ranging from 1μW to 100μW, while an hybrid watch could indefinitely be powered with 1-hour of direct light per day. With the highest DC-conversion efficiency, the Nowi power management integrated circuit (IC) has emerged as the world's most advanced energy harvesting design. Moreover, the company has achieved solutions for the power bottleneck in products ranging from Wearables to Internet of Things sensors.

Appendix C

Appendices for Chapter 3

C.1 Simplified form of expression for non-linear EH model

Depending on the results provided in [59, 60], the expression for non-linear EH model (based on) the proposed frameworks is approximated by

$$\mathcal{E}_{\ell}^{\mathcal{N}} = \frac{\mathcal{E}'}{1-\varkappa} \cdot \left(\frac{1}{1+\exp(-\alpha\rho_{\ell}\sum_{k=1}^{K}\sum_{n=1}^{N}\sum_{n'=1}^{N} p_{2,n',k}|h_{2,n',k,\ell}|^2 + \alpha\beta)} - \varkappa \right). \tag{C.1}$$

Therefore, the corresponding constraint in (3.16) becomes

$$\frac{\mathcal{E}'}{1-\varkappa} \cdot \left(\frac{1}{1+\exp(-\alpha\rho_{\ell}\sum_{k=1}^{K}\sum_{n=1}^{N}\sum_{n'=1}^{N} p_{2,n',k}|h_{2,n',k,\ell}|^2 + \alpha\beta)} - \varkappa \right) \geq \xi_{\ell}. \tag{C.2}$$

Further simplification of (C.2) leads to

$$\rho_{\ell} \geq \frac{-\ln\left(\frac{(\mathcal{E}'-\xi_{\ell})(1-\varkappa)}{\mathcal{E}'\varkappa+\xi_{\ell}(1-\varkappa)}\right) + \alpha\beta}{\alpha\sum_{k=1}^{K}\sum_{n=1}^{N}\sum_{n'=1}^{N} p_{2,n',k}|h_{2,n',k,\ell}|^2}. \tag{C.3}$$

In this regard, it is noteworthy that for corresponding estimated values for $\mathcal{E}'$, α and β, the feasibility space of the original problem shrinks so much that $\rho_{\ell} \in [0,1)$ may not be satisfied anymore. Therefore, motivated from previous analysis in (3.12) (from prior works with linear EH expressions), we simplify the expression in (C.1) to provide more tractability while ensuring $\rho_{\ell} \in [0,1)$, as follows

$$\mathcal{E}_{\ell}^{\mathcal{N}} = \rho_{\ell}\sum_{k=1}^{K}\sum_{n=1}^{N}\sum_{n'=1}^{N} \frac{\mathcal{E}'}{1-\varkappa} \cdot \left(\frac{1}{1+\exp(-\alpha p_{2,n',k}|h_{2,n',k,\ell}|^2 + \alpha\beta)} - \varkappa \right). \tag{C.4}$$

Therefore, the corresponding expression in (C.4) is considered for analysis throughout the Chapter 3.

C.2 Derivation of Optimal Solution $\boldsymbol{p}^*$ in (3.35) and (3.36)

Using the short notations: $x_1 = \frac{|h_{1,n,k}|^2}{\sigma_k^2}$, $x_2 = \frac{|h_{2,n',k,\ell}|^2}{\sigma_{d_\ell}^2}$, $p_1 = p_{1,n}$ and $p_2 = p_{2,n',k}$, the derivative of (3.25) with respect to p_1 is represented as

$$\frac{\partial \mathcal{L}_{(n,n'),k,\ell}}{\partial p_1} = -\lambda_S + \frac{1}{2} \cdot \frac{(1-\rho_\ell)^2 \cdot x_1 \cdot x_2^2 \cdot p_2^2}{(x_1 \cdot p_1 + (1-\rho_\ell) \cdot x_2 \cdot p_2)} \cdot \frac{1}{(x_1 \cdot p_1 + (1-\rho_\ell) \cdot x_2 \cdot p_2 + (1-\rho_\ell) \cdot x_1 \cdot x_2 \cdot p_1 \cdot p_2)}. \quad \text{(C.5)}$$

Similarly, the derivative of (3.25) with respect to p_2 is represented as

$$\frac{\partial \mathcal{L}_{(n,n'),k,\ell}}{\partial p_2} = -\lambda_{R,k} + \frac{1}{2} \cdot \frac{(1-\rho_\ell) \cdot x_1^2 \cdot x_2 \cdot p_1^2}{(x_1 \cdot p_1 + (1-\rho_\ell) \cdot x_2 \cdot p_2)} \cdot \frac{1}{(x_1 \cdot p_1 + (1-\rho_\ell) \cdot x_2 \cdot p_2 + (1-\rho_\ell) \cdot x_1 \cdot x_2 \cdot p_1 \cdot p_2)}. \quad \text{(C.6)}$$

Firstly, we consider the condition when both p_1^* and p_2^* are positive. Equating (C.5) and (C.6), we get

$$\lambda_{R,k} \cdot (1-\rho_\ell) \cdot x_2 \cdot p_2^2 = \lambda_S \cdot x_1 \cdot p_1^2. \quad \text{(C.7)}$$

This yields

$$c = \sqrt{\frac{\lambda_{R,k} \cdot (1-\rho_\ell) \cdot x_2}{\lambda_S \cdot x_1}}. \quad \text{(C.8)}$$

In order to let $p_1^* > 0$, the factor c should be positive, which is true in general. Substituting (C.8) into (C.5), we get

$$p_2^* = \left(\frac{1}{c_{(n,n'),k,\ell}(1-\rho_\ell) x_1 x_2} \right) \cdot \left(\frac{(1-\rho_\ell)^2 x_1 x_2^2 - (2\lambda_S)(c_{(n,n'),k,\ell} x_1 + (1-\rho_\ell) x_2)^2}{2\lambda_S (c_{(n,n'),k,\ell} x_1 + (1-\rho_\ell) x_2)} \right). \quad \text{(C.9)}$$

If the value of (C.9) is negative, the p_2^* should be set to zero. For such cases, the optimal power allocation in the first hop should follow the expression of conventional water-filling approach

$$p_1^* = \left(\frac{1}{\lambda_S} - \frac{1}{x_1} \right)^+. \quad \text{(C.10)}$$

Thus, the optimality of solution $\boldsymbol{p}^*$ in (3.35) and (3.36) is proved.

Appendix D

Appendices for Chapter 4

D.1 Conversion of Non-Linear Energy Harvesting constraint to Linear Constraint

The non-linear EH constraint at the i^{th} user is given by

$$\frac{\mathcal{E}'}{1-\phi}\cdot\left(\frac{1}{1+e^{(-\alpha(\sum_{k=1}^{\Psi}|\mathbf{w}_k^H\mathbf{h}_i|^2)+\alpha\beta)}}-\phi\right)\geq\xi_i, \tag{D.1}$$

where ξ_i is the harvested energy demand at the i^{th} user.

The expression in (D.1) can be re-arranged and written as

$$\frac{\mathcal{E}'}{1-\phi}\cdot\left(\frac{1}{1+e^{(-\alpha\mathcal{E}_i^{\mathcal{L}}/\zeta_i+\alpha\sigma_{R,i}^2+\alpha\beta)}}-\phi\right)\geq\xi_i. \tag{D.2}$$

Further simplification of (D.2) leads to the equivalent linear EH constraint

$$\mathcal{E}_i^{\mathcal{L}}\geq\xi_i', \tag{D.3}$$

where

$$\xi_i'=\zeta_i\left(\sigma_{R,i}^2+\beta-\frac{1}{\alpha}\ln\left(\frac{(1-\phi)(\mathcal{E}'-\xi_i)}{(1-\phi)\mathcal{E}'+\phi\xi_i}\right)\right). \tag{D.4}$$

From (D.4), it is clear that ξ_i' is an up-scaled version of ξ_i and that the constraints in (4.8) and (D.3) are equivalent. QED. ■

D.2 Proof of Proposition 1

Consider the following expression, synonymous to the sub-term of (4.5),

$$\mathrm{F}(x)=\frac{1}{1+\exp(-ax+b)}. \tag{D.5}$$

It is clear that the optimization of $\mathcal{E}_j^{\mathcal{N}}(\mathbf{w})$ with respect to $\mathbf{w}$ would affect only the sub-term of (4.5), as represented in (D.5). Therefore, in order to understand the nature of $F(x)$, we

express the first and second order derivative of the function with respect to x, respectively, as follows

$$\frac{\partial \mathrm{F}(x)}{\partial x} = \frac{a \exp(-ax+b)}{(1+\exp(-ax+b))^2}, \tag{D.6}$$

$$\frac{\partial^2 \mathrm{F}(x)}{\partial x^2} = \frac{-a^2 \exp(-ax+b)(1-(\exp(-ax+b))^2)}{(1+\exp(-ax+b))^4}. \tag{D.7}$$

The parameters a and b may assume any value defined in [222], corresponding to the received input power (x) in the μW regime. Based on these parameter selections, it is explicit that $0 < \exp(-ax+b) < 1$. Therefore we have,

$$\frac{\partial^2 \mathrm{F}(x)}{\partial x^2} < 0, \tag{D.8}$$

which implies that the $\mathrm{F}(x)$ is a concave function within the specified limits of a, b and x. Hence proved. ■

Appendix E

Appendices for Chapter 5

E.1 Analysis of different possibilities from KKT Conditions for Data Maximization Problem

We analyze all the cases corresponding to (5.9) – (5.21) in order to obtain a feasible solution as follows

Case I: $\lambda_1 = 0 \implies G(\varpi_i, \tau_i, P_{\mathcal{R}_i}) \neq 0$; $\lambda_2 \neq 0 \implies H(\varpi_i, \tau_i, P_{\mathcal{R}_i}) = 0$
From (5.15), we find that $\lambda_2 = 0$, which is contradictory. Hence, this case is not possible.

Case II: $\lambda_1 = 0 \implies G(\varpi_i, \tau_i, P_{\mathcal{R}_i}) \neq 0$; $\lambda_2 = 0 \implies H(\varpi_i, \tau_i, P_{\mathcal{R}_i}) \neq 0$
This case is not acceptable as $B\log_2(1+\Upsilon_{\mathcal{R}_i,\mathcal{D}}) \neq 0$.

Case III: $\lambda_1 \neq 0 \implies G(\varpi_i, \tau_i, P_{\mathcal{R}_i}) = 0$; $\lambda_2 = 0 \implies H(\varpi_i, \tau_i, P_{\mathcal{R}_i}) \neq 0$
From (5.17), we find that $\lambda_1 = 1$ which implies that $P_{\mathcal{S}} \to 0$. Therefore, this is not a feasible solution.

Case IV: $\lambda_1 \neq 0 \implies G(\varpi_i, \tau_i, P_{\mathcal{R}_i}) = 0$; $\lambda_2 \neq 0 \implies H(\varpi_i, \tau_i, P_{\mathcal{R}_i}) = 0$
For $\lambda_1 \neq 0 \implies G(x, P_{\mathcal{R}_i}) = 0$; $\lambda_2 \neq 0 \implies H(x, P_{\mathcal{R}_i}) = 0$, we deduce to the following equations

$$-\lambda_1[\tau_i(B\log_2(1+\Upsilon_{\mathcal{S},\mathcal{R}_i}) + (\delta_i \cdot r))] + \lambda_2[\zeta\tau_i(P_{\mathcal{S}} d^{-\vartheta}_{\mathcal{S},\mathcal{R}_i}|h_{\mathcal{S},\mathcal{R}_i}|^2 + \sigma^2_{n_{R_i}})] = 0, \quad \text{(E.1)}$$

$$-B\log_2(1+\Upsilon_{\mathcal{R}_i,\mathcal{D}}) + \lambda_1\Big(B\log_2(1+\Upsilon_{\mathcal{R}_i,\mathcal{D}}) + (1-\varpi_i)\Big(B\log_2(1+\Upsilon_{\mathcal{S},\mathcal{R}_i}) + (\delta_i \cdot r\Big)\Big) + \lambda_2\Big(P_{\mathcal{R}_i} + \zeta\varpi_i(P_{\mathcal{S}} d^{-\vartheta}_{\mathcal{S},\mathcal{R}_i}|h_{\mathcal{S},\mathcal{R}_i}|^2 + \sigma^2_{n_{R_i}})\Big) = 0, \quad \text{(E.2)}$$

$$\frac{\ln(2) d^{-\vartheta}_{\mathcal{R}_i,\mathcal{D}}|h_{\mathcal{R}_i,\mathcal{D}}|^2}{\sigma^2_{n_{\mathcal{D}}} + P_{\mathcal{R}_i} d^{-\vartheta}_{\mathcal{R}_i,\mathcal{D}}|h_{\mathcal{R}_i,\mathcal{D}}|^2} - \lambda_1\left(\frac{\ln(2) d^{-\vartheta}_{\mathcal{R}_i,\mathcal{D}}|h_{\mathcal{R}_i,\mathcal{D}}|^2}{\sigma^2_{n_{\mathcal{D}}} + P_{\mathcal{R}_i} d^{-\vartheta}_{\mathcal{R}_i,\mathcal{D}}|h_{\mathcal{R}_i,\mathcal{D}}|^2}\right) - \lambda_2 = 0, \quad \text{(E.3)}$$

$$(1-\tau_i)B\log_2(1+\Upsilon_{\mathcal{R}_i,\mathcal{D}}) - (1-\varpi_i)\tau_i\Big(B\log_2(1+\Upsilon_{\mathcal{S},\mathcal{R}_i}) + (\delta_i \cdot r)\Big) = 0. \quad \text{(E.4)}$$

$$(1-\tau_i)P_{\mathcal{R}_i} - \zeta\varpi_i\tau_i(P_{\mathcal{S}} d^{-\vartheta}_{\mathcal{S},\mathcal{R}_i}|h_{\mathcal{S},\mathcal{R}_i}|^2 + \sigma^2_{n_{R_i}}) - E_{ext} = 0. \quad \text{(E.5)}$$

From (E.1) and (E.3) we have

$$\lambda_1 = \frac{\chi_1(\zeta(P_{\mathcal{S}} d^{-\vartheta}_{\mathcal{S},\mathcal{R}_i}|h_{\mathcal{S},\mathcal{R}_i}|^2 + \sigma^2_{n_{R_i}}))}{\chi_2}, \quad \text{(E.6)}$$

$$\lambda_2 = \frac{\chi_1(B\log_2(1+\Upsilon_{\mathcal{S},\mathcal{R}_i}) + (\delta_i \cdot r))}{\chi_2}, \quad \text{(E.7)}$$

where $\chi_1 = (\ln(2) d_{\mathcal{R}_i,\mathcal{D}}^{-\vartheta} |h_{\mathcal{R}_i,\mathcal{D}}|^2)$, and $\chi_2 = (\ln(2) d_{\mathcal{R}_i,\mathcal{D}}^{-\vartheta} |h_{\mathcal{R}_i,\mathcal{D}}|^2)(\zeta(P_{\mathcal{S}} d_{\mathcal{S},\mathcal{R}_i}^{-\vartheta} |h_{\mathcal{S},\mathcal{R}_i}|^2 + \sigma_{n_{R_i}}^2)) + (\sigma_{n_{\mathcal{D}}}^2 + P_{\mathcal{R}_i} d_{\mathcal{R}_i,\mathcal{D}}^{-\vartheta} |h_{\mathcal{R}_i,\mathcal{D}}|^2)(B \log_2(1 + \Upsilon_{\mathcal{S},\mathcal{R}_i}) + (\delta_i \cdot r))$.

Assuming $\kappa = 1 + \Upsilon_{\mathcal{R}_i,\mathcal{D}}$ and substituting (E.6) and (E.7) in (E.2), we obtain the following equation

$$\mathcal{A} + \kappa[\ln(2) - B \log_2(\kappa)] = 0, \tag{E.8}$$

where $\mathcal{A} = \frac{(\ln(2) d_{\mathcal{R}_i,\mathcal{D}}^{-\vartheta} |h_{\mathcal{R}_i,\mathcal{D}}|^2)(\zeta(P_{\mathcal{S}} d_{\mathcal{S},\mathcal{R}_i}^{-\vartheta} |h_{\mathcal{S},\mathcal{R}_i}|^2 + \sigma_{n_{R_i}}^2))}{\sigma_{n_{\mathcal{D}}}^2}$. The solution of this equation is obtained in a closed form as follows

$$\kappa = \exp\left(\mathcal{W}\left(\frac{\mathcal{A}}{B} \exp\left(-\frac{1}{B} \log^2(2) \right) * \log(2) \right) + \frac{\log^2(2)}{B} \right), \tag{E.9}$$

where $\mathcal{W}(\cdot)$ is the Lambert W function [282].

Using (E.9), (E.4) and (E.5), we obtain the following

$$\tau_i = \frac{\varphi_1 \cdot \varphi_2 + P_{\mathcal{R}_i} - E_{ext} \cdot \varphi_3}{\varphi_1 \cdot \varphi_2 + \varphi_2 \cdot \varphi_3 + P_{\mathcal{R}_i} \cdot \varphi_3}, \tag{E.10}$$

where $\varphi_1 = B \log_2(1 + \Upsilon_{\mathcal{R}_i,\mathcal{D}})$, $\varphi_2 = \zeta(P_{\mathcal{S}} d_{\mathcal{S},\mathcal{R}_i}^{-\vartheta} |h_{\mathcal{S},\mathcal{R}_i}|^2 + \sigma_{n_{R_i}}^2)$, and $\varphi_3 = B \log_2(1 + \Upsilon_{\mathcal{S},\mathcal{R}_i}) + (\delta_i \cdot r)$.

$$\varpi_i = \frac{(1 - \tau_i) P_{\mathcal{R}_i} - E_{ext}}{\zeta \tau_i (P_{\mathcal{S}} d_{\mathcal{S},\mathcal{R}_i}^{-\vartheta} |h_{\mathcal{S},\mathcal{R}_i}|^2 + \sigma_{n_{R_i}}^2)}. \tag{E.11}$$

E.2 Analysis of different possibilities from KKT Conditions for Maximization Problem of Energy Stored at the Relay

We analyze all the cases in order to obtain a feasible solution corresponding to (5.28) – (5.40). The analysis is as follows

Case I: $\mu_1 = 0 \implies G(\hat{\varpi}_i, \hat{\tau}_i, P_{\mathcal{R}_i}) \neq 0$; $\mu_2 = 0 \implies H(\hat{\varpi}_i, \hat{\tau}_i, P_{\mathcal{R}_i}) \neq 0$; $\mu_3 = 0 \implies I(\hat{\varpi}_i, \hat{\tau}_i, P_{\mathcal{R}_i}) \neq 0$

From (5.34) and (5.35), we find that $P_{\mathcal{R}_i} = -\zeta(P_{\mathcal{S}}|g|^2 + \sigma_{n_{R_i}}^2)$ or $P_{\mathcal{R}_i} = 0$ respectively. Since both these solutions cannot be accepted, therefore this case is not possible.

Case II: $\mu_1 = 0 \implies G(\hat{\varpi}_i, \hat{\tau}_i, P_{\mathcal{R}_i}) \neq 0$; $\mu_2 = 0 \implies H(\hat{\varpi}_i, \hat{\tau}_i, P_{\mathcal{R}_i}) \neq 0$; $\mu_3 \neq 0 \implies I(\hat{\varpi}_i, \hat{\tau}_i, P_{\mathcal{R}_i}) = 0$

This case again leads us to the unacceptable solution as in the previous case, therefore this case can be excluded.

Case III: $\mu_1 = 0 \implies G(\hat{\varpi}_i, \hat{\tau}_i, P_{\mathcal{R}_i}) \neq 0$; $\mu_2 \neq 0 \implies H(\hat{\varpi}_i, \hat{\tau}_i, P_{\mathcal{R}_i}) = 0$; $\mu_3 = 0 \implies I(\hat{\varpi}_i, \hat{\tau}_i, P_{\mathcal{R}_i}) \neq 0$

From the optimality conditions, we deduce that $\mu_2 = 1$ with no solutions for $\hat{\varpi}_i$, $\hat{\tau}_i$, and $P_{\mathcal{R}_i}$. Hence, this case is not admissible.

Case IV: $\mu_1 \neq 0 \implies G(\hat{\varpi}_i, \hat{\tau}_i, P_{\mathcal{R}_i}) = 0$; $\mu_2 = 0 \implies H(\hat{\varpi}_i, \hat{\tau}_i, P_{\mathcal{R}_i}) \neq 0$; $\mu_3 = 0 \implies I(\hat{\varpi}_i, \hat{\tau}_i, P_{\mathcal{R}_i}) \neq 0$

Herein, we find that $\mu_1 < 0$; which violates the non-negativity condition. Thus, this case is infeasible.

Case V: $\mu_1 = 0 \implies G(\hat{\varpi}_i, \hat{\tau}_i, P_{\mathcal{R}_i}) \neq 0$; $\mu_2 \neq 0 \implies H(\hat{\varpi}_i, \hat{\tau}_i, P_{\mathcal{R}_i}) = 0$; $\mu_3 \neq 0 \implies I(\hat{\varpi}_i, \hat{\tau}_i, P_{\mathcal{R}_i}) = 0$

For this case, we can represent the following equations in their simplified forms

$$[\zeta(P_{\mathcal{S}} d_{\mathcal{S},\mathcal{R}_i}^{-\vartheta} |h_{\mathcal{S},\mathcal{R}_i}|^2 + \sigma_{n_{R_i}}^2) + P_{\mathcal{R}_i}] + \mu_2[P_{\mathcal{R}_i} + \zeta(P_{\mathcal{S}} d_{\mathcal{S},\mathcal{R}_i}^{-\vartheta} |h_{\mathcal{S},\mathcal{R}_i}|^2 + \sigma_{n_{R_i}}^2)] - \mu_3[B \log_2(1 + \Upsilon_{\mathcal{R}_i,\mathcal{D}})] = 0, \tag{E.12}$$

$$P_{\mathcal{R}_i} + \mu_2[P_{\mathcal{R}_i}] - \mu_3[B\log_2(1+\Upsilon_{\mathcal{R}_i,\mathcal{D}})] = 0, \tag{E.13}$$

$$1 + \mu_2 - \mu_3\left(\frac{\ln(2)d_{\mathcal{R}_i,\mathcal{D}}^{-\vartheta}|h_{\mathcal{R}_i,\mathcal{D}}|^2}{\sigma_{n_\mathcal{D}}^2 + P_{\mathcal{R}_i}d_{\mathcal{R}_i,\mathcal{D}}^{-\vartheta}|h_{\mathcal{R}_i,\mathcal{D}}|^2}\right) = 0, \tag{E.14}$$

$$(1-(\hat{\varpi}_i+\hat{\tau}_i))P_{\mathcal{R}_i} - \zeta\hat{\varpi}_i(P_\mathcal{S}d_{\mathcal{S},\mathcal{R}_i}^{-\vartheta}|h_{\mathcal{S},\mathcal{R}_i}|^2 + \sigma_{n_{R_i}}^2) - E_{ext} = 0, \tag{E.15}$$

$$r - (1-(\hat{\varpi}_i+\hat{\tau}_i))B\log_2(1+\Upsilon_{\mathcal{R}_i,\mathcal{D}}) = 0. \tag{E.16}$$

Solving the above equations, we obtain solutions for $P_{\mathcal{R}_i}$ as follows

$$P_{\mathcal{R}_i} = \max(\exp\Big(\mathcal{W}(\exp(-\log^2(2)) + \log(2)) + \log^2(2)\Big), \exp\Big(\mathcal{W}_{-1}(\exp(-\log^2(2)) + \log(2)) + \log^2(2)\Big)), \tag{E.17}$$

where $\mathcal{W}(\cdot)$ is the LambertW function or the product log function and $\mathcal{W}_k(\cdot)$ is the analytic continuation of the product log function [260]. As the solution is independent of $P_\mathcal{S}$, it is reasonable to discard this solution.

Case VI: $\mu_1 \neq 0 \implies G(\hat{\varpi}_i, \hat{\tau}_i, P_{\mathcal{R}_i}) = 0$; $\mu_2 = 0 \implies H(\hat{\varpi}_i, \hat{\tau}_i, P_{\mathcal{R}_i}) \neq 0$; $\mu_3 \neq 0 \implies I(\hat{\varpi}_i, \hat{\tau}_i, P_{\mathcal{R}_i}) = 0$

We can represent the following equations in their simplified forms

$$[\zeta(P_\mathcal{S}d_{\mathcal{S},\mathcal{R}_i}^{-\vartheta}|h_{\mathcal{S},\mathcal{R}_i}|^2 + \sigma_{n_{R_i}}^2) + P_{\mathcal{R}_i}] + \mu_1[B\log_2(1+\Upsilon_{\mathcal{R}_i,\mathcal{D}})] - \mu_3[B\log_2(1+\Upsilon_{\mathcal{R}_i,\mathcal{D}})] = 0, \tag{E.18}$$

$$P_{\mathcal{R}_i} + \mu_1[B\log_2(1+\Upsilon_{\mathcal{R}_i,\mathcal{D}}) + (B\log_2(1+\Upsilon_{\mathcal{S},\mathcal{R}_i}) + (\delta_i\cdot r))] - \mu_3[B\log_2(1+\Upsilon_{\mathcal{R}_i,\mathcal{D}})] = 0, \tag{E.19}$$

$$1 + \mu_2 - \mu_3\left(\frac{\ln(2)d_{\mathcal{R}_i,\mathcal{D}}^{-\vartheta}|h_{\mathcal{R}_i,\mathcal{D}}|^2}{\sigma_{n_\mathcal{D}}^2 + P_{\mathcal{R}_i}d_{\mathcal{R}_i,\mathcal{D}}^{-\vartheta}|h_{\mathcal{R}_i,\mathcal{D}}|^2}\right) = 0, \tag{E.20}$$

$$(1-(\hat{\varpi}_i+\hat{\tau}_i))P_{\mathcal{R}_i} - \zeta\hat{\varpi}_i(P_\mathcal{S}d_{\mathcal{S},\mathcal{R}_i}^{-\vartheta}|h_{\mathcal{S},\mathcal{R}_i}|^2 + \sigma_{n_{R_i}}^2) - E_{ext} = 0, \tag{E.21}$$

$$r - (1-(\hat{\varpi}_i+\hat{\tau}_i))B\log_2(1+\Upsilon_{\mathcal{R}_i,\mathcal{D}}) = 0. \tag{E.22}$$

From (E.18) and (E.19), we obtain

$$\mu_1 = \frac{\zeta(P_\mathcal{S}d_{\mathcal{S},\mathcal{R}_i}^{-\vartheta}|h_{\mathcal{S},\mathcal{R}_i}|^2 + \sigma_{n_{R_i}}^2)}{B\log_2(1+\Upsilon_{\mathcal{S},\mathcal{R}_i}) + (\delta_i\cdot r)}. \tag{E.23}$$

Substituting (E.23) in (E.20), we find the following

$$\mu_3 = \left(\frac{\sigma_{n_\mathcal{D}}^2 + P_{\mathcal{R}_i}d_{\mathcal{R}_i,\mathcal{D}}^{-\vartheta}|h_{\mathcal{R}_i,\mathcal{D}}|^2}{\ln(2)d_{\mathcal{R}_i,\mathcal{D}}^{-\vartheta}|h_{\mathcal{R}_i,\mathcal{D}}|^2}\right) + \left(\frac{\zeta(P_\mathcal{S}d_{\mathcal{S},\mathcal{R}_i}^{-\vartheta}|h_{\mathcal{S},\mathcal{R}_i}|^2 + \sigma_{n_{R_i}}^2)}{B\log_2(1+\Upsilon_{\mathcal{S},\mathcal{R}_i}) + (\delta_i\cdot r)}\right). \tag{E.24}$$

Substituting (E.23) and (E.24) in (E.19), and assuming $\nu = 1 + \Upsilon_{\mathcal{R}_i,\mathcal{D}}$, we obtain the following equation

$$\nu[B\log_2(\nu) - \ln(2)] + \mathcal{A} = 0, \tag{E.25}$$

where $\mathcal{A} = \ln(2) - \left(\frac{\zeta}{\sigma_{n_\mathcal{D}}^2}\right)(\ln(2)d_{\mathcal{R}_i,\mathcal{D}}^{-\vartheta}|h_{\mathcal{R}_i,\mathcal{D}}|^2)(P_\mathcal{S}d_{\mathcal{S},\mathcal{R}_i}^{-\vartheta}$
$|h_{\mathcal{S},\mathcal{R}_i}|^2 + \sigma_{n_{R_i}}^2)$.

The solution of the above expression can be expressed as follows

$$\nu = \exp\left(\mathcal{W}\left(-\frac{\mathcal{A}}{B}\exp\left(-\frac{1}{B}\log^2(2)\right)*\log(2)\right) + \frac{\log^2(2)}{B}\right). \tag{E.26}$$

Consequently, the we obtain the following

$$P^{\dagger}_{\mathcal{R}_i} = (\nu - 1)\left(\frac{\sigma^2_{n_{\mathcal{D}}}}{d^{-\vartheta}_{\mathcal{R}_i,\mathcal{D}}|h_{\mathcal{R}_i,\mathcal{D}}|^2}\right). \tag{E.27}$$

From (E.21) and (E.22), and using (E.26), we obtain

$$\hat{\tau}^{\dagger}_i = \frac{r}{B\log_2(1+\Upsilon_{\mathcal{S},\mathcal{R}_i}) + (\delta_i \cdot r)}. \tag{E.28}$$

Finally, substituting (5.42) in (E.22), we find the following

$$\hat{\varpi}^{\dagger}_i = 1 - r\left(\frac{1}{B\log_2(1+\Upsilon_{\mathcal{S},\mathcal{R}_i}) + (\delta_i \cdot r)} + \frac{1}{B\log_2\left(1+\frac{P^{\dagger}_{\mathcal{R}_i} d^{-\vartheta}_{\mathcal{R}_i,\mathcal{D}}|h_{\mathcal{R}_i,\mathcal{D}}|^2}{\sigma^2_{n_{\mathcal{D}}}}\right)}\right), \tag{E.29}$$

where $P^{\dagger}_{\mathcal{R}_i}$, $\hat{\tau}^{\dagger}_i$, and $\hat{\varpi}^{\dagger}_i$ are the optimal values obtained for $P_{\mathcal{R}_i}$, $\hat{\tau}_i$, and $\hat{\varpi}_i$, respectively.

Case VII: $\mu_1 \neq 0 \implies G(\hat{\varpi}_i, \hat{\tau}_i, P_{\mathcal{R}_i}) = 0$; $\mu_2 \neq 0 \implies H(\hat{\varpi}_i, \hat{\tau}_i, P_{\mathcal{R}_i}) = 0$; $\mu_3 = 0 \implies I(\hat{\varpi}_i, \hat{\tau}_i, P_{\mathcal{R}_i}) \neq 0$

The simplified equations for this case can be represented as follows

$$[\zeta(P_{\mathcal{S}} d^{-\vartheta}_{\mathcal{S},\mathcal{R}_i}|h_{\mathcal{S},\mathcal{R}_i}|^2 + \sigma^2_{n_{R_i}}) + P_{\mathcal{R}_i}] + \mu_1[B\log_2(1+\Upsilon_{\mathcal{R}_i,\mathcal{D}})] + \mu_2[P_{\mathcal{R}_i} + \zeta(P_{\mathcal{S}} d^{-\vartheta}_{\mathcal{S},\mathcal{R}_i}|h_{\mathcal{S},\mathcal{R}_i}|^2 + \sigma^2_{n_{R_i}})] = 0, \tag{E.30}$$

$$P_{\mathcal{R}_i} + \mu_1[B\log_2(1+\Upsilon_{\mathcal{R}_i,\mathcal{D}}) + (B\log_2(1+\Upsilon_{\mathcal{S},\mathcal{R}_i}) + (\delta_i \cdot r))] + \mu_2[P_{\mathcal{R}_i}] = 0, \tag{E.31}$$

$$1 + \mu_1\left(\frac{\ln(2) d^{-\vartheta}_{\mathcal{R}_i,\mathcal{D}}|h_{\mathcal{R}_i,\mathcal{D}}|^2}{\sigma^2_{n_{\mathcal{D}}} + P_{\mathcal{R}_i} d^{-\vartheta}_{\mathcal{R}_i,\mathcal{D}}|h_{\mathcal{R}_i,\mathcal{D}}|^2}\right) + \mu_2 = 0, \tag{E.32}$$

$$(1 - (\hat{\varpi}_i + \hat{\tau}_i))B\log_2(1+\Upsilon_{\mathcal{R}_i,\mathcal{D}}) - \hat{\tau}_i[B\log_2(1+\Upsilon_{\mathcal{S},\mathcal{R}_i}) + (\delta_i \cdot r)] = 0, \tag{E.33}$$

$$(1 - (\hat{\varpi}_i + \hat{\tau}_i))P_{\mathcal{R}_i} - \zeta\hat{\varpi}_i(P_{\mathcal{S}} d^{-\vartheta}_{\mathcal{S},\mathcal{R}_i}|h_{\mathcal{S},\mathcal{R}_i}|^2 + \sigma^2_{n_{R_i}}) - E_{ext} = 0. \tag{E.34}$$

From (E.31) and (E.32), and assuming $\mu = 1 + \Upsilon_{\mathcal{R}_i,\mathcal{D}}$, we obtain the following equation

$$\mu(B\log_2(\mu) + B\log_2(1+\Upsilon_{\mathcal{S},\mathcal{R}_i}) + (\delta_i \cdot r) - \ln(2)) + \ln(2) = 0. \tag{E.35}$$

Since the solution of (E.35) is composed of complex values, therefore this case is not acceptable.

Case VIII: $\mu_1 \neq 0 \implies G(\hat{\varpi}_i, \hat{\tau}_i, P_{\mathcal{R}_i}) = 0$; $\mu_2 \neq 0 \implies H(\hat{\varpi}_i, \hat{\tau}_i, P_{\mathcal{R}_i}) = 0$; $\mu_3 \neq 0 \implies I(\hat{\varpi}_i, \hat{\tau}_i, P_{\mathcal{R}_i}) = 0$

The equations to be used for computation of $\hat{\varpi}_i$, $\hat{\tau}_i$, and $P_{\mathcal{R}_i}$ in this case can be written as

$$[\zeta(P_{\mathcal{S}} d^{-\vartheta}_{\mathcal{S},\mathcal{R}_i}|h_{\mathcal{S},\mathcal{R}_i}|^2 + \sigma^2_{n_{R_i}}) + P_{\mathcal{R}_i}] + \mu_1[B\log_2(1+\Upsilon_{\mathcal{R}_i,\mathcal{D}})] + \mu_2[P_{\mathcal{R}_i} + \zeta(P_{\mathcal{S}} d^{-\vartheta}_{\mathcal{S},\mathcal{R}_i}|h_{\mathcal{S},\mathcal{R}_i}|^2 + \sigma^2_{n_{R_i}})] - \mu_3[B\log_2(1+\Upsilon_{\mathcal{R}_i,\mathcal{D}})] = 0, \tag{E.36}$$

$$P_{\mathcal{R}_i} + \mu_1[B\log_2(1+\Upsilon_{\mathcal{R}_i,\mathcal{D}}) + (B\log_2(1+\Upsilon_{\mathcal{S},\mathcal{R}_i}) + (\delta_i \cdot r))] + \mu_2[P_{\mathcal{R}_i}] - \mu_3[B\log_2(1+\Upsilon_{\mathcal{R}_i,\mathcal{D}})] = 0, \tag{E.37}$$

$$1 + \mu_1\left(\frac{\ln(2) d^{-\vartheta}_{\mathcal{R}_i,\mathcal{D}}|h_{\mathcal{R}_i,\mathcal{D}}|^2}{\sigma^2_{n_{\mathcal{D}}} + P_{\mathcal{R}_i} d^{-\vartheta}_{\mathcal{R}_i,\mathcal{D}}|h_{\mathcal{R}_i,\mathcal{D}}|^2}\right) + \mu_2 - \mu_3\left(\frac{\ln(2) d^{-\vartheta}_{\mathcal{R}_i,\mathcal{D}}|h_{\mathcal{R}_i,\mathcal{D}}|^2}{\sigma^2_{n_{\mathcal{D}}} + P_{\mathcal{R}_i} d^{-\vartheta}_{\mathcal{R}_i,\mathcal{D}}|h_{\mathcal{R}_i,\mathcal{D}}|^2}\right) = 0, \tag{E.38}$$

$$(1 - (\hat{\varpi}_i + \hat{\tau}_i))B\log_2(1 + \Upsilon_{\mathcal{R}_i,\mathcal{D}}) - \hat{\tau}_i[B\log_2(1 + \Upsilon_{\mathcal{S},\mathcal{R}_i}) + (\delta_i \cdot r)] = 0, \quad \text{(E.39)}$$

$$(1 - (\hat{\varpi}_i + \hat{\tau}_i))P_{\mathcal{R}_i} - \zeta\hat{\varpi}_i(P_{\mathcal{S}}d_{\mathcal{S},\mathcal{R}_i}^{-\vartheta}|h_{\mathcal{S},\mathcal{R}_i}|^2 + \sigma_{n_{R_i}}^2) - E_{ext} = 0, \quad \text{(E.40)}$$

$$r - (1 - (\hat{\varpi}_i + \hat{\tau}_i))B\log_2(1 + \Upsilon_{\mathcal{R}_i,\mathcal{D}}) = 0. \quad \text{(E.41)}$$

From (E.39) and (E.41), we obtain

$$\hat{\tau}_i = \frac{r}{B\log_2(1 + \Upsilon_{\mathcal{S},\mathcal{R}_i}) + (\delta_i \cdot r)}. \quad \text{(E.42)}$$

Similarly, from (E.40) and (E.41), we find

$$\hat{\varpi}_i = \frac{rP_{\mathcal{R}_i} - E_{ext}B\log_2(1 + \Upsilon_{\mathcal{R}_i,\mathcal{D}})}{\zeta(P_{\mathcal{S}}d_{\mathcal{S},\mathcal{R}_i}^{-\vartheta}|h_{\mathcal{S},\mathcal{R}_i}|^2 + \sigma_{n_{R_i}}^2)}. \quad \text{(E.43)}$$

Substituting (E.42) and (E.43) in (E.41), and assuming $\tilde{\eta} = 1 + \Upsilon_{\mathcal{R}_i,\mathcal{D}}$ we obtain the following equation

$$\mathcal{A} - B\log_2(\tilde{\eta})[\mathcal{B} + \mathcal{C}\tilde{\eta} + \mathcal{D}B\log_2(\tilde{\eta})] = 0, \quad \text{(E.44)}$$

where $\mathcal{A} = a \cdot b \cdot r$, $\mathcal{B} = a \cdot b + a \cdot r \cdot \left(\frac{\sigma_{n_{\mathcal{D}}}^2}{d_{\mathcal{R}_i,\mathcal{D}}^{-\vartheta}|h_{\mathcal{R}_i,\mathcal{D}}|^2}\right) - b \cdot r$, $\mathcal{C} = -a \cdot r \cdot \left(\frac{\sigma_{n_{\mathcal{D}}}^2}{d_{\mathcal{R}_i,\mathcal{D}}^{-\vartheta}|h_{\mathcal{R}_i,\mathcal{D}}|^2}\right)$, and $\mathcal{D} = a \cdot E_{ext}$, where $a = B\log_2(1 + \Upsilon_{\mathcal{S},\mathcal{R}_i}) + (\delta_i \cdot r)$, and $b = \zeta(P_{\mathcal{S}}d_{\mathcal{S},\mathcal{R}_i}^{-\vartheta}|h_{\mathcal{S},\mathcal{R}_i}|^2 + \sigma_{n_{R_i}}^2)$.

Considering $\mathcal{F}(\tilde{\eta}) = \mathcal{A} - B\log_2(\tilde{\eta})[\mathcal{B} + \mathcal{C}\tilde{\eta} + \mathcal{D}B\log_2(\tilde{\eta})]$, we have a nonlinear equation of the type

$$\mathcal{F}(\tilde{\eta}) = 0. \quad \text{(E.45)}$$

Let us assume that $\tilde{\eta}$ is a simple or one of the multiple roots of (E.45), and $\tilde{\eta}_0$ is an initial point prediction sufficiently near to $\tilde{\eta}$. Using the Taylor's series expansion, we can express the following

$$\mathcal{F}(\tilde{\eta}_0) + (\tilde{\eta} - \tilde{\eta}_0)\mathcal{F}'(\tilde{\eta}_0) + \frac{1}{2}(\tilde{\eta} - \tilde{\eta}_0)^2\mathcal{F}''(\tilde{\eta}_0) = 0. \quad \text{(E.46)}$$

In order to solve the nonlinear equation $\mathcal{F}(\tilde{\eta}) = 0$, an alternative equivalence formulation has been used to develop a class of iterative methods. Simplified form of (E.46) can be re-written as

$$\mathcal{F}''(\tilde{\eta}_0)(\tilde{\eta} - \tilde{\eta}_0)^2 + 2\mathcal{F}'(\tilde{\eta}_0)(\tilde{\eta} - \tilde{\eta}_0) + 2\mathcal{F}(\tilde{\eta}_0) = 0. \quad \text{(E.47)}$$

It is clear that the equation in (E.47) is of the quadratic form. Hence, the corresponding roots can be expressed as

$$\tilde{\eta} - \tilde{\eta}_0 = \frac{-\mathcal{F}'(\tilde{\eta}_0) \pm \sqrt{[\mathcal{F}'(\tilde{\eta}_0)]^2 - 2\mathcal{F}''(\tilde{\eta}_0)\mathcal{F}(\tilde{\eta}_0)}}{\mathcal{F}''(\tilde{\eta}_0)}. \quad \text{(E.48)}$$

Depending on the sign of proceeding the radical term, the formula in (E.48) provides the following two possibilities

$$\tilde{\eta} = \tilde{\eta}_0 - \frac{\mathcal{F}'(\tilde{\eta}_0) + \sqrt{[\mathcal{F}'(\tilde{\eta}_0)]^2 - 2\mathcal{F}''(\tilde{\eta}_0)\mathcal{F}(\tilde{\eta}_0)}}{\mathcal{F}''(\tilde{\eta}_0)}. \quad \text{(E.49)}$$

$$\tilde{\eta} = \tilde{\eta}_0 - \frac{\mathcal{F}'(\tilde{\eta}_0) - \sqrt{[\mathcal{F}'(\tilde{\eta}_0)]^2 - 2\mathcal{F}''(\tilde{\eta}_0)\mathcal{F}(\tilde{\eta}_0)}}{\mathcal{F}''(\tilde{\eta}_0)}. \quad \text{(E.50)}$$

Using the fixed point formulations in (E.49) and (E.50), and in order to maximize the objective in (5.26), the following formula for an approximate solution $\tilde{\eta}_{k+1}$ can be used to find the larger root iteratively [283]

$$\tilde{\eta}_{k+1} = \tilde{\eta}_k - \frac{\mathcal{F}'(\tilde{\eta}_k) - \sqrt{[\mathcal{F}'(\tilde{\eta}_k)]^2 - 2\mathcal{F}''(\tilde{\eta}_k)\mathcal{F}(\tilde{\eta}_k)}}{\mathcal{F}''(\tilde{\eta}_k)}. \tag{E.51}$$

It should be noted that the denominator of (E.51) is independent of $\mathcal{F}'(\tilde{\eta}_k)$ which makes it specially fit to find the largest root of the (E.45).

Since the nonlinear equation in (E.44) involves the logarithmic terms, the number of iterations required to find the optimal largest root may be higher for the chosen value of $\tilde{\eta}_0$. In that case, Halley's method (2) or the modified Chebyshev's method (39) in [284] may also be used to reduce the number of iterations.

Finally, we obtain the following solutions for this case

$$P^*_{\mathcal{R}_i} = (\tilde{\eta} - 1)\left(\frac{\sigma^2_{n_\mathcal{D}}}{d^{-\vartheta}_{\mathcal{R}_i,\mathcal{D}}|h_{\mathcal{R}_i,\mathcal{D}}|^2}\right), \tag{E.52}$$

$$\hat{\tau}^*_i = \frac{r}{B\log_2(1+\Upsilon_{\mathcal{S},\mathcal{R}_i}) + (\delta_i \cdot r)}, \tag{E.53}$$

$$\hat{\varpi}^*_i = \frac{rP^*_{\mathcal{R}_i} - E_{ext}B\log_2\left(1 + \frac{P^*_{\mathcal{R}_i} d^{-\vartheta}_{\mathcal{R}_i,\mathcal{D}}|h_{\mathcal{R}_i,\mathcal{D}}|^2}{\sigma^2_{n_\mathcal{D}}}\right)}{\zeta(P_\mathcal{S} d^{-\vartheta}_{\mathcal{S},\mathcal{R}_i}|h_{\mathcal{S},\mathcal{R}_i}|^2 + \sigma^2_{n_{R_i}})}, \tag{E.54}$$

where $P^*_{\mathcal{R}_i}$, $\hat{\tau}^*_i$, and $\hat{\varpi}^*_i$ are the optimal values obtained for $P_{\mathcal{R}_i}$, $\hat{\tau}_i$, and $\hat{\varpi}_i$, respectively in this case.

E.3 TS Factors' Selection for Uniformity in the assumed Convention

In this chapter, we have investigated two problems for maximization of throughput and stored energy at the relay by using two distinct time-conventions, respectively. This facilitates the reader to independently adopt any of the presented conventions for further analysis in similar directions. Herein, we intend to accomplish the relationship between the two conventions as presented in Fig. 5.3 and Fig. 5.4, respectively, in order to impose uniformity in the analysis.

Assuming the TS convention as in Fig. 5.3, the corresponding conventions for Fig. 5.4 can be represented in terms of the metrics in Fig. 5.3 as follows

$$\hat{\varpi}_i = \varpi_i \cdot \tau_i, \text{ and } \hat{\tau}_i = (1 - \varpi_i) \cdot \tau_i, \tag{E.55}$$

where i is the index of the chosen relay.

Similarly, if the TS convention as in Fig. 5.4 is assumed throughout, then the metrics in Fig. 5.3 can be represented as

$$\varpi_i = \frac{\hat{\varpi}_i}{\hat{\varpi}_i + \hat{\tau}_i}, \text{ and } \tau_i = \hat{\varpi}_i + \hat{\tau}_i. \tag{E.56}$$

Bibliography

[1] Charles Coulston Gillispie, Frederic Lawrence Holmes, Noretta Koertge, and Thomson Gale, *Complete Dictionary of Scientific Biography*, Detroit, Mich. : Charles Scribner's Sons, 2008.

[2] Luke Goodman and et. al., "The feasibility of wireless energy," *Available online at https : //www.wpi.edu/Pubs/E − project/Available/E − project − 051713 − 222152/unrestricted/wireless − energy − iqp.pdf*, 2013.

[3] Sumit Gautam, *Simultaneous Wireless Information and Energy Transfer in Multicarrier and Cooperative Communication Systems*, MS Thesis: International Institute of Information Technology Hyderabad, 2017.

[4] Sumit Sharma, "Advanced trends in wireless electricity transmission using semiconductor devices," *International Journal of Scientific & Engineering Research*, pp. 188–194, December 2013.

[5] Geoffrey A. Landis, "Applications for space power by laser transmission," 1994, vol. 2121, pp. 252–255.

[6] G.A. Landis, M. Stavnes, S. Oleson, and J. Bozek, *Space transfer with ground-based laser/electric propulsion*, Jul 1992.

[7] T. Gangale, "Globalization of space - the astrosociological approach," *American Institute of Aeronautics and Astronautics*, September 2007.

[8] N. Shinohara, "Wireless power transmission for solar power satellite (sps) (second draft) 1. theoretical background," *Available on-line at http://citeseerx.ist.psu.edu/viewdoc/summary?doi=10.1.1.372.4940.*

[9] L. S. Luk, "Point-to-point wireless power transportation in reunion island," in *International Astronautical Congress, 48th, Turin, Italy*, 1997.

[10] AFP-JIJI, "The japan times," *Available on-line at http : //www.japantimes.co.jp/news/2015/03/13/national/science − health/japan − space − scientists − make − wireless − energy − breakthrough/#.V3KcYDH3QUV*, 2015.

[11] Powercast Corporation, "Powercast," *www.powercastco.com.*

[12] N. Shinohara, "Development of rectenna with wireless communication system," in *Proceedings of the 5th European Conference on Antennas and Propagation (EUCAP)*, April 2011, pp. 3970–3973.

[13] I. Krikidis, S. Timotheou, S. Nikolaou, G. Zheng, D. W. K. Ng, and R. Schober, "Simultaneous wireless information and power transfer in modern communication systems," *IEEE Commun. Mag.*, vol. 52, no. 11, pp. 104–110, 2014.

[14] NEOS Guide: Companion Site to the NEOS Server, "Optimization taxonomy," `https://neos-guide.org/content/optimization-taxonomy`, [Online].

[15] S. Gautam, E. Lagunas, S. Chatzinotas, and B. Ottersten, "Relay Selection and Resource Allocation for SWIPT in Multi-User OFDMA Systems," *IEEE Trans. Wireless Comm.*, vol. 18, no. 5, pp. 2493–2508, May 2019.

[16] S. Gautam and P. Ubaidulla, "Relay Selection and Transceiver Design for Joint Wireless Information and Energy Transfer in Cooperative Networks," in *85th Veh. Tech. Conf. (VTC), 2017-Spring*, June 2017.

[17] S. Gautam, E. Lagunas, S. K. Sharma, S. Chatzinotas, and B Ottersten, "Relay Selection Strategies for SWIPT-Enabled Cooperative Wireless Systems," in *28th Annual IEEE Int. Symp. on Personal, Indoor and Mobile Radio Comm. (PIMRC)*, October 2017.

[18] S. Gautam, E. Lagunas, S. Chatzinotas, and B. Ottersten, "Resource allocation and relay selection for multi-user OFDM-based cooperative networks with SWIPT," in *2018 15th International Symposium on Wireless Communication Systems (ISWCS)*. IEEE, 2018, pp. 1–5.

[19] S. Gautam, E. Lagunas, S. Chatzinotas, and B. Ottersten, "Sequential Resource Distribution Technique for Multi-User OFDM-SWIPT Based Cooperative Networks," in *IEEE Global Communication Conference (GLOBECOM)*, Dec 2018, pp. 1–7.

[20] S. Gautam, E. Lagunas, S. Vuppala, S. Chatzinotasy, and B. Ottersten, "QoS-Constrained Sum-Harvested Energy Maximization in OFDMA-based Wireless Cooperative Networks," in *2018 IEEE International Conference on Advanced Networks and Telecommunications Systems (ANTS)*. IEEE, 2018, pp. 1–6.

[21] S. Gautam, E. Lagunas, S. Vuppala, S. Chatzinotas, and B. Ottersten, "Pricing Perspective for SWIPT in OFDM-based Multi-User Wireless Cooperative Systems," in *2019 IEEE Wireless Communications and Networking Conference (WCNC)*, April 2019, pp. 1–7.

[22] S. Gautam, E. Lagunas, A. Bandi, S. Chatzinotas, S. K. Sharma, T. X. Vu, S. Kisseleff, and B. Ottersten, "Multigroup Multicast Precoding for Energy Optimization in SWIPT Systems with Heterogeneous Users," *IEEE Open Journal of the Communications Society*, pp. 1–1, 2019.

[23] S. Gautam, E. Lagunas, S. Chatzinotas, and B. Ottersten, "Wireless Multi-group Multicast Precoding with Selective RF Energy Harvesting," in *27th European Signal Processing Conference (EUSIPCO)*. IEEE, 2019, `http://orbilu.uni.lu/handle/10993/39760`.

[24] S. Gautam, E. Lagunas, S. Kisseleff, S. Chatzinotas, and B. Ottersten, "Successive Convex Approximation for Transmit Power Minimization in SWIPT-Multicast Systems," *accepted to 2020 IEEE International Conference on Communications (ICC): Green Communication Systems and Networks Symposium (IEEE ICC'20 - GCSN Symposium)*, June 2020.

[25] T. X. Vu, S. Chatzinotas, S. Gautam, E. Lagunas, and B. Ottersten, "Joint Optimization for PS-based SWIPT Multiuser Systems with Non-linear Energy Harvesting," *submitted to 2020 IEEE Wireless Communications and Networking Conference (WCNC) (IEEE WCNC 2020)*, Apr. 2020.

[26] S. Gautam, T. X. Vu, S. Chatzinotas, and B. Ottersten, "Cache-Aided Simultaneous Wireless Information and Power Transfer (SWIPT) With Relay Selection," *IEEE J. Sel. Areas Commun.*, vol. 37, no. 1, pp. 187–201, Jan 2019.

[27] S. Gautam, T. X. Vu, S. Chatzinotas, and B. Ottersten, "Joint wireless information and energy transfer in cache-assisted relaying systems," in *IEEE Wireless Communications and Networking Conference (WCNC)*, April 2018, pp. 1–6.

[28] Muhammad Saad, "Feasibility of energy efficient wireless power transmission in electric vehicles," *Available on-line at https : //www.researchgate.net/publication/*283265634*_Feasibility_of_Energy_Efficient_Wireless_Power_Transmission_in_Electric_Vehicles*, 2014.

[29] William C Brown, "The history of wireless power transmission," *Solar energy*, vol. 56, no. 1, pp. 3–21, January 1996.

[30] W. C. Brown, "The History of Power Transmission by Radio Waves," *IEEE Trans. Microw. Theory Techn.*, vol. 32, no. 9, pp. 1230–1242, Sep 1984.

[31] Z. Ding, C. Zhong, D. Wing Kwan Ng, M. Peng, H. A. Suraweera, R. Schober, and H. V. Poor, "Application of smart antenna technologies in simultaneous wireless information and power transfer," *IEEE Communications Magazine*, vol. 53, no. 4, pp. 86–93, April 2015.

[32] Namrata Naha - STSTW Media, "Tesla Tower: The Tragic Story of Nikola Tesla's Wardenclyffe Wireless Station," `https://www.ststworld.com/tesla-tower/`, 7 Oct. 2018, [Online].

[33] R. D. Fernandes, J. N. Matos, and N. B. Carvalho, "Resonant Electrical Coupling: Circuit Model and First Experimental Results," *IEEE Trans. Microw. Theory Techn.*, vol. 63, no. 9, pp. 2983–2990, 2015.

[34] Mainland High School ISTF Volusia County Schools, "William C. Brown," `http://mainland.cctt.org/istf2008/brown.asp`, 2008, [Online].

[35] William C Brown, "The history of the development of the rectenna," in *Solar Power Satellite Microwave Power Transmission and Reception*, 1980, vol. 2141, pp. 271–280.

[36] A. K. RamRakhyani, S. Mirabbasi, and M. Chiao, "Design and optimization of resonance-based efficient wireless power delivery systems for biomedical implants," *IEEE Trans. Biomed. Circuits Syst*, vol. 5, no. 1, pp. 48–63, 2011.

[37] K. Agarwal, R. Jegadeesan, Y.-X. Guo, and N. V. Thakor, "Wireless power transfer strategies for implantable bioelectronics," *IEEE Rev. Biomed. Eng.*, vol. 10, pp. 136–161, 2017.

[38] Slideshare, "Wireless power transmission," `https://www.slideshare.net/rakeshkk/wireless-power-transmission`, 31 Aug. 2010, [Online].

[39] Andre Kurs, *Power transfer through strongly coupled resonances*, Ph.D. thesis, Massachusetts Institute of Technology, 2007.

[40] Wikipedia, "Resonant inductive coupling," `https://en.wikipedia.org/wiki/Resonant_inductive_coupling`, [Online].

[41] Slideshare, "WiTricity," `https://www.slideshare.net/SouvikDolui/wi-tricity-35160759`, 27 May 2014, [Online].

[42] Mystica Augustine Michael Duke, "Wireless power transmission," *International Journal of Scientific & Engineering Research*, vol. 5, no. 10, pp. 125–129, October 2014.

[43] SDAK, "How Lightning Works," `http://infotech-spots.blogspot.com/2009/04/how-lightning-works.html`, 17 Apr. 2009, [Online].

[44] James Benford, John A Swegle, and Edl Schamiloglu, *High power microwaves*, CRC Press, 2015.

[45] Wikipedia, "Wireless power transfer," `https://en.wikipedia.org/wiki/Wireless_power_transfer`, [Online].

[46] Parina Hassani - Systweak Blog, "Future of Power Distribution," `https://blogs.systweak.com/future-of-power-distribution/`, 14 Oct. 2016, [Online].

[47] W. F. Pickard, A. Q. Shen, and N. J. Hansing, "Parking the power: Strategies and physical limitations for bulk energy storage in supply–demand matching on a grid whose input power is provided by intermittent sources," *Renewable and Sustainable Energy Reviews*, vol. 13, no. 8, pp. 1934–1945, 2009.

[48] V. A. Vanke, H. Matsumoto, N. Shinohara, and A. Kita, "High Power Converter of Microwaves into DC," *Journal of Radioelectronics*, , no. 9, August 30 1999.

[49] S. Sood, S. Kullanthasamy, and M. Shahidehpour, "Solar power transmission: from space to earth," in *IEEE Power Engineering Society General Meeting, 2005*, June 2005, pp. 605–610 Vol. 1.

[50] Wikipedia, "Space-based solar power," `https://en.wikipedia.org/wiki/Space-based_solar_power`, [Online].

[51] C. Mikeka and H. Arai, *Design issues in radio frequency energy harvesting system*, INTECH Open Access Publisher, 2011.

[52] Henry Liu, "Maximizing efficiency of wireless power transfer with resonant Inductive Coupling," 2011.

[53] Kurs Andre and et. al., "Wireless power transfer via strongly coupled magnetic resonances," *Science*, vol. 317, no. 5834, pp. 83–86, 2007.

[54] M. V. Reddy, K. S. Hemanth, and C. H. V. Mohan, "Microwave power transmission–a next generation power transmission system," *IOSR Journal of Electrical and Electronics Engineering (IOSRJEEE), e-ISSN*, pp. 2278–1676, 2013.

[55] P. N. Alevizos and A. Bletsas, "Sensitive and nonlinear far-field RF energy harvesting in wireless communications," *IEEE Trans. Wireless Commun.*, vol. 17, no. 6, pp. 3670–3685, 2018.

[56] C. Konstantopoulos, E. Koutroulis, N. Mitianoudis, and A. Bletsas, "Converting a plant to a battery and wireless sensor with scatter radio and ultra-low cost," *IEEE Trans. Instrum. Meas.*, vol. 65, no. 2, pp. 388–398, 2015.

[57] S. D. Assimonis, S.-N. Daskalakis, and A. Bletsas, "Sensitive and efficient RF harvesting supply for batteryless backscatter sensor networks," *IEEE Trans. Microw. Theory Techn.*, vol. 64, no. 4, pp. 1327–1338, 2016.

[58] U. Olgun, C.-C. Chen, and J. L. Volakis, "Investigation of rectenna array configurations for enhanced RF power harvesting," *IEEE Antennas Wireless Propag. Lett.*, vol. 10, pp. 262–265, 2011.

[59] J. Guo, H. Zhang, and X. Zhu, "Theoretical analysis of RF-DC conversion efficiency for class-F rectifiers," *IEEE Trans. Microw. Theory Techn.*, vol. 62, no. 4, pp. 977–985, 2014.

[60] K. Xiong, B. Wang, and K. J. R. Liu, "Rate-energy region of SWIPT for MIMO broadcasting under nonlinear energy harvesting model," *IEEE Trans. Wireless Commun.*, vol. 16, no. 8, pp. 5147–5161, 2017.

[61] Y. Chen, K. T. Sabnis, and R. A. Abd-Alhameed, "New formula for conversion efficiency of RF EH and its wireless applications," *IEEE Trans. Veh. Tech.*, vol. 65, no. 11, pp. 9410–9414, 2016.

[62] L. Shi, L. Zhao, and K. Liang, "Power allocation for wireless powered MIMO transmissions with non-linear RF energy conversion models," *China Communications*, vol. 14, no. 2, pp. 57–64, 2017.

[63] J. Kang, I. Kim, and D. I. Kim, "Joint Tx Power Allocation and Rx Power Splitting for SWIPT System With Multiple Nonlinear Energy Harvesting Circuits," *IEEE Wireless Comm. Lett.*, vol. 8, no. 1, pp. 53–56, Feb 2019.

[64] G. Ma, J. Xu, Y. Zeng, and M. R. V. Moghadam, "A Generic Receiver Architecture for MIMO Wireless Power Transfer With Nonlinear Energy Harvesting," *IEEE Signal Process. Lett.*, vol. 26, no. 2, pp. 312–316, Feb 2019.

[65] R. Zhang and C. K. Ho, "MIMO broadcasting for simultaneous wireless information and power transfer," *IEEE Trans. Wireless Commun.*, vol. 12, no. 5, pp. 1989–2001, 2013.

[66] X. Zhou, R. Zhang, and C. K. Ho, "Wireless Information and Power Transfer in Multiuser OFDM Systems," *IEEE Trans. Wireless Commun.*, vol. 13, no. 4, pp. 2282–2294, April 2014.

[67] G. Lu, L. Shi, and Y. Ye, "Maximum Throughput of TS/PS Scheme in an AF Relaying Network With Non-Linear Energy Harvester," *IEEE Access*, vol. 6, pp. 26617–26625, 2018.

[68] L. R. Varshney, "Transporting information and energy simultaneously," in *2008 IEEE International Symposium on Information Theory*, July 2008, pp. 1612–1616.

[69] P. Grover and A. Sahai, "Shannon meets Tesla: Wireless information and power transfer," in *2010 IEEE International Symposium on Information Theory*, June 2010, pp. 2363–2367.

[70] A. M. Fouladgar and O. Simeone, "On the Transfer of Information and Energy in Multi-User Systems," *IEEE Commun. Lett.*, vol. 16, no. 11, pp. 1733–1736, November 2012.

[71] P. Popovski, A. M. Fouladgar, and O. Simeone, "Interactive joint transfer of energy and information," *IEEE Trans. Commun.*, vol. 61, no. 5, pp. 2086–2097, May 2013.

[72] M. Peng, Y. Liu, D. Wei, W. Wang, and H. Chen, "Hierarchical cooperative relay based heterogeneous networks," *IEEE Wireless Commun.*, vol. 18, no. 3, pp. 48–56, June 2011.

[73] B. Zhou, H. Hu, S. Huang, and H. Chen, "Intracluster Device-to-Device Relay Algorithm With Optimal Resource Utilization," *IEEE Trans. Veh. Tech.*, vol. 62, no. 5, pp. 2315–2326, Jun 2013.

[74] J. N. Laneman and G. W. Wornell, "Energy-efficient antenna sharing and relaying for wireless networks," in *2000 IEEE Wireless Communications and Networking Conference. Conference Record (Cat. No.00TH8540)*, Sep. 2000, vol. 1, pp. 7–12 vol.1.

[75] J. N. Laneman, D. N. C. Tse, and G. W. Wornell, "Cooperative diversity in wireless networks: Efficient protocols and outage behavior," *IEEE Trans. Inf. Theory*, vol. 50, no. 12, pp. 3062–3080, Dec 2004.

[76] H. Chen, Y. Li, J. L. Rebelatto, B. F. Uchôa-Filho, and B. Vucetic, "Harvest-Then-Cooperate: Wireless-Powered Cooperative Communications," *IEEE Trans. Sig. Proc.*, vol. 63, no. 7, pp. 1700–1711, April 2015.

[77] A. Rajaram, D. N. K. Jayakody, and V. Skachek, "Store-then-cooperate: Energy harvesting scheme in cooperative relay networks," in *2016 International Symposium on Wireless Communication Systems (ISWCS)*, Sep. 2016, pp. 445–450.

[78] W. Huang, H. Chen, Y. Li, and B. Vucetic, "On the Performance of Multi-antenna Wireless-Powered Communications With Energy Beamforming," *IEEE Trans. Veh. Tech.*, vol. 65, no. 3, pp. 1801–1808, March 2016.

[79] I. Krikidis, G. Zheng, and B. Ottersten, "Harvest-use cooperative networks with half/full-duplex relaying," in *2013 IEEE Wireless Communications and Networking Conference (WCNC)*, April 2013, pp. 4256–4260.

[80] A. A. Nasir, X. Zhou, S. Durrani, and R. A. Kennedy, "Relaying Protocols for Wireless Energy Harvesting and Information Processing," *IEEE Trans. Wireless Commun.*, vol. 12, no. 7, pp. 3622–3636, July 2013.

[81] Z. Ding, I. Krikidis, B. Sharif, and H. V. Poor, "Wireless Information and Power Transfer in Cooperative Networks With Spatially Random Relays," *IEEE Trans. Wireless Commun.*, vol. 13, no. 8, pp. 4440–4453, Aug 2014.

[82] Z. Hu, C. Yuan, F. Zhu, and F. Gao, "Weighted sum transmit power minimization for full-duplex system with SWIPT and self-energy recycling," *IEEE Access*, vol. 4, pp. 4874–4881, 2016.

[83] M. Gao, H. H. Chen, Y. Li, M. Shirvanimoghaddam, and J. Shi, "Full-duplex wireless-powered communication with antenna pair selection," in *2015 IEEE Wireless Communications and Networking Conference (WCNC)*. IEEE, 2015, pp. 693–698.

[84] J. I. Choi, M. Jain, K. Srinivasan, P. Levis, and S. Katti, "Achieving single channel, full duplex wireless communication," in *Proceedings of the sixteenth annual international conference on Mobile computing and networking*. ACM, 2010, pp. 1–12.

[85] D. N. K. Jayakody, J. Thompson, S. Chatzinotas, and S. Durrani, *Wireless Information and Power Transfer: A New Paradigm for Green Communications*, Springer, 2017.

[86] M. Duarte, C. Dick, and A. Sabharwal, "Experiment-driven characterization of full-duplex wireless systems," *IEEE Trans. Wireless Commun.*, vol. 11, no. 12, pp. 4296–4307, 2012.

[87] E. Aryafar, M. A. Khojastepour, K. Sundaresan, S. Rangarajan, and M. Chiang, "Midu: Enabling mimo full duplex," in *Proceedings of the 18th annual international conference on Mobile computing and networking*. ACM, 2012, pp. 257–268.

[88] E. Ahmed and A. M. Eltawil, "All-digital self-interference cancellation technique for full-duplex systems," *IEEE Trans. Wireless Commun.*, vol. 14, no. 7, pp. 3519–3532, 2015.

[89] A. A. Okandeji, M. R. A. Khandaker, and K.-K. Wong, "Wireless information and power transfer in full-duplex communication systems," in *2016 IEEE International Conference on Communications (ICC)*. IEEE, 2016, pp. 1–6.

[90] Y. Zeng and R. Zhang, "Full-duplex wireless-powered relay with self-energy recycling," *IEEE Wireless Commun. Lett.*, vol. 4, no. 2, pp. 201–204, 2015.

[91] M. Maso, C.-F. Liu, C.-H. Lee, T. Q. S. Quek, and L. S. Cardoso, "Energy-recycling full-duplex radios for next-generation networks," *IEEE J. Sel. Areas Commun.*, vol. 33, no. 12, pp. 2948–2962, 2015.

[92] H. Ju and R. Zhang, "Optimal resource allocation in full-duplex wireless-powered communication network," *IEEE Trans. Commun.*, vol. 62, no. 10, pp. 3528–3540, 2014.

[93] X. Kang, C. K. Ho, and S. Sun, "Full-duplex wireless-powered communication network with energy causality," *IEEE Trans. Wireless Commun.*, vol. 14, no. 10, pp. 5539–5551, 2015.

[94] S. Leng, D. W. K. Ng, N. Zlatanov, and R. Schober, "Multi-objective resource allocation in full-duplex SWIPT systems," in *2016 IEEE International Conference on Communications (ICC)*. IEEE, 2016, pp. 1–7.

[95] V.-D. Nguyen, H. V. Nguyen, G.-M. Kang, H. M. Kim, and O.-S. Shin, "Sum rate maximization for full duplex wireless-powered communication networks," in *2016 24th European Signal Processing Conference (EUSIPCO)*. IEEE, 2016, pp. 798–802.

[96] X. Lu, P. Wang, D. Niyato, D. I. Kim, and Z. Han, "Wireless Networks With RF Energy Harvesting: A Contemporary Survey," *IEEE Commun. Surveys Tuts.*, vol. 17, no. 2, pp. 757–789, Secondquarter 2015.

[97] X. Lu, P. Wang, D. Niyato, and E. Hossain, "Dynamic spectrum access in cognitive radio networks with RF energy harvesting," *IEEE Wireless Commun.*, vol. 21, no. 3, pp. 102–110, June 2014.

[98] J. Lee and S. Nam, "Fundamental Aspects of Near-Field Coupling Small Antennas for Wireless Power Transfer," *IEEE Trans. Antennas Propag.*, vol. 58, no. 11, pp. 3442–3449, Nov 2010.

[99] A. Naeem, M. H. Rehmani, Y. Saleem, I. Rashid, and N. Crespi, "Network Coding in Cognitive Radio Networks: A Comprehensive Survey," *IEEE Commun. Surveys Tuts.*, vol. 19, no. 3, pp. 1945–1973, thirdquarter 2017.

[100] Z. Hu, N. Wei, and Z. Zhang, "Optimal Resource Allocation for Harvested Energy Maximization in Wideband Cognitive Radio Network With SWIPT," *IEEE Access*, vol. 5, pp. 23383–23394, 2017.

[101] A. El Shafie, N. Al-Dhahir, and R. Hamila, "Cooperative Access Schemes for Efficient SWIPT Transmissions in Cognitive Radio Networks," in *2015 IEEE Globecom Workshops (GC Wkshps)*, Dec 2015, pp. 1–6.

[102] S. K. Sharma, T. E. Bogale, S. Chatzinotas, B. Ottersten, L. B. Le, and X. Wang, "Cognitive Radio Techniques Under Practical Imperfections: A Survey," *IEEE Commun. Surveys Tuts.*, vol. 17, no. 4, pp. 1858–1884, Fourthquarter 2015.

[103] D. W. K. Ng, E. S. Lo, and R. Schober, "Wireless information and power transfer: Energy efficiency optimization in OFDMA systems," *IEEE Trans. Wireless Commun.*, vol. 12, no. 12, pp. 6352–6370, 2013.

[104] S. M. R. Islam, N. Avazov, O. A. Dobre, and K.-S. Kwak, "Power-domain non-orthogonal multiple access (NOMA) in 5G systems: Potentials and challenges," *IEEE Commun. Surveys Tuts.*, vol. 19, no. 2, pp. 721–742, 2016.

[105] Z. Ding, X. Lei, G. K. Karagiannidis, R. Schober, J. Yuan, and V. K. Bhargava, "A survey on non-orthogonal multiple access for 5G networks: Research challenges and future trends," *IEEE J. Sel. Areas Commun.*, vol. 35, no. 10, pp. 2181–2195, 2017.

[106] Z. Ding, Mu. Peng, and H. V. Poor, "Cooperative non-orthogonal multiple access in 5G systems," *IEEE Commun. Lett.*, vol. 19, no. 8, pp. 1462–1465, 2015.

[107] Y. Liu, Z. Ding, M. Elkashlan, and H. V. Poor, "Cooperative non-orthogonal multiple access with simultaneous wireless information and power transfer," *IEEE J. Sel. Areas Commun.*, vol. 34, no. 4, pp. 938–953, 2016.

[108] Z. Chen, Z. Ding, X. Dai, and G. K. Karagiannidis, "On the application of quasi-degradation to MISO-NOMA downlink," *IEEE Trans. Signal Process.*, vol. 64, no. 23, pp. 6174–6189, 2016.

[109] Z. Chen, Z. Ding, P. Xu, and X. Dai, "Optimal precoding for a QoS optimization problem in two-user MISO-NOMA downlink," *IEEE Commun. Lett.*, vol. 20, no. 6, pp. 1263–1266, 2016.

[110] N. T. Do, D. B. da Costa, T. Q. Duong, and B. An, "Transmit antenna selection schemes for MISO-NOMA cooperative downlink transmissions with hybrid SWIPT protocol," in *2017 IEEE International Conference on Communications (ICC)*. IEEE, 2017, pp. 1–6.

[111] L. Lu, G. Y. Li, A. L. Swindlehurst, A. Ashikhmin, and R. Zhang, "An Overview of Massive MIMO: Benefits and Challenges," *IEEE J. Sel. Topics Signal Process.*, vol. 8, no. 5, pp. 742–758, Oct 2014.

[112] G. Amarasuriya and H. V. Poor, "Wireless Information and Power Transfer in Multi-Way Relay Networks with Massive MIMO," in *2015 IEEE Global Communications Conference (GLOBECOM)*, Dec 2015, pp. 1–7.

[113] D. Kwon, H. S. Kang, and D. K. Kim, "Robust Interference Exploitation-Based Precoding Scheme With Quantized CSIT," *IEEE Commun. Lett.*, vol. 20, no. 4, pp. 780–783, April 2016.

[114] S. Timotheou, G. Zheng, C. Masouros, and I. Krikidis, "Symbol-level precoding in MISO broadcast channels for SWIPT systems," in *2016 23rd International Conference on Telecommunications (ICT)*, May 2016, pp. 1–5.

[115] M. Alodeh, S. Chatzinotas, and B. Ottersten, "Constructive Interference through Symbol Level Precoding for Multi-Level Modulation," in *2015 IEEE Global Communications Conference (GLOBECOM)*, Dec 2015, pp. 1–6.

[116] H. Stockman, "Communication by means of reflected power," *Proceedings of the IRE*, vol. 36, no. 10, pp. 1196–1204, 1948.

[117] G. Vannucci, A. Bletsas, and D. Leigh, "A software-defined radio system for backscatter sensor networks," *IEEE Trans. Wireless Commun.*, vol. 7, no. 6, pp. 2170–2179, 2008.

[118] N. Fasarakis-Hilliard, P. N. Alevizos, and A. Bletsas, "Coherent detection and channel coding for bistatic scatter radio sensor networking," *IEEE Trans. Commun.*, vol. 63, no. 5, pp. 1798–1810, 2015.

[119] M. Marcus and B. Pattan, "Millimeter wave propagation: spectrum management implications," *IEEE Microw. Mag.*, vol. 6, no. 2, pp. 54–62, 2005.

[120] A. Al-Hourani, S. Chandrasekharan, and S. Kandeepan, "Path loss study for millimeter wave device-to-device communications in urban environment," in *2014 IEEE international conference on communications workshops (ICC)*. IEEE, 2014, pp. 102–107.

[121] J. Lillibridge, R. Scharroo, S. Abdalla, and D. Vandemark, "One-and two-dimensional wind speed models for Ka-band altimetry," *J. Atmos. Ocean. Technol.*, vol. 31, no. 3, pp. 630–638, 2014.

[122] L. Wang, M. Elkashlan, R. W. Heath, M. Di Renzo, and K.-K. Wong, "Millimeter wave power transfer and information transmission," in *2015 IEEE Global Communications Conference (GLOBECOM)*. IEEE, 2015, pp. 1–6.

[123] S. Ladan, A. B. Guntupalli, and K. Wu, "A high-efficiency 24 GHz rectenna development towards millimeter-wave energy harvesting and wireless power transmission," *IEEE Trans. Circuits Syst. I, Reg. Papers*, vol. 61, no. 12, pp. 3358–3366, 2014.

[124] A. Nesic, Z. Micic, S. Jovanovic, and I. Radnovic, "Millimeter wave printed antenna array with high side lobe suppression," in *2006 IEEE Antennas and Propagation Society International Symposium*. IEEE, 2006, pp. 3051–3054.

[125] M. Peer, N. Jain, and V. A. Bohara, "A hybrid spectrum sharing protocol for energy harvesting wireless sensor nodes," in *2016 IEEE 17th International Workshop on Signal Processing Advances in Wireless Communications (SPAWC)*. IEEE, 2016, pp. 1–6.

[126] I. F. Akyildiz, T. Melodia, and K. R. Chowdhury, "A survey on wireless multimedia sensor networks," *Comput. Netw.*, vol. 51, no. 4, pp. 921–960, 2007.

[127] B. Tong, Z. Li, G. Wang, and W. Zhang, "How wireless power charging technology affects sensor network deployment and routing," in *2010 IEEE 30th International Conference on Distributed Computing Systems*. IEEE, 2010, pp. 438–447.

[128] Zoya Popović, Erez Avigdor Falkenstein, Daniel Costinett, and Regan Zane, "Low-power far-field wireless powering for wireless sensors," *Proceedings of the IEEE*, vol. 101, no. 6, pp. 1397–1409, 2013.

[129] S. Guo, C. Wang, and Y. Yang, "Mobile data gathering with wireless energy replenishment in rechargeable sensor networks," in *2013 Proceedings IEEE INFOCOM*. IEEE, 2013, pp. 1932–1940.

[130] S. Guo, C. Wang, and Y. Yang, "Joint mobile data gathering and energy provisioning in wireless rechargeable sensor networks," *IEEE Trans. Mobile Comput.*, vol. 13, no. 12, pp. 2836–2852, 2014.

[131] C. Wang, J. Li, F. Ye, and Y. Yang, "NETWRAP: An NDN based real-timewireless recharging framework for wireless sensor networks," *IEEE Trans. Mobile Comput.*, vol. 13, no. 6, pp. 1283–1297, 2014.

[132] S. Zhang, J. Wu, and S. Lu, "Collaborative mobile charging for sensor networks," in *2012 IEEE 9th international conference on mobile ad-hoc and sensor systems (MASS 2012)*. IEEE, 2012, pp. 84–92.

[133] J. Johnson, E. Basha, and C. Detweiler, "Charge selection algorithms for maximizing sensor network life with UAV-based limited wireless recharging," in *2013 IEEE Eighth International Conference on Intelligent Sensors, Sensor Networks and Information Processing*. IEEE, 2013, pp. 159–164.

[134] M. Y. Naderi, K. R. Chowdhury, S. Basagni, W. Heinzelman, S. De, and S. Jana, "Experimental study of concurrent data and wireless energy transfer for sensor networks," in *2014 IEEE Global Communications Conference*. IEEE, 2014, pp. 2543–2549.

[135] H. Xing, K.-K. Wong, A. Nallanathan, and R. Zhang, "Wireless powered cooperative jamming for secrecy multi-AF relaying networks," *IEEE Trans. Wireless Commun.*, vol. 15, no. 12, pp. 7971–7984, 2016.

[136] L. Dong, Z. Han, A. P. P., and H. V. Poor, "Improving wireless physical layer security via cooperating relays," *IEEE Trans. Signal Process.*, vol. 58, no. 3, pp. 1875–1888, 2009.

[137] J. Li, A. P. Petropulu, and S. Weber, "On cooperative relaying schemes for wireless physical layer security," *IEEE Trans. Signal Process.*, vol. 59, no. 10, pp. 4985–4997, 2011.

[138] M. Zhang and Y. Liu, "Energy harvesting for physical-layer security in OFDMA networks," *IEEE Trans. Inf. Forensics Security*, vol. 11, no. 1, pp. 154–162, 2015.

[139] M. Zhang, Y. Liu, and R. Zhang, "Artificial noise aided secrecy information and power transfer in OFDMA systems," *IEEE Trans. Wireless Commun.*, vol. 15, no. 4, pp. 3085–3096, 2016.

[140] G. Pan, C. Tang, T. Li, and Y. Chen, "Secrecy performance analysis for SIMO simultaneous wireless information and power transfer systems," *IEEE Trans. Commun.*, vol. 63, no. 9, pp. 3423–3433, 2015.

[141] G. Pan, H. Lei, Y. Deng, L. Fan, J. Yang, Y. Chen, and Z. Ding, "On secrecy performance of MISO SWIPT systems with TAS and imperfect CSI," *IEEE Trans. Commun.*, vol. 64, no. 9, pp. 3831–3843, 2016.

[142] Y. Yang, Q. Li, W.-K. Ma, J. Ge, and P. C. Ching, "Cooperative secure beamforming for AF relay networks with multiple eavesdroppers," *IEEE Signal Process. Lett.*, vol. 20, no. 1, pp. 35–38, 2012.

[143] H. Xing, L. Liu, and R. Zhang, "Secrecy wireless information and power transfer in fading wiretap channel," *IEEE Trans. Veh. Tech.*, vol. 65, no. 1, pp. 180–190, 2015.

[144] Y. Liu, "Wireless information and power transfer for multirelay-assisted cooperative communication," *IEEE Commun. Lett.*, vol. 20, no. 4, pp. 784–787, 2016.

[145] L.-G. Tran, H.-K. Cha, and W.-T. Park, "A compact wireless power transfer system at 915 MHz with supercapacitor for optogenetics applications," *Sensors and Actuators A: Physical*, vol. 285, pp. 386–394, 2019.

[146] Vaisleib, V. and Mor, O. and Alpert, O., "Wi-Charge," `https://wi-charge.com/`, [Online].

[147] Energous Corporation, "Watt-Up," `https://www.energous.com/`, [Online].

[148] Bohn, F. and Hajimiri, A. and Abiri, B., "GuRu," `https://guru.inc/`, [Online].

[149] Ossia, "Cota," `https://www.ossia.com/`, [Online].

[150] Powercast Corporation, "Powercast : Wireless Power for a Wireless World," `https://www.powercastco.com/`, [Online].

[151] Soljačić, M., "WiTricity," `https://witricity.com/`, [Online].

[152] Qi Wireless, "Qi (Standard)," `http://www.qiwireless.com/`, [Online].

[153] MacDonald, J. and Shi, L., "Spansive (formely Pi)," `https://www.spansive.com/`, [Online].

[154] Freevolt, "Freevolt," `https://getfreevolt.com/`, [Online].

[155] NOWI B.V., "NOWI: Enabling the Internet of Things," `nowi-energy.com`, [Online].

[156] J. N. Laneman, D. N. C. Tse, and G. W. Wornell, "Cooperative Diversity in Wireless Networks: Efficient Protocols and Outage Behavior," *IEEE Trans. Inf. Theory*, vol. 50, no. 12, pp. 3062–3080, Dec. 2010.

[157] A. S. Ibrahim, A. K. Sadek, W. Su, and K. J. R. Liu, "Cooperative Communications with Relay-Selection: When to Cooperate and Whom to Cooperate With?," *IEEE Trans. Wireless Commun.*, vol. 7, no. 7, pp. 2814–2827, Jul. 2008.

[158] F. Atay, *Cooperative diversity relaying techniques in wireless communication networks*, Ph.D. thesis, Citeseer, 2009.

[159] S. Sesia, I. Toufik, and M. Baker, *Orthogonal Frequency Division Multiple Access (OFDMA)*, p. 792, Wiley Telecom, 2011.

[160] M. S. Alam, J. W. Mark, and X. S. Shen, "Relay Selection and Resource Allocation for Multi-User Cooperative OFDMA Networks," *IEEE Trans. Wireless Commun.*, vol. 12, no. 5, pp. 2193–2205, May 2013.

[161] J. Luo, R .S. Blum, L. J. Greenstein, L. J. Cimini, and A. M. Haimovich, "Practical Relay Networks: A Generalization of Hybrid-ARQ," *IEEE J. Select. Areas Commun.*, vol. 23, no. 1, pp. 7–18, Jan. 2005.

[162] B. Medepally and N. B. Mehta, "Voluntary Energy Harvesting Relays and Selection in Cooperative Wireless Networks," *IEEE Trans. Wireless Commun.*, vol. 9, no. 11, pp. 3543–3553, Nov. 2010.

[163] A. Bletsas, A. Khisti, and M. Z. Win, "Opportunistic Cooperative Diversity with Feedback and Cheap Radios," *IEEE Trans. Wireless Commun.*, vol. 7, no. 5, pp. 1823–1827, May 2008.

[164] W. Dang, M. Tao, H. Mu, and J. Huang, "Subcarrier-Pair Based Resource Allocation for Cooperative Multi-Relay OFDM Systems," *IEEE Trans. Wireless Commun.*, vol. 9, no. 5, pp. 1640–1649, May 2010.

[165] I. Hammerstrom and A. Wittneben, "Power Allocation Schemes for Amplify-and-Forward MIMO-OFDM Relay Links," *IEEE Trans. Wireless Commun.*, vol. 6, no. 8, pp. 2798–2802, Aug. 2007.

[166] L. Dai, B. Gui, and L. J. Cimini Jr., "Selective Relaying in OFDM Multihop Cooperative Networks," in *2007 IEEE Wireless Communications and Networking Conference*, March 2007, pp. 963–968.

[167] S. Gautam and P. Ubaidulla, "Simultaneous transmission of information and energy in OFDM systems," in *Proc. 18th Wireless Personal Multimedia Communications (WPMC)*, December 2015.

[168] T. D. P. Perera, D. N. K. Jayakody, S. K. Sharma, S. Chatzinotas, and J. Li, "Simultaneous Wireless Information and Power Transfer (SWIPT): Recent Advances and Future Challenges," *IEEE Commun. Surveys Tuts.*, 2017.

[169] Z. Ding, C. Zhong, D. W. K. Ng, M. Peng, H. A. Suraweera, R. Schober, and H. V. Poor, "Application of smart antenna technologies in simultaneous wireless information and power transfer," *IEEE Commun. Mag.*, vol. 53, no. 4, pp. 86–93, April 2015.

[170] K. Huang and E. Larsson, "Simultaneous Information and Power Transfer for Broadband Wireless Systems," *IEEE Trans. Signal Process.*, vol. 61, no. 23, pp. 5972–5986, Dec 2013.

[171] X. Zhou, R. Zhang, and C. K. Ho, "Wireless Information and Power Transfer: Architecture Design and Rate-Energy Tradeoff," *IEEE Trans. Commun.*, vol. 61, no. 11, pp. 4754–4767, November 2013.

[172] L. Jiang, C. Qin, X. Zhang, and H. Tian, "Secure beamforming design for SWIPT in cooperative D2D communications," *China Communications*, vol. 14, no. 1, pp. 20–33, Jan 2017.

[173] Z. Ali, G. A. S. Sidhu, S. Zhang, L. Xing, and F. Gao, "Achieving Green Transmission With Energy Harvesting Based Cooperative Communication," *IEEE Access*, pp. 1–1, 2018.

[174] Y. Feng, V. C. M. Leung, and F. Ji, "Performance Study for SWIPT Cooperative Communication Systems in Shadowed Nakagami Fading Channels," *IEEE Trans. Wireless Commun.*, vol. 17, no. 2, pp. 1199–1211, Feb 2018.

[175] A. Farjami, V. T. Vakili, and S. S. Moghaddam, "A simple relay selection algorithm in multi user OFDM based cooperative CR networks," in *2014 7th Int. Symp. on Telecomm. (IST)*, Sept 2014, pp. 118–122.

[176] B. Razeghi, M. Hatamian, A. Naghizadeh, S. Sabeti, and G. A. Hodtani, "A novel relay selection scheme for multi-user cooperation communications using fuzzy logic," in *2015 IEEE 12th Int. Conf. on Networking, Sensing and Control*, April 2015, pp. 241–246.

[177] C. Qin and K. Xiao, "Performance analysis of a multi-user relay selection scheme with predicted SINR in the presence of co-channel interference," in *2016 8th IEEE International Conference on Communication Software and Networks (ICCSN)*, June 2016, pp. 171–176.

[178] D. S. Michalopoulos, H. A. Suraweera, and R. Schober, "Relay Selection for Simultaneous Information Transmission and Wireless Energy Transfer: A Tradeoff Perspective," *IEEE J. Sel. Areas Commun.*, vol. 33, no. 8, pp. 1578–1594, Aug. 2015.

[179] D. Wang, R. Zhang, X. Cheng, and L. Yang, "Relay selection in two-way full-duplex energy-harvesting relay networks," in *Global Communications Conference (GLOBECOM), 2016 IEEE*. IEEE, 2016, pp. 1–6.

[180] S. Guo, F. Wang, Y. Yang, and B. Xiao, "Energy-efficient cooperative transmission for simultaneous wireless information and power transfer in clustered wireless sensor networks," *IEEE Trans. Commun.*, vol. 63, no. 11, pp. 4405–4417, 2015.

[181] T. P. Do, I. Song, and Y. H. Kim, "Simultaneous wireless transfer of power and information in a decode-and-forward two-way relaying network," *IEEE Trans. Wireless Commun.*, vol. 16, no. 3, pp. 1579–1592, 2017.

[182] N. Zhao, R. Chai, Q. Hu, J. K. Zhang, et al., "Energy efficiency optimization based joint relay selection and resource allocation for SWIPT relay networks," in *2015 10th Int. Conf. on Comm. and Net. in China (ChinaCom)*. IEEE, 2015, pp. 503–508.

[183] Y. Ye, Y. Li, D. Wang, F. Zhou, R. Q. Hu, and H. Zhang, "Optimal Transmission Schemes for DF Relaying Networks Using SWIPT," *IEEE Trans. Veh. Technol.*, 2018.

[184] S. Modem and S. Prakriya, "Performance of analog network coding based two-way EH relay with beamforming," *IEEE Trans. Commun.*, vol. 65, no. 4, pp. 1518–1535, 2017.

[185] S. Gautam and P. Ubaidulla, "Simultaneous transmission of information and RF energy in multicarrier systems," in *23rd Int. Conf. on Telecom. (ICT)*, May 2016, pp. 1–5.

[186] L. Liu, R. Zhang, and K. C. Chua, "Wireless Information and Power Transfer: A Dynamic Power Splitting Approach," *IEEE Trans. Commun.*, vol. 61, no. 9, pp. 3990–4001, September 2013.

[187] X. Zhou, R. Zhang, and C. K. Ho, "Wireless Information and Power Transfer in Multiuser OFDM Systems," *IEEE Trans. Wireless Commun.*, vol. 13, no. 4, pp. 2282–2294, April 2014.

[188] Y. Chen, K. T. Sabnis, and R. A. Abd-Alhameed, "New formula for conversion efficiency of RF EH and its wireless applications," *IEEE Trans. Veh. Technol.*, vol. 65, no. 11, pp. 9410–9414, 2016.

[189] Z. Chang, L. Lei, H. Zhang, T. Ristaniemi, S. Chatzinotas, B. Ottersten, and Z. Han, "Energy-Efficient and Secure Resource Allocation for Multiple-Antenna NOMA with Wireless Power Transfer," *IEEE Trans. Green Commun. Netw*, pp. 1–1, 2018.

[190] W. Yu and R. Lui, "Dual methods for nonconvex spectrum optimization of multicarrier systems," *IEEE Trans. Commun.*, vol. 54, no. 7, pp. 1310–1322, July 2006.

[191] S. Boyd and L. Vandenberghe, *Convex optimization*, Cambridge university press, 2004.

[192] H. W. Kuhn, "The Hungarian method for the assignment problem," *Naval Research Logistics (NRL)*, vol. 2, no. 1-2, pp. 83–97, 1955.

[193] P. Series, "Propagation data and prediction methods for the planning of indoor radiocommunication systems and radio local area networks in the frequency range 900 MHz to 100 GHz," *Recommendation ITU-R*, pp. 1238–7, 2012.

[194] J. G. Proakis, *Digital Communications*, 4th Edition, McGraw-Hill, 2001.

[195] Q. Shi, L. Liu, W. Xu, and R. Zhang, "Joint Transmit Beamforming and Receive Power Splitting for MISO SWIPT Systems," *IEEE Trans. Wireless Commun.*, vol. 13, no. 6, pp. 3269–3280, June 2014.

[196] S. Gautam and P. Ubaidulla, "Relay Selection and Transceiver Design for Joint Wireless Information and Energy Transfer in Cooperative Networks," in *85th Veh. Tech. Conf. (Spring)*. IEEE, 2017, pp. 1–5.

[197] D. Mishra, G. C. Alexandropoulos, and S. De, "Harvested Power Fairness Optimization in MISO SWIPT Multicasting IoT with Individual Constraints," in *IEEE International Conference on Communications (ICC)*, May 2018, pp. 1–6.

[198] M. Sivakumaran and P. Iacopino, "The Mobile Economy 2018," `https://www.gsma.com/mobileeconomy/wp-content/uploads/2018/05/The-Mobile-Economy-2018.pdf`, 2018.

[199] R. Tandon, S. A. Jafar, S. Shamai, and H. V. Poor, "On the Synergistic Benefits of Alternating CSIT for the MISO Broadcast Channel," *IEEE Trans. Inf. Theory*, vol. 59, no. 7, pp. 4106–4128, July 2013.

[200] L. R. Varshney, "Transporting information and energy simultaneously," in *IEEE International Symposium on Information Theory*, July 2008, pp. 1612–1616.

[201] M. R. A. Khandaker and K. Wong, "SWIPT in MISO Multicasting Systems," *IEEE Wireless Commun. Lett.*, vol. 3, no. 3, pp. 277–280, June 2014.

[202] Z. Ding, C. Zhong, D. W. K. Ng, M. Peng, H. A. Suraweera, R. Schober, and H. V. Poor, "Application of smart antenna technologies in simultaneous wireless information and power transfer," *IEEE Comm. Mag.*, vol. 53, no. 4, pp. 86–93, April 2015.

[203] N. D. Sidiropoulos and T. N. Davidson and, "Transmit beamforming for physical-layer multicasting," *IEEE Trans. Signal Process.*, vol. 54, no. 6, pp. 2239–2251, June 2006.

[204] Q. Shi, C. Peng, W. Xu, M. Hong, and Y. Cai, "Energy Efficiency Optimization for MISO SWIPT Systems With Zero-Forcing Beamforming," *IEEE Trans. Signal Process.*, vol. 64, no. 4, pp. 842–854, Feb 2016.

[205] J. Xu, L. Liu, and R. Zhang, "Multiuser MISO Beamforming for Simultaneous Wireless Information and Power Transfer," *IEEE Trans. Signal Process.*, vol. 62, no. 18, pp. 4798–4810, Sep. 2014.

[206] S. Timotheou, G. Zheng, C. Masouros, and I. Krikidis, "Symbol-level precoding in MISO broadcast channels for SWIPT systems," in *23rd International Conference on Telecommunications (ICT)*, May 2016, pp. 1–5.

[207] N. Janatian, I. Stupia, and L. Vandendorpe, "Joint multi-objective transmit precoding and receiver time switching design for MISO SWIPT systems," in *17th International Workshop on Signal Processing Advances in Wireless Communications (SPAWC)*, July 2016, pp. 1–5.

[208] G. Venkatraman, A. Tölli, M. Juntti, and L. Tran, "Multigroup Multicast Beamformer Design for MISO-OFDM With Antenna Selection," *IEEE Trans. Signal Proc.*, vol. 65, no. 22, pp. 5832–5847, Nov 2017.

[209] E. Karipidis, N. D. Sidiropoulos, and Zhi-Quan Luo, "Convex Transmit Beamforming for Downlink Multicasting to Multiple Co-Channel Groups," in *2006 IEEE International Conference on Acoustics Speech and Signal Processing Proceedings*, May 2006, vol. 5, pp. V–V.

[210] M. Alodeh, S. Chatzinotas, and B. Ottersten, "User Selection for Symbol-Level Multigroup Multicasting Precoding in the Downlink of MISO Channels," in *IEEE International Conference on Communications (ICC)*, May 2018, pp. 1–7.

[211] D. Christopoulos, S. Chatzinotas, and B. Ottersten, "Weighted Fair Multicast Multigroup Beamforming under Per-antenna Power Constraints," *IEEE Trans. Signal Process.*, vol. 62, no. 19, pp. 5132–5142, 2014.

[212] A. Z. Yalcin and M. Yuksel, "Precoder Design For Multi-Group Multicasting With a Common Message," *IEEE Trans. Comm.*, vol. 67, no. 10, pp. 7302–7315, Oct 2019.

[213] Ö. T. Demir and T. E. Tuncer, "Multi-group multicast beamforming for simultaneous wireless information and power transfer," in *23rd European Signal Processing Conference (EUSIPCO)*, Aug 2015, pp. 1356–1360.

[214] Ö. T. Demir and T. E. Tuncer, "Antenna Selection and Hybrid Beamforming for Simultaneous Wireless Information and Power Transfer in Multi-Group Multicasting Systems," *IEEE Trans. Wireless Comm.*, vol. 15, no. 10, pp. 6948–6962, Oct 2016.

[215] M. Alodeh, D. Spano, A. Kalantari, C. G. Tsinos, D. Christopoulos, S. Chatzinotas, and B. Ottersten, "Symbol-Level and Multicast Precoding for Multiuser Multiantenna Downlink: A State-of-the-Art, Classification, and Challenges," *IEEE Commun. Surveys Tuts.*, vol. 20, no. 3, pp. 1733–1757, thirdquarter 2018.

[216] M. R. A. Khandaker and K. Wong, "SWIPT in MISO Multicasting Systems," *IEEE Wireless Commun. Lett.*, vol. 3, no. 3, pp. 277–280, June 2014.

[217] D. Mishra, G. C. Alexandropoulos, and S. De, "Energy Sustainable IoT With Individual QoS Constraints Through MISO SWIPT Multicasting," *IEEE Internet Things J.*, vol. 5, no. 4, pp. 2856–2867, Aug 2018.

[218] E. Karipidis, N. D. Sidiropoulos, and Z. Luo, "Far-Field Multicast Beamforming for Uniform Linear Antenna Arrays," *IEEE Trans. Signal Proc.*, vol. 55, no. 10, pp. 4916–4927, Oct 2007.

[219] D. Christopoulos, S. Chatzinotas, and B. Ottersten, "Multicast Multigroup Precoding and User Scheduling for Frame-Based Satellite Communications," *IEEE Trans. Wireless Comm.*, vol. 14, no. 9, pp. 4695–4707, Sep. 2015.

[220] H. Zhou and M. Tao, "Joint multicast beamforming and user grouping in massive MIMO systems," in *2015 IEEE International Conference on Communications (ICC)*, June 2015, pp. 1770–1775.

[221] B. Clerckx and E. Bayguzina, "Waveform Design for Wireless Power Transfer," *IEEE Trans. Signal Process.*, vol. 64, no. 23, pp. 6313–6328, 2016.

[222] J. Guo, H. Zhang, and X. Zhu, "Theoretical analysis of RF-DC conversion efficiency for class-F rectifiers," *IEEE Trans. Microw. Theory Techn.*, vol. 62, no. 4, pp. 977–985, 2014.

[223] A. Wiesel, Y. C. Eldar, and S. Shamai, "Linear precoding via conic optimization for fixed MIMO receivers," *IEEE Trans. Signal Process.*, vol. 54, no. 1, pp. 161–176, Jan 2006.

[224] S. Boyd and L. Vandenberghe, *Convex optimization*, Cambridge university press, 2004.

[225] M. Grant and S. Boyd, "CVX: Matlab software for disciplined convex programming, version 2.1," `http://cvxr.com/cvx`, Mar. 2014.

[226] M. Grant and S. Boyd, "Graph implementations for nonsmooth convex programs," in *Recent Advances in Learning and Control*, V. Blondel, S. Boyd, and H. Kimura, Eds., Lecture Notes in Control and Information Sciences, pp. 95–110. Springer-Verlag Limited, 2008, `http://stanford.edu/~boyd/graph_dcp.html`.

[227] M. Bengtsson and B. Ottersten, "Optimum and Suboptimum Transmit Beamforming," in *Handbook of Antennas in Wireless Communications*. CRC press, 2001.

[228] K. Krishnan, *Linear programming (LP) approaches to semidefinite programming (SDP) problems*, Ph.D. thesis, Citeseer, 2002.

[229] D. Christopoulos, S. Chatzinotas, and B. Ottersten, "Multicast multigroup beamforming under per-antenna power constraints," in *IEEE International Conference on Communications (ICC)*, June 2014, pp. 4704–4710.

[230] O. Mehanna, K. Huang, B. Gopalakrishnan, A. Konar, and N. D. Sidiropoulos, "Feasible point pursuit and successive approximation of non-convex QCQPs," *IEEE Signal Process. Lett.*, vol. 22, no. 7, pp. 804–808, 2014.

[231] FCC Notice of Proposed Rule Making, "Revision of Part 15 of the Commission's Rules Regarding Ultrawideband Transmission Systems," `https://transition.fcc.gov/Bureaus/Engineering_Technology/Orders/2002/fcc02048.pdf`, Apr. 2002.

[232] L. Zhang, Y. Xin, and Y.-C. Liang, "Weighted sum rate optimization for cognitive radio MIMO broadcast channels," *IEEE Trans. Wireless Comm.*, vol. 8, no. 6, pp. 2950–2959, 2009.

[233] R. Madani, G. Fazelnia, and J. Lavaei, "Rank-2 matrix solution for semidefinite relaxations of arbitrary polynomial optimization problems," *constraints*, vol. 21, pp. 25, 2014.

[234] A. Bozorgchenani, D. Tarchi, and G. E. Corazza, "Centralized and Distributed Architectures for Energy and Delay Efficient Fog Network-Based Edge Computing Services," *IEEE Trans. Green Commun. Netw.*, vol. 3, no. 1, pp. 250–263, March 2019.

[235] Y. Yang, Z. Liu, X. Yang, K. Wang, X. Hong, and X. Ge, "POMT: Paired Offloading of Multiple Tasks in Heterogeneous Fog Networks," *IEEE Internet Things J.*, vol. 6, no. 5, pp. 8658–8669, Oct 2019.

[236] AIR802, "IEEE 802.11 a/b/g/n Wi-Fi Standards and Facts ," `https://www.air802.com/ieee-802.11-standards-facts-amp-channels.html`.

[237] B. Mitchell, "Learn Exactly How "Fast" a Wi-Fi Network Can Move," 2019, `https://www.lifewire.com/how-fast-is-a-wifi-network-816543`.

[238] N. Janatian, I. Stupia, and L. Vandendorpe, "Optimal resource allocation in ultra-low power fog-computing SWIPT-based networks," in *2018 IEEE Wireless Communications and Networking Conference (WCNC)*, April 2018, pp. 1–6.

[239] S. Zhou, J. Gong, Z. Zhou, W. Chen, and Z. Niu, "GreenDelivery: proactive content caching and push with energy-harvesting-based small cells," *IEEE Commun. Mag.*, vol. 53, no. 4, pp. 142–149, April 2015.

[240] ERICSSON white paper, "More than 50 Billion Connected Devices ," `https://www.ericsson.com/openarticle/mwc-connected-devices_1686565587_c`, 2011, [Online].

[241] Q. Gu, G. Wang, R. Fan, Z. Zhong, K. Yang, and H. Jiang, "Rate-Energy Tradeoff in Simultaneous Wireless Information and Power Transfer over Fading Channels with Uncertain Distribution," *IEEE Trans. Veh. Technol.*, vol. PP, no. 99, pp. 1–1, 2017.

[242] J. Park, B. Clerckx, C. Song, and Y. Wu, "An Analysis of the Optimum Node Density for Simultaneous Wireless Information and Power Transfer in Ad Hoc Networks," *IEEE Trans. Veh. Technol.*, vol. PP, no. 99, pp. 1–1, 2017.

[243] B. Clerckx, "Waveform and Transceiver Design for Simultaneous Wireless Information and Power Transfer," *CoRR*, vol. abs/1607.05602, 2016.

[244] I. Bang, S. M. Kim, and D. K. Sung, "Adaptive Multiuser Scheduling for Simultaneous Wireless Information and Power Transfer in a Multicell Environment," *IEEE Trans. Wireless Commun.*, vol. 16, no. 11, pp. 7460–7474, Nov. 2017.

[245] S. Mahama, D. K. P. Asiedu, and K. J. Lee, "Simultaneous Wireless Information and Power Transfer for Cooperative Relay Networks With Battery," *IEEE Access*, vol. 5, pp. 13171–13178, 2017.

[246] A. A. Nasir and X. Zhou and S. Durrani and R. A. Kennedy, "Relaying Protocols for Wireless Energy Harvesting and Information Processing," *IEEE Trans. Wireless Commun.*, vol. 12, no. 7, pp. 3622–3636, July 2013.

[247] J. Huang, C. C. Xing, and C. Wang, "Simultaneous Wireless Information and Power Transfer: Technologies, Applications, and Research Challenges," *IEEE Commun. Mag.*, vol. 55, no. 11, pp. 26–32, Nov. 2017.

[248] S. Borst, V. Gupta, and A. Walid, "Distributed Caching Algorithms for Content Distribution Networks," in *Proc. IEEE Int. Conf. Comput. Commun.*, Mar. 2010, pp. 1–9.

[249] M. A. Maddah-Ali and U. Niesen, "Fundamental Limits of Caching," *IEEE Trans. Inf. Theory*, vol. 60, no. 5, pp. 2856–2867, May 2014.

[250] T. X. Vu, S. Chatzinotas, B. Ottersten, and T. Q. Duong, "Energy Minimization for Cache-assisted Content Delivery Networks with Wireless Backhaul," *IEEE Wireless Commun. Lett.*, vol. 7, no. 3, pp. 332 – 335, Jun 2018.

[251] T. X. Vu, S. Chatzinotas, and B. Ottersten, "Edge-Caching Wireless Networks: Performance analysis and optimization," *IEEE Trans. Wireless Commun.*, vol. 17, no. 7, pp. 2827 – 2839, Apr 2018.

[252] S. Vuppala, T. X. Vu, S. Gautam, S. Chatzinotas, and B. Ottersten, "Cache-Aided Millimeter Wave Ad-Hoc Networks with Contention-Based Content Delivery," *IEEE Trans. Commun.*, vol. 66, no. 8, pp. 3540 – 3554, Aug 2018.

[253] A. Kumar and W. Saad, "On the tradeoff between energy harvesting and caching in wireless networks," in *2015 IEEE International Conference on Communication Workshop (ICCW)*, Jun. 2015, pp. 1976–1981.

[254] D. Niyato, D. I. Kim, P. Wang, and L. Song, "A novel caching mechanism for Internet of Things (IoT) sensing service with energy harvesting," in *Proc. IEEE Int. Conf. Commun.*, May 2016, pp. 1–6.

[255] S. Zhang, N. Zhang, X. Fang, P. Yang, and X. S. Shen, "Cost-effective vehicular network planning with cache-enabled green roadside units," in *Proc. IEEE Int. Conf. Commun.*, May 2017, pp. 1–6.

[256] I. Krikidis and S. Timotheou and S. Nikolaou and G. Zheng and D. W. K. Ng and R. Schober, "Simultaneous wireless information and power transfer in modern communication systems," *IEEE Commun. Mag.*, vol. 52, no. 11, pp. 104–110, Nov 2014.

[257] L. Xiang and D. W. K. Ng and T. Islam and R. Schober and V. W. S. Wong and J. Wang, "Cross-Layer Optimization of Fast Video Delivery in Cache- and Buffer-Enabled Relaying Networks," *IEEE Trans. Veh. Technol.*, vol. 66, no. 12, pp. 11366–11382, Dec 2017.

[258] S. Lohani, R. A. Loodaricheh, E. Hossain, and V. K. Bhargava, "On Multiuser Resource Allocation in Relay-Based Wireless-Powered Uplink Cellular Networks," *IEEE Trans. Wireless Commun.*, vol. 15, no. 3, pp. 1851–1865, March 2016.

[259] F. Benkhelifa and M. S. Alouini, "Precoding Design of MIMO Amplify-and-Forward Communication System With an Energy Harvesting Relay and Possibly Imperfect CSI," *IEEE Access*, vol. 5, pp. 578–594, 2017.

[260] T. Le, K. Mayaram, and T. Fiez, "Efficient Far-Field Radio Frequency Energy Harvesting for Passively Powered Sensor Networks," *IEEE Journal of Solid-State Circuits*, vol. 43, no. 5, pp. 1287–1302, May 2008.

[261] U. Muncuk and K. Alemdar and J. D. Sarode and K. R. Chowdhury, "Multi-band Ambient RF Energy Harvesting Circuit Design for Enabling Battery-less Sensors and IoTs," `http://krc.coe.neu.edu/sites/krc.coe.neu.edu/files/papers/IOTJournal18%20.pdf`, *accepted to IEEE Internet Things J.*, Feb 2018, [Online].

[262] B. Clerckx, "Waveform optimization for SWIPT with nonlinear energy harvester modeling," in *20th International ITG Workshop on Smart Antennas*. VDE, 2016, pp. 1–5.

[263] D. I. Kim, J. H. Moon, and J. J. Park, "New SWIPT using PAPR: How it works," *IEEE Wireless Commun. Lett.*, vol. 5, no. 6, pp. 672–675, 2016.

[264] J. J. Park, J. H. Moon, K.-Y. Lee, and D. I. Kim, "Dual mode SWIPT: Waveform design and transceiver architecture with adaptive mode switching policy," in *2018 IEEE 87th Vehicular Technology Conference (VTC Spring)*. IEEE, 2018, pp. 1–5.

[265] H. Sun, Z. Zhong, and Y.-X. Guo, "An adaptive reconfigurable rectifier for wireless power transmission," *IEEE Microw. Wireless Compon. Lett*, vol. 23, no. 9, pp. 492–494, 2013.

[266] M. Varasteh, B. Rassouli, and B. Clerckx, "SWIPT Signalling over Frequency-Selective Channels with a Nonlinear Energy Harvester: Non-Zero Mean and Asymmetric Inputs," *arXiv preprint arXiv:1901.01740*, 2019.

[267] S. T. Shah, K. W. Choi, T.-J. Lee, and M. Y. Chung, "Outage probability and throughput analysis of SWIPT enabled cognitive relay network with ambient backscatter," *IEEE Internet Things J.*, vol. 5, no. 4, pp. 3198–3208, 2018.

[268] P. N. Alevizos and A. Bletsas, "Industrial SWIPT: Backscatter Radio and RFIDs," *Wireless Information and Power Transfer: Theory and Practice*, pp. 61–79, 2018.

[269] N. Van Huynh, D. T. Hoang, X. Lu, D. Niyato, P. Wang, and D. I. Kim, "Ambient backscatter communications: A contemporary survey," *IEEE Commun. Surveys Tuts.*, vol. 20, no. 4, pp. 2889–2922, 2018.

[270] J. Qian, F. Gao, and G. Wang, "Signal detection of ambient backscatter system with differential modulation," in *2016 IEEE International Conference on Acoustics, Speech and Signal Processing (ICASSP)*. IEEE, 2016, pp. 3831–3835.

[271] B. Lyu, Z. Yang, G. Gui, and Y. Feng, "Wireless powered communication networks assisted by backscatter communication," *IEEE Access*, vol. 5, pp. 7254–7262, 2017.

[272] N. Janatian, I. Stupia, and L. Vandendorpe, "Optimal Offloading Strategy and Resource Allocation in SWIPT-based Mobile-Edge Computing Networks," in *2018 15th International Symposium on Wireless Communication Systems (ISWCS)*, Aug 2018, pp. 1–6.

[273] A. I. Akin, N. Janatian, I. Stupia, and L. Vandendorpe, "SWIPT-based real-time mobile computing systems: A stochastic geometry perspective," in *2019 IEEE Wireless Communications and Networking Conference (WCNC)*. IEEE, 2019, pp. 1–7.

[274] H. Mirghasemi, I. Stupia, and L. Vandendorpe, "Optimal Compression and Transmission Policies for Energy Harvesting Nodes," in *2018 15th International Symposium on Wireless Communication Systems (ISWCS)*. IEEE, 2018, pp. 1–6.

[275] Y. Mao, B. Clerckx, and V. O. Li, "Rate-Splitting for Multi-User Multi-Antenna Wireless Information and Power Transfer," *arXiv preprint arXiv:1902.07851*, 2019.

[276] mathapptician, "Graphical method - solving an optimization problem," `https://www.youtube.com/watch?v=fY4DiobykXY`, 28 Aug. 2012, [Online].

[277] M. Bierlaire, "Duality: Lagrangian and dual problem," `https://www.youtube.com/watch?v=4OifjG2kIJQ`, 19 Mar. 2019, [Online].

[278] OnMyPhD, "Karush-Kuhn-Tucker (KKT) conditions," `http://www.onmyphd.com/?p=kkt.karush.kuhn.tucker`, [Online].

[279] WikiAudio, "Semidefinite programming," `https://www.youtube.com/watch?v=Sm0IUpxBHNs`, 29 Jan. 2016, [Online].

[280] R. M. Freund, "Introduction to Semidefinite Programming (SDP)," `https://ocw.mit.edu/courses/electrical-engineering-and-computer-science/6-251j-introduction-to-mathematical-programming-fall-2009/readings/MIT6_251JF09_SDP.pdf`, [Online].

[281] Wikipedia, "Slack variable," `https://en.wikipedia.org/wiki/Slack_variable`, [Online].

[282] Robert M. Corless, Gaston H. Gonnet, David E. G. Hare, David J. Jeffrey, and Donald E. Knuth, "On the LambertW function," *Advances in Computational mathematics*, vol. 5, no. 1, pp. 329–359, 1996.

[283] Z. Hong-bin, "A Novel Method Finding Multiple Roots of Nonlinear Equations," in *2009 Fifth International Conference on Natural Computation*, Aug 2009, vol. 6, pp. 299–302.

[284] Beny Neta, "New third order nonlinear solvers for multiple roots," *Applied Mathematics and Computation*, vol. 202, no. 1, pp. 162–170, 2008.